EVALUATING THE MECHANISMS OF 2-HYDROXYPROPYL-β-CYCLODEXTRIN

AND LIVER X RECEPTOR AGONISTS AS POTENTIAL THERAPIES

FOR NIEMANN-PICK TYPE C DISEASE

APPROVED BY SUPERVISORY COMMITTEE

Joyce Repa, Ph.D.

Carole Mendelson, Ph.D.

Steven Kliewer, Ph.D.

Joel Goodman, Ph.D.

DEDICATION

I would like to dedicate this dissertation work to two very important people in my life, who I have not yet truly had the opportunity to get to know:

The first is my paternal grandfather, Stanley Leroy Miller. He was born on February 6, 1931 and was a loving son, husband, father, grandfather, and friend. When my grandfather was 17 years old, he joined the U.S. army where he served for 20 years starting out as a cook and working his way up through the ranks to master sergeant. After retiring from the military, he moved his family to Pineville, Louisiana, where he worked at Pineville Kraft Paper Mill. As he had always been a very health conscious and athletic man, everyone was concerned when he began falling without explanation. At the age of 54, he was diagnosed at the Brooke Army Medical Center in San Antonio, TX with Amyotrophic Lateral Sclerosis, a progressive motor neuron disease for which there is no cure. Although he was given only a couple years to live, my grandfather was a fighter who did not give up easily, a trait that runs in the family. I was just 3 years old when he passed away on March 22, 1990. My first memories are saying goodbye to him, seeing a soldier hand my grandmother a folded flag, and hearing the gun shots and bugle play at his funeral. At the time, I was far too young to appreciate the life that my grandfather lived, but his untimely death left a lasting impression on me and has been my inspiration to study another neurologic disease for which there is no cure.

The second person is my daughter. Although she is probably not aware of what is going on around her, she has been with me, literally, through every step of writing and defending my dissertation. I am looking forward to meeting her in the next few weeks and helping her to grow up into the young woman she will become. I hope my dissertation research will inspire my daughter to reach for the stars and to never give up on her dreams, however big or small they may seem at the time. I want her to know that her father and I will support her whether she wants to be a famous artist or follow in my footsteps and pursue her Ph.D. or whatever her future goal may be. Although her life is just beginning, she has motivated me to look towards the future. I envision a future in which there is hope for a patient diagnosed with a neurologic disease.

ACKNOWLEDGEMENTS

As with any of one's major life accomplishments, this dissertation would not have been possible without the help of many people who inspired, encouraged, and supported me along the way. I would like to first and foremost acknowledge my research advisor, Dr. Joyce Repa. Joyce not only taught me how to do "good science" and to confidently present my research; but she also went above and beyond the typical role of a mentor to be an invaluable asset at the bench for many of the mouse studies presented in this dissertation. In addition, I would like to thank my dissertation committee, Drs. Carole Mendelson, Steven Kliewer and Joel Goodman, who stuck with me even when it seemed as if I would not make it through my first committee meeting. Their scientific advice and expertise greatly enhanced my dissertation research and helped to mold me into a better scientist.

I would especially like to express my gratitude to my fellow labmates, who were much more than just colleagues: Lilja Kjalarsdottir, Yelenis Mari, Bing Liu, Ryan Jones, and Ernest Tong. They were my daily support and will be dearly missed as I move on from UT Southwestern. Furthermore, I would like to acknowledge the collaboration and support from Drs. John Dietschy, Steven Turley, Benny Liu, and Charina Ramirez, who allowed me to play a role in the original work uncovering cyclodextrin's therapeutic potential for Niemann-Pick Type C disease. I would also like to recognize the financial as well as the scientific support provided by the predoctoral Pharmacology training grant at UT Southwestern and the Ara Parseghian Medical Research Foundation.

Last but definitely not least, I would like to acknowledge my husband, parents, grandparents, and siblings. Specifically, my father, Dale Miller, taught me that anything was attainable with hard work; and my mother, Debra Miller, prayed for me through every test and trial I encountered along the way. My dear husband, John Taylor, encouraged me to follow my dreams and never to limit myself, even though it meant sacrifices for him. Whether it was by getting up early to drop me off at the lab before the sun came up or staying up late to read the final draft of my papers, John has been my constant help and companion throughout the past 4 years. I would never have had the courage to pursue my doctorate without the love and support of my entire family.

EVALUATING THE MECHANISMS OF 2-HYDROXYPROPYL-β-CYCLODEXTRIN

AND LIVER X RECEPTOR AGONISTS AS POTENTIAL THERAPIES

FOR NIEMANN-PICK TYPE C DISEASE

by

ANNA MARIE TAYLOR

DISSERTATION

Presented to the Faculty of the Graduate School of Biomedical Sciences

The University of Texas Southwestern Medical Center at Dallas

In Partial Fulfillment of the Requirements

For the Degree of

DOCTOR OF PHILOSOPHY

The University of Texas Southwestern Medical Center

Dallas, Texas

May, 2013

EVALUATING THE MECHANISMS OF 2-HYDROXYPROPYL-β-CYCLODEXTRIN

AND LIVER X RECEPTOR AGONISTS AS POTENTIAL THERAPIES

FOR NIEMANN-PICK TYPE C DISEASE

ANNA MARIE TAYLOR, Ph.D.

The University of Texas Southwestern Medical Center at Dallas, 2013

JOYCE REPA, Ph.D.

Cholesterol is essential to life; therefore, the synthesis, entry, and efflux of cholesterol are tightly regulated. In some rare disease states, such as in Niemann-Pick Type C, cholesterol balance is lost leading to detrimental effects. In Niemann-Pick Type C, mutations in either of the cholesterol trafficking proteins, NPC1 or NPC2, lead to the entrapment of unesterified cholesterol within the lysosome. The accumulated cholesterol promotes increased inflammation and apoptosis throughout the body resulting in premature death, which typically occurs during adolescence in humans. Currently there are no therapies proven to halt the progression of Niemann-Pick Type C in patients; however, two separate compounds (an LXR agonist and a cyclodextrin) have been shown to increase lifespan in the $Npc1^{-/-}$ mouse model. Although both of these potential therapies are known to alter cholesterol dynamics in the cell, the molecular mechanism(s) through which they are able to correct the defect in Niemann-Pick Type C and ultimately to

enhance survival have not been fully elucidated, which is the goal of this work. As *Abcg1* is a LXR target gene and a potential mechanism through which cholesterol is trafficked from *Npc1$^{-/-}$* cells after LXR agonist treatment, the *Npc1$^{-/-}$Abcg1$^{-/-}$* mouse was generated and evaluated. These mice die significantly earlier than *Npc1$^{-/-}$* littermates and suggest that ABCG1 plays a vital role in reducing inflammation in Niemann-Pick Type C. In addition, comprehensive studies were done within 24 hours of cyclodextrin administration in *Npc1$^{-/-}$* mice. These results show that cyclodextrin works in *Npc1$^{-/-}$* mice by freeing the trapped cholesterol from the lysosome of each cell very rapidly and then releasing the cholesterol intracellularly for normal sterol processing. Finally, *Npc1$^{-/-}$* mice were treated in combination with the LXR agonist and cyclodextrin to test if dual treatment had an additive effect on relieving Niemann-Pick Type C disease progression. The combination therapy had no further benefit over cyclodextrin alone, which implies that the two agents are acting by similar mechanism(s). Overall, this work further clarifies the molecular mechanism(s) of LXR agonists and cyclodextrins in Niemann-Pick Type C disease progression, which could lead to the development of more effective therapies for patients.

TABLE OF CONTENTS

CHAPTER ONE: INTRODUCTION

CHAPTER TWO: INVESTIGATING THE ROLE OF ABCG1 IN

THE PROGRESSION OF NIEMANN PICK TYPE C DISEASE

APPENDIX A: TESTING HISTONE DEACETYLASE INHIBITORS AS

POTENTIAL THERAPIES FOR NIEMANN PICK TYPE C DISEASE

APPENDIX B: EVALUATING CYCLODEXTRIN'S EFFECTS ON HEARING IN MICE

APPENDIX C: PRIMERS USED FOR QUANTITATIVE REAL-TIME PCR

PRIOR PUBLICATIONS

Miller, A. M.*, C. Crumbley and K. Prüfer. 2009. N-terminal nuclear localization sequences of liver X receptors alpha and beta bind to importin alpha and are essential for both nuclear import and transactivating functions. *Int. J. Biochem. Cell Biol.* 41: 834-843. PMID: 18773967

Liu, B., S. D. Turley, D. K. Burns, **A. M. Miller***, J. J. Repa and J. M. Dietschy. 2009. Reversal of defective lysosomal transport in NPC disease ameliorates the liver dysfunction and neurodegeneration in *npc1-/-* mouse. *Proc. Natl. Acad. Sci. USA* 106: 2377-2382. PMID: 19171898

Liu, B., C. M. Ramirez, **A. M. Miller***, J. J. Repa, S. D. Turley and J. M. Dietschy. 2009. Cyclodextrin reverses the transport defect in the NPC1 mouse at any age and in nearly every organ leading to excretion of sequestered cholesterol as bile acid. *J. Lipid Res.* 51:933-944. PMID: 19965601

Ramirez, C. M., B. Liu, **A. M. Taylor**, J. J. Repa, D. K. Burns, A. G. Weinberg, S. D. Turley and J. M. Dietschy. 2010. Weekly cyclodextrin administration normalizes cholesterol metabolism in nearly every organ of the Niemann-Pick Type C1 mouse and markedly prolongs life. *Pediatr. Res.* 68: 309-15. PMID: 20581737

Ramirez, C.M., B. Liu, A. Aqul, **A. M. Taylor**, J. J. Repa, S. D. Turley and J. M. Dietschy. 2011. Quantitative role of LAL, NPC2, and NPC1 in lysosomal cholesterol processing defined by genetic and pharmacological manipulations. *J. Lipid Res.* 52(4):688-98. PMID: 21289032

Taylor, A. M, B. Liu, Y. Mari, B. Liu, and J.J. Repa. 2012. Cyclodextrin mediates rapid changes in lipid balance in *Npc1$^{-/-}$* mice without carrying cholesterol through the bloodstream. *J. Lipid Res.* Aug. 14 [ePub ahead of print]. PMID: 22892156

Jones, R. D., **A. M. Taylor**, E. Tong, and J.J. Repa. 2012. Carboxylesterases are uniquely expressed among tissues and regulated by nuclear hormone receptors in the mouse. *Drug Metab. Dispos.* Sept. 25 [ePub ahead of print]. PMID: 23011759

*Anna M. Miller married in 2009, becoming Anna M. Taylor

LIST OF FIGURES

LIST OF TABLES

LIST OF APPENDICES

LIST OF ABBREVIATIONS

Aβ, β-amyloid
ABC, ATP-binding cassette transporter
ABR, Auditory Brainstem Response
ACAT, acetyl-CoA acetyltransferase
AD, Alzheimer disease
AKLP, alkaline phosphatase
ALT, alanine aminotransferase
ANOVA, analysis of variance
API, apoptosis inhibitor
APO, Apolipoprotein
Ara-C, Arabinofuranosyl Cytidine
ASM, acid sphingomyelinase
AST, aspartate aminotransferase
BA, Bile Acids
BUN, blood urea nitrogen
bw, body weight
C, free (unesterified) cholesterol
C24OH, 24-hydroxycholesterol
Casp, Caspase
cDNA, complementary Deoxyribonucleic acid
CD, cyclodextrin
CE, cholesteryl ester
CESD, Cholesterol Ester Storage disease
CH25H, Cholesterol 25-hydroxylase
CHO, Chinese hamster ovary
CM, chylomicrons
CMr, remnant of chylomicrons
CNS, Central Nervous System
CoA, Coenzyme A
C_T, comparative cycle number at threshold
CYP7A1, Cholesterol 7α-hydroxylase
CYP46, Cholesterol 24-hydroxylase
DAB, 3,3'-Diaminobenzidine
DAPI, 4',6-diamidino-2-phenylindole
dB, decibel
DMEM, Dulbecco's Modified Eagle Medium
DMSO, Dimethyl sulfoxide
DPS, digitonin-precipitable sterols
EDTA, Ethylenediaminetetraacetic acid
EM, electron microscopy
ER, endoplasmic reticulum
EtOH, ethanol
FBS, fetal bovine serum
FDA, US Food and Drug Administration
FH, Familial hypercholesterolemia
FPLC, Fast protein liquid chromatography
GC, gas chromatography
GD, Gaucher disease

gDNA, genomic deoxyribonucleic acid
h, hours
HD, Huntington disease
Hdacs, histone deacetylases
HDACi, histone deacetylase inhibitors
HDL, high-density lipoprotein
HMG-CoA, 3-hydroxy-3-methyl-glutaryl-CoA
HP-β-CD, 2-hydroxypropyl-β-cyclodextrin
IFN, interferon
IL, interleukin
INSIG-1, insulin-induced gene 1 protein
ip, intraperitoneal
LAL, lysosomal acid lipase
LE/L, late endosome/lysosome
LDL, low-density lipoprotein
LDLc, LDL associated cholesterol
LDLR, low-density lipoprotein receptor
LPS, Lipopolysaccharides
LXR, liver X receptor
LXRE, LXR Response Elements
M-β-CD, methyl-β-cyclodextrin
Miglustat, N-butyldeoxynojirimycin
MIP, macrophage inflammatory protein
MLPA, Multiplex Ligation-dependent Probe Amplification
mpk, mg/kg body weight
mRNA, messenger ribonucleic acid
MW, Molecular Weight
NCTR, National Center for Toxicological Research
NIH, National Institutes of Health
NPA, Niemann-Pick type A
NPB, Niemann-Pick type B
NPC, Niemann-Pick type C
NPC1L1, NPC1 Like 1
NPD, Niemann-Pick type D
OCT, optimal cutting temperature compound
OHCs, outer hairs cells
PBS, phosphate buffered saline
PCR, polymerase chain reaction
PD, Parkinson disease
Penh, enhanced paused
Pen/Strep, Penicillin/Streptomycin
qPCR, quantitative real-time PCR
RXR, Retinoid X Receptor
SBE-β-CD, Sulfobutylether-β-cyclodextrin
sc, subcutaneous
SCAP, SREBP cleavage activating protein
SEM, standard error of the mean
SLOS, Smith-Lemli Opitz Syndrome
SREBP, sterol regulatory element-binding protein
SRE, SREBP Response Elements

Tcmpd, T0901317
TNF, tumor necrosis factor
US, The United States of America
VLDL, very-low-density lipoprotein
VLDLr, remnant of very-low-density lipoprotein
WD, Wolman's disease
ZT, Zeitgeber time

Introduction

1.1 Cholesterol Metabolism

   Proper balance of cholesterol is essential to mammalian life. Unesterified cholesterol (**Fig. 1.1**) is an integral component of plasma membranes and myelin sheaths and serves as the precursor to steroid hormones, vitamin D, and bile acids, which are all vital for survival. Almost every cell in the body is capable of synthesizing cholesterol *de novo* from acetyl-CoA through the mevalonate pathway. Although humans can also acquire cholesterol through intestinal absorption from dietary sources such as beef, pork, poultry, fish, cheese, and egg yolks, this external supply of cholesterol is not necessary for life and may in fact lead to excess storage of cholesterol as cholesteryl esters in the body. In order to achieve cholesterol turnover while maintaining cholesterol balance, new cholesterol is synthesized at the level in which cholesterol is removed from cells. Regardless of the source, cholesterol and its derivates must be excreted from the body as humans have no enzymes capable of breaking down the sterol core of the cholesterol molecule (Dietschy, 1984). This removal of cholesterol is achieved daily by sloughing off of skin cells and by excretion of neutral and acidic (bile acids) sterols through the feces or more rarely the urine.

Cholesterol Regulation in Cells

   As even small alterations in the total levels of cholesterol can lead to detrimental effects in cells, the synthesis, entry, and efflux of cholesterol are tightly maintained in animals. To accomplish cellular cholesterol homeostasis, two master regulators of cholesterol have evolved: the sterol regulatory element-binding proteins (SREBPs) and the oxysterol-responsive nuclear hormone receptors, liver X receptors (LXRs).

   SREBPs. In mammals, three closely related isoforms of SREBP are present: SREBP1a, SREBP1c, and SREBP2. While all SREBPs are capable of regulating cholesterol synthesis when over-expressed,
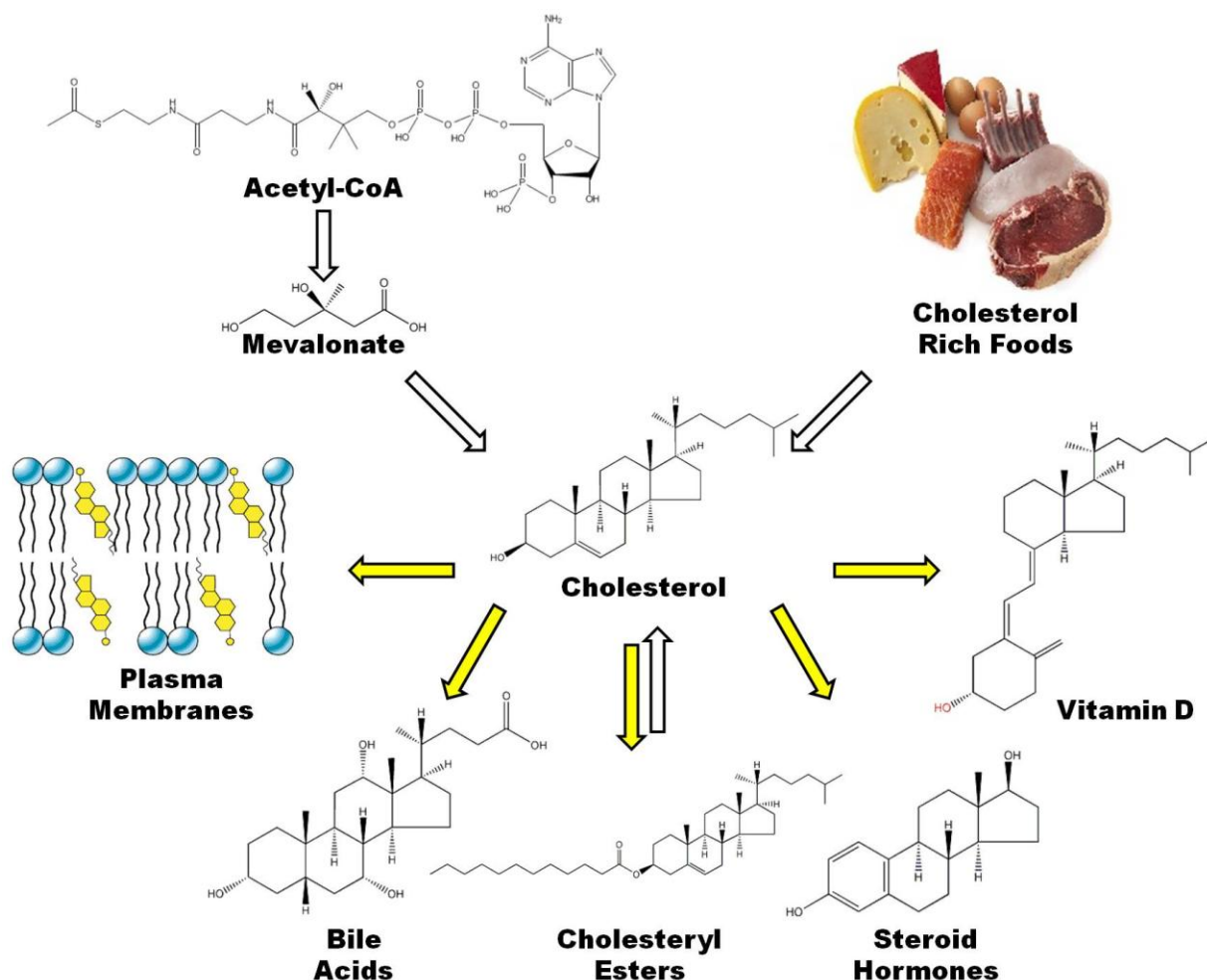
Figure 1.1 *Sources by which the body acquires and eliminates cholesterol.* Mammals acquire cholesterol through *de novo* cholesterol synthesis or from intestinal absorption of cholesterol through diet. Unesterified cholesterol from either source can be incorporated into plasma membranes and freely converted to and from cholesteryl esters. Unesterified cholesterol is also required for the production of bile acids, steroid hormones, and Vitamin D. Chemical structures were downloaded from the Lipid Maps database (http://www.lipidmaps.org). Pictures of cholesterol rich foods and plasma membranes were modified from http://healthimpactnews.com and http://www.uic.edu, respectively.

only SREBP1a and SREBP2 do so under physiologic conditions (Horton et al., 2002). On the other hand,

SREBP1a and SREBP1c but not SREBP2 regulate fatty acid synthesis. Regardless of their targets,

SREBPs are active when cholesterol levels are low in cells. When SREBPs are synthesized in the

endoplasmic reticulum (ER), they are immediately bound by the SREBP cleavage activating protein

[SCAP]. SCAP acts as an escort for the SREBPs to the Golgi apparatus, where the SREBPs are cleaved

by proteases. This releases the active fragment of SREBP, which can then enter the nucleus to regulate

transcription (Goldstein et al., 2006). Specifically, activated SREBP2 (**Fig. 1.2**) upregulates the entry of

cholesterol into cells through increased expression of low-density lipoprotein receptor (LDLR) and the *de*

novo synthesis of cholesterol from acetyl-CoA through enhanced levels of 3-hydroxy-3-methyl-glutaryl-

CoA (HMG-CoA) reductase, synthase, and virtually every enzyme in the cholesterol synthesis pathway

(Horton et al., 2002). Once cellular cholesterol levels have increased and cholesterol has begun to build

up in the ER membrane, insulin-induced gene 1 protein (INSIG-1) will bind to SCAP preventing the

SCAP/SREBP complex from exiting the ER (Goldstein et al., 2006). Thus the activity of SREBP2 is

prevented post-transcriptionally in response to high concentrations of sterols in the ER, which allows

cellular cholesterol levels to decrease.
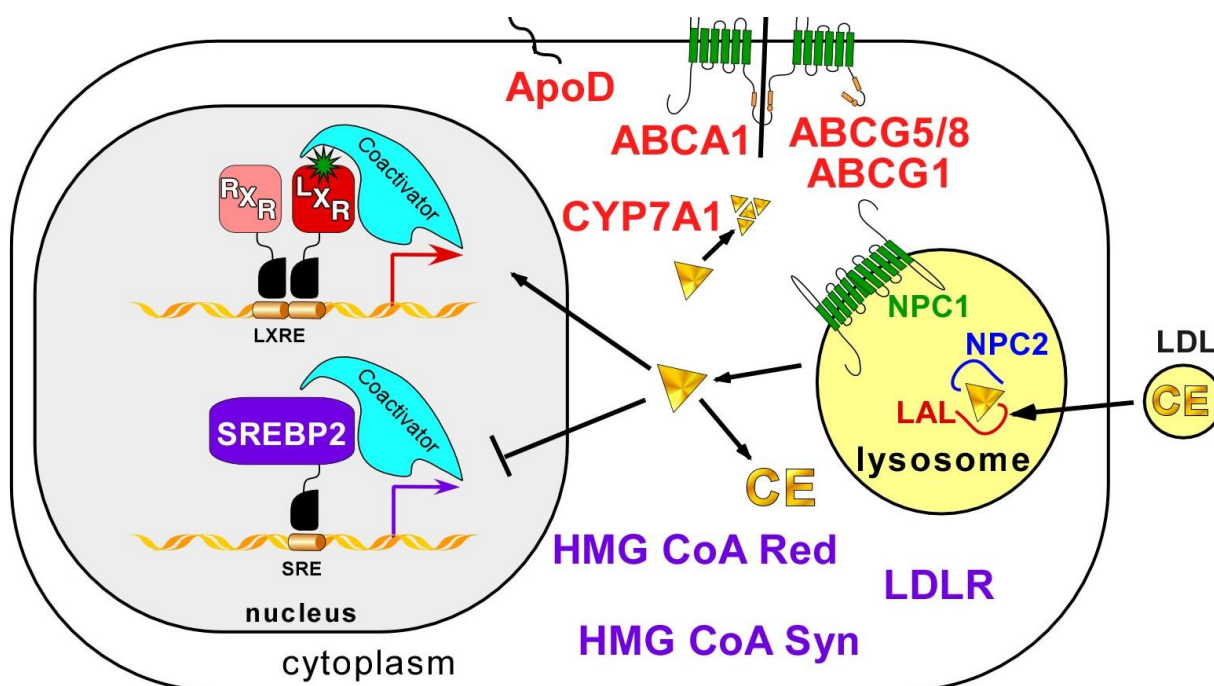
Figure 1.2 *Cholesterol regulation and trafficking in wildtype cells.* LDL moves cholesteryl esters (**CE**) into the lysosomal compartment of cells, where the LAL cleaves the ester group yielding free cholesterol (**triangle**). NPC2 then binds and hands off cholesterol to NPC1, which through an unknown mechanism facilitates the egress of cholesterol out of the lysosome into the cytosol. When cholesterol levels in the cytosol are low, SREBP2 is cleaved and enters the nucleus where it upregulates its target genes, which increase intracellular cholesterol levels: the LDLR promotes entry of LDL carrying cholesterol into cells, while HMGCoARed/Syn are required for the *de novo* synthesis of cholesterol. When intracellular levels of cholesterol are high, cholesterol is converted to cholesteryl esters and oxysterols (**star**). The oxysterols activate LXR, which upregulates its target genes to reduce cholesterol levels in cells: the ABC transporters and ApoD assist in the efflux of cholesterol from cells, while CYP7A1 promotes the breakdown of cholesterol into bile acids (broken **triangle**).

LXRs. While SREBP is active when cholesterol levels are low, the LXRs are active when cholesterol

levels are elevated and promote the egress of cholesterol from cells. High levels of cholesterol lead to the

production of oxysterols, which are natural byproducts of cholesterol and are the endogenous agonists for

LXRs (Janowski et al., 1999). In mammals, there are two isoforms of the Liver X Receptor: LXRα and

LXRβ. While LXRβ is considered to be ubiquitously expressed, LXRα is most highly expressed in the

liver and is generally limited to other metabolically active tissues (Repa et al., 2000b). Both LXRs form

obligate heterodimers with the retinoid X receptor (RXR) (Willy et al., 1997), and LXR/RXR binds to

LXR Response Elements (LXREs), which are two direct repeats of the hexanucleotide motif (AGGTCA)

with four nucleotides in between. When bound by oxysterol, LXR/RXR (**Fig. 1.2**) upregulates the efflux

of cholesterol from cells through the ATP-binding cassette (ABC) transporters, such as ABCA1 and

ABCG1/5/8, as well as, the conversion of cholesterol into bile acids through cholesterol 7α-hydroxylase

(CYP7A1) in the liver (Repa et al., 2002). The reduction of cellular cholesterol leads to a decrease in

oxysterol concentrations and LXR activation, which allows cholesterol levels to increase. Thus, LXRs

and SREBPs serve as a check-and-balance system for intracellular cholesterol levels.

Extracellular and Intracellular Trafficking of Cholesterol

Although all organs are capable of synthesizing cholesterol *de novo*, cholesterol must be moved

throughout the body in order to achieve cholesterol turnover. As cholesterol is insoluble, it is packaged

into lipoprotein particles to be carried through the bloodstream from one organ to the next. There are

several types of lipoproteins particles detectable in plasma: chylomicrons (CM), very-low-density

lipoprotein (VLDL), low-density lipoprotein (LDL), and high-density lipoprotein (HDL). Dietary lipids

are absorbed into the intestine, where they are packaged into CM. CM move from the intestine to adipose

and muscle, which sequester free fatty acids from the CM leaving a remnant. The remnant of CM (CMr)

contains most of the dietary cholesterol and continues through the bloodstream to be taken up by the liver.

The liver packages cholesterol in VLDL particles to send it to other perpherial organs, and remnants of

VLDL (VLDLr) can be converted to LDL, which is returned to the liver (Dietschy, 1998). Cholesterol can also be packaged by peripheral organs into HDL particles to facility cholesterol delivery back to the liver.

Lipoprotein particles enter cells either through receptor-mediated or bulk-phase endocytosis. The upake of LDL (**Fig. 1.2**), for instance, is mediated via endocytosis through the cell surface LDL receptor (LDLR). When bound by LDL, LDLR is internalized through clathrin-coated pits and then moves into the late endosome/early lysosome (LE/L), where the acidic environment causes a release of the lipids it carried. Then, the LDLRs are recycled back to the cell surface, and cholesteryl ester moves through the LE/L (Goldstein et al., 2009). Within the LE/L, the lysosomal acid lipase (LAL, also known as LIPA), which is a soluble protein of 399 amino acids, first hydrolyzes the ester group yielding free cholesterol (Du et al., 1996). Then, the small (132 amino acids) soluble protein, Niemann Pick Type C 2 (NPC2), binds to the isooctyl side chain of cholesterol leaving the hydroxyl end of the sterol exposed, for another protein, Niemann Pick Type C 1 (NPC1) to bind in the opposite orientation. Although NPC1 is a large 13 transmembrane protein of 1228 amino acids, only the N-terminal domain which projects into the lumen of the lysosome binds cholesterol (Kwon et al., 2009). Once NPC2 has handed-off unesterified cholesterol to NPC1, the mechanism(s) by which NPC1 or a yet unidentified "NPC3" protein mediates egress of cholesterol out of the lysosome into the cytosol remains to be solved. Once cholesterol is liberated from the lysosome, it joins the metabolically active pool of cholesterol (**Fig. 1.3A**), which can be incorporated into membranes, including that of the ER to regulate SREBPs, and broken down into byproducts, such as oxysterols, to regulate LXRs.

Cholesterol Metabolism in the Brain vs. Peripheral Tissues

Although peripheral organs dominate the synthesis, transport, and turnover of cholesterol in the body, it is important to consider how cholesterol is metabolized in the Central Nervous System (CNS). The
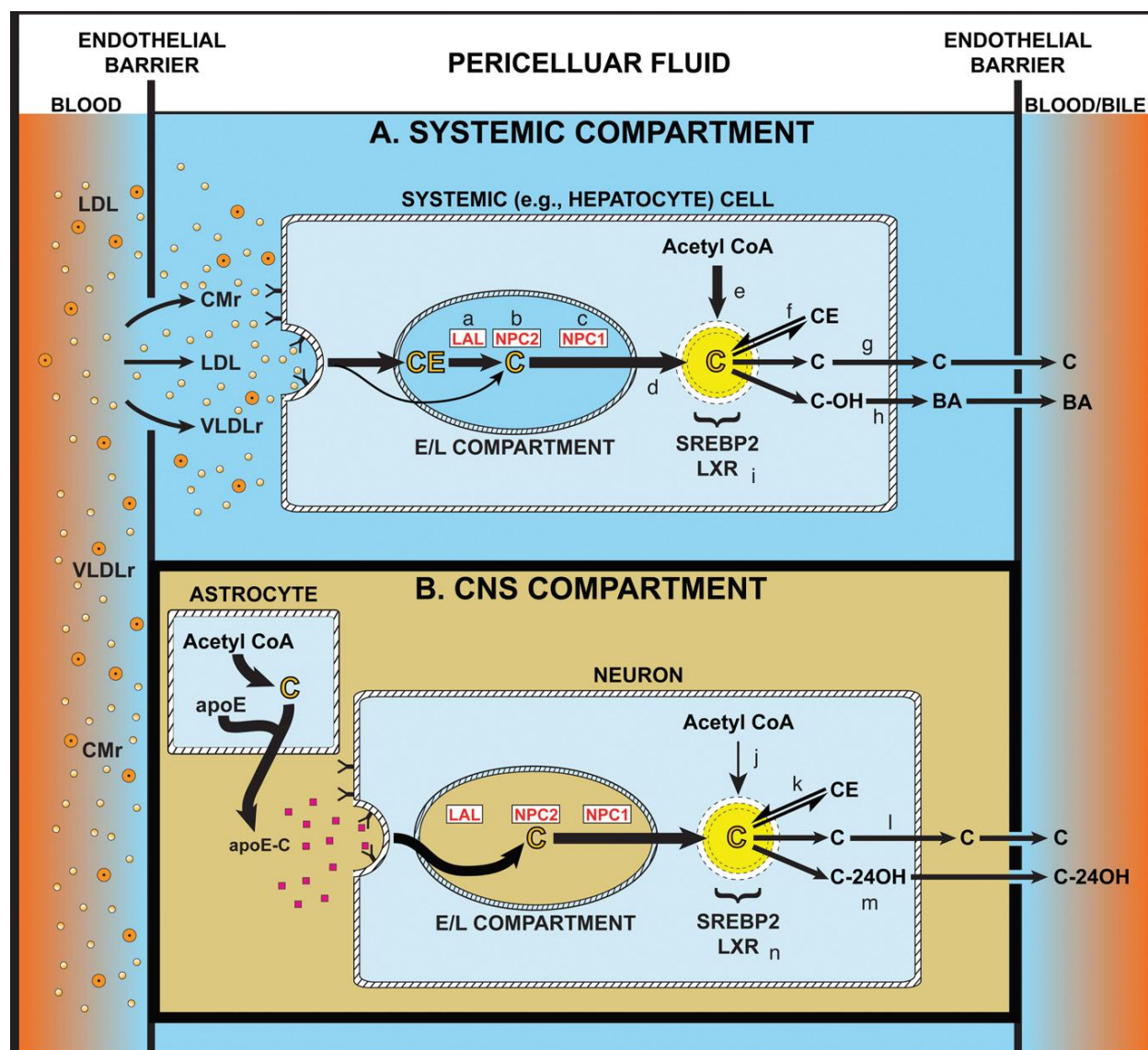
Figure 1.3 *Cholesterol trafficking in peripheral tissues versus the central nervous system (CNS).*
In the systemic compartment represented by a hepatocyte (**A**), lipoproteins including LDL, the remnants of chylomicrons (CMr), and very-low-density lipoproteins (VLDLr) deliver cholesteryl ester (CE) into the late LE/L compartment of cells, where LAL (**a**) cleaves the ester group yielding free cholesterol (C). NPC2 (**b**) then binds and hands off cholesterol to NPC1 (**c**), which facilitates the egress of cholesterol out of the lysosome (**d**) to join the newly synthesized C (**e**) in a metabolically active pool in the cytosol. Depending of the cell type, C can be incorporated into plasma membrane (**g**) or converted to CE (**f**), oxysterols (**h**), and, in liver, bile acids (BA). This intracellular pool of C is tightly regulated by SREBP2 and LXR (**i**).
In the CNS (**B**), the endothelial barrier is impermeable to plasma lipoproteins and thus all C must be synthesized within the compartment. It is postulated that C is synthesized mainly by astrocytes and is carried with apoE to neurons, where it moves through the LE/L compartment into the cytosol. Neurons presumably can also synthesize C *de novo* (**j**). In the CNS, the metabolically active pool of C can be incorporated into membranes including myelin sheaths (**l**), converted to CE (**k**), or metabolized into the oxysterol, 24(S)-hydroxycholesterol (C24OH) (**m**), for excretion across the blood brain barrier. As in peripheral tissues, SREBP2 and LXR (**n**) tightly regulate the intracellular pool of C in the CNS. This figure was used from (Aqul et al., 2011).

CNS, which consists of the brain and spinal cord, only accounts for a small portion (2.1%) of body mass in mammals; however, it has been estimated to contain almost a quarter (23%) of the unesterified cholesterol in the body (Dietschy et al., 2004). This is remarkable considering that the endothelial barrier surrounding the CNS is impermeable to plasma lipoproteins, and thus all cholesterol in the brain and spinal cord must be synthesized *de novo* (**Fig. 1.3B**). Although all cells in the CNS including neurons are capable of synthesizing cholesterol, it is postulated that *de novo* synthesis from acetyl-CoA is mainly performed by glial cells, specifically by oligodendrocytes, which incorporate large quantities of cholesterol into membrane to myelinate the axons of neurons, and by astrocytes, which transport cholesterol to neurons (Dietschy, 2009). Once synthesized, cholesterol can be transported from one cell to another in complex with Apolipoprotein E (apoE), which is internalized into the LE/L compartment of a cell through receptor-mediated endocytosis. As unesterified cholesterol is likely delivered by apoE, it bypasses the need for LAL; and the free cholesterol can be directly bound by NPC2 and handed off to NPC1 (Aqul et al., 2011). Once cholesterol is released from the lysosome, it joins the metabolically active pool of cholesterol, where it can be utilized by the cell just as in peripheral tissues. A principal difference is that cholesterol must be metabolized into the oxysterol, 24-hydroxycholesterol (C24OH), by cholesterol 24-hydroxylase (CYP46) for transport across the blood brain barrier and ultimately for clearance by the liver (Russell et al., 2009). Turnover of cholesterol in the brain is known to be required in the hippocampus for learning (Kotti et al., 2006); thus, cholesterol is continuously synthesized at a low rate in the brain and released from the CNS as C24OH (Dietschy, 2009).

1.2 Cholesterol disruption leading to disease

Whenever cholesterol balance is lost in mammals, a variety of detrimental conditions can result. The most common concern with cholesterol in humans is hypercholesterolemia, which can either be caused by enhanced dietary uptake or diminished clearance of cholesterol. In addition, mutations in genes required

for cholesterol synthesis and trafficking lead to devastating lipid storage conditions that often result in death during childhood. Disruption in cholesterol metabolism has also been linked to many chronic neurodegenerative diseases, highlighting the importance of cholesterol regulation in the brain (Vance, 2012).

High Cholesterol and Atherosclerosis

High levels of cholesterol in the bloodstream are known as hypercholesterolemia and are a well-established risk factor for cardiovascular disease, the leading cause of death in the Western world. Hypercholesterolemia increases the storage of cholesteryl esters in macrophages, which are the foundation for plaque buildup in arteries, termed atherosclerosis, and ultimately promote heart disease. Reducing the circulating levels of LDL cholesterol (LDLc) has been proven to lower the incidence of coronary heart disease; thus, LDLc levels lower than 100 mg/dL are currently recommended for patients with cardiovascular disease (Grundy et al., 2004; Costet, 2010). There are a couple different approaches to lower LDLc. The first is obvious, although often difficult in Western culture where large quantities of lipid-rich food are consumed, and involves decreasing the dietary intake of cholesterol. As humans are capable of synthesizing all the cholesterol their cells require *de novo*, there is no need for added cholesterol through the diet. However, dietary changes are often not enough to reduce LDLc to the recommended levels, and pharmaceutical intervention is required. Statins, which are the most commonly prescribed cholesterol-lowering drug class, serve as competitive inhibitors for HMGCoARed and work by blocking the *de novo* synthesis of cholesterol (Grundy et al., 2004). In addition to statins, another commonly used LDLc lowing therapy is ezetimibe, which can be given to block the intestinal absorption of cholesterol through Niemann Pick Type C 1 Like 1 (NPC1L1), the protein responsible for the transport of cholesterol across the plasma membrane into enterocytes (Costet, 2010).

Disorders Caused by Mutations in Cholesterol Genes

Familial hypercholesterolemia. Although high plasma cholesterol levels can be caused by dietary intake of cholesterol, they can also be caused through a variety of genetic mutations, which result in a family of disorders classified as Familial Hypercholesterolemia (FH). The most common cases of FH are caused by autosomal dominant inactivating mutations in the *LDLR* gene, which are found in 1:500 people. Individuals with a single affected allele exhibit plasma LDLc levels of 350-550 mg/dL and have increased risks of early cardiovascular events. Patients homozygous for mutations in *LDLR* are much rarer (1:1,000,000) and have plasma LDLc concentration exceeding 650 mg/dL (Goldstein et al., 1995). These extremely high levels of circulating LDL lead to large depositions of cholesterol as xanthomas on tendons and skin and as extensive plaque formation on the artery walls, resulting in heart attacks in early childhood (Goldstein et al., 2009). Currently, cholesterol-lowering therapies, such as statins, are used to treat FH and have been shown to extend survival in homozygous cases into mid-adulthood; however, new therapeutics to further extend survival and improve quality of life are being pursued (Parihar et al., 2012; Raal et al., 2012).

Smith-Lemli Opitz Syndrome. Mutations in the enzymes of the mevalonate pathway required to synthesis cholesterol *de novo* from acetyl-CoA are known to lead to several rare human diseases, including: lathosterolosis, desmosterolosis, cerebrotendious xanthomatosis, and Smith-Lemli Opitz Syndrome (SLOS). SLOS is the most prevalent of these disorders affecting 1:20,000 live births and is caused by an autosomal recessive mutation in *7-dehydrocholesterol reductase*, which catalyzes the conversion of 7-dehydrocholesterol into cholesterol, the final step of the cholesterol synthesis pathway (Vance, 2012). SLOS presents as severe developmental abnormalities, intellectual impairment, and behavior disabilities. The severity of disease, which often correlates to the extent of developmental malformations, can range from death in infancy to survival into adulthood. As SLOS is plagued by extremely reduced levels of cholesterol and elevated levels of 7-dehydrocholesterol, therapies aimed at increasing cholesterol levels while reducing levels of sterol intermediates by turning off cholesterol synthesis have been used with reported success, although the results are controversial (DeBarber et al.,

2011).

Niemann Pick Type C Disease. Niemann Pick Type C (NPC) disease is a rare lysosomal storage disorder, which is estimated to affect 1:120,000 live births. NPC is transmitted by autosomal recessive inheritance, in which both parents are silent carriers of inactivating mutations in one of two proteins required to transport free cholesterol from the lysosomal compartment: mutations in *NPC1* represent 95% of NPC cases, while mutations in *NPC2* account for the remaining NPC cases where the genetic cause has been identified (Ory, 2004; Vanier, 2010; Patterson et al., 2012). Regardless of the underlying mutation, patients with NPC typically suffer from progressive neurodegeneration (which presents in late infancy/early childhood with vertical supranuclear gaze palsy, cerebellar ataxia, gelastic cataplexy, and seizures) and die between 10 and 25 years of age (Vanier, 2010). In addition to the prominent neurological symptoms, children with NPC also suffer from systemic disease, including liver dysfunction, hepatosplenomegaly, and chronic pulmonary disease (Patterson et al., 2012). Currently there are no therapies which have been approved by the Food and Drug Administration (FDA) of the United States to extend lifespan in children with NPC.

Wolman's Disease. Like NPC disease, Wolman's disease (WD) is a rare lysosomal storage disease in which cholesterol is trapped within the lysosome. WD is estimated to effect 1:300,000 live births and is caused by autosomal recessive mutations in *LAL* (Du et al., 2008). Typically WD is used to refer to cases of LAL (lysosomal acid lipase) deficiency, which result in death in early childhood; while Cholesterol Ester Storage disease (CESD) represents patients with more mild cases of the deficiency that can survive into adulthood. Patients with WD display hepatosplenomegaly, malabsorption, and adrenal calcification (Assmann et al., 2001). As with NPC, there is no approved therapy for patients with WD. However, enzyme replacement therapy with hLAL was shown to be effective in mice and is currently being tested in a human trial (Du et al., 2008). Interestingly, although both NPC (unesterified cholesterol) and WD (cholesteryl esters) are caused by entrapment of cholesterol in the lysosome, only NPC has effects in the brain. This is likely because unesterified cholesterol can enter into the lysosome directly via ApoE

mediated trafficking, thus bypassing the need for LAL in cells of the CNS (**Fig. 1.3B**) (Aqul et al., 2011).

Cholesterol Dysregulation in Other Neurodegenerative Diseases

Alzheimer disease. The most common neurodegenerative disorder is Alzheimer disease (AD), which leads to a progressive decline in cognition and loss of memory. Although often the cause of AD is unknown, it is predicted to affect 1 in 8 adults over the age of 65 and nearly 50% of individuals by the age of 85 ("2012 Alzheimer's disease facts and figures,"). Cholesterol dysregulation has been linked to the pathology of AD in several ways. Many studies, although not all, have reported an increased prevalence of AD in patients with high circulating levels of cholesterol; and statins have been suggested to protect against AD (Vance, 2012). Although these links to cholesterol are debated, the isoform of the cholesterol-carrying APOE is clearly associated with the risk factors for developing AD. There are three different isoforms of APOE (APOE2, APOE3, and APOE4), which vary by only a single amino acid substitution. While two copies of the APOE4 allele greatly increases one's chances of developing AD, the APOE2 allele is protective (Liu et al., 2010b). Although the cause is still uncertain, it has been shown that APOE is involved in β-amyloid (Aβ) degradation and that the APOE4 isoform leads to enhanced Aβ deposition. High levels of circulating cholesterol have also been shown to lead to an increase in Aβ plaques which contain cholesterol (Orth et al., 2012). Intriguingly, many of the brain pathologies classically present in AD, including neurofibrillary tangles, hyperphosphorylation of tau, and increased Aβ burden, have also been reported in NPC patients (Kodam et al., 2010; Peake et al., 2010), further linking AD to cholesterol dysfunction. Currently, there are no approved therapies to halt the progression of AD.

Parkinson disease. Parkinson disease (PD) is the second most common neurodegenerative disorder and is estimated to affect 13 out of every 100,000 individuals with its prevalence greatly increasing in adults over 60 years of age (Van Den Eeden et al., 2003). PD is characterized by progressive tremors, increasing difficulty to move, and ultimately cognitive impairment. The motor symptoms occur from a lack of dopamine that results as dopaminergic neurons are degenerated and can be reversed, at least

temporarily, by the administration of levodopa, which is converted into dopamine (Vance, 2012).

Cholesterol metabolites have been shown to be increased in dying dopaminergic neurons and to lead to an

acceleration of α-synuclein aggregation, which is believed to contribute to the pathogenesis of PD (Liu et

al., 2010b). Consistent with this finding, statins have been shown to protect dopaminergic neurons from

degeneration in PD and have been suggested to lead to a reduced incidence of PD. However, the role of

statins in PD is extremely controversial as patients with PD overall have lower levels of LDLc than

unaffected individuals. It has been postulated that the benefits of statins are due to anti-inflammatory

instead of cholesterol-lowering effects (Roy et al., 2011). Thus, potential roles of cholesterol metabolism

in PD will require further investigation.

Huntington disease. Unlike AD and PD, the genetic cause of Huntington's disease (HD), which

occurs in 3 out of every 100,000 individuals, is well characterized (Pringsheim et al., 2012). HD is caused

by an autosomal dominate mutation in the gene encoding the huntingtin protein, which leads to a

polyglutamate repeat at the N-terminus of the protein. The mutant huntingtin protein is toxic and causes

neurodegeneration (Vance, 2012). HD presents as progressive behavioral abnormalities, movement

difficulties, and dementia. Recently, patients and animal models of HD have been shown to have reduced

rates of cholesterol synthesis and increased levels of cholesterol accumulation in the brain, while plasma

levels of cholesterol and 24(S)-hydroxycholesterol are reduced (Karasinska et al., 2011). Although the

link between the mutant huntingtin protein and cholesterol is still unknown, it is clear that cholesterol

metabolism is dysregulated in HD. As there is no approved treatment to prevent the progression of HD,

cholesterol-altering therapies, including LXR agonists, are being evaluated (Karasinska et al., 2011).

1.3 Niemann-Pick Type C Disease

In NPC, mutations in the lysosomal proteins, NPC1 or NPC2, lead to the entrapment and subsequent

accumulation of unesterified cholesterol within the LE/L, where it cannot be properly sensed or utilized

by the cell. Although there is an excess of cholesterol within the LE/L, NPC (**Fig. 1.4**) leads to enhanced

cellular sterol synthesis through SREBP2 and reduced cholesterol elimination through a lack of LXR

activation (Xie et al., 1999b; Li et al., 2005). Ultimately, this causes increased inflammation and

apoptosis throughout the body resulting in premature death, which typically occurs during adolescence in

humans (Vanier, 2010).
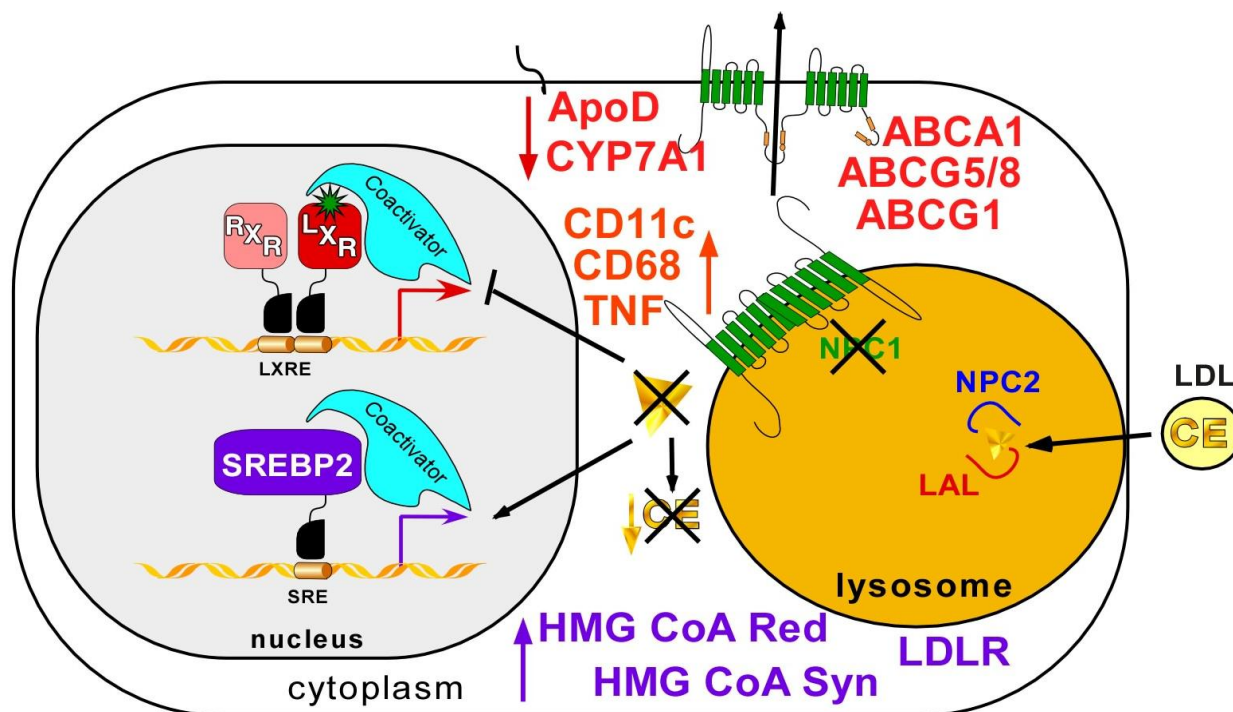
Figure 1.4 *The dysregulation of cellular cholesterol homeostasis in Niemann-Pick Type C Disease.* In cells without functional NPC1, the egress of free cholesterol (triangle) from the lysosome is blocked leading to massive lipid accumulation, enhanced cellular sterol synthesis (via activation of SREBP2), decreased cholesteryl ester (CE) formation, reduced oxysterol formation and, in turn, decreased sterol elimination (via lack of LXR activation), and increased **cytokine production**. Ultimately this leads to increased inflammation and cell death.

History of Niemann-Pick Type C Disease

Initial Characterization. In 1914, a German pediatrician by the name of Alfred Niemann described

the first known case of Niemann-Pick disease, an infant who presented with neurodegeneration and

hepatosplenomegaly that resembled Gaucher disease (GD), another rare neurological disorder. A decade

later, Ludwig Pick, who was a German pathologist, distinguished Niemann's original description from

GD; and the term "Niemann-Pick disease" was coined. A breakthrough in the field occurred in 1958

when Drs. Sidney Farber and Alan Crocker of Boston Children's Hospital described the clinical

manifestations in 18 individuals which had been diagnosed with Niemann-Pick disease (Patterson et al.,

2001; Schuchman et al., 2001; Pentchev, 2004; Vanier, 2010). They found wide variation in the age of

onset and spectrum of symptoms and suggested that diagnosis should be based on the presence of foam

cells and excess sphingomyelin in tissues.

Separation into Niemann Pick A-D. Crocker further split Niemann-Pick disease into 4 disorders: A to

D (Crocker, 1961). Niemann-Pick Type A (NPA), which presents as neurodegeneration leading to death

in infancy, was characterized by massive sphingomyelin storage in the brain and peripheral tissues; while

Niemann-Pick Type B (NPB) had similar sphingomyelin storage as in NPA but lacked neurological

symptoms. Niemann-Pick Type C (NPC) presented with a progressive neurodegeneration and had less

storage of sphingomyelin but increased accumulation of cholesterol in peripheral tissues compared to

NPA and NPB. Niemann-Pick Type D (NPD) had an identical clinical presentation to NPC, except all of

the patients under this classification were of Nova Scotia origin (Patterson et al., 2001; Vanier, 2010). Just

a few years later at the National Institutes of Health (NIH) in 1966, Dr. Roscoe Brady discovered NPA

and NPB to be caused by deficiencies in acid sphingomyelinase (ASM), which were later linked to

mutations in *SMPD1*; however, the cause(s) of NPC and NPD was still unknown (Pentchev, 2004).

Cloning of Npc1 and Npc2. In 1979 under Dr. Brady at NIH, Dr. Peter Pentchev began work on a

spontaneous mouse model with a lipid storage disease (Morris et al., 1982) that would turn out to be the

first animal model of NPC disease. Unlike wildtype mice which store cholesteryl esters in their liver after

being fed a high cholesterol diet, these mice were shown by Pentchev to accumulate large amounts of

unesterified cholesterol (Boothe et al., 1984). This finding lead to the discovery that the delivery of LDLc

to cells, which were derived from mutant mice or from patients with NPC disease, could not activate the

formation of cholesteryl esters through the protein, acetyl-CoA acetyltransferase (ACAT). The deficiency

in LDLc-stimulated cholesterol esterification was shown not to be through a defect in ACAT activity, as

cell lysates derived from the mutant cells were just as capable of forming cholesteryl esters as wildtype

cell lystates. After this work, NPC disease was found to be a defect in the trafficking of cholesterol from the lysosomal compartment, and the hunt was on to clone the gene(s) responsible (Pentchev, 2004).

Using genomic libraries from NPC patients, two distinct mutant loci were predicted. In 1997, the first gene, which was named *Niemann Pick Type C 1* (*NPC1*), was found on chromosome 18 by positional cloning in both human (Carstea et al., 1997) and mouse (Loftus et al., 1997). The *NPC1* gene predicted a protein with at least 13 transmembrane domains that had high homology to several proteins involved in cholesterol balance. Mutations in *NPC1* were found in the majority of NPC cases and in all accounts of NPD; therefore, patients with NPD are no longer considered to have a distinct disorder and are incorporated under NPC disease (Patterson et al., 2001). In 2000, the second gene, which was named *Niemann Pick Type C 2* (*NPC2*), was found on chromosome 14 (Naureckiene et al., 2000). Mutations in *NPC2* were found to be rare (representing less than 5% of NPC cases) compared to those in *NPC1* (Vanier, 2010).

Initial Therapeutic Trials. No specific treatments are recommended for NPC disease. Initially bone marrow and liver transplants were attempted in humans, but there was no evidence of altered disease progression (Patterson et al., 2001). After the identification of cholesterol trafficking defects as the cause of NPC disease, several treatment strategies to reduce cholesterol levels were attempted, including low cholesterol diets, statins, and ezetimibe. Although these therapies had modest success at reducing the storage of cholesterol in peripheral organs, such as the liver; this did not alter the progression of the disease or extend lifespan (Patterson et al., 2001). It is important to remember that while cells with mutations in *NPC1* or *NPC2* have an accumulation of cholesterol within the lysosome (**Fig. 1.4**), they also have a deficiency in the metabolic active pool of cholesterol that can be sensed and utilized by the cell. Therefore, while reducing cholesterol in cells by blocking *de novo* synthesis and dietary absorption may lead to less cholesterol accumulation in peripheral organs; it does not repair the shortage of cholesterol in cells, which would also need to be corrected to see improvements in NPC disease.

Current Recommendations for Niemann-Pick Type C Patients

Diagnosis Strategy. Before the cloning of *NPC1* and *NPC2*, diagnosis of NPC was a very lengthy

process, which required identification of the clinical manifestations of the disease and then ruling out

every other potential disease that could lead to the symptoms reported. Pathologically, foamy cells and

sea-blue histiocytes in tissue biopsies were used to suggest NPC (Patterson et al., 2001). The linkage of

altered cholesterol trafficking to NPC disease lead to a vast improvement in diagnostic testing for NPC.

First of all, biochemical testing could be used to confirm the deficiency in LDLc-stimulated cholesterol

esterification in patient-derived fibroblast, as was done by Pentchev. Secondly, it led to the development

of filipin staining as a way to fluorescently label unesterified cholesterol in the lysosome, a method which

quickly became the standard diagnostic test for the positive identification of NPC disease (Pentchev,

2004).

The procedure to accurately diagnose NPC has been greatly enhanced over the last decade; however,

it is still a process which involves ruling out other disorders, such as GD and the ASM deficiencies that

cause NPA and NPB (**Fig. 1.5A**). When NPC disease is suspected, physicians should take a skin biopsy to

be used for a fibroblast culture and subsequent filipin staining, as well as, a blood sample for gDNA

sequencing of *NPC1* and *NPC2*. A flowchart has been created to aid in the positive diagnosis of NPC

disease (**Fig. 1.5A**) (Patterson et al., 2012).

Clinical Manifestations. Although it has long been recognized that there is large variability in the

clinical onset and lifespan of patients with NPC, recently it has been proposed that the clinical

manifestations of NPC could best be described when split into 5 subcategories: perinatal; early-infantile;

late-infantile; juvenile; and adolescent/adult (**Fig. 1.5B**) (Patterson et al., 2012). With perinatal

presentation, NPC presents as severe liver failure or pulmonary distress, and the patient succumbs to this

disease in infancy before neurological symptoms have had the chance to present. Early-infantile cases

A

Clinical manifestations

Useful preliminary tests:
Chitotriosidase — Exclude GD and ASM deficiencies | Foam cells in bone marrow — If liver biopsy: EM study | **Plasma oxysterol profile**[a]

(EM study of skin) ←------

Skin biopsy Fibroblast culture | **EDTA-blood gDNA**

Filipin test (Two separate experiments)[b] + **NPC1 & NPC2 sequencing** (wherever possible) (minimum: all exons and junctions)*

Highly + 'Classical'[c] = NP-C

80–85% of NP-C patients

Moderately + 'Variant'[d] = Probable NP-C

~15% of NP-C patients

Mildly + or ± (uncertain) = Possible NP-C?

<5% of NP-C patients (most cases = not NP-C)

Clearly negative = Likely not NP-C

Sequence if high clinical suspicion

Two (or one homozygous) known or pathogenic mutation(s) = NP-C

Two mutant alleles with one or two novel[e,f] mutations = Possible NP-C

One mutant Allele = ?

No mutant allele = likely not NP-C but: If filipin + or high clinical suspicion

MLPA

Most common result = negative

Interpretation of combined results

NP-C confirmed if repeated highly + filipin (whatever the mutation profile)

NP-C confirmed if two pathogenic mutations (whatever the filipin profile)

*NP-C almost certain if variant filipin and two novel mutant alleles or one** pathogenic mutant allele*

*Doubt may remain if filipin uncertain and only one mutation***

Almost certainly not NP-C if mildly + or even variant filipin and no mutation

NP-C discounted if no mutation and filipin - (or uncertain)

More refined tests in research laboratories needed to solve the (few) remaining difficult cases

Database

*Numerous polymorphisms — check allele segregation from parental study; conclude quickly on NPC2 in children <8–10 months
**Profile also seen in heterozygote subjects

B

Hepatosplenomegaly
● Absent in ~15% of cases
● Age of onset is variable[†]
● May regress with age

Neonatal cholestasis

Systemic involvement
Liver
Neonatal fatal*
Hepatosplenomegaly

Age, years

Birth 1 2 3 6 10 20 30 40 50 60

Neurological involvement

Early infantile
Late infantile
Juvenile
Adolescent/Adult

Delay in motor milestones
Hypotonia

Gait problems
Clumsiness
Speech delay
Cataplexy

School problems
Ataxia
(Seizures)
(Cataplexy)

Psychiatric problems
Ataxia
Dystonia
Dementia

Vertical supranuclear gaze palsy

Neurological involvement ---- Period of onset ☐ Duration

Figure 1.5 *Current recommendations for the diagnosis and classification of NPC disease.* A schematic to assist physicians in the positive diagnosis of NPC disease (**A**) and to inform them of the clinical spectrums of NPC disease (**B**). Abbrev.: GD, Gaucher disease; ASM, acid sphingomyelinase; EM, electron microscopy; MLPA, Multiplex Ligation-dependent Probe Amplification. This figure was adapted from (Patterson et al., 2012).

include children who present with neurological symptoms before the age of 2 and often never learn to walk. They frequently have hepatosplenomegaly at birth and die by the age of 5. Children with the late-infantile form also present with hepatosplenomegaly at birth but will reach all developmental milestones, although they may be delayed compared to normal children. Between the ages of 3-5, neurological symptoms, which are typical of NPC (including vertical supranuclear gaze palsy, cerebellar ataxia, gelastic cataplexy, and frequent seizures) will develop. Death in late-infantile NPC often precedes the age of 12. The most common form of NPC is a juvenile presentation, where neurological systems develop in school-aged (6-15) children and are usually first misdiagnosed as learning disabilities. In these cases, splenomegaly and prolonged jaundice are typically present at birth. Although lifespan is more variable in juvenile cases, death commonly occurs between 10 and 25 years of age. In the adolescent/adult form of NPC, symptoms are much more unpredictable. In addition to the prominent neurological signs and splenomegaly, psychiatric disturbances are common. At end-stage of disease, the adult form is very similar to that of the childhood forms of NPC (Vanier, 2010).

Treatment Plans. Once a patient has been diagnosed with NPC, there is very little that can be done to halt the progression of the disease. The prevailing management plan for NPC in patients is to treat individual symptoms as they present in order to improve quality of life. For example, anti-epileptic therapy can be prescribed to control seizures, and CNS stimulates may alleviate cataplexy (Patterson et al., 2012).

1.4 Animal Models of Niemann-Pick Type C Disease

As NPC1 and NPC2 are highly conserved proteins, animal models of NPC have proven invaluable to biochemical and molecular characterization of the disease, as well as to the discovery of potential therapies. Although primary human fibroblasts from patients with a variety of mutations leading to NPC disease are readily available to investigators from the Coriell Institute, these cultured cells have many

limitations. First of all, the cells are an *in vitro* system that may not reflect cholesterol movement through the body. Also, the cells are derived from skin, which is not considered a prominent target organ for NPC; although, some recent advancements have been made with stem cell technology to convert human NPC fibroblasts into neurons and other cell types of interest (Swaroop et al., 2012). Together, the *in vivo* animal models and the *in vitro* human fibroblasts have helped investigators move the NPC field forward.

NIH Balb-c *Npc1$^{-/-}$* mouse

In March of 1975, an unusual mouse was discovered in a wildtype Balb/c colony at the National Center for Toxicological Research (NCTR) in Jefferson, Arkansas. The mouse displayed a progressive neurological disorder leading to premature death. The parents of this mouse were used to generate a colony, which was originally referred to as the NCTR-BALB/c colony, of the mice carrying the spontaneous mutation, which were found to have excess storage of unesterified cholesterol in perpherial tissues in addition to neurodegeneration (Morris et al., 1982). Work by Dr. Peter Pentchev at the NIH proved that this mouse was a model for NPC disease (Pentchev, 2004), and the mouse was renamed the *Npc1^{NIH}* model. In 1997, the *Npc1^{NIH}* mutation was found to be caused by a spontaneous insertion of a large retrotransposon-like sequence that lead to a frameshift in the *Npc1* gene (Loftus et al., 1997). The resulting truncated *Npc1* mRNA does not yield any detectable protein (Maue et al., 2012).

Of all of the animal models available for NPC, the *Npc1^{NIH}* has been the most commonly studied. When *Npc1^{NIH}* mice on a pure BALB/c background are fed a standard rodent chow containing low (0.02% w/w) cholesterol, they live to be 12 weeks old (Liu et al., 2008). At 7 weeks of age (Li et al., 2005) these *Npc1^{NIH}* mice begin losing weight and displaying neurological symptoms; therefore, they are commonly studied at 49 days of age. The *Npc1^{NIH}* mice display a progressive loss of Purkinje cells of the cerebellum and an increase in microglia load in the brain (**Fig. 1.6**), which has been well characterized (German et al., 2001a; German et al., 2001b; Ong et al., 2001; German et al., 2002; Li et al., 2005). Virtually all organs in *Npc1^{NIH}* mice have dramatically increased total cholesterol concentrations,

decreased levels of cholesterol esters, and upregulated rates of cholesterol synthesis compared to wildtype

mice (Xie et al., 1999a; Xie et al., 1999b). In addition to cholesterol, these mice also accumulate

gangliosides (Zervas et al., 2001a). Overall, the symptoms observed in the $Npc1^{NIH}$ mice very closely

resemble those found in human NPC patients.
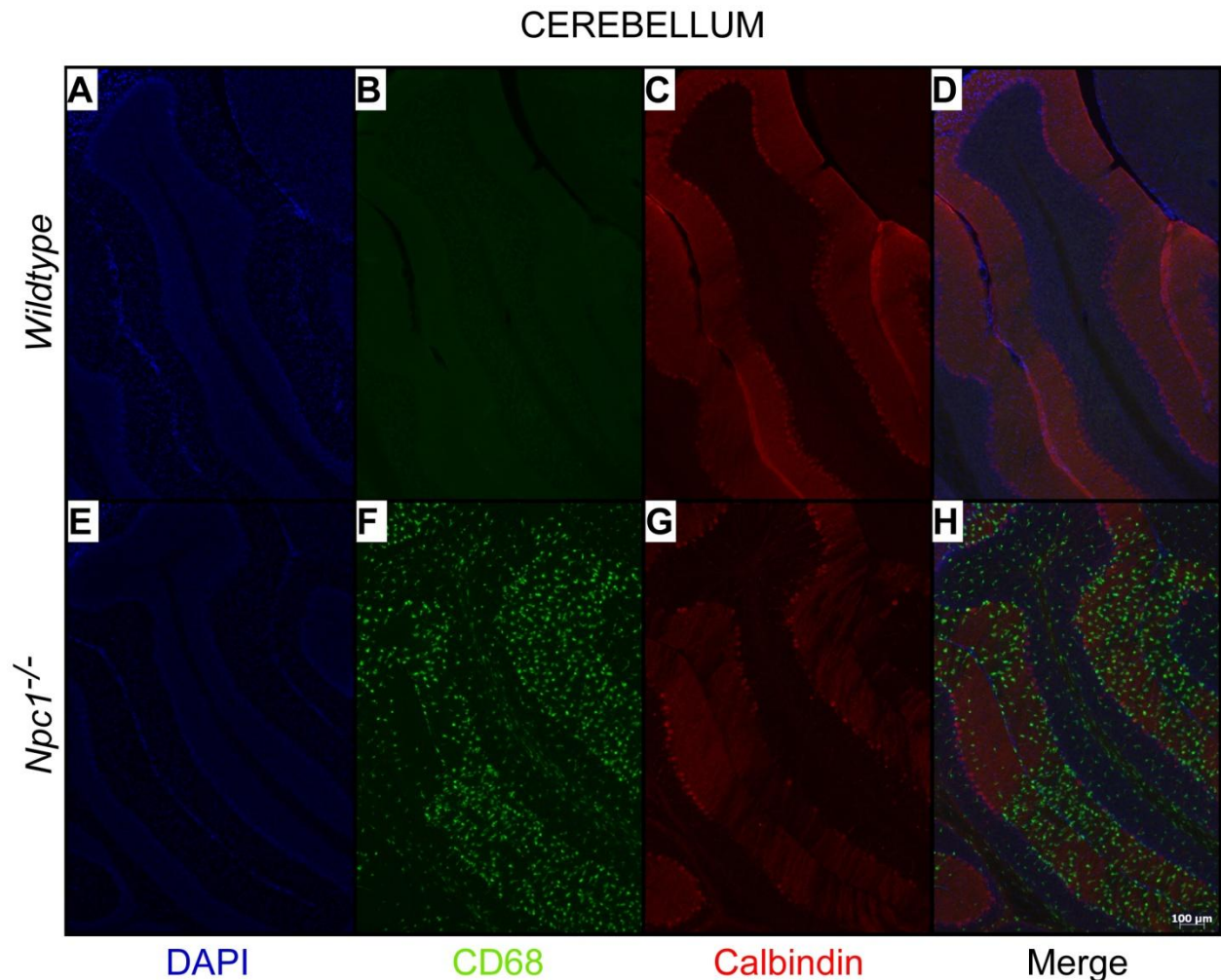
Figure 1.6 *Purkinje cell survival and microglia burden in the cerebella of Npc1$^{-/-}$ mice.* 50-day-old *wildtype* (**A-D**) and *Npc1$^{-/-}$* mice (**E-H**) were perfused through the heart with saline followed by formalin. Brains were harvested and cryo-preserved in sucrose for sectioning at 40uM. Free-floating cerebellar sections were co-stained for calbindin immunoreactivity (**red**) to show Purkinje cell structure, for CD68 immunoreactivity (**green**) to indicate microglia burden, and with DAPI (**blue**) to show cell nuclei. Each image shown is a representative histological section from 3 or more cerebellar slices stained from 4 animals per genotype.

Other Mouse Models

In addition to the commonly studied spontaneous mouse model for NPC, $Npc1^{NIH}$, several other

mouse models have been generated:

Npc2$^{-/-}$ model. After the discovery of NPC2, a second mouse model for NPC was produced to represent the 5% of human cases caused by mutations in *NPC2*. This *Npc2$^{-/-}$* mouse was described as a hypomorph as 0-4% of residual protein was found in testis and epididymis (Sleat et al., 2004). However as these tissues are only found in males and both genders display equivalent symptoms, it is unlikely that this residual NPC2 protein is having any effect in the mice. Although *Npc2$^{-/-}$* mice were found to survive significantly longer (16 weeks) compared to the *Npc1^{NIH}* and *Npc1^{NIH}Npc2$^{-/-}$* mice (12 weeks), overall the mice displayed similar loss of neurons and accumulation of cholesterol and gangliosides (Sleat et al., 2004). At 7 weeks of age, the *Npc2$^{-/-}$* mice were further shown to have a significantly smaller total pool of cholesterol (4,337 mg/kg) than occurs in the *Npc1^{NIH}* mouse (5,408 mg/kg) (Ramirez et al., 2011), which may explain why their extended lifespan.

Npc1 cholesterol-binding mutant. Two amino acid residues (proline-202 and phenylalanine-203) in the N-terminus of the NPC1 protein were shown to be required for cholesterol binding (Kwon et al., 2009). In order to test the role of cholesterol binding in NPC disease progression, a knock-in mouse (*Npc1$^{pf/pf}$*) was created, in which proline-202 and phenylalanine-203 within *Npc1* were mutated to alanine. Although higher than wildtype levels of the mutant NPC1 protein were present in the *Npc1$^{pf/pf}$* mouse, these mice completely phenocopied the *Npc1^{NIH}* mouse (Xie et al., 2011). These mouse harboring mutations in the critical cholesterol-binding residues clearly establish that cholesterol binding is an essential function of the NPC1 protein.

Point mutation in Npc1. Although the progression of NPC disease in the *Npc1^{NIH}* mouse model highly resembles that found in humans, the mutation in this mouse leads to no detectable NPC1 protein. This does not represent the common loss-of-function missense mutations in humans, where mutant NPC1 protein is often produced but fails to be properly trafficked to the lysosome. Using a mutagenesis screen, a novel mouse model (*Npc1^{NMF164}*) with a point mutation in *Npc1* leading to a single amino acid substitution (aspartate-1005-glycine) was generated and described (Maue et al., 2012). Although this mouse model displayed similar phenotypes to other NPC mouse models, the *Npc1^{NMF164}* disease

progression was significantly slower and lead to a 50% increase in lifespan compared to the $Npc1^{NIH}$ (Maue et al., 2012). This mouse may serve as a model of the adolescent/adult form of NPC and as a useful system to test potential therapies which could successfully deliver trafficking-detective NPC1 protein to the lysosome.

Conditional Npc1 Knockout models. In order to directly test the role of NPC1 in specific cell types, a conditional null mouse mutant of the *Npc1* gene ($Npc1^{flox}$) was created utilizing Cre-loxP technology to mimic the frameshift mutation found in the $Npc1^{NIH}$ mouse model (Elrick et al., 2010). First, $Npc1^{flox}$ were bred to mice with a Cre recombinase under a ubiquitous promoter in order to generate global $Npc1^{-/-}$, which phenocopied the $Npc1^{NIH}$ on a similar background strain. Next, the $Npc1^{flox}$ were bred to *Pcp2-Cre* mice to generate mice without *Npc1* only in Purkinje neurons. As expected, these mice displayed a progressive neurodegeneration of Purkinje cells and impairment of motor tasks; however, these mice, surprisingly, did not lose weight or die prematurely (at least up until 20 weeks of age) as is typical of global $Npc1^{-/-}$ (Elrick et al., 2010). In addition, the $Npc1^{flox}$ mouse was used to create mice lacking *Npc1* in all neurons or in astrocytes. While loss of *Npc1* in astrocytes did not lead to NPC disease, the loss of *Npc1* in all neurons led to equivalent progressive neurodegeneration and reduced survival as reported with global $Npc1^{-/-}$ mice (Yu et al., 2011). As Cre mice are available to generate mice with mutations in almost every subset of cells known, the potential uses of this $Npc1^{flox}$ mouse are vast.

Other Animal Models

Although mouse models are valuable tools for research of human diseases, there are limitations to using these small mammals. The rate of metabolism and the lifespan of mice are accelerated compared to humans. In addition, the small size of mice mandates that most studies be endpoint in order to harvest enough tissue for analyses; while with larger mammals, it may be possible to do tissue biopsies from the same animal throughout life. Even though mice are small, they are often not practical models for large-scale genomic or compound screens, which could be easily performed in smaller non-mammalian species.

Thus several other animal models of NPC have been generated.

Feline model. Besides the mouse, the feline model of NPC is the best characterized. Like the $Npc1^{NIH}$ mouse, the NPC feline model arose from a spontaneous mutation, which was discovered when in a domestic kitten displayed a progressive neurological disease and accumulation of lipids (Lowenthal et al., 1990). A colony of cats carrying the NPC mutation was generated, which was further characterized as having hepatosplenomegaly at birth, progressive loss of Purkinje cells, and positive filipin staining as seen in humans with NPC (Brown et al., 1994). In 2003, the mutation in NPC felines was mapped to a point mutation in *Npc1* leading to a single amino acid shift (cysteine-955-serine) (Somers et al., 2003). The feline model of NPC has been a valuable tool for confirming therapies that are shown to extend lifespan in NPC mouse models before they are tested in a clinical population.

Canine model. Similar to the feline model, a canine model of NPC was found in a domestic animal. A single report describing progressive neurodegeneration and cholesterol accumulation in a boxer puppy was published (Kuwamura et al., 1993). A colony was not generated for further characterization.

Others models. In addition to mammalian models of NPC disease, models have been described in *Caenorhabditis elegans* (Sym et al., 2000; Li et al., 2004), *Drosophila melanogaster* (Huang et al., 2005; Huang et al., 2007), and *Saccharomyces cerevisiae* (Malathi et al., 2004). Although recent work has been conducted using the yeast model (Munkacsi et al., 2011), the majority of ongoing research in NPC is being performed in either cultured cells or the mouse and feline models.

1.5 Potential Treatments Discovered in the *Npc1^{-/-}* mouse

As there are no pharmacological agents approved by the United States FDA to extend lifespan in patients with NPC disease, many research teams have sought to identify small-molecule therapeutics, which increase the lifespan of animal models for NPC. Using the $Npc1^{NIH}$ mouse (which will be represented by $Npc1^{-/-}$ from here out), several potential therapies for NPC have been discovered to reduce

neurodegeneration and to ultimately extend lifespan, including: an inhibitor of glucosylceramide synthase (N-butyldeoxynojirimycin or miglustat) (Zervas et al., 2001b); a Liver X Receptor agonist (T0901317 or Tcmpd) (Repa et al., 2007); and a modified cyclodextrin (2-hydroxypropyl-β-cyclodextrin or HP-β-CD) (Liu et al., 2009).

Miglustat

Miglustat was originally characterized and FDA-approved as a therapy for Gaucher disease (GD), which is a lysosomal storage disease in which the primary defect is reduced glucocerebrosidase activity leading to massive LE/L accumulation of glucosylceramide. Treatment with miglustat inhibits glucosylceramide synthase, which is a pivotal enzyme in the production of glycosphingolipids, preventing the accumulation of glucosylceramide in GD. As glycosphingolipids are also known to accumulate in the lysosome of NPC patients secondary to the accumulation of cholesterol, miglustat was tested as a therapy in the $Npc1^{-/-}$ mouse, where it was shown to reduce neurological dysfunction and lead to a 30% increase in survival compared to untreated $Npc1^{-/-}$ mice (Zervas et al., 2001b). Miglustat was the first therapy moved into a clinical trial in NPC patients, after being shown to extend lifespan in the $Npc1^{-/-}$ mouse. Although it was inconclusive whether this drug extended lifespan in patients, neurological symptoms were delayed compared to untreated controls (Patterson et al., 2007). While miglustat was approved as a therapy for NPC in the European Union, the United State FDA denied the request, as severe side effects including weight loss and tremors were reported (Patterson et al., 2012). Thus, no therapies are currently approved for the treatment of NPC in the United States.

LXR agonists

As there are decreased levels of oxysterols (Frolov et al., 2003) and diminished LXR activation in NPC (Li et al., 2005), it was hypothesized that LXR agonists could enhance the level of cholesterol efflux and serve as a potential therapy for NPC. Treatment of human NPC patient fibroblasts for 48 hours with

endogenous oxysterols, 25 and 27-hydroxycholesterol, was shown by filipin staining to decrease LE/L accumulation of cholesterol (Frolov et al., 2003). As the synthetic LXR agonist, T0901317 (Tcmpd), had been previously shown to cross the blood brain barrier and achieve concentrations in the CNS above the EC_{50} for LXRα/β (Whitney et al., 2002), oral administration to the $Npc1^{-/-}$ mouse model was tested. In these studies, Tcmpd treatment compared to vehicle treatment in $Npc1^{-/-}$ mice was shown to lead to a significant reduction in inflammation, improvement in neuronal survival, and a slight but significant extension of lifespan by 10 days (Repa et al., 2007). In addition, deletion of LXRβ, the most prevalent isoform of LXR in the brain, in the $Npc1^{-/-}$ mouse model was shown to lead to a statistically significant reduction in lifespan compared to the $Npc1^{-/-}$ mutant (Repa et al., 2007). Although these studies demonstrated the importance of LXR in maintaining cholesterol homeostasis in the NPC brain; no analyses were performed on perpheral tissues, nor was a molecular mechanism(s) by which Tcmpd extended lifespan identified.

Cyclodextrins

2-hydroxypropyl-β-cyclodextrin (HP-β-CD) is a cyclic oligosaccharide composed of 7 glucopyranosides that form a barrel-shaped molecule. HP-β-CD has a hydrophilic exterior that makes the compound water-soluble and a hydrophobic core that can harbor small hydrophobic molecules, such as lipids. Both of these properties make HP-β-CD, which has been approved by the FDA as a delivery agent, an ideal vehicle to increase the solubility of hydrophobic drugs (Irie et al., 1992; Thompson, 1997; Gould et al., 2005; Stella et al., 2008). HP-β-CD was considered to possess no therapeutic effect even in NPC (Camargo et al., 2001) (Griffin et al., 2004); that is until 2009 when a single dose of HP-β-CD in 7-day-old $Npc1^{-/-}$ pups was shown to led to dramatic sterol balance changes in just 24h and to a significant extension by 40% in the lifespan of $Npc1^{-/-}$ mice (Liu et al., 2009).

Since the initial study, many studies have been undertaken to better understand the potential of HP-β-CD therapy in NPC. Notably, serial injections of HP-β-CD were shown to double the lifespan of the

Npc1^{-/-} mouse (Davidson et al., 2009; Ramirez et al., 2010), and continuous intracerebroventricular administration was shown to dramatically rescue Purkinje cell loss in the cerebellum (Aqul et al., 2011). In addition, HP-β-CD can bypass mutations in either *NPC1* or *NPC2*, as HP-β-CD has been shown to significantly decrease hepatic cholesterol synthesis in just 24h in the *Npc1*^{-/-}, *Npc2*^{-/-}, and the rare *Npc1*^{-/-} *Npc2*^{-/-} double knockout mice (Ramirez et al., 2011). Further work has shown that HP-β-CD is beneficial in every organ except lung (Ramirez et al., 2010; Muralidhar et al., 2011). Studies performed in the feline model of NPC have confirmed HP-β-CD effectiveness at extending lifespan, but have also uncovered a previously unreported side effect. Although this has not yet been tested in the mouse, a single high dose of HP-β-CD can lead to an immediate and irreversible hearing loss in both wildtype and NPC-affected cats (Ward et al., 2010).

Several studies have also been performed to determine the molecular mechanism(s) through which HP-β-CD therapy works. A single HP-β-CD injection to 7- or 49-day-old *Npc1*^{-/-} mice has been shown in just 24 h to lead to the following: a decrease in cholesterol synthesis rates; an increase in the ratio of esterified/ unesterified cholesterol; down-regulation of the sterol regulatory element-binding protein 2 (SREBP2) and its target genes; and increased expression of liver X receptor (LXR) target genes (Liu et al., 2009; Liu et al., 2010a). These measurable shifts in sterol homeostasis serve as surrogate markers, which indicate that the *Npc1*^{-/-} cells are responding to cytosolic cholesterol excess. Since these changes were observed only after HP-β-CD administration to *Npc1*^{-/-} mice and not seen in wildtype mice, they further suggest that the excess unesterified cholesterol is being released from the LE/L compartment in *Npc1*^{-/-} cells. In support of this, a methyl-β-CD conjugated to a dextran with AlexaFluor546 was shown to enter the lysosome of fibroblasts from NPC patients and was able to diminish filipin staining of unesterified sterol within the lysosome (Rosenbaum et al., 2010). Overall these data suggest that HP-β-CD is able to facilitate the release of the lysosomal pool of unesterified cholesterol from NPC-deficient cells within 24 h. However many questions remain to be answered: how is HP-β-CD releasing cholesterol from the lysosome; why is HP-β-CD not affecting lung; does HP-β-CD cause deafness in other models

beyond the cat; and ultimately, will HP-β-CD extend lifespan in patients with NPC?

Other Therapies

Preliminary reports have suggested additional therapeutic agents for the treatment of NPC disease. *Histone deacetylase inhibitors* (HDACi's) have recently been shown to reduce the storage of cholesterol in cultured human fibroblasts from NPC patients (Pipalia et al., 2011) and in a yeast model of NPC disease (Munkacsi et al., 2011). HDACi are currently being tested in the $Npc1^{-/-}$ mouse model. ***Imatinib***, which inhibits the proapoptotic c-Abl, was found to improve neurological symptoms and extend lifespan in the $Npc1^{-/-}$ mouse. Like HP-β-CD, imatinib only improved lifespan when it was given to 7-day-old pups, suggesting that it can not cross the blood brain barrier of a mature animal, and thus future studies are required to test if direct delivery into the CNS is effective (Alvarez et al., 2008). ***Ibuprofen***, the non-steroidal anti-inflammatory drug, was also shown to further extend lifespan in the $Npc1^{-/-}$ mouse when given alone or in combination with miglustat; although, some toxic effects were reported (Smith et al., 2009). ***δ-tocopherol***, a form of vitamin E, was very recently shown to reduce cholesterol accumulation in cultured human fibroblasts deficient in NPC1, NPC2, or LAL. While more studies are required, δ-tocopherol shows potential to be used for treatment of a variety of lysosomal storage diseases (Xu et al., 2012).

Although NPC is a very rare disorder that only affects 1 in 120,000 individuals, uncovering potential NPC therapies could have a broad impact in other neurodegenerative diseases where cholesterol is dysregulated, such as SLOS, AD, PD, and HD. Furthermore, discovering the molecular mechanism(s) through which these therapies overcome the cholesterol trafficking defect in NPC disease could lead to novel insights on how cells maintain the synthesis, entry, and efflux of cholesterol.

CHAPTER TWO:

Investigating the Role of ABCG1 in the Progression of Niemann Pick Disease

2.1 Abstract

Proteins, NPC1 and NPC2, are required to traffic cholesterol from the lysosome. Mutations in either gene lead to entrapment of cholesterol in the lysosome and cause Niemann Pick Type C (NPC) disease. NPC disease presents as hepatic steatosis, splenomegaly, pulmonary dysfunction, and neurodegeneration resulting in premature death. There are no approved pharmacological agents that extend the lifespan of patients with NPC; however, two separate compounds (an LXR agonist and a cyclodextrin) have been identified that increase lifespan in the $Npc1^{-/-}$ mouse model. After either drug treatment, mRNA analyses of a variety of tissues show an upregulation of the LXR target gene, ATP-binding cassette transporter G1 (ABCG1), leading to the hypothesis that ABCG1 plays a pivotal role in relieving NPC disease progression. To test this, *wildtype*, $Abcg1^{-/-}$, $Npc1^{-/-}$, and $Npc1^{-/-}Abcg1^{-/-}$ littermate mice were enrolled into a survival study to monitor longevity. $Npc1^{-/-}Abcg1^{-/-}$ exhibited significantly reduced survival (81d) compared to $Npc1^{-/-}$ littermates (96d), which is consistent with the 10d reduction in lifespan measured in the $Npc1^{-/-}Lxr\beta^{-/-}$. In order to determine why survival was reduced in $Npc1^{-/-}Abcg1^{-/-}$, tissues were harvested from 50-day-old mice for sterol balance studies, histological evaluation, and mRNA analysis. Cholesterol synthesis in liver, lung, spleen, brain, and whole animal was not altered between *wildtype* and $Abcg1^{-/-}$ mice or between $Npc1^{-/-}$ and $Npc1^{-/-}Abcg1^{-/-}$ mice. There were no differences evident in Purkinje cell survival or neuroinflammatory burden in the cerebella of $Npc1^{-/-}$ and $Npc1^{-/-}Abcg1^{-/-}$ mice. Pro-inflammatory mRNA markers and foamy macrophages were significantly increased in peripheral organs of $Npc1^{-/-}Abcg1^{-/-}$ compared to $Npc1^{-/-}$ mice. Finally, ABCG1 was not required for the beneficial effects of the LXR agonist or cyclodextrin therapy in the $Npc1^{-/-}$ mice. Overall these data suggest that ABCG1 plays an important role in reducing inflammation in NPC disease progression. Thus other treatments which increase the expression of *Abcg1*, like LXR agonists and cyclodextrin, could be beneficial to NPC.

28

2.2 Introduction

Cholesterol is an integral component of cellular membranes and myelin sheaths and serves as the precursor to steroid hormones, vitamin D, and bile acids, which are all essential for the survival of mammals. Small alterations in cholesterol homeostasis can lead to detrimental effects in animals; thus, the synthesis, entry, and efflux of cholesterol are tightly maintained within each cell by two regulators of transcription: sterol regulatory element-binding protein 2 (SREBP2) and the oxysterol-responsive nuclear receptor, liver X receptor (LXR). When cholesterol levels are low, SREBP2 is activated which upregulates the entry of cholesterol through the low-density lipoprotein receptor (LDLR) and *de novo* synthesis of cholesterol from acetyl-CoA through 3-hydroxy-3-methyl-glutaryl-CoA (HMG-CoA) reductase and synthase (Horton et al., 2002). Alternatively, high levels of cholesterol lead to the production of oxysterols, cholesterol derivatives that serve as endogenous ligands for LXR (Janowski et al., 1999). Activated LXR upregulates the efflux of cholesterol from cells through the ATP-binding cassette (ABC) transporters, such as ABCA1 and ABCG1/5/8, and enhances the conversion of cholesterol into bile acids through cholesterol 7α-hydroxylase (CYP7A1) (Repa et al., 2002).

In some rare disease states, such as in Niemann Pick Type C disease (NPC), cholesterol balance is lost (Ory, 2004). In NPC, mutations in the lysosomal proteins, NPC1 or NPC2, lead to the entrapment and accumulation of unesterified cholesterol within the late endosome/early lysosome (LE/L), where it cannot be properly sensed and utilized by the cell (Patterson, 2003; Vance, 2006). Although there is an excess of cholesterol within the LE/L, NPC leads to enhanced cellular sterol synthesis through SREBP2 and reduced sterol elimination through a lack of LXR activation (Xie et al., 1999a; Li et al., 2005). Ultimately, this causes increased macrophage infiltration, inflammation, and cell death throughout the body resulting in premature death, which typically occurs during adolescence in humans (Vanier, 2010) and before 11 weeks of age in the *Npc1$^{-/-}$* mouse model (Liu et al., 2008).

As there are decreased levels of oxysterols (Frolov et al., 2003) and diminished LXR activation in NPC (Li et al., 2005), it was hypothesized that LXR agonists could enhance the level of cholesterol efflux

and serve as a potential treatment for NPC for which there are no approved therapeutic agents. Treatment of human NPC patient fibroblasts for 48 hours with endogenous oxysterols, 25 and 27-hydroxycholesterol, was shown by filipin staining to decrease LE/L accumulation of cholesterol (Frolov et al., 2003). Then using the $Npc1^{-/-}$ mouse model, the Repa lab further showed that oral administration of the synthetic LXR agonist, T0901317 (Tcmpd), could significantly reduce inflammation, improve neuronal survival, and extend lifespan (Repa et al., 2007). In addition, it was demonstrated that deletion of $Lxr\beta$, the most prevalent isoform of LXR in the brain, in the $Npc1^{-/-}$ mouse model led to a statistically significant reduction in lifespan compared to the $Npc1^{-/-}$ mutant (Repa et al., 2007). In an attempt to identify the molecular mechanism(s) by which Tcmpd extended lifespan and $Lxr\beta$ deletion shortened lifespan, the effect of the loss of the ABC transporter, ABCA1, on NPC disease progression was tested. ABCA1 is known to be required for cholesterol efflux in the brain; however, it appears ABCA1 is not involved in mediating LXR actions in NPC disease, as $Abca1^{-/-} Npc1^{-/-}$ mice lived as long as their $Npc1^{-/-}$ littermates (Repa et al., 2007).

Comparable to ABCA1, ABCG1, another LXR target, is also expressed in mouse brain and important for the efflux of cholesterol from cells, in particular macrophages (Baldan et al., 2006a; Kim et al., 2008). Intriguingly, ABCG1, which has been traditionally characterized as a plasma membrane protein, was recently shown to co-localize with NPC1 within the LE/L compartment and has been suggested to transport cholesterol intracellularly (Tarling et al., 2011). In $Npc1^{-/-}$ mice, the relative expression of $Abcg1$ was enhanced in liver, lung, and brain 12h after Tcmpd administration (unpublished data), suggesting that it could play a pivotal role in relieving NPC disease progression. Furthermore, $Abcg1$ is increased in the liver of 7-day-old $Npc1^{-/-}$ mice 24h after 2-hydroxypropyl-β-cyclodextrin (HP-β-CD), which has also been shown to lead to a significant extension of lifespan in $Npc1^{-/-}$ mice (Liu et al., 2009). Therefore, a series of studies was performed to evaluate the role of ABCG1 in the progression of NPC utilizing *wildtype*, $Abcg1^{-/-}$, $Npc1^{-/-}$, and $Npc1^{-/-}Abcg1^{-/-}$ littermate mice. The experiments were designed: 1) to characterize NPC disease progression (survival, cholesterol homeostasis, neuronal loss, inflammation) in the absence

of endogenous ABCG1; 2) to determine ABCG1's role in the anti-inflammatory effects of an LXR

agonist in $Npc1^{-/-}$ macrophages; and 3) to evaluate the contributions of ABCG1 to the cholesterol-altering

effects of HP-β-CD in $Npc1^{-/-}$ mice. Together, these studies show that ABCG1 plays an important role in

slowing NPC disease progression and suggest this is due to a reduction in peripheral inflammation.

2.3 Materials and Methods

Animals and Treatments

Heterozygous $Abcg1^{+/-}$ mice on a C57BL/6 background were acquired from Alan R. Tall (Columbia

U), which were originally produced by Deltagen (San Mateo, CA) (Kennedy et al., 2005). These mice

were bred to heterozygous ($Npc1^{+/-}$) mice on a BALB/c background (Loftus et al., 1997) to generate

mixed strain double heterozygous ($Npc1^{+/-}Abcg1^{+/-}$) breeding pairs, which spawned the *wildtype* ($Npc1^{+/+}$

$Abcg1^{+/+}$), $Abcg1^{-/-}$ ($Npc1^{+/+}Abcg1^{-/-}$), $Npc1^{-/-}$ ($Npc1^{-/-}Abcg1^{+/+}$), and *double knockout* ($Npc1^{-/-}Abcg1^{-/-}$)

mice used for the following studies. Litters were genotyped upon weaning, between 19-21 days of age.

Mice were group-housed in plastic cages containing wood chip bedding in an animal facility with

temperature-controlled rooms (23 ± 1°C) and a maintained light cycle (12h light on/12h off). The mice

were allowed *ad libitum* access to water and a standard rodent chow containing 0.02% w/w cholesterol

(7001; Harlan Teklad, Madison, WI).

For survival studies, mice were given easy access to food and water, by providing a powdered form

of 7001 diet in glass containers on the floor of their cage and by using water bottles with long spouts. At

end-stage of life, mice were monitored twice daily. When a mouse could no longer intake food or water,

this point was considered death and the mouse was euthanized. For studies testing the effectiveness of 2-

hydroxypropyl-β-cyclodextrin (HP-β-CD), 49-day-old mice were given a single subcutaneous (sc)

injection of HP-β-CD (H107, Sigma) at 4000 mg per kg body weight [mpk] or vehicle [saline at

equivalent volume of 20 μl/g body weight (bw)]. All studies in this chapter, except those in cell culture,

utilized equal numbers of age-matched males and females per group. When mice were used as a source of cells for culture, macrophages were obtained from 2-month-old male mice. All animal research was conducted in conformity with the Public Health Service Policy on Humane Care and Use of Laboratory Animals, and all experiments were performed with prior approval from the University of Texas Southwestern Medical Center's Institutional Animal Care and Use Committee.

Measures of cholesterol balance in mice

49-day-old *wildtype, Abcg1^{-/-}, Npc1^{-/-},* and *Npc1^{-/-}Abcg1^{-/-}* mice (n=3 to 5 mice/group) were given a sc injection of saline or HP-β-CD. 24h after the injection, the mice were weighed and euthanized (exsanguinated under deep anesthesia) to harvest tissues for the following analyses:

Sterol synthesis rates. Exactly 1h prior to euthanasia and tissue harvest, mice were given an intraperitoneal (ip) injection of 1.76 mCi of [3H] water per g bw. Liver, spleen, lung, and brain were quickly removed, weighed, and saponified in alcoholic KOH. The remaining carcass was also weighed and saponified in alcoholic KOH to determine whole animal synthesis rates. Organ contents of [3H]-labeled digitonin-precipitable sterols (DPS) were determined as previously described (Dietschy et al., 1984). The rate of sterol synthesis within each organ is reported as the nmol of [3H] incorporated into DPS per hour per gram of tissue. The total rate of sterol synthesis within the whole animals was calculated by combining the rate of sterol synthesis within the individual organs with that of the remaining carcass and is reported as the μmol of [3H] incorporated into DPS per hour per 100 gram of bw.

Tissue Cholesterol Concentrations. The liver, spleen, lung, brain, and remaining carcass in KOH used for the synthesis determinations were also used to measure total cholesterol content. Briefly, the cholesterol was extracted and quantified by gas chromatography (GC) with a stigmastanol internal standard as previously described (Turley et al., 1994). The total cholesterol concentration of each organ is expressed as the mg of cholesterol per gram of tissue. The total cholesterol content within the whole animal was calculated by combining the cholesterol concentrations within the individual organs with that

of the remaining carcass and is reported as the mg of total cholesterol per 100 gram of bw.

Histological examination of tissues

Tissues. Wildtype, *Abcg1*^{-/-}, *Npc1*^{-/-}, and *Npc1*^{-/-}*Abcg1*^{-/-} mice (n=4 mice/group) were euthanized at exactly 50 days of age at the same point during the light cycle (3h after lights on or Zeitgeber time (ZT) 3). Under deep anesthesia, mice were perfused through the heart with saline (until the liver was completed blanched and the run-off was clear) followed by a 4% formaldehyde solution (HT501320, Sigma) for ~10 min (until all exposed organs were stiff to the touch). Lungs were inflated by injecting 2mL of 4% formaldehyde directly into the trachea. Lungs, spleen, and brain were carefully removed from the animal into a jar of 4% formaldehyde, which was kept during the day at ~23°C and overnight at 4°C. The following day, the tissues were washed 3x with PBS. At this point, the brains were submerged in a 20% sucrose/PBS/0.02% Sodium Azide solution for cryoprotection and stored at 4°C. Once the brain sunk in the sucrose solution (~2 days), the brains were frozen at -80°C until cryosectioning was performed. Meanwhile, the spleen and lungs were further washed with increasing concentrations of EtOH in PBS until 70% EtOH was reached. Once in 70% EtOH, the remaining tissues were stored at -20°C until being cleared with xylene and embedded in paraplast plus (P3683, Sigma) for sectioning.

H&E Staining. Paraffin embedded lungs and spleen were sectioned at 5 μm and stained with hematoxylin and eosin by the Molecular Pathology Core at the University of Texas Southwestern Medical Center. Each image shown is a representative histological section from 3 or more tissue slices stained from n=4 animals/genotype.

Immunohistochemistry. Cryopreserved cerebella were embedded in optimal cutting temperature compound (4583, Tissue-Tek) and sectioned along the sagital plane at 40 μm thickness with a Leica CM 1850 cryostat. Sections were stored in a PBS/0.02% sodium azide solution at 4°C until the day of staining. To show Purkinje cell structure, free-floating cerebellar sections were stained for calbindin immunoreactivity (Frank et al., 2003; Repa et al., 2007). At room temperature, sections were blocked in

0.3% H_2O_2 for 0.5 h to quench endogenous peroxidases and then with 3% goat serum and 0.25% Triton

X-100 for 2h to permeabilize the cells. The sections were incubated with anti-calbindin D-28K (1:5000;

AB1778, Millipore, Billerica, MA) overnight at 4°C. The next day at room temperature, the sections were

washed and then incubated with a biotinylated goat anti-rabbit antibody (1:1000; BA-1000, Vector

Laboratories, Burlingame, CA) for 2 h followed by NeutrAvidin-HRP (1:5000; 31030, Pierce, Rockford,

IL) for 1 h. The tissue-bound peroxidase activity was revealed by incubating the sections in a 0.04%

DAB/0.01% H_2O_2 (SK-4100, Vector Laboratories) for 2-3 min. Tissue sections were mounted on slides,

dehydrated with increasing concentrations of EtOH, and then coverslipped with permount (SP15-100,

Fisher).

For microglia characterization, free-floating cerebellar sections were stained for CD68

immunoreactivity. At room temperature, sections were blocked with 3% goat serum and 0.25% Triton X-

100 for 2 h to permeabilize the cells. Then, sections were incubated with anti-CD68 (1:500; MCA1957T,

AbD Serotec, Raleigh, NC) overnight at 4°C. The next day at room temperature, the sections were

washed and then incubated in goat anti-rat Alexa 488 (1:1000; Invitrogen) for 2 h in the dark. Tissue

sections were mounted on slides and coverslipped with VectaShield Mounting medium w/ DAPI (H-

1200, Vector Laboratories). Each image shown is a representative histological section from 3 or more

cerebellar slices stained from n=4 animals/genotype.

Measurement of relative mRNA levels

Tissues. Wildtype, Abcg1^{-/-}, Npc1^{-/-}, and Npc1^{-/-}Abcg1^{-/-} mice (n=6 mice/group) were euthanized at

exactly 50 days of age at the same point during the light cycle (ZT 2). Mice were exsanguinated; then

liver, spleen, lung, and brain were collected and flash-frozen in liquid nitrogen. The tissues were stored at

-80°C until total RNA was isolated using RNA STAT-60 (Tel-Test, Inc.). RNA concentrations were

determined by absorbance at 260nm with a Thermo Scientific Nanodrop 100 Spectrophotometer. 2 ug of

total RNA was treated with RNase-free DNase (Roche) and reverse-transcribed into cDNA with

SuperScript II (Invitrogen) as previously described (Kurrasch et al., 2004; Valasek et al., 2005b). The

cDNA was used to perform quantitative real-time PCR (qPCR) with the Applied Biosystems 7900HT

sequence detection system. Each qPCR was analyzed in duplicate and contained in a final volume of 10

µl: 25 ng of cDNA, each primer at 150 nM, and 5 µl of 2x SYBR Green PCR Master Mix (Applied

Biosystems). The nucleotide sequences of the primers used in this chapter are listed in Table C.1 of

Appendix C. Results were evaluated by the comparative cycle number at threshold (C_T) method

(Schmittgen et al., 2008) using cyclophilin as the invariant housekeeping gene (Dheda et al., 2004; Kosir

et al., 2010), and mRNA levels were arithmetically adjusted to a unit of 1 for the *wildtype* untreated

group.

    Primary Macrophages. Npc1$^{-/-}$ and *Npc1$^{-/-}$Abcg1$^{-/-}$* mice (n=2 mice/group) received a 1 mL i.p.

injection of 3% thioglycollate (autoclaved and aged for 3 months; #211717, Becton Dickinson) to elicit

macrophages. Three days later, mice were euthanized, and macrophages were harvested from the

peritoneal cavity by sterile lavage using ice-cold PBS. Lavage solutions from mice of the same genotype

were pooled together, and cells were collected by centrifugation for 5 min at 150x g at 4°C. Cell pellets

were resuspended in medium [high-glucose DMEM (Invitrogen) containing 10% heat-inactivated fetal

calf serum (FBS; Atlanta Biologicals) and 1% Pen/Strep (Invitrogen)]. The primary macrophages were

counted and plated at 1.05×10^5 cells/cm^2 on tissue-culture treated plates (Corning). Once plated, the cells

were maintained in a humid incubator at 37°C with 5% CO_2. Six hours later, cells were washed with PBS

and exposed to fresh media with FBS containing either vehicle (1uL of DMSO/mL of media) or at 1 µM

of the synthetic LXR agonist, T0901317 (Tcmpd, #71810, Cayman Chemicals, Ann Arbor, MI) prepared

in DMSO. After 16 h of treatment, culture medium was aspirated from each well, and 500 uL of RNA-

STAT60 was used to lyse cells and obtain RNA for analysis by qPCR as described above for tissues.

Measurement of secreted cytokine concentrations

    Thioglycollate-elicited peritoneal macrophages were harvested from *Npc1$^{-/-}$* and *Npc1$^{-/-}$Abcg1$^{-/-}$* mice

as described above. The macrophages were plated at a density of 2.1×10^5 cells/cm^2 on tissue-culture treated plates, were allowed to adhere for 6 h, and then were treated in fresh media with DMSO or 1μM Tcmpd. After 16 h of treatment, the macrophages were challenged with Lipopolysaccharide (LPS; L4391, Sigma) prepared in saline by replacing the culture media with fresh media containing: vehicle alone (DMSO and saline), Tcmpd alone (1 μM Tcmpd and saline), LPS alone (DMSO and 100 ng of LPS/mL of media), or Tcmpd with LPS (1 μM Tcmpd and 100 ng of LPS/mL of media). After 4h, the culture medium from each well was transferred to a tube, flash frozen in liquid nitrogen, and stored at -80°C until analyses for cytokine levels were performed. 25 μL of each sample was analyzed in duplicate, alongside cytokine standards, on a 7-plex mouse cytokine plate (#K15012B-1, MesoScale Discovery, Gaithersburg, Maryland) according to the manufacturer's instructions. The plate was analyzed using a SECTOR® Imager 2400 instrument (MesoScale Discovery). Concentrations for IFNγ, IL-1β, IL-6, IL-10, IL-12p70, KC/GRO, and TNF are reported as pg of protein per mL of media.

Data Analysis

All data are presented as the mean ± SEM. Statistically significant differences (*P*-value <0.05) between groups were determined using a one-way ANOVA followed by the Newman-Keuls multiple comparison test and are indicated by different letters. Significant differences in survival curves were determined by the Wilcoxon-Gehar and Log-rank analyses and are represented by *** (p<0.001). Significant differences in body weight curves were determined by calculating the area under the curve from 4 to 10 weeks and then performing a one-way ANOVA, which are also represented by *** (p<0.001). All statistical tests were performed using GraphPad Prism5 software (GraphPad Software, Inc. San Diego, CA).

2.4 Results

Deletion of *Abcg1* significantly reduced lifespan in *Npc1*^{-/-} mice:

Npc1^{-/-} mice accumulate unesterified cholesterol within the lysosome, which leads to increased inflammation, progressive neurodegeneration, and ultimately a shortened lifespan compared to their wildtype littermates. When *Npc1*^{-/-} mice on a pure BALB/c background are fed a standard rodent chow containing low (0.02% w/w) cholesterol, they live to be ~85d (Liu et al., 2008). Breeding mice onto a *Lxrβ*-deficient background significantly reduced the lifespan of the *Npc1*^{-/-} mouse by ~10d (Repa et al., 2007). In order to determine the role of the LXR target gene, *Abcg1*, on the progression of NPC disease, *Npc1*^{-/-} mice were bred onto an *Abcg1*-deficient background, which alone does not alter viability or lifespan in mice (Kennedy et al., 2005). Importantly as genetic background has both been shown to alter the lifespan of *Npc1*^{-/-} mice (Liu et al., 2008), all mice used in this study were from the same generation on an identical mixed-strained background. In this survival study, *Npc1*^{-/-} lived to a median age of 93.5d, while their *Npc1*^{-/-}*Abcg1*^{-/-} littermates exhibited significantly reduced survival of only 81d (**Fig. 2.1A**). *Abcg1*^{-/-} survived as long as *wildtype* mice (data not shown). The significant reduction in lifespan by the functional deletion of ABCG1 in *Npc1*^{-/-} mice mirrors that which was reported for LXRβ.
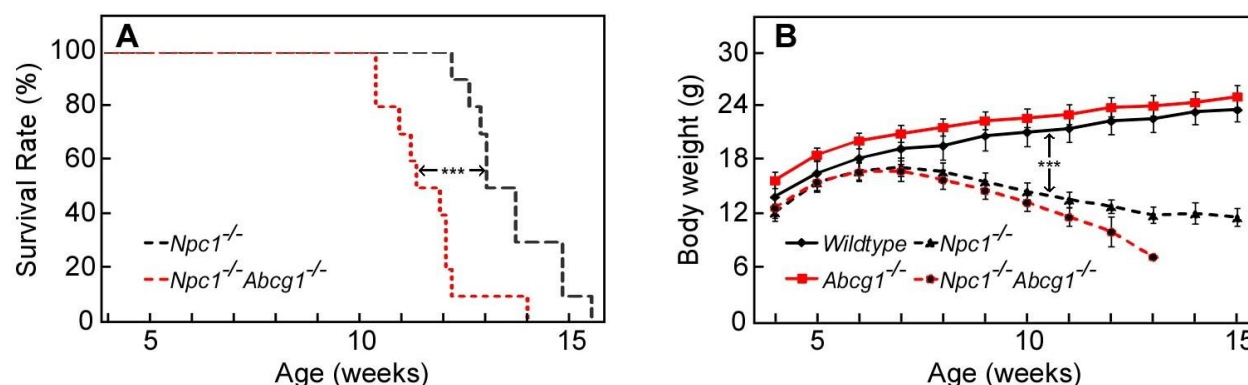
Figure 2.1 *Effect of the functional deletion of ABCG1 on lifespan and body weight in the Npc1*^{-/-} *mice.* Mice were weaned at 21d and enrolled (n=5 females and n=5 males/genotype) into a survival study. Mice were group-housed and fed standard chow (0.02% cholesterol). (**A**) *Npc1*^{-/-}*Abcg1*^{-/-} exhibited significantly reduced survival (81d) compared to *Npc1*^{-/-} littermates (93.5d, p<0.001). Significant differences in survival curves were determined by Wilcoxon-Gehar and Log-rank analyses using GraphPad Prism software. (**B**) Body weights were recorded weekly.
Not Depicted: *Abcg1*^{-/-} survived as long as wildtype mice.

Weekly body weights were recorded during the survival study, which showed that both the *Npc1*^{-/-}

and $Npc1^{-/-}Abcg1^{-/-}$ gained weight until 7 weeks of age and then gradually began losing weight until death (**Fig. 2.1B**). Although there was a trend towards the $Npc1^{-/-}Abcg1^{-/-}$ group losing weight more rapidly than the $Npc1^{-/-}$, the only statistically significant differences were when comparing the *wildtype* and $Abcg1^{-/-}$ mouse groups with the $Npc1^{-/-}$ and $Npc1^{-/-}Abcg1^{-/-}$ mice.

Deletion of *Abcg1* does not affect sterol synthesis in wildtype or $Npc1^{-/-}$ mice:

As $Npc1^{-/-}Abcg1^{-/-}$ mice survived ~10 d less than their $Npc1^{-/-}$ littermates, a series of studies were performed to address which mechanism(s) were involved. A logical starting point was to determine if aspects of sterol balance, which are dysregulated in NPC disease, are further altered by the deletion of *Abcg1*. Virtually all organs in $Npc1^{-/-}$ mice, with the exception of brain (due to demyelination), have dramatically increased total cholesterol concentrations, decreased levels of cholesterol esters, and upregulated rates of cholesterol synthesis compared to wildtype mice (Xie et al., 1999a). $Abcg1^{-/-}$ mice have been shown to display a progressive accumulation of cholesterol within lung that reaches significance compared to wildtype mice by 6 months of age (Baldan et al., 2006b); however, *in vivo* cholesterol synthesis rates within any tissue of the $Abcg1^{-/-}$ mice have not been previously reported. Therefore for these studies, organ weights (**Fig. 2.2 A, B**), total cholesterol concentrations (**Fig. 2.2 C, D**), and *in vivo* cholesterol synthesis rates (**Fig. 2.2 E, F**) were determined for liver, spleen, lung, and brain, as well as, from the whole body of *wildtype*, $Abcg1^{-/-}$, $Npc1^{-/-}$, and $Npc1^{-/-}Abcg1^{-/-}$ mice.

As previously described, $Npc1^{-/-}$ mice displayed significant hepatomegaly and splenomegaly compared to *wildtype* controls (**Fig. 2.2 A**). Whereas $Abcg1^{-/-}$ animals had organ masses and a total body weight equivalent to *wildtype* mice, at 50 days of age $Npc1^{-/-}Abcg1^{-/-}$ mice were similarly matched with $Npc1^{-/-}$ animals (**Fig. 2.2 A, B**). The only novel difference found was a significantly higher relative lung weight in $Npc1^{-/-}Abcg1^{-/-}$ ($1.19 \pm 0.10\%$) compared to *wildtype* ($0.78 \pm 0.10\%$) and $Abcg1^{-/-}$ ($0.82 \pm 0.06\%$); however, the lungs of $Npc1^{-/-}$ mice ($1.05 \pm 0.06\%$) were not significantly different from any group (**Fig. 2.2 A**). Consistent with the increased organ weights, $Npc1^{-/-}$ and $Npc1^{-/-}Abcg1^{-/-}$ mice had increased

cholesterol concentrations in liver, spleen, and lung, as well as whole body compared to *wildtype* and

Abcg1^{-/-} animals **(Fig. 2.2 B, C)**. The only difference measured between *wildtype* and *Abcg1*^{-/-} mice was a

significant increase in cholesterol content in lung **(Fig. 2.2 B)**. Measurements of *in vivo* cholesterol

synthesis rates showed no differences between *wildtype* and *Abcg1*^{-/-} mice or between *Npc1*^{-/-} and *Npc1*^{-/-}
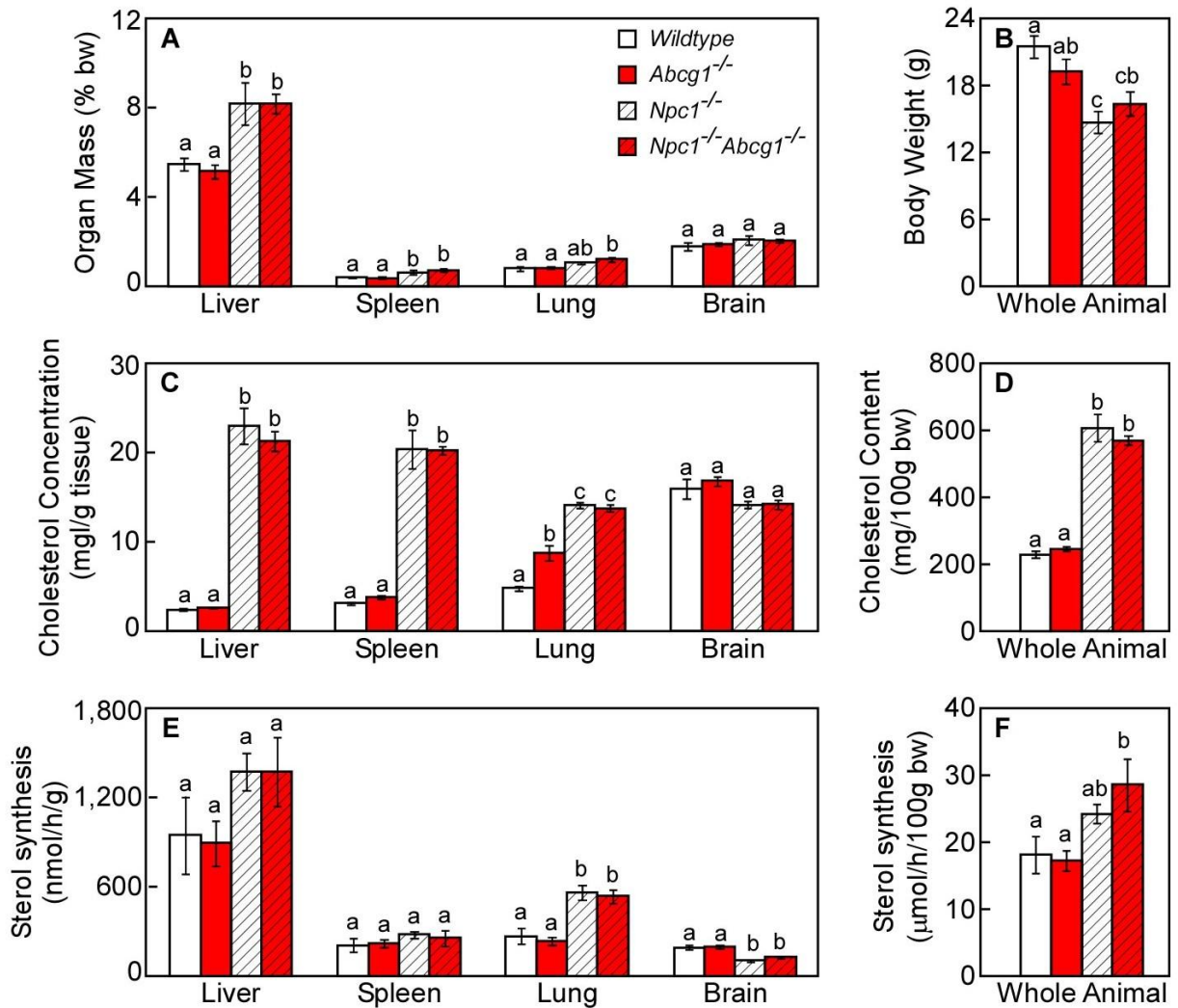
Abcg1^{-/-} mice.

Figure 2.2 *Effect of the functional deletion of ABCG1 on tissue cholesterol content and sterol synthesis rates in Npc1*^{-/-} *mice.* 50-day-old *wildtype*, *Abcg1*^{-/-}, *Npc1*^{-/-}, and *Npc1*^{-/-}*Abcg1*^{-/-} mice were injected with [3H]-water, and tissues were harvested exactly 1h later. Organ weights were measured for liver, spleen, lung, and brain (**A**) and expressed relative to the total body weight (**B**). The tissues were saponified to measure the total concentration of cholesterol (**C, D**) by GC and the rates of cholesterol synthesis (**E, F**) by the [3H]-water method. Each bar represents the mean $\pm$ SEM for 3-5 mice. Statistically significant differences (P <0.05) between genotypes are indicated by different letters.
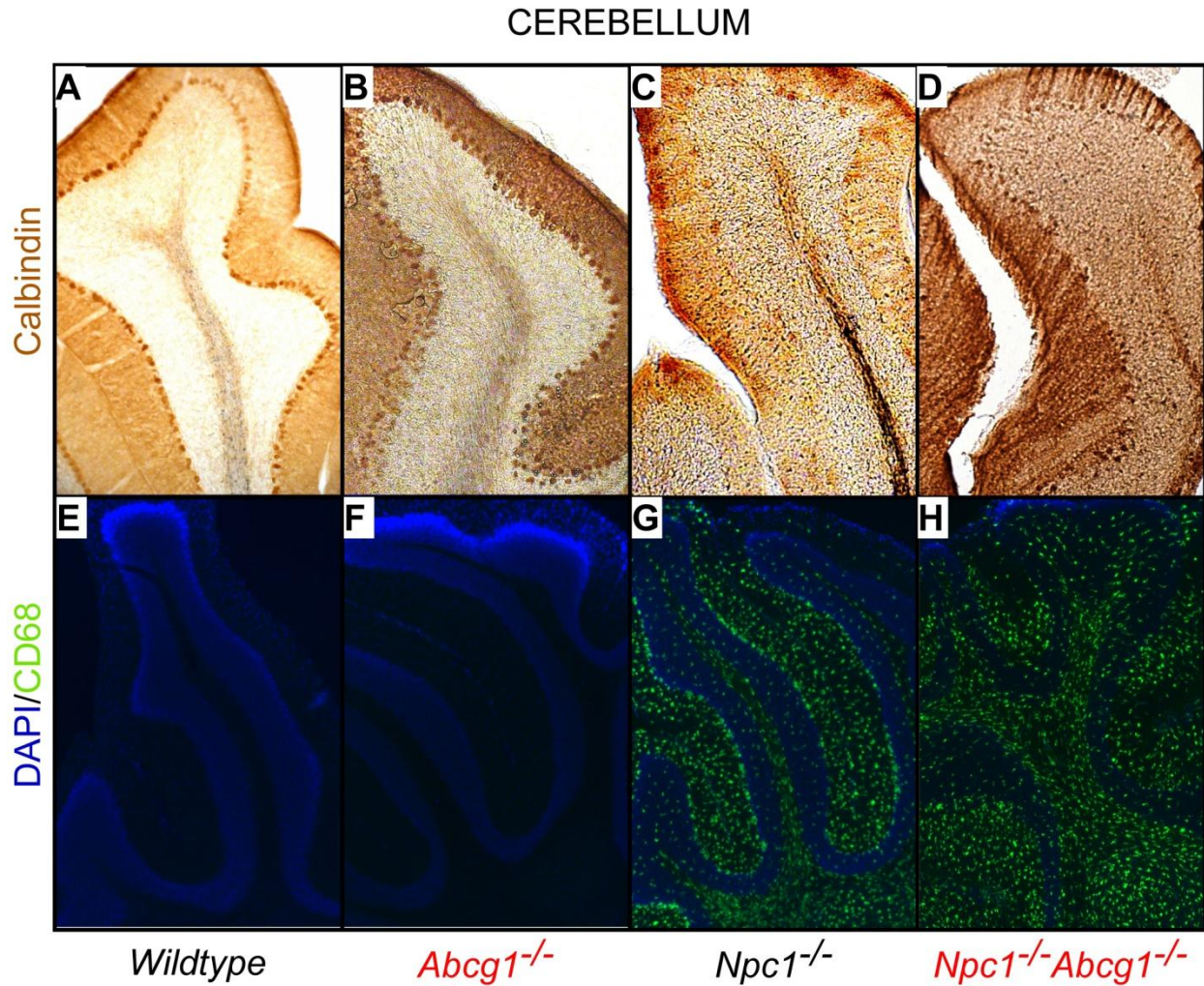
CEREBELLUM

Figure 2.3 *Effect of the functional deletion of ABCG1 on Purkinje cell survival and inflammation in the cerebella of Npc1-/- mice.* 50-day-old *wildtype*, *Abcg1-/-*, *Npc1-/-*, and *Npc1-/-Abcg1-/-* mice were perfused through the heart with saline followed by formalin. Brains were harvested and cryo-preserved in sucrose for sectioning at 40 μm. Free-floating cerebellar sections were stained for calbindin immunoreactivity (**brown**) to show Purkinje cell structure (**A-D**) or for CD68 immunoreactivity (**green**) to indicate microglia burden and co-stained with DAPI (**blue**) to show cell nuclei (**E-H**). Each image shown is a representative histological section from 3 or more cerebellar slices stained from n=4 animals/genotype.

Deletion of *Abcg1* does not alter Purkinje cell survival or microglia burden in *Npc1-/-* mice:

As no substantial differences were found in sterol balance between *Npc1-/-* and *Npc1-/-Abcg1-/-* mice that explained the difference in survival, next the cerebella of the mice were evaluated. By 7 weeks of age, *Npc1-/-* mice have lost an extensive number of Purkinje cells (**Fig. 2.3C**) and have a dramatic increase in microglia (**Fig. 2.3G**) compared to *wildtype* controls (**Fig. 2.3A, E**). Like *wildtype* mice, *Abcg1-/-*

littermates **(Fig. 2.3B, F)** showed no neuronal loss or microglia infiltration. Importantly, there were no significant differences between the number of remaining Purkinje cells or microglia present in the cerebella of *Npc1*$^{-/-}$ **(Fig. 2.3C, G)** and *Npc1*$^{-/-}$*Abcg1*$^{-/-}$ **(Fig. 2.3D, H)**. In support of the histological evaluation, mRNA markers for *Purkinje cell proteins (Pcp) 2* and *4* were significantly reduced while markers for *Caspase 1 and 3* were significant increased in the cerebella of *Npc1*$^{-/-}$ and *Npc1*$^{-/-}$*Abcg1*$^{-/-}$ compared to *wildtype* and *Abcg1*$^{-/-}$ littermates **(Fig. 2.5 E,** *Casp1* not shown**)**. The mRNA level for the *macrophage inflammatory protein* (*Mip*) *1α* was likewise found to be significantly higher in the cerebella of *Npc1*$^{-/-}$ and *Npc1*$^{-/-}$*Abcg1*$^{-/-}$ compared to *wildtype* and *Abcg1*$^{-/-}$ mice **(Fig. 2.5 F)**; however, *Mip1α* was also significantly reduced by >25% in the *Npc1*$^{-/-}$*Abcg1*$^{-/-}$ compared to *Npc1*$^{-/-}$ mice.

Deletion of *Abcg1* increases inflammation in the peripheral organs of *Npc1*$^{-/-}$ mice:

Although neural inflammation and neurodegeneration were unchanged in *Npc1*$^{-/-}$*Abcg1*$^{-/-}$ mice compared to *Npc1*$^{-/-}$, levels of inflammation were examined in spleen and lung. 50-day-old *Npc1*$^{-/-}$ mice had large foamy macrophages (arrowheads, **Fig. 2.4C**) scattered within alveolar spaces of the lung that were not found within any *wildtype* lung sections **(Fig. 2.4A)**. The lungs of *Abcg1*$^{-/-}$ **(Fig. 2.4B)** also had significant macrophage infiltration within almost every alveolar space, although these macrophages appeared smaller and less foamy that those of *Npc1*$^{-/-}$ mice. These two phenotypes combined in the lungs of *Npc1*$^{-/-}$*Abcg1*$^{-/-}$ mice **(Fig. 2.4D)** yielding very large, foamy macrophages clustered within almost every alveolar space. While no abnormalities were apparent within the spleens of *wildtype* and *Abcg1*$^{-/-}$ mice **(Fig. 2.4E, F),** a few abnormal macrophages were seen in *Npc1*$^{-/-}$ spleens (arrowheads, **Fig. 2.4G**). A striking phenotype of very large foamy macrophages throughout the spleen was found in *Npc1*$^{-/-}$*Abcg1*$^{-/-}$ mice **(Fig. 2.4H)**.

In addition to histology, mRNA levels of select genes related to cholesterol metabolism and pro-inflammatory state were evaluated in liver **(Fig. 2.5A, B)**, spleen **(Fig. 2.5C, D)**, and lung **(Fig. 2.6)**. The mRNA levels for *Abcg1* and *Npc1* were measured in all tissues to confirm genotypes **(Fig. 2.5-6)**.

Intriguingly in only liver, the mRNA levels of *Abcg1* was significantly increased by knockout of *Npc1;*

while *Npc1* was significantly decreased by knockout of *Abcg1* (**Fig. 2.5A**). Another LXR target gene,

Abca1, was upregulated in *Abcg1*^{-/-} and *Npc1*^{-/-}*Abcg1*^{-/-} spleens possibly to compensate for the loss of

ABCG1 (**Fig. 2.5C**). The mRNA levels of the *de novo* cholesterol synthesis regulator, SREBP2, and its

target genes, *Hmg CoA Reductase* (*Hmg CoA Red*) and *low density lipoprotein receptor* (*Ldlr*) were

upregulated in the liver, spleen, and lung of *Npc1*^{-/-} and *Npc1*^{-/-}*Abcg1*^{-/-} mice compared to *wildtype* and

Abcg1^{-/-} littermates; although only the increases in *Hmg CoA Red* and *Ldlr* within lung (**Fig. 2.6A**) and

Hmg CoA Red within spleen were significant (**Fig. 2.5C**).
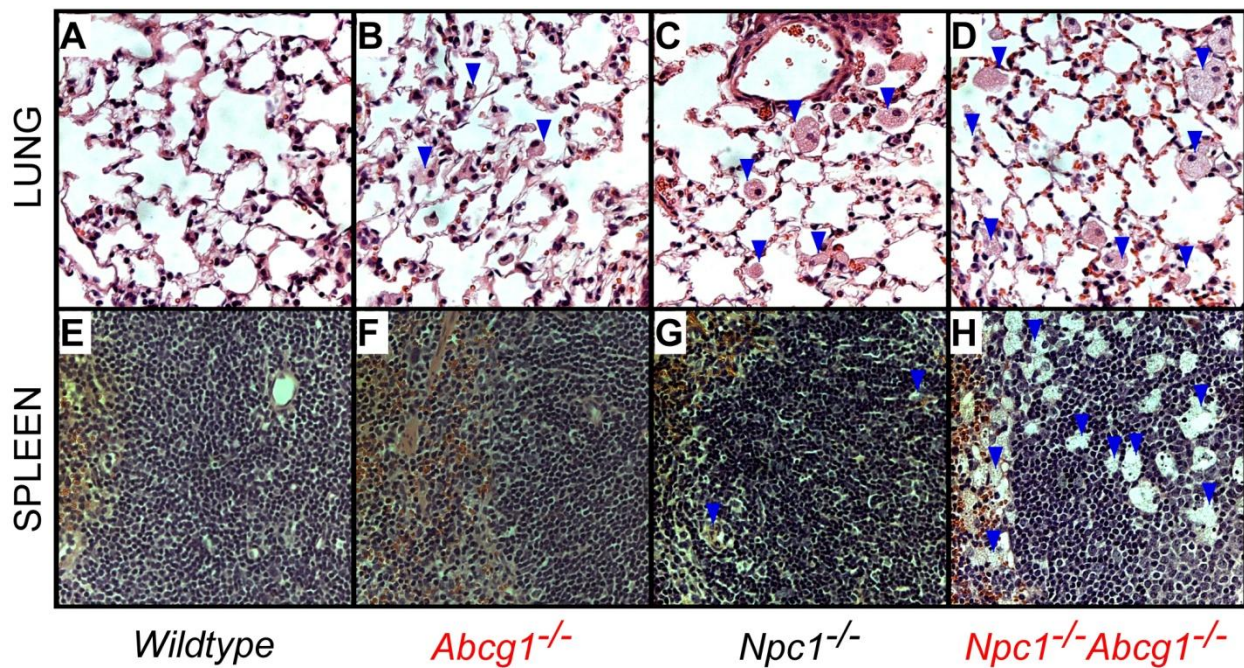
Figure 2.4 *Effect of the functional deletion of ABCG1 on lung and spleen histology in Npc1*^{-/-} *mice.* 50-day-old *wildtype*, *Abcg1*^{-/-}, *Npc1*^{-/-}, and *Npc1*^{-/-}*Abcg1*^{-/-} mice were perfused through the heart with saline followed by formalin. Lungs were inflated by injecting formalin directly into the trachea. Lungs and spleen were harvested and embedded in paraplast. 5 μm sections of lung (**A-D**) and spleen (**E-H**) were stained with hematoxylin (**purple**) and eosin (**pink**). Arrowheads (▼) within images point out macrophages. Each image shown is a representative histological section from 3 or more slices stained from n=4 animals/genotype.

While there was no increase in microglia load or mRNA levels of proinflammatory genes in the

cerebella of *Npc1*^{-/-}*Abcg1*^{-/-} in contrast to *Npc1*^{-/-} mice, there was an increase in macrophage load in spleen

LIVER
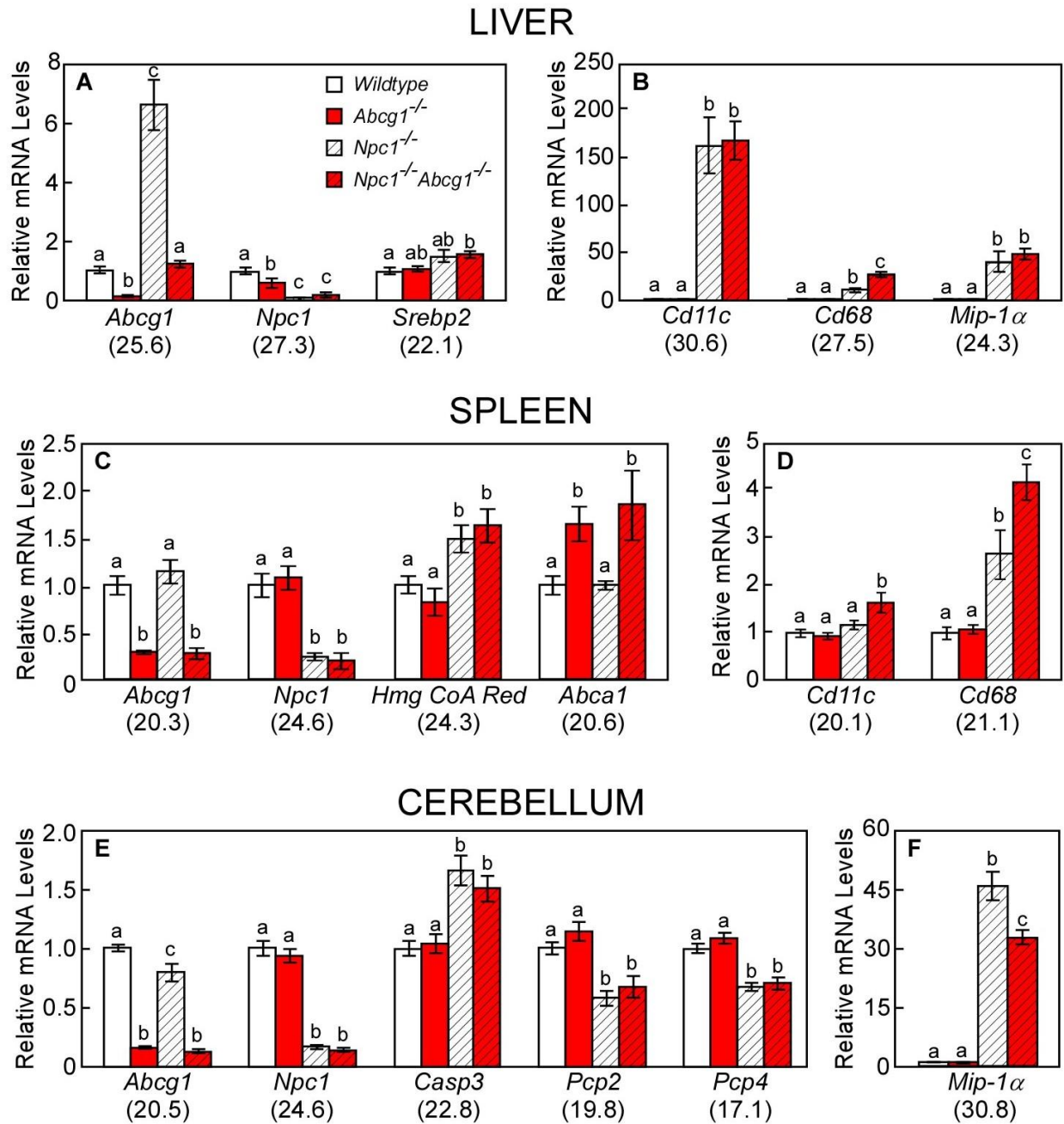
SPLEEN

CEREBELLUM

Figure 2.5 *Effect of functional deletion of ABCG1 on hepatic, spleen, and cerebellar mRNA levels in Npc1⁻ᐟ⁻ mice.* Tissues were harvested from 50-day-old *wildtype*, *Abcg1⁻ᐟ⁻*, *Npc1⁻ᐟ⁻*, and *Npc1⁻ᐟ⁻Abcg1⁻ᐟ⁻* mice, and total RNA was extracted. Relative mRNA levels of select genes in liver (**A, B**), spleen (**C, D**), and cerebellum (**E, F**) were measured by qPCR using cyclophilin as the invariant housekeeping gene. Each bar represents the mean ± SEM for 6 mice. Statistically significant differences (P <0.05) between genotypes are indicated by different letters. Average Ct values for the *wildtype* group within a given tissue are indicated below each gene symbol.

and lung. Corresponding with the changes in histology, a significant increase in the mRNA levels of

Cd68 (macrosialin, a cell surface marker of monocytes and macrophages) was measured in liver (**Fig.**
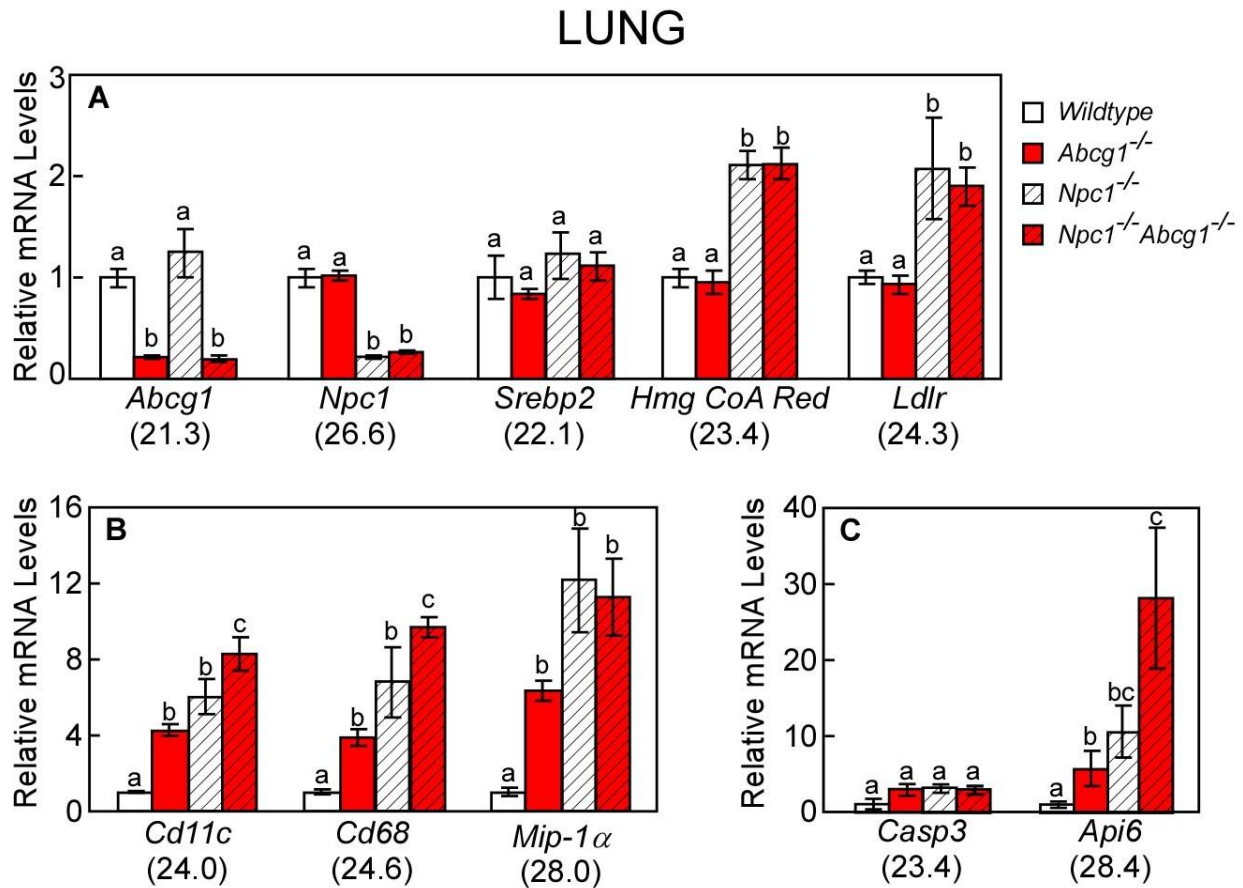
LUNG

Figure 2.6 *Effect of the functional deletion of ABCG1 on pulmonary mRNA levels in Npc1$^{-/-}$ mice.* Lungs were harvested from 50-day-old *wildtype*, *Abcg1$^{-/-}$*, *Npc1$^{-/-}$*, and *Npc1$^{-/-}$Abcg1$^{-/-}$* mice, and total RNA was extracted. Relative mRNA levels of select genes related to cholesterol metabolism (**A**), pro-inflammatory state (**B**), and apoptosis (**C**) were measured by qPCR using cyclophilin as the invariant housekeeping gene. Each bar represents the mean ± SEM for 6 mice. Statistically significant differences (P <0.05) between genotypes are indicated by different letters. Average Ct values within lung for the *wildtype* group are indicated below each gene symbol.

2.5B), spleen **(Fig. 2.5D)**, and lung **(Fig. 2.6B)** from *Npc1$^{-/-}$Abcg1$^{-/-}$* compared to *Npc1$^{-/-}$* indicating

enhanced macrophage infiltration in these peripheral tissues. As in cerebellum, there was no increase in

the mRNA levels of pro-inflammation cytokines, *Mip1α* and *Cd11c,* in liver **(Fig. 2.5B)**; however, Cd11c

was significantly increased in *Npc1$^{-/-}$Abcg1$^{-/-}$* spleen **(Fig. 2.5D)** and lung **(Fig. 2.6B)** in contrast to *Npc1$^{-/-}$*

mice. Additionally in lung, significant increases were measured in the mRNA levels of *apoptosis*

inhibitor 6 (*Api6*) but not *Caspase 3 and 6* **(Fig. 2.6C,** *Casp6* not shown)**. Although cholesterol balance

and neurodegeneration were unchanged in *Npc1$^{-/-}$Abcg1$^{-/-}$* mice compared to *Npc1$^{-/-}$*, markers of

inflammation were significantly increased in spleen and lung, which could possibly provide an

explanation for the decreased survival rate.

ABCG1 is not required for the anti-inflammatory effects of LXR agonist in *Npc1*$^{-/-}$ mice:

Administration of the LXR agonist, T0901317 (Tcmpd), was shown to significantly extend lifespan by ~10 days and to have anti-inflammatory effects in *Npc1*$^{-/-}$ mice (Repa et al., 2007). As *Abcg1* is upregulated by Tcmpd administration and may play an important role in limiting macrophage infiltration and the inflammatory response in peripheral organs of *Npc1*$^{-/-}$ mice, experiments were designed to determine if ABCG1 was required for the anti-inflammatory effects of an LXR agonist in *Npc1*$^{-/-}$ mice. To test this, primary macrophages were harvested from the peritoneal cavity of *Npc1*$^{-/-}$ and *Npc1*$^{-/-}$*Abcg1*$^{-/-}$ mice and then were treated in culture with Tcmpd (1μM) in order to measure levels of cytokine secretion as well as relative mRNA levels of pro-inflammatory cytokines **(Fig. 2.7)**. Of the 7 cytokines (IFNγ, IL-1β, IL-6, IL-10, IL-12p70, KC/GRO, and TNF) measured, all showed a trend to be secreted at a higher concentration from *Npc1*$^{-/-}$*Abcg1*$^{-/-}$ macrophages compared to *Npc1*$^{-/-}$; although, only TNF was significantly different between the two genotypes **(Fig. 2.7A)**. Regardless of the presence of ABCG1, Tcmpd was able to significantly reduce the level of secretion for all 7 cytokines tested compared to vehicle treated controls **(Fig. 2.7A-C,** not shown for IL-1β, IL-6, IL-12p70, or KC).

As Tcmpd treatment brought the "resting" cytokine secretion down to an undetectable level in both *Npc1*$^{-/-}$ and *Npc1*$^{-/-}$*Abcg1*$^{-/-}$ macrophages, lipopolysaccharide (LPS), which is known to elicit an immune response, was used to challenge the macrophages and then the effects of Tcmpd were reevaluated. After 4 h of LPS stimulation, the secretion of TNF **(Fig. 2.7A)**, IFNγ **(Fig. 2.7B)**, and IL-10 **(Fig. 2.7C)** from vehicle treated *Npc1*$^{-/-}$*Abcg1*$^{-/-}$ macrophages was significantly higher than the cytokine secretion from *Npc1*$^{-/-}$ macrophages. Tcmpd administration was able to significantly reduce the level of cytokine secretion from *Npc1*$^{-/-}$*Abcg1*$^{-/-}$ macrophages compared to vehicle treated; although, it was unable to reduce the level to as low as what was measured in Tcmpd treated *Npc1*$^{-/-}$ macrophages after LPS stimulation **(Fig. 2.7A-C)**.

In order to further test the effectiveness of an LXR agonist at reducing inflammation in *Npc1*$^{-/-}$*Abcg1*$^{-/-}$ mice, the relative mRNA levels of select LXR target genes and pro-inflammatory cytokines were
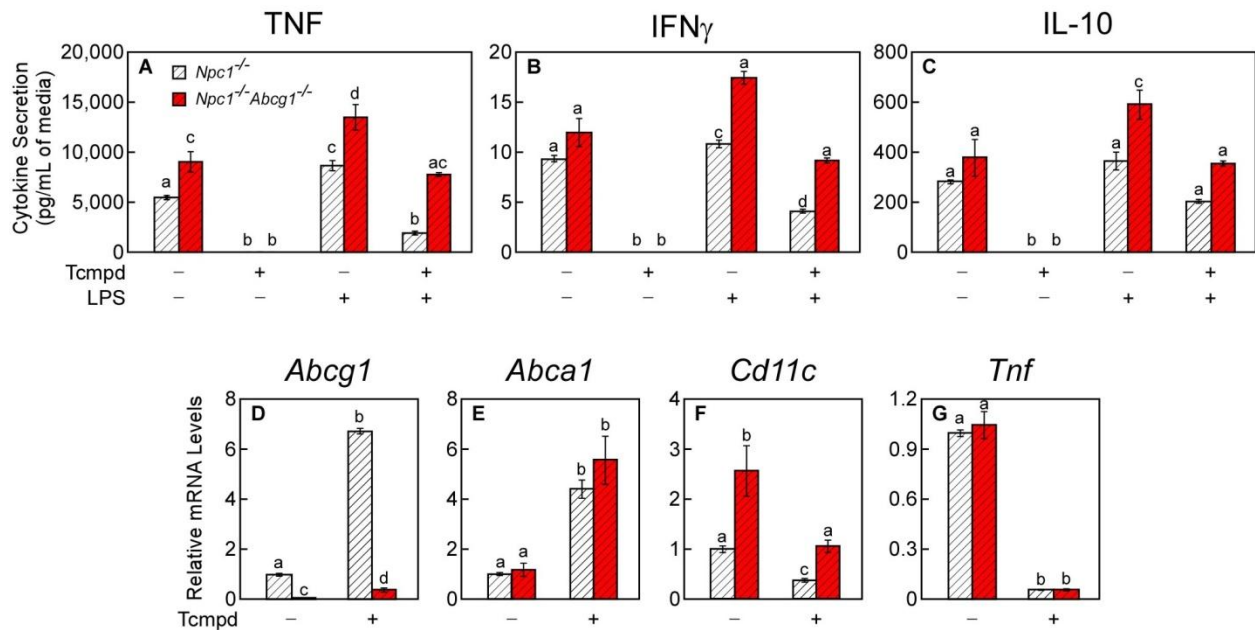
Figure 2.7 *Effect of Abcg1 deletion on the anti-inflammatory effects of Tcmpd in Npc1⁻/⁻ mice.* Thioglycollate-elicited peritoneal macrophages (from 50-day-old mice) were obtained from *Npc1⁻/⁻* and *Npc1⁻/⁻Abcg1⁻/⁻* mice. These cells were plated in FBS-containing culture media, pretreated for 16h with vehicle or T0901317 (Tcmpd, 1µM), and then stimulated for 4hr with lipopolysaccharide (LPS, 100ng/mL). Media was harvested to measure the protein levels of cytokines secreted by the macrophages: TNF (**A**), INF-γ (**B**), and IL-10 (**C**). Another set of macrophages were harvested for RNA isolation 16h after treatment with vehicle or T0901317 (1µM). The relative mRNA levels of LXR target genes, *Abcg1* (**D**) and *Abca1* (**E**), and pro-inflammatory cytokines, *Cd11c* (**F**) and *Tnf* (**G**) were determined by qPCR using β-actin as the invariant housekeeping gene. Each bar represents the mean ± SEM of triplicate wells. Statistically significant differences (P <0.05) are indicated by different letters.

measured in macrophages after Tcmpd treatment. The mRNA levels for *Abcg1* and *Npc1* were measured

to confirm the genotype of the macrophages. *Npc1* was not detectable compared to *wildtype* control

macrophages for any of the *Npc1⁻/⁻* or *Npc1⁻/⁻Abcg1⁻/⁻* groups (data not shown). The mRNA level of *Abcg1*

was only detectable at levels comparable with *wildtype* in the *Npc1⁻/⁻* group; however, it was significantly

upregulated by treatment with Tcmpd in both groups, albeit to a much smaller extent in *Npc1⁻/⁻Abcg1⁻/⁻*

cells **(Fig. 2.7D)**. *Abca1* was expressed at the same level in vehicle-treated *Npc1⁻/⁻* and *Npc1⁻/⁻Abcg1⁻/⁻*

macrophages and was significantly increased by Tcmpd treatment **(Fig. 2.7E)**. Although a significant

difference was measured between genotypes in the protein level of TNF **(Fig. 2.7A)**, only the mRNA

level of *Cdllc* **(Fig. 2.7G)** not *Tnf* **(Fig. 2.7H)** was significantly increased in *Npc1⁻/⁻Abcg1⁻/⁻* cells

compared to in *Npc1⁻/⁻* macrophages. As with the protein levels of cytokines regardless of the presence of

ABCG1, Tcmpd was able to significantly reduce the mRNA levels of *Cdllc* and *Tnf* **(Fig. 2.7G-H)**,

although it was not to the same extent as in Tcmpd-treated *Npc1*$^{-/-}$ macrophages for *Cdllc*. Thus ABCG1 is not required for the effects of LXR through Tcmpd; however, it likely contributes to the overall pro-inflammatory effect in *Npc1*$^{-/-}$ mice.

ABCG1 is not required for the cholesterol altering effects of HP-β-CD in *Npc1*$^{-/-}$ mice:

A single injection of 2-hydroxypropyl-β-cyclodextrin (HP-β-CD) to a 7-day-old *Npc1*$^{-/-}$ pup was shown to significantly expand lifespan by ~25 days and to dramatically alter cholesterol synthesis within 24h (Liu et al., 2009). In addition, HP-β-CD administration to 7-day-old *Npc1*$^{-/-}$ pups significant altered mRNA levels of cholesterol and inflammation related genes in liver, as shown by: a decrease in the expression of SREBP2 target genes; an increase in the expression of LXR target genes, including *Abcg1*; and a reduction in the level of pro-inflammatory cytokines (Liu et al., 2009). As the mRNA level of *Abcg1* was upregulated after HP-β-CD, experiments were performed to determine whether ABCG1 was required for the beneficial effects of HP-β-CD in *Npc1*$^{-/-}$ mice. To test this, 4,000 mpk of HP-β-CD was administered to 49-day-old mice from each genotype and *in vivo* cholesterol synthesis rates were measured 24h after. As previously shown (Liu et al., 2010a), HP-β-CD had no effect on sterol synthesis rates in adult *wildtype* animals, but dramatically decreased the rate of synthesis in liver **(Fig. 2.8A)**, spleen **(Fig. 2.8B)**, and the whole body **(Fig. 2.8C)** of *Npc1*$^{-/-}$ mice just 24h after injection. Additionally, HP-β-CD had no effect on sterol synthesis in *Abcg1*$^{-/-}$ animals, but significantly reduced the rate in liver, spleen, and whole animal of *Npc1*$^{-/-}$*Abcg1*$^{-/-}$ mice **(Fig. 2.8A-C)**. Cholesterol synthesis rates were also significantly reduced in the kidney, adrenal, and white adipose tissue but not in lung or brain from *Npc1*$^{-/-}$ and *Npc1*$^{-/-}$*Abcg1*$^{-/-}$ mice (data not shown).

In addition to measuring the effects of HP-β-CD on *in vivo* cholesterol synthesis in *wildtype*, *Abcg1*$^{-/-}$, *Npc1*$^{-/-}$, and *Npc1*$^{-/-}$*Abcg1*$^{-/-}$ mice, livers were harvested 24h after HP-β-CD administration to evaluate the mRNA levels of pro-inflammatory and cholesterol related genes. As no significant shifts were seen in the expression of any gene after HP-β-CD in *wildtype* or *Abcg1*$^{-/-}$, only the results from *Npc1*$^{-/-}$ and *Npc1*$^{-/-}$
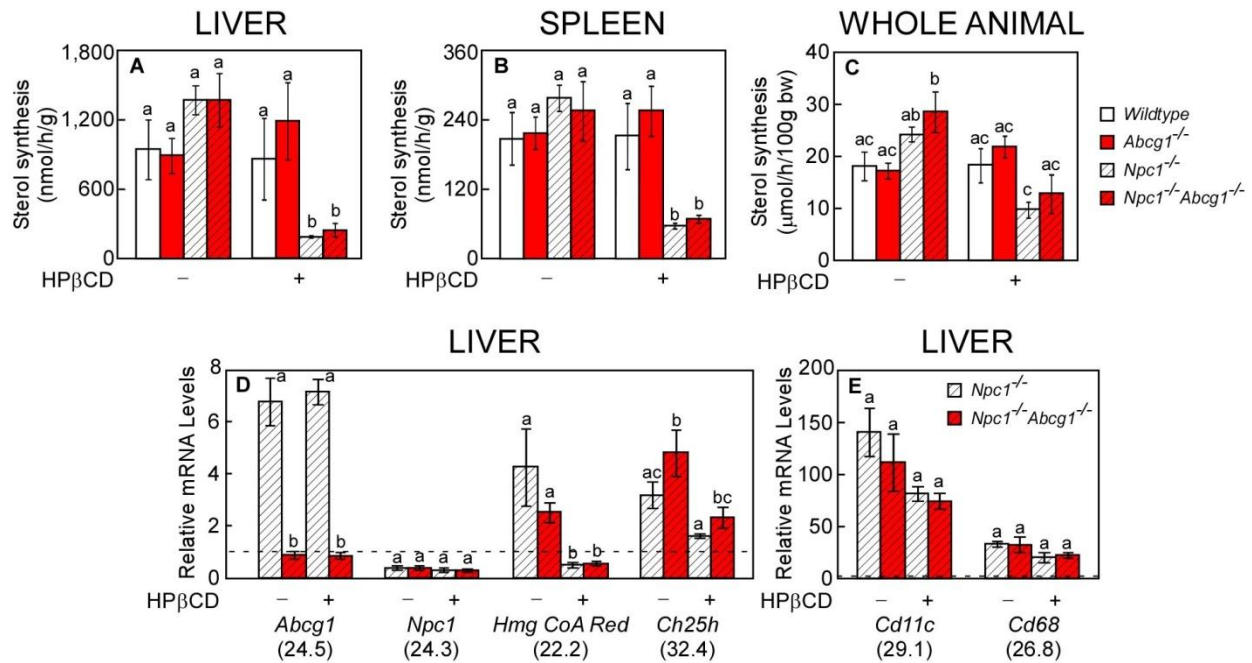
Figure 2.8 *Effect of Abcg1 deletion on the cholesterol altering effects of HP-β-CD in Npc1⁻ mice.* 49-day-old *wildtype*, *Abcg1⁻ᐟ⁻*, *Npc1⁻ᐟ⁻*, and *Npc1⁻ᐟ⁻Abcg1⁻ᐟ⁻* mice (n=3-5/group) were injected with saline or a 4,000 mpk bolus of HP-β-CD, and livers and spleens were harvested 24h later. The tissues were saponified to measure the rate of cholesterol synthesis (**A-C**) by the [³H]-water method. A second cohort of 49-day-old mice (n=6/group) were injected with saline or HP-β-CD, and livers were harvested for RNA isolation 24h later. Relative mRNA levels of select genes related to cholesterol metabolism (**D**) and pro-inflammatory state (**E**) were measured by qPCR using cyclophilin as the invariant housekeeping gene. The dotted line represents the expression level in the *wildtype* group for each gene. Average Ct values within liver for the *wildtype* vehicle-treated group are indicated below each gene symbol. Each bar represents the mean ± SEM. Statistically significant differences (P <0.05) between genotypes are indicated by different letters.

Abcg1⁻ᐟ⁻ mice are presented here (the dotted line represents the expression level in the vehicle-treated

wildtype group; **Fig. 2.8D, E**). Genotypes were confirmed by the mRNA expression of *Abcg1* and *Npc1*,

which were not altered by HP-β-CD **(Fig. 2.8D)**. Consistent with the reduction in cholesterol synthesis

rates, the SREBP2 target gene, *HmgCoARed*, was significantly reduced by HP-β-CD administration in

both *Npc1⁻ᐟ⁻* and *Npc1⁻ᐟ⁻Abcg1⁻ᐟ⁻* livers. There was a trend towards decrease expression of *cholesterol 25-*

hydroxylase (*Ch25h*) after HP-β-CD. Although there was a reduction in mRNA levels of the macrophage

marker, *Cd68*, and the pro-inflammatory cytokine, *Cd11c*; these changes were not significant 24h after

HP-β-CD administration to 49-day-old *Npc1⁻ᐟ⁻* and *Npc1⁻ᐟ⁻Abcg1⁻ᐟ⁻* mice. Overall, these data provide

evidence that ABCG1 is not required for the cholesterol altering effects of HP-β-CD in *Npc1⁻ᐟ⁻* mice.

2.5 Discussion

Niemann Pick Type C Disease (NPC) is a disorder in which free cholesterol is trapped in the lysosome, which leads to a disruption in cholesterol balance resulting in accumulating inflammation and cell death. This causes progressive hepatomegaly, splenomegaly, pulmonary dysfunction, and neurodegeneration until the body succumbs to premature death. Increasing LXR activation by administration of a synthetic ligand (Tcmpd) was shown to extend the lifespan of the $Npc1^{-/-}$ mouse model by approximately 10 d; while a reduction in LXR activity by genetic deletion of $Lxr\beta$ in the $Npc1^{-/-}$ mouse was shown to decrease the survival rate by 10 d (Repa et al., 2007). Tcmpd was shown to increase cholesterol efflux from the brain, reduce neuroinflammation, and enhance neuronal survival (Repa et al., 2007); however, the molecular mechanism through which LXR activation was modulating NPC disease progression was not further elucidated. As Tcmpd treatment significantly increased the expression of two cholesterol efflux ABC transporters, $Abca1$ and $Abcg1$, in the brain, they serve as likely molecular candidates. While loss of ABCA1 was shown to have no effect of lifespan in $Npc1^{-/-}$ mouse (Repa et al., 2007), this present study showed that the functional deletion of ABCG1 lead to a significant decrease in lifespan in $Npc1^{-/-}$ mouse (**Fig. 2.1**), which mirrored the 10d reduction in survival observed in the $Npc1^{-/-}$ $Lxr\beta^{-/-}$. This novel finding suggests that ABCG1 plays a role in preventing NPC disease progression, but why did the $Npc1^{-/-}Abcg1^{-/-}$ die earlier than their $Npc1^{-/-}$ littermates? In order to establish why survival was reduced in the $Npc1^{-/-}Abcg1^{-/-}$ mice, tissues were collected from 50-day-old *wildtype*, $Abcg1^{-/-}$, $Npc1^{-/-}$, and $Npc1^{-/-}Abcg1^{-/-}$ mice for sterol balance studies, histological evaluation, and mRNA analysis.

No significant differences were uncovered between relative organ weights, cholesterol concentration, or cholesterol synthesis rates in any organ from $Npc1^{-/-}Abcg1^{-/-}$ compared with $Npc1^{-/-}$ mice (**Fig. 2.2**). Previously, lipid content had been measured in $Abcg1^{-/-}$ mice, which had a more dramatic response to being fed a high-fat, high-cholesterol diet than wildtypes, as their livers and lungs had significantly higher concentrations of cholesterol, phospholipids, and triglyercides (Kennedy et al., 2005). However, this is the first study to evaluate *de novo* cholesterol synthesis rates in $Abcg1^{-/-}$ mice. Unlike $Npc1^{-/-}$ mice which

have increased sterol synthesis in virtually every tissue tested with the exception of brain (Xie et al., 1999a), *Abcg1*^{-/-} mice on a standard chow with low cholesterol content showed no change in sterol synthesis compared to *wildtype* animals (**Fig. 2.2E, F**). However, future studies to further evaluate cholesterol synthesis in *Abcg1*^{-/-} mice after a high-fat, high-cholesterol diet as was used in Kennedy's study may be informative. The only significant difference in sterol measured between *Abcg1*^{-/-} and *wildtype* mice in this study was an increase in the cholesterol concentration in *Abcg1*^{-/-} lung (**Fig. 2.2C**). This is not unexpected as even on a low cholesterol diet, *Abcg1*^{-/-} mice have been shown to progressively accumulate cholesterol within lung (Baldan et al., 2006b; Wojcik et al., 2008); however, this is the first report showing a significant difference in the total cholesterol concentration within lung as early as 7 weeks of age. This anomaly is likely due to a difference in the background of the *Abcg1*^{-/-} mice strain used as the mice in this study were on a mixed C57BL/6-BALB/c background while all previous studies utilized *Abcg1*^{-/-} mice on a pure C57BL/6 background.

There was also no difference evident in Purkinje cell survival or neuroinflammatory burden in the cerebella of *Npc1*^{-/-} and *Npc1*^{-/-}*Abcg1*^{-/-} mice by histological analysis (**Fig. 2.3)** or by measurement of relative mRNA levels of Purkinje cell and inflammation markers (**Fig. 2.5E, F**). This suggests that loss of ABCG1 in brain does not worsen neurodegeneration in NPC disease progression; however, it does not address the effects of an increase in Abcg1 expression as was seen after Tcmpd administration in *Npc1*^{-/-} mice. Although Abcg1 is expressed in neurons, astrocytes, and microglia (Tarr et al., 2008) and is thought to play an important role in transporting cholesterol within the brain (Karten et al., 2006), no obvious neuronal phenotype was been reported in *Abcg1*^{-/-} mice (Kennedy et al., 2005; Bojanic et al., 2010). This was perplexing to the field until another ABC transporter, ABCG4, was found to be coexpressed and to have overlapping functions with ABCG1 only in brain (Tarr et al., 2008). While *Abcg1* is broadly expressed throughout the body and is regulated by LXR, *Abcg4* has only been identified in mouse brain and retina and is not an LXR target gene (Tarr et al., 2008). It is possible that ABCG4 is compensating for the loss of ABCG1 in the brains of *Npc1*^{-/-}*Abcg1*^{-/-} mice; therefore, it may be valuable to overexpress

Abcg1 in *Npc1⁻ᐟ⁻* mice using a transgenic mouse in order to determine the direct of effects of ABCG1 on

neurodegeneration in NPC disease.
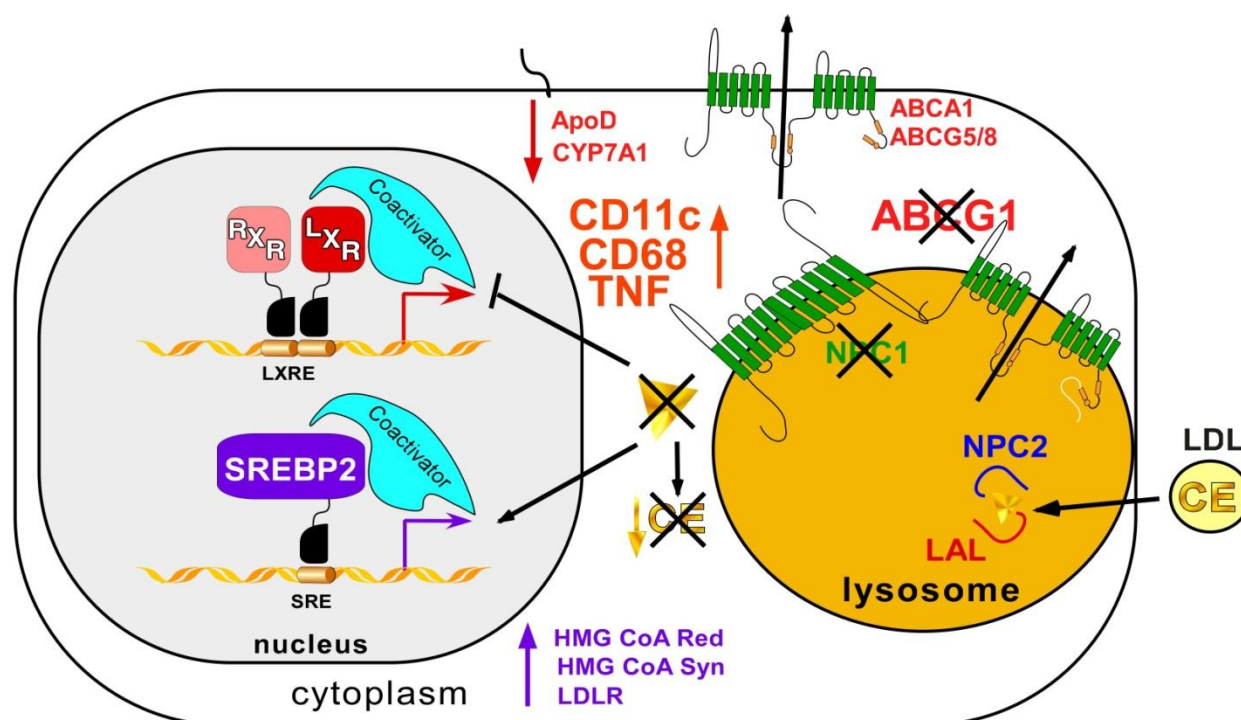
Figure 2.9 *Proposed mechanism for the effect of ABCG1 deletion in Npc1⁻ᐟ⁻ mice.* In cells without functional NPC1, the egress of free cholesterol (triangle) from the lysosome is blocked leading to massive lipid accumulation, enhanced cellular sterol synthesis (via activation of SREBP2), decreased cholesteryl ester (CE) formation, reduced oxysterol formation and in turn sterol elimination (via lack of LXR activation), and increased inflammation. When the ABC transporter, ABCG1, which was recently found to be located within the lysosomal compartment, is further deleted, this does not increase overall cholesterol levels, but instead leads to increased cytokine production and inflammation. This is likely due to ABCG1's role in the intracellular transport of cholesterol in macrophages.

While there were no changes in brain, infiltration of foamy macrophages (**Fig. 2.4**) and pro-

inflammatory mRNA markers (**Fig. 2.5-6**) were significantly increased in peripheral organs, particularly

in lung and spleen, of *Npc1⁻ᐟ⁻Abcg1⁻ᐟ⁻* compared to *Npc1⁻ᐟ⁻* mice. Numerous studies have reported a critical

role of ABCG1 in maintaining pulmonary cholesterol homeostasis and that *Abcg1⁻ᐟ⁻* mice have a

progressive increase in foamy macrophages within the alveolar spaces of the lungs (Baldan et al., 2006b;

Thomassen et al., 2007; Baldan et al., 2008; Wojcik et al., 2008)). This, however, is the first account

comparing the lungs from *wildtype*, *Abcg1⁻ᐟ⁻*, *Npc1⁻ᐟ⁻*, and *Npc1⁻ᐟ⁻Abcg1⁻ᐟ⁻* mice. Since total levels of

cholesterol in lung were increased as early 7 weeks of age, it was not unanticipated that *Abcg1⁻ᐟ⁻* lungs

contained small infiltrating macrophages (**Fig. 2.4B**) and had increased levels pro-inflammatory cytokines compared to wildtype controls (**Fig. 2.6B**). The increase in cytokines (**Fig. 2.6B**) and the large foamy macrophages scattered through the lungs of *Npc1*$^{-/-}$ mice (**Fig. 2.4C**) had also been previously reported (Ramirez et al., 2010); but, in this study it was shown that *Npc1*$^{-/-}$*Abcg1*$^{-/-}$ had more invading macrophages (**Fig. 2.4D**) and higher expression of cytokines (**Fig. 2.6B**) and apoptotic genes (**Fig. 2.6C**) in lung than either *Npc1*$^{-/-}$ or *Abcg1*$^{-/-}$ mice alone.
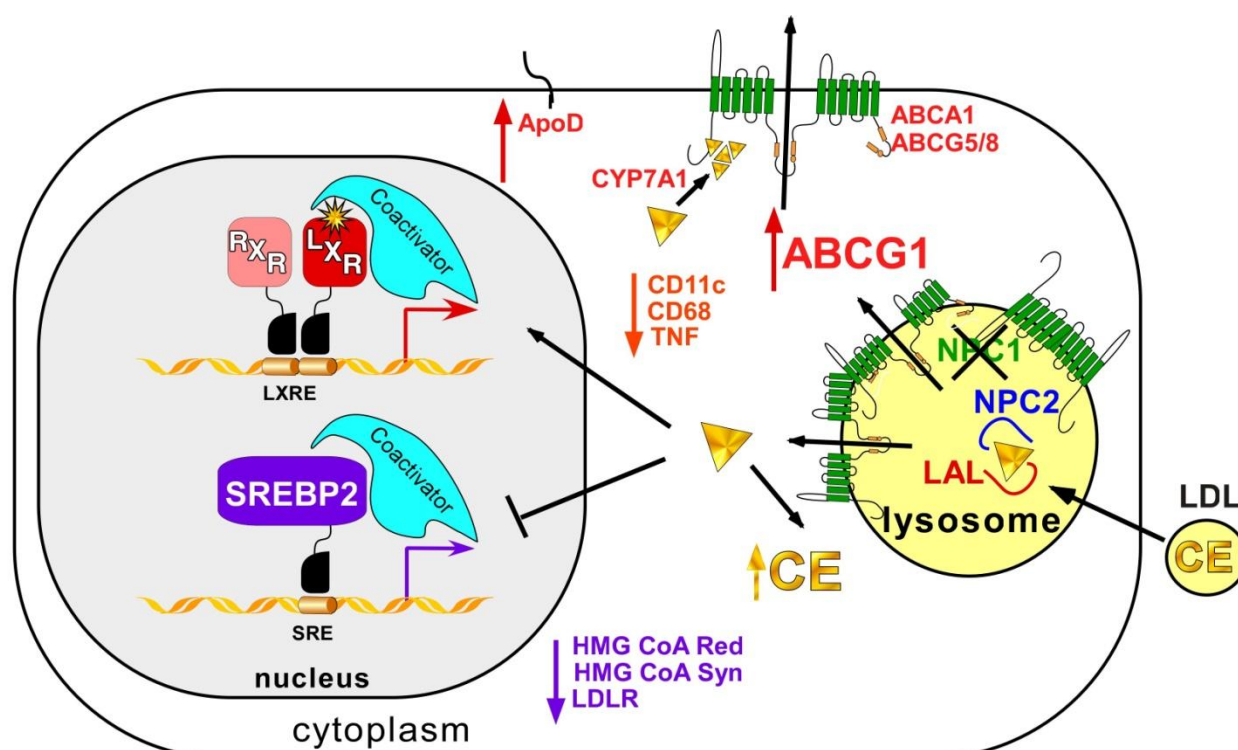
Figure 2.10 *Hypothetical model of the potential beneficial of overexpressing ABCG1 in Npc1*$^{-/-}$ *mice.* In cells without functional NPC1, the egress of free cholesterol (triangle) from the lysosome is blocked leading to massive lipid accumulation, which leads to increased sterol synthesis (via SREBP2), reduced oxysterol formation and in turn sterol elimination through the ABC transporters (via lack of LXR activation), and increased inflammation. Increasing the expression or the activity of ABCG1, which was recently found to be located within the lysosomal compartment, could provide an alternative mechanism to NPC1 to promote the efflux of cholesterol from the lysosome allowing for: rapid decreases in sterol synthesis rates (via SREBP2), increases in cholesteryl ester (CE) formation and activation of LXR which would further increase sterol efflux (via ABC transporters), and ultimately decreases inflammation, which could promote cell survival.

The most startling phenotype was seen in spleens of *Npc1*$^{-/-}$*Abcg1*$^{-/-}$, which had not been previously reported in *Abcg1*$^{-/-}$ mice. Whereas only a few small scattered macrophages could be found in *Npc1*$^{-/-}$ mice (**Fig. 2.4G**), an overwhelming number of very large foamy macrophages were found throughout the

spleen of $Npc1^{-/-}Abcg1^{-/-}$ mice (**Fig. 2.4H**). This was supported by a significant increase in the mRNA levels of Cd11c and Cd68 in spleens of $Npc1^{-/-}Abcg1^{-/-}$ compared to $Npc1^{-/-}$ or $Abcg1^{-/-}$ mice alone (**Fig. 2.6D**). In addition to its role in inflammation, Abcg1 has been suggested to be involved in surfactant secretion from type II alveolar epithelial cells, as 8 month old $Abcg1^{-/-}$ have abnormally large lamellar bodies and dysregulated levels of surfactant genes and lipids (Baldan et al., 2006b). Changes in the mRNA levels of surfactant proteins were not seen in whole lungs of the $Abcg1^{-/-}$, $Npc1^{-/-}$, and $Npc1^{-/-}Abcg1^{-/-}$ compared to *wildtype* littermates at any point in the $Npc1^{-/-}Abcg1^{-/-}$ lifespan (measured weekly until 80 days of age, data not shown). It is possible that other cell types in lung masked the differences and that changes may have been uncovered if primary type II alveolar epithelial cells were evaluated, which will be addressed in future studies.

Finally, although *Abcg1* expression was shown to be increased in $Npc1^{-/-}$ tissues after administration of therapeutic agents that extended lifespan, ABCG1 was not shown not to be required for the beneficial effects of the LXR agonist (**Fig. 2.7**) or HP-β-CD (**Fig. 2.8**) in the $Npc1^{-/-}$ mice. While Tcmpd treatment was able to significantly decrease LPS-stimulated cytokine secretion in $Npc1^{-/-}Abcg1^{-/-}$ macrophages, it was not reduced to the same extent as in $Npc1^{-/-}$ macrophages (**Fig. 2.7**). This suggests that although ABCG1 is not necessary for the reduction in inflammation seen after Tcmpd in $Npc1^{-/-}$ mice, it does contribute to the effect. As for ABCG1's role in HP-β-CD, lack of functional ABCG1 had no effect on the cholesterol altering effects of HP-β-CD in 50-day-old $Npc1^{-/-}$ mice (**Fig. 2.8**). Although the overall conclusion from the treatment studies in $Npc1^{-/-}Abcg1^{-/-}$ mice is that ABCG1 is not necessary for the effects; these studies do not rule out that an increase in *Abcg1* expression alone could have a beneficial effect in $Npc1^{-/-}$ mice. Given the importance of ABCG1 in cholesterol trafficking in lung and the fact that HP-β-CD, the most promising treatment for NPC, has no effect on the pulmonary disease in NPC (Ramirez et al., 2010), it may be particularly interesting to overexpress *Abcg1* in $Npc1^{-/-}$ mice and evaluate the lung phenotype. If ABCG1 is shown to have beneficial effects, it may be possible to co-administer a drug which increases *Abcg1* expression along with HP-β-CD.

Overall these data suggest that ABCG1 plays an important role in NPC disease progression (**Fig. 2.9**), as $Npc1^{-/-}Abcg1^{-/-}$ die significantly earlier than their $Npc1^{-/-}$ littermates. This is not due to changes in cholesterol balance or neurodegeneration, but instead appears to be through increased inflammation in peripheral organs, particularly in lung and spleen. Therefore, it will be of interest to investigate whether overexpression of *Abcg1* (**Fig. 2.10**) or treatments with compounds that increase the *Abcg1* expression or activity could be beneficial to NPC.

CHAPTER THREE:

Evaluating the Acute Effects of Cyclodextrin in the Mouse Model for Niemann Pick Type C Disease

3.1 Abstract

A single injection of 2-hydroxypropyl-β-cyclodextrin (HP-β-CD) to *Npc1*$^{-/-}$ mice results in delayed neurodegeneration, decreased inflammation, and prolonged lifespan. Changes in sterol balance observed in *Npc1*$^{-/-}$ mice 24h after HP-β-CD administration suggest that HP-β-CD promotes the release of lysosomal cholesterol, which accumulates in Niemann Pick Type C disease. To further elucidate HP-β-CD's mechanism of action, studies were performed to evaluate the time course of the HP-β-CD's effects. Within 3h after HP-β-CD administration, decreases in cholesterol synthesis and corresponding gene expression levels, as well as increases in hepatic cholesteryl ester levels occurred in *Npc1*$^{-/-}$ mice. In addition, no changes in cholesterol content in plasma or urine were observed after HP-β-CD, which suggest that HP-β-CD does not simply carry cholesterol from the lysosome into the bloodstream for urinary excretion. Although mRNA levels of proinflammatory cytokines are significantly reduced 24h after HP-β-CD, these changes were not apparent within 12h of treatment. Finally, gene expression changes related to sterol homeostasis in *Npc1*$^{-/-}$ mice following HP-β-CD were confirmed in primary cultured cells. Taken together, these results show that HP-β-CD works in *Npc1*$^{-/-}$ mice by freeing the trapped cholesterol from the lysosome of each cell very rapidly and then releasing the cholesterol intracellularly for normal sterol processing.

3.2 Introduction

Cyclodextrins (CDs) are cyclic oligosaccharides composed of 6, 7, or 8 glucopyranosides, which are called α, β, or γ-CD respectively. CDs have a distinctive barrel shape with a hydrophilic exterior that makes the compound water-soluble and with a hydrophobic core that prefers to be filled with small

hydrophobic molecules, such as lipids. Both of these properties make CDs ideal vehicles to increase the solubility of hydrophobic drugs; thus, CDs have been approved by the Food and Drug Administration (FDA) as delivery agents (Irie et al., 1992; Thompson, 1997; Gould et al., 2005; Stella et al., 2008). In addition to the natural CDs that are products of starch, several modified forms of β-CD have been synthesized which have fewer toxic effects *in vivo*, including 2-hydroxypropyl (HP-β-CD) and sulfobutylether (SBE-β-CD). These CDs were considered to possess no therapeutic effect and to simply serve as benign carriers of therapeutics, which would be released into the bloodstream, allowing CDs to be excreted intact separately through the kidneys (Stella et al., 2008). That is until 2009 when a single dose of HP-β-CD led to dramatic sterol balance changes in 7-day-old $Npc1^{-/-}$ pups in just 24h and significantly extended their lifespan (Liu et al., 2009).

Niemann-Pick Type C (NPC) disease is a rare autosomal recessive disorder in which a defect disrupts the intracellular transport of cholesterol from the late endosome/early lysosome (LE/L) leading to massive lipid accumulation. Mutations in NPC1 or more rarely in NPC2, both lysosomal proteins required to traffic cholesterol, lead to NPC (Patterson et al., 2001; Patterson, 2003). NPC disease presents as hepatic steatosis, splenomegaly, pulmonary dysfunction, and neurodegeneration resulting in premature death, which typically occurs during adolescence in humans (Vanier, 2010) and around 85d in the $Npc1^{-/-}$ mouse model (Liu et al., 2008). As there are no FDA approved treatments to extend lifespan for NPC patients, the $Npc1^{-/-}$ mouse has been used as a model in an attempt to identify an effective therapy. Therefore when HP-β-CD was shown to extend the lifespan of $Npc1^{-/-}$ mice to 118d (Liu et al., 2009), it quickly became the focus of the NPC research community.

Since the initial study, HP-β-CD therapy has been moved into patients with NPC disease, and much work has been undertaken to better understand how CD is working in $Npc1^{-/-}$ animal models. Notably, serial injections of HP-β-CD were shown to double the lifespan of the $Npc1^{-/-}$ mouse (Davidson et al., 2009; Ramirez et al., 2010), and continuous intracerebroventricular administration was shown to dramatically rescue Purkinje cell loss of the cerebellum (Aqul et al., 2011). In addition, HP-β-CD does

not require a functional NPC1 or NPC2 protein to work, as HP-β-CD has been shown to significantly decrease hepatic cholesterol synthesis in just 24h in the $Npc1^{-/-}$, $Npc2^{-/-}$, and the rare $Npc1^{-/-}Npc2^{-/-}$ double knockout mice (Ramirez et al., 2011). Studies performed within a variety of tissues harvested 24h after a single HP-β-CD injection to 7- or 49-day-old $Npc1^{-/-}$ mice have shown dramatic changes in sterol balance, including: a decrease in cholesterol synthesis rates; an increase in the ratio of esterified/unesterified cholesterol; down-regulation of the sterol regulatory element-binding protein 2 (SREBP2) and its target genes; and increased expression of liver X receptor (LXR) target genes (Liu et al., 2009; Liu et al., 2010a). These measurable shifts in sterol homeostasis serve as surrogate markers to indicate that the cell is responding to a state of cytosolic cholesterol excess. Since these changes were observed after HP-β-CD administration to $Npc1^{-/-}$ mice only and not seen for wildtype mice, they further suggest that the excess unesterified cholesterol is being released from the LE/L compartment in $Npc1^{-/-}$ mice. Overall these data suggest that HP-β-CD is able to facilitate the release of the lysosomal pool of unesterified cholesterol from NPC-deficient cells within 24h.

Although virtually all studies thus far have been performed 24h after HP-β-CD, a single time course experiment using ^{14}C-labelled HP-β-CD in 49-day-old mice demonstrated that it is cleared from the plasma within 3h and from the whole body within 6h after a subcutaneous dose of 4000 mg/kg body weight [mpk] (Liu et al., 2010a). Therefore, a series of studies were performed in $Npc1^{-/-}$ mice to evaluate the time course of changes elicited by HP-β-CD, 1-12h after administration, to further understand its mechanism of action. The experiments were designed: 1) to measure the rate of change in lipid balance and corresponding mRNA levels; 2) to determine whether a CD/cholesterol complex is evident at any time in plasma or urine; 3) to evaluate how rapidly inflammation is reduced; and 4) to assess the direct effects of HP-β-CD and SBE-β-CD on primary cells (neurons and macrophages) in culture. Together, these studies provide novel insights into the mechanism by which HP-β-CD frees trapped unesterified cholesterol from the LE/L of cells lacking NPC1.

3.3 Materials and Methods

Animals and Treatments

Heterozygous (*Npc1*^{+/-}) mice on a BALB/c background were bred to generate wildtype (*Npc1*^{+/+}) and

homozygous-null (*Npc1*^{-/-}) littermates (Loftus et al., 1997). Mice were group-housed in plastic cages

containing wood chip bedding in an animal facility with temperature-controlled rooms (23 ± 1°C) and a

maintained light cycle (12h light on/12h off). The mice were allowed *ad libitum* access to water and a

standard rodent chow containing 0.02% w/w cholesterol (7001; Harlan Teklad, Madison, WI). Mice were

genotyped (Loftus et al., 1997) upon weaning, between 19-21 days of age. For all *in vivo* studies, 49-day-

old mice were given a single subcutaneous (sc) injection of HP-β-CD (H107, Sigma) at 4000 mpk or

vehicle (saline at equivalent volume of 20 μl/g body weight (bw)). When mice were used as a source of

cells for culture, macrophages were obtained from 2-month-old mice, and hippocampal neurons from 1-

day-old pups. As no differences in response to HP-β-CD were evident between male and female mice in

previous reports (Liu et al., 2008; Liu et al., 2009; Liu et al., 2010a; Ramirez et al., 2010; Aqul et al.,

2011; Ramirez et al., 2011), these studies utilized either equal numbers of males and females per group

(**Figs. 3.1, 3.4D, 3.5-7, 3.9**) or only females (**Figs. 3.2, 3.3, 3.4A-C**). All animal research was conducted

in conformity with the Public Health Service Policy on Humane Care and Use of Laboratory Animals,

and all experiments were performed with prior approval from University of Texas Southwestern Medical

Center's Institutional Animal Care and Use Committee.

Measures of cholesterol balance in mice

Npc1^{+/+} and *Npc1*^{-/-} mice (n=4 to 6 mice/group) were given a sc injection of HP-β-CD or saline. At

time points ranging from 0 to 12h after the injection, the mice were weighed and euthanized

(exsanguinated under deep anesthesia) to harvest tissues for the following analyses:

Sterol synthesis rates. Exactly 1h prior to euthanasia and tissue harvest, one cohort of mice were

given an intraperitoneal (ip) injection of 1.76 mCi of [3H] water per g bw. Aliquots of liver and spleen

were quickly removed, weighed, and saponified in alcoholic KOH. Organ contents of [^{3}H]-labeled digitonin-precipitable sterols (DPS) were determined as previously described (Dietschy et al., 1984). The rate of sterol synthesis is reported as the nmol of [^{3}H] incorporated into DPS per hour per gram of tissue.

Tissue Cholesterol Concentrations. The aliquots of liver and spleen in KOH used for the synthesis determination were also used to measure total cholesterol content. Briefly, the cholesterol was extracted and quantified by gas chromatography (GC) with a stigmastanol internal standard as previously described (Turley et al., 1994). The total cholesterol concentration of each organ is expressed as the mg of cholesterol per gram of tissue.

Unesterified/Esterified Cholesterol Determinations. From a different cohort of mice, livers were flash frozen and were crushed into a powder, which was weighed and digested in a 2:1 chloroform to methanol solution. Free and esterified cholesterol were separated using a silica column (Sep-Pak Vac RC; Waters Corp., Milford, MA) and were quantified by GC as previously described (Beltroy et al., 2007). The cholesterol concentration of each organ is reported as the mg of unesterified cholesterol or cholesteryl ester per gram of tissue.

Plasma Lipoprotein Profiles. Blood samples were collected using EDTA coated syringes from the ascending vena cava of anesthetized mice. Injection times for HP-β-CD were staggered so that all animals were exsanguinated at the same point during the light cycle (9h after lights on or Zeitgeber time (ZT) 9). Plasma was separated from red blood cells by centrifugation at 1×10^4x g for 10min at 4°C. Equal volumes of plasma/mouse were pooled for similarly treated animals (n=2/group) and samples were provided to a core facility where lipoprotein profiles were obtained using fast protein liquid chromatography (FPLC) as described previously (Valasek et al., 2005b). Total cholesterol concentrations in eluted fractions were measured using both an enzyme-based method (Infinity Cholesterol Reagent: 401-500P, Sigma) and by solvent extraction followed with measurement by GC (as explained above). No differences were found between the two methods, so only values from the enzyme-based method, expressed as μg of total cholesterol per fraction, are reported.

Urine Cholesterol Concentration. After receiving an injection of saline or HP-β-CD 2h before lights out (ZT 10), a separate cohort of mice were placed immediately into individual metabolic chambers in a maintained animal facility to collect urine. While in the chamber, the mice were allowed *ad libitum* access to food and water. 48h later the collection was stopped. The screens above urine collection tubes were cleared of feces and food crumbles. The dried urine was rehydrated with sterile water and allowed to drip into the collection tube. Urine collections were spun at 1×10^4x g for 5 min at 4°C, and the supernantants were stored at 4°C. Later, the samples were dried down and then saponified in alcoholic KOH. Total cholesterol was extracted and measured by GC as described above. The cholesterol content of each urine sample is reported as μg of total cholesterol per 24h.

Measurement of relative mRNA levels

Tissues. *Npc1*$^{+/+}$ or *Npc1*$^{-/-}$ mice (n=4 mice/group) were given a single sc injection of HP-β-CD (4,000 mpk) or saline and were euthanized 0 to 12h later. Injection times were staggered so that all tissues were harvested at the same point during the light cycle (ZT 9). Mice were exsanguinated; then liver, spleen, and ileum (defined as the mucosae from the distal third of the small intestine) were collected and flash-frozen in liquid nitrogen. The tissues were stored at -80°C until total RNA was isolated using RNA STAT-60 (Tel-Test, Inc.). RNA concentrations were determined by absorbance at 260nm with a Thermo Scientific Nanodrop 100 Spectrophotometer. 2 μg of total RNA was treated with RNase-free DNase (Roche) and reverse-transcribed into cDNA with SuperScript II (Invitrogen) as previously described (Kurrasch et al., 2004; Valasek et al., 2005b). The cDNA was used to perform quantitative real-time PCR (qPCR) with the Applied Biosystems 7900HT sequence detection system. Each qPCR was analyzed in duplicate and contained in a final volume of 10 μl: 25 ng of cDNA, each primer at 150 nM, and 5 μl of 2x SYBR Green PCR Master Mix (Applied Biosystems). The nucleotide sequences of the primers used in this chapter are listed in Table C.2 of Appendix C. Results were evaluated by the comparative cycle number at threshold (C_T) method (Schmittgen et al., 2008) using cyclophilin as the

invariant housekeeping gene (Dheda et al., 2004; Kosir et al., 2010), and mRNA levels were arithmetically adjusted to a unit of 1 for the control group.

Primary Macrophages. Npc1$^{+/+}$ or *Npc1$^{-/-}$* mice (n=4 to 6 mice/group) received a 1 mL ip injection of 3% thioglycollate (autoclaved and aged for 3 months; 211717, Becton Dickinson) to elicit macrophages. Three days later, mice were euthanized, and macrophages were harvested from the peritoneal cavity by sterile lavage using ice-cold PBS. Lavages from mice of the same genotype were pooled together, and cells were collected by centrifugation for 5min at 150x g at 4°C. Cell pellets were resuspended in in medium [high-glucose DMEM (Invitrogen) containing 10% heat-inactivated fetal calf serum (FBS; Atlanta Biologicals) and 1% Pen/Strep (Invitrogen)]. The primary macrophages were counted and plated at 1.05x10^5 cells/cm^2 in tissue-culture treated plates (Corning). Once plated, the cells were maintained in a humid incubator at 37°C with 5% CO_2. Six hours later, cells were washed with PBS and exposed to fresh media with FBS containing either vehicle (PBS) or treatment. For the CD dose-response experiments, cells were treated for 4 h with varying amounts of a 250 mM solution of HP-β-CD (H107; Sigma) made in PBS to yield concentrations of 0.3, 0.75, and 1.5 mM. For experiments to compare HP-β-CD and SBE-β-CD (Captisol™, CYDEX Pharmaceuticals, Inc.), cells were treated for 16h with 0.3 mM of either compound from a 250 mM stock solution made in PBS. After treatment, culture medium was aspirated from each well, and 500uL of RNA-STAT60 was used to lyse cells and obtain RNA for analysis by qPCR (as described above for tissues).

Primary Hippocampal Neurons. At birth, pups from *Npc1$^{+/-}$* breeding mice were genotyped and sacrificed hours later by decapitation. Under a dissecting scope, the hippocampus was removed, minced, and incubated at 37°C in 10% trypsin (Sigma) for 10 min. Cells were collected by centrifugation for 5 min at 300x g, and the cell pellet was resuspended in in medium [high-glucose DMEM (Invitrogen) containing 10% heat-inactivated FBS (Atlanta Biologicals) and 1% neurobasal B27 supplement (Invitrogen)]. The primary hippocampal cells were counted and plated at 2.55x10^5 cells/cm^2 on a poly-L-lysine coated plate. Once plated, the cells were maintained in a humid incubator at 37°C with 5% CO_2.

The next day, cells were exposed to 5 μM Ara-C (Sigma, to reduce astrocyte contamination) in DMEM supplemented with 2 mM L-glutamine. On culture day 8, cells were provided fresh media containing vehicle or treatment and then harvested for RNA using the experimental designs described above for macrophage cultures.

Measurement of plasma cytokine concentrations

For the 0h time point, 60 μL of blood was harvested from the tail vein of $Npc1^{+/+}$ or $Npc1^{-/-}$ mice. The mice were allowed to recover for 1 day, and then mice were injected with HP-β-CD or saline. Then 3, 6, 12, and 24h later, another 60 μL aliquot of blood was harvested from the tail. Each tail-blood isolation was collected into a tube with 3 μL of 0.5 M EDTA on ice. Blood was centrifuged at $1x10^4$x g for 10 min at 10°C, and plasma was moved to a fresh tube, flash frozen in liquid nitrogen, and stored at -80°C until analyses for cytokine levels were performed. 10 μL of each sample was analyzed in duplicate, alongside standard curves, on a 7-plex ultra-sensitive pro-inflammatory mouse cytokine plate (#K11012C-1, MesoScale Discovery, Gaithersburg, Maryland) according to the manufacturer's instructions. The plate was read using a SECTOR® Imager 6000 instrument (MesoScale Discovery). Concentrations for IFNγ, IL-1β, IL-6, IL-10, IL-12p70, KC/GRO, and TNF are reported as pg of protein per mL of plasma.

Data Analysis

All data are presented as the mean ± SEM. Statistically significant differences (*P*-value <0.05) between the $Npc1^{+/+}$ controls and the 0h CD or saline-treated $Npc1^{-/-}$ group were tested using an unpaired Student's t-test and are represented by ‡. Significant differences between $Npc1^{-/-}$ mice studied 0h after CD treatment and those studied at later time points were determined using a one-way ANOVA followed by Dunnett's post-hoc analysis and are represented by * (P <0.05) to *** (P <0.0005). All statistical tests were performed using GraphPad Prism5 software (GraphPad Software, Inc. San Diego, CA).

3.4 Results

De novo cholesterol synthesis rates are reduced in *Npc1*$^{-/-}$ mice 3h after HP-β-CD injection:

As HP-β-CD is cleared within 3 to 6h from the plasma and total body of 49-day-old mice (Liu et al., 2010a), it is probable that HP-β-CD pharmacologic effect on *Npc1*$^{-/-}$ mice is occurring within this timeframe. To test this, 49-day-old *Npc1*$^{-/-}$ mice were given a single dose of HP-β-CD and then harvested 0 to 12h later to measure sterol balance. Significant increases in organ weights, tissue total cholesterol content, and cholesterol synthesis rates in *Npc1*$^{-/-}$ mice compared to their wildtype littermates were evident at the outset (0h) of this study (**Fig. 3.1**), which are consistent with previous reports (Li et al., 2005). As expected within 12h after receiving a single dose of HP-β-CD, there were no differences in liver and spleen weights or cholesterol concentration in the *Npc1*$^{-/-}$ (**Fig. 3.1A-D**). However, a significant decrease in cholesterol synthesis in both liver and spleen was measured after just 3h of HP-β-CD administration in the *Npc1*$^{-/-}$ (**Fig. 3.1E-F**). By 6h after HP-β-CD administration, hepatic cholesterol synthesis rates in *Npc1*$^{-/-}$ mice leveled off at a rate of 197 nmol/g/h and then remained steady for the duration of the 12h study (**Fig. 3.1E**). This was a reduction of ~80% compared to the initial rate (*Npc1*$^{-/-}$ 0h, 1010 nmol/g/h) in liver and was even less than that measured in *Npc1*$^{+/+}$ mice (580 nmol/g/h). A similar steady state from 6 to 12h after HP-β-CD was measured in spleen of *Npc1*$^{-/-}$ mice; although, the absolute rates of cholesterol synthesis were much lower compared to liver (**Fig. 3.1F**).

Hepatic cholesteryl ester content is increased in *Npc1*$^{-/-}$ mice 3h after HP-β-CD injection:

Although there was no measurable change in hepatic total cholesterol content within the first 12h after HP-β-CD (**Fig. 3.1C**), it is still plausible that in this timeframe there could be a shift in the ratio of unesterified to esterified cholesterol as was observed 24h after HP-β-CD (Liu et al., 2010a). A modest, although not statistically significant decrease in hepatic unesterified cholesterol from 20.5 mg/g at 0h to 17.1mg/g (**Fig. 3.2A**) was observed 12h after HP-β-CD injection in *Npc1*$^{-/-}$ mice. In contrast, hepatic

cholesteryl ester concentration in $Npc1^{-/-}$ mice was significantly increased by 3h after HP-β-CD injection and reached a plateau at 6h (**Fig. 3.2B**). The rate of change in cholesteryl ester content after HP-β-CD administration is in $Npc1^{-/-}$ mice is consistent with the timeframe observed for cholesterol synthesis reduction (**Fig. 3.2E-F**).
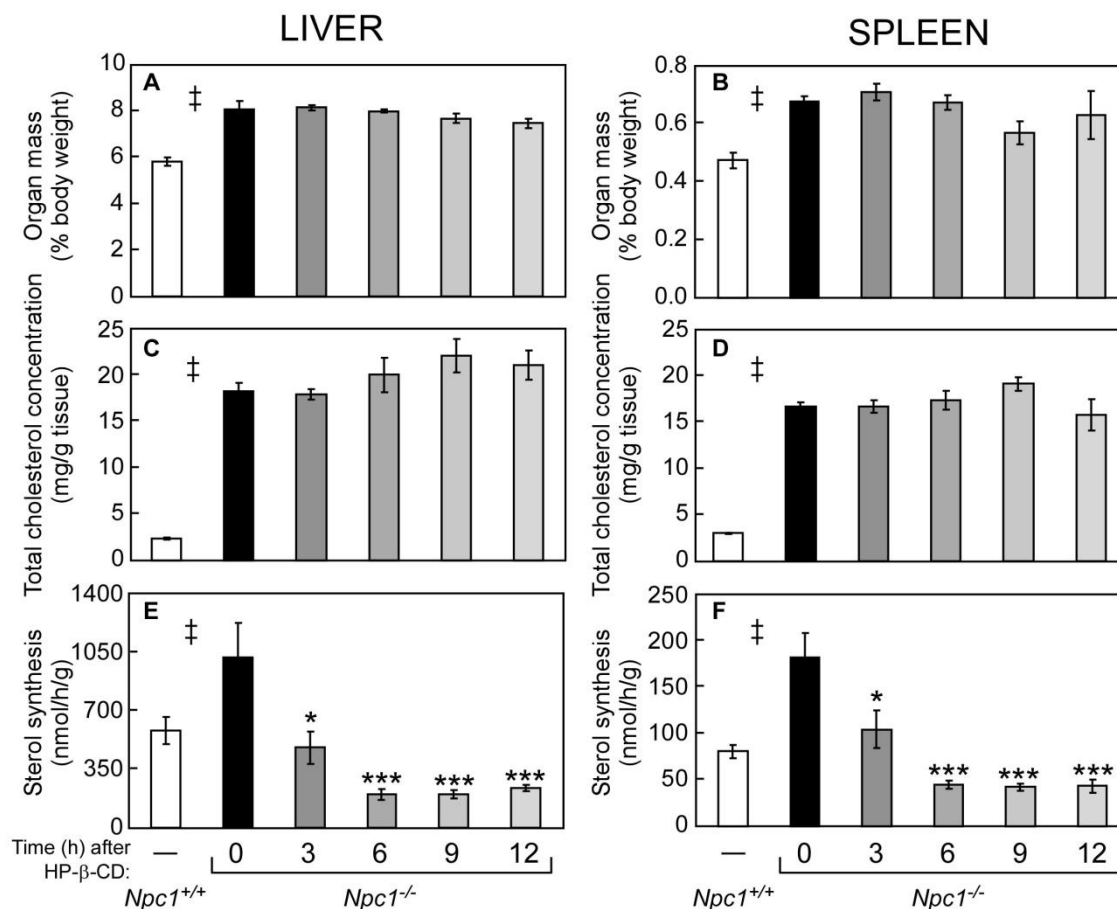
Figure 3.1 *Time course of HP-**β**-CD's effects on tissue cholesterol content and sterol synthesis rates in Npc1$^{-/-}$ mice.* 49-day-old $Npc1^{-/-}$ mice were injected at time 0 with a 4,000 mpk bolus of HP-β-CD, and tissues were harvested after 0, 3, 6, 9, or 12 h. $Npc1^{+/+}$ controls were studied 24h after an injection of HP-β-CD. Organ weights were measured and expressed relative to the total body weight for liver (**A**) and spleen (**B**). Liver and spleen tissues were saponified to measure the total concentration of cholesterol (**C, D**) by GC and the rates of cholesterol synthesis (**E, F**) by the [^{3}H]-water method. Each bar represents the mean ± SEM for 4-6 mice. Statistically significant differences ($P < 0.05$) between the $Npc1^{+/+}$ and the $Npc1^{-/-}$ (0h) groups are represented by ‡, while differences occurring in $Npc1^{-/-}$ mice following injection with HP-β-CD are indicated by * ($P < 0.05$) to *** ($P < 0.0005$) versus the 0h group.
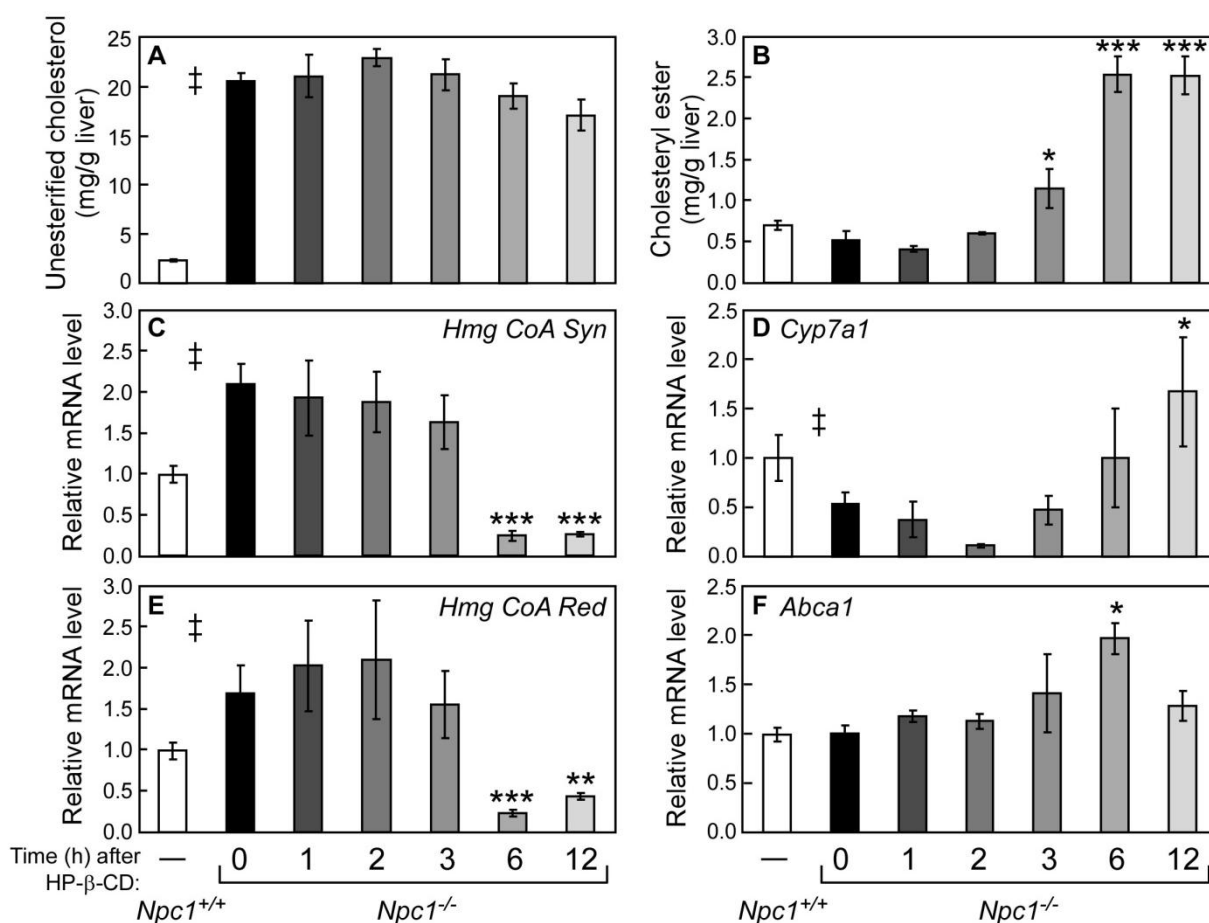
Figure 3.2 *Time course of HP-β-CD's effects on hepatic esterified and unesterified cholesterol concentrations and sterol-regulated mRNA levels in Npc1⁻/⁻ mice.* 49-day-old *Npc1⁻/⁻* mice were injected at time 0 with a 4,000 mpk bolus of HP-β-CD, and tissues were harvested after 0, 1, 2, 3, 6, or 12h. Injection times were staggered so that all tissues were harvested at the same point during the light cycle (ZT 9). Concentrations of hepatic unesterified cholesterol (**A**) and cholesteryl ester (**B**) were determined at all-time points. Relative mRNA levels in liver for SREBP2 target genes, *Hmg CoA Syn* (**C**) and *Hmg CoA Red* (**E**), and for LXR target genes, *Cyp7a1* (**D**) and *Abca1* (**F**), were measured by qPCR using cyclophilin as the invariant housekeeping gene. Values represent the mean ± SEM for 4-6 mice per group. Statistically significant differences (*P* <0.05) between the *Npc1⁺/⁺* and the *Npc1⁻/⁻* (0h) groups are represented by ‡, while differences occurring in *Npc1⁻/⁻* mice following injection with HP-β-CD are indicated by * (P <0.05) to *** (P <0.0005) versus the 0h group.

Significant changes in mRNA levels are observed 6h after HP-β-CD injection in *Npc1⁻/⁻* mice:

To identify molecular mechanisms that could account for the changes in cholesterol balance measured in *Npc1⁻/⁻* mice just 3h after HP-β-CD administration, mRNA levels for cholesterol-related genes were measured. After 24h of HP-β-CD treatment in *Npc1⁻/⁻* mice, there were significant increases in the expression of target genes of the oxysterol-responsive nuclear hormone receptor, LXR, as well as a decrease in the mRNA levels of target genes of the *de novo* cholesterol synthesis regulator, SREBP2 (Liu

et al., 2009). These observed mRNA changes are consistent with a cellular state where more cholesterol is available to be metabolized, which would reduce *de novo* cholesterol synthesis via SREBP2 and enhance cholesterol efflux and catabolism via LXR. As shown in Fig. 3.2, these changes were observed in *Npc1$^{-/-}$* liver as early as 6h after HP-β-CD treatment. By 6h after HP-β-CD, the mRNA levels of the SREBP2 target genes, *Hmg CoA Synthase* (*Hmg CoA Syn*) and *Reductase* (*Hmg CoA Red*), were significantly reduced by >85% compared to *Npc1$^{-/-}$* mice at 0h and were at levels even lower than those measured in *Npc1$^{+/+}$* mice (**Fig. 3.2C, E**). A reduction in the mRNA levels of *Srebp2* and its target genes were also seen in spleen and ileum as early as 3h after HP-β-CD treatment in *Npc1$^{-/-}$* (**Fig 3.3A, B**); although, the decrease observed in these tissues was not as profound as in liver.
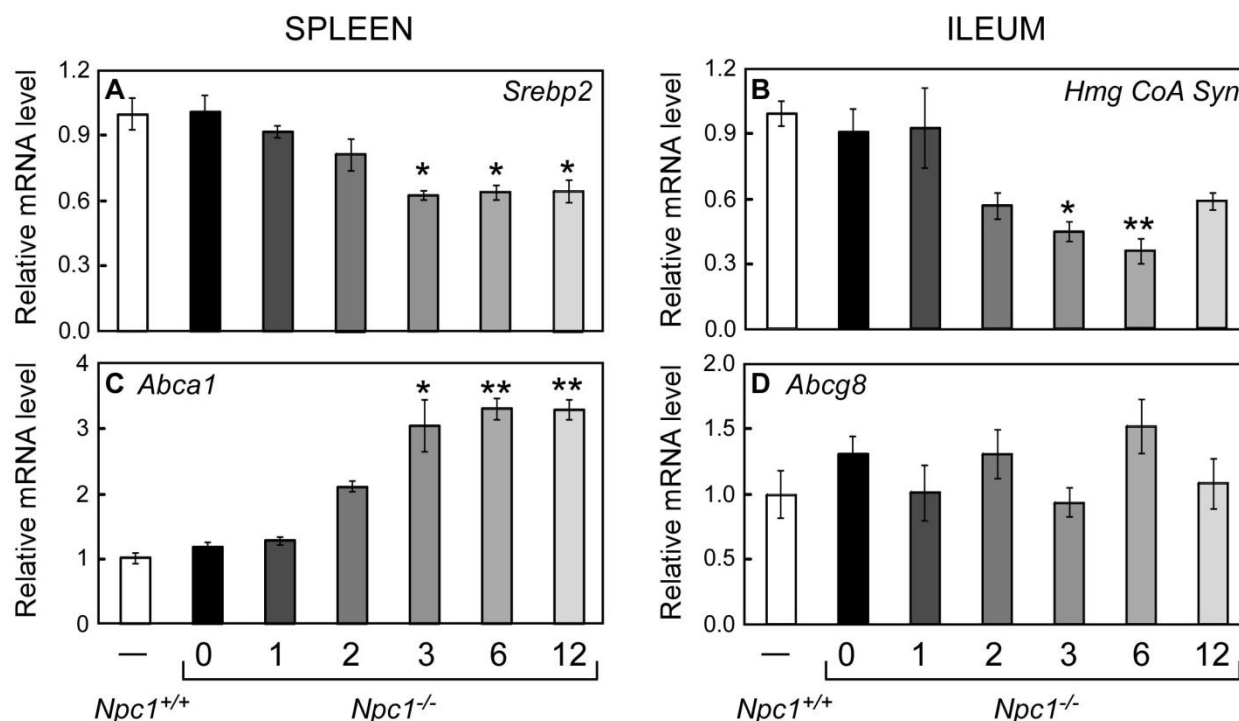
Figure 3.3 *Time course of HP-β-CD's effects on spleen and ileum mRNA levels.* Refer to the legend of Fig. 2 for experimental details and statistical analyses. Spleen and ileum (defined as the scraped mucosae from the distal third of small intestine) were harvested and processed for RNA. The relative mRNA levels of SREBP2 (**A**) and its target gene, *Hmg CoA Syn* (**B**), and LXR target genes, *Abca1* (**C**) and *Abcg8* (**D**), were measured by qPCR using cyclophilin as the invariant housekeeping gene.

Cholesterol 7α-hydroxylase (*Cyp7a1*), the LXR target gene in mice, is a rate-limiting enzyme for conversion of cholesterol to bile acids in liver. It should be noted that hepatic *Cyp7a1* mRNA levels

exhibit a pronounced circadian rhythm (Panda et al., 2002); thus, this study design utilized staggered HP-β-CD injection times to limit tissue harvesting to a single time of day (ZT 9). *Cyp7a1* mRNA levels were reduced by 50% in $Npc1^{-/-}$ mice compared to $Npc1^{+/+}$ littermates. In $Npc1^{-/-}$ mice, HP-β-CD administration resulted in increased *Cyp7a1* mRNA levels with a trend observed as early as 6h and a significant increase (3-fold) evident at 12h (**Fig. 3.2D)**. The mRNA level of *ATP-binding cassette transporter a1* (*Abca1*), another LXR target gene, was shown to be only transiently increased in livers of $Npc1^{-/-}$ mice at 6h after HP-β-CD (**Fig. 3.2F**). These results from liver are in contrast to *Abca1* mRNA levels in spleen (**Fig. 3.3C**), where its expression was significantly increased by 3h after HP-β-CD in $Npc1^{-/-}$ mice and remained at this level throughout the 12h study. Within the first 12h following HP-β-CD treatment, no changes in mRNA levels were seen in *Abcg8*, which like *Abca1* is an LXR target gene and an ABC transporter, in either liver (data not shown) or in ileum (**Fig. 3.2D**).

No change in plasma lipoprotein cholesterol levels nor evidence of a CD/cholesterol complex was observed in either plasma or urine within 12h after a HP-β-CD injection in $Npc1^{-/-}$ mice:

As HP-β-CD is cleared within 6h from mature mice while changes in cholesterol balance in $Npc1^{-/-}$ mice are observed as early as 3h and plateau by 6h, one might hypothesize that HP-β-CD is carrying the excess cholesterol from $Npc1^{-/-}$ cells out of the body. An alternative hypothesis is that HP-β-CD is only briefly shuttling cholesterol from the lysosome of $Npc1^{-/-}$ cells and then is releasing the previously trapped cholesterol within the cell. In order to test these hypotheses, the level of cholesterol in the plasma and urine after HP-β-CD injections were measured at various times consistent with the renal clearance rates of intact HP-β-CD (Stella et al., 2008).

To measure plasma cholesterol, FPLC gel filtration for fractionation of lipoproteins was performed on pooled plasma from blood samples collected 0 to 12h after HP-β-CD injections in $Npc1^{-/-}$ (**Fig. 3.4**). First plasma lipoprotein profiles of $Npc1^{+/+}$ and $Npc1^{-/-}$ were compared, and it was observed that the High Density Lipoprotein (HDL) peak (represented by fractions 23-35, **Fig. 3.4A**) was higher in the $Npc1^{-/-}$

mouse, which is consistent with a previous report (Xie et al., 2000). During the first 3h following an injection when the HP-β-CD was still present in the plasma, there was no apparent shift in the plasma lipoprotein cholesterol levels of $Npc1^{-/-}$ mice (**Fig. 3.4B**). In addition, there were no changes 6h or 12h after HP-β-CD (**Fig. 3.4C**), which are representative of time points when HP-β-CD is no longer detectable in the whole animal and yet sterol balance changes are occurring. Notably, there was no shift in sterol within any fractions nor in the eluate collected 20 minutes before and after fractionation (data not shown); therefore, no increase in the level of total cholesterol was measurable in the bloodstream at any time to suggest the presence of a CD/cholesterol complex.
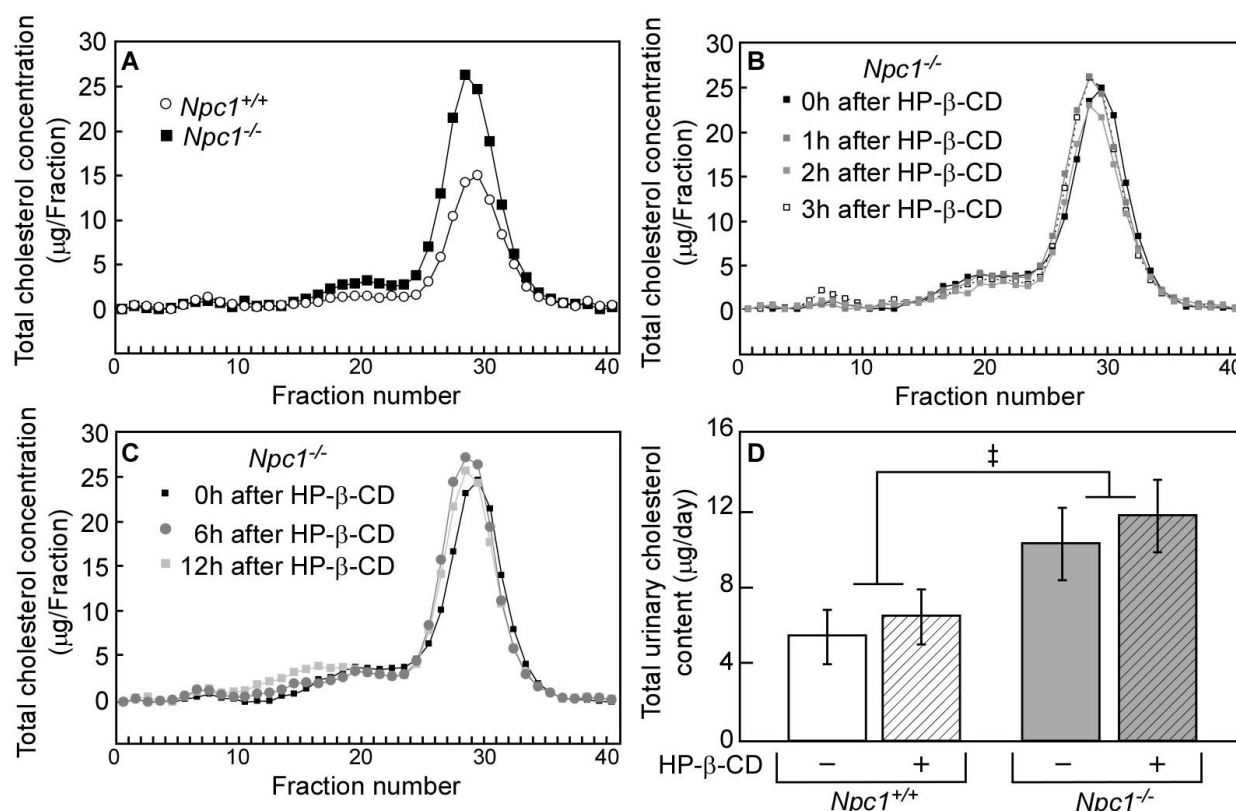
Figure 3.4 *Cholesterol distribution in plasma and urine of Npc1$^{-/-}$ mice after HP-β-CD injection.* Plasma samples were collected from 49-day-old $Npc1^{+/+}$ and $Npc1^{-/-}$ mice 0, 1, 2, 3, 6, and 12h after an injection with HP-β-CD (4,000 mpk, sc) or equivalent volume of vehicle (saline). Plasmas were pooled (n=2 pooled samples/group), and lipoprotein profiles were generated by FPLC. Lipoprotein profiles were plotted to allow comparison between: (**A**) saline-treated $Npc1^{+/+}$ and $Npc1^{-/-}$ mice; (**B**) the very early time points, 0-3h, after HP-β-CD injection of $Npc1^{-/-}$ mice; and (**C**) later time points, 6-12h, after HP-β-CD injection of $Npc1^{-/-}$ mice. Urine samples were collected from 49-day-old $Npc1^{+/+}$ and $Npc1^{-/-}$ mice over a 48-h period after a HP-β-CD (4,000 mpk, sc) or vehicle (saline) injection. The total urinary cholesterol (**D**) values depict the mean ± SEM for 6 mice/group. A significant difference (P <0.05) between the $Npc1^{+/+}$ and $Npc1^{-/-}$ groups is represented by ‡.

HP-β-CD is excreted intact into urine (Stella et al., 2008), thus urine samples were collected from mice after saline or HP-β-CD injections to determine whether cholesterol was present as a complex with excreted CD (**Fig. 3.4D**). Because of the extremely low excretion rate of cholesterol in mouse urine, a 48h urine collection was needed in order to accurately measure the concentration of cholesterol within the urine. Over 48h following an injection with HP-β-CD, there was no change in the amount of cholesterol secreted in the urine in either $Npc1^{+/+}$ and $Npc1^{-/-}$ mice (**Fig. 3.4D**). There was however a significant difference between the basal amount of cholesterol secreted in the urine of $Npc1^{+/+}$ (a rate of 6.1±1.5μg/day) and that of $Npc1^{-/-}$ (a rate of 11.2±2.0μg/day), which was not dependent on treatment. This difference was not accounted for by a difference in body weight between the groups as there still was a significant difference between the $Npc1^{+/+}$ urine cholesterol excretion rate of 0.33±0.1μg/day/g of bw and the $Npc1^{-/-}$ rate of 0.72±0.1μg/day/g of bw. It is important to note that the amount of cholesterol excreted in urine of mice is insignificant compared to the amount of sterol secreted from the body by the feces which was 126μg/day/g of bw in $Npc1^{+/+}$ and was 199μg/day/g of bw in $Npc1^{-/-}$ (Liu et al., 2010a).

Very few changes were observed in proinflammatory cytokines and their mRNA levels within 12h after a HP-β-CD injection in $Npc1^{-/-}$ mice:

Many molecular markers of the proinflammatory state have been shown to be dramatically elevated in virtually all tissues and to increase with age in untreated $Npc1^{-/-}$ mice compared to $Npc1^{+/+}$ controls (Li et al., 2005; Wu et al., 2005; Langmade et al., 2006). These same markers have been shown to be reduced when $Npc1^{-/-}$ are provided with a therapy, such as HP-β-CD, which relieves lysosomal lipid accumulation and extends lifespan (Langmade et al., 2006; Repa et al., 2007; Liu et al., 2009; Ramirez et al., 2010). In liver, the mRNA levels of *Cd68* (macrosialin, a cell surface marker of monocytes and macrophages) and cytokines *Mip1α*, *Il-12p40*, *Ifn-γ*, *Cxcl1*, and *Tnfα* were dramatically increased in $Npc1^{-/-}$ mice compared with $Npc1^{+/+}$ mice (**Fig. 3.5A**), and similar elevations were observed for selected cytokines in other organs (spleen, **Fig. 3.5E** and ileum, **Fig. 3.5F**). 24h after a single injection of HP-β-CD, the mRNA

levels of elevated inflammation markers in $Npc1^{-/-}$ liver were significantly reduced (**Fig. 3.5A**), and comparable changes were observed for the hepatic protein levels of IFN-γ, CXCL1, and TNFα (data not shown).
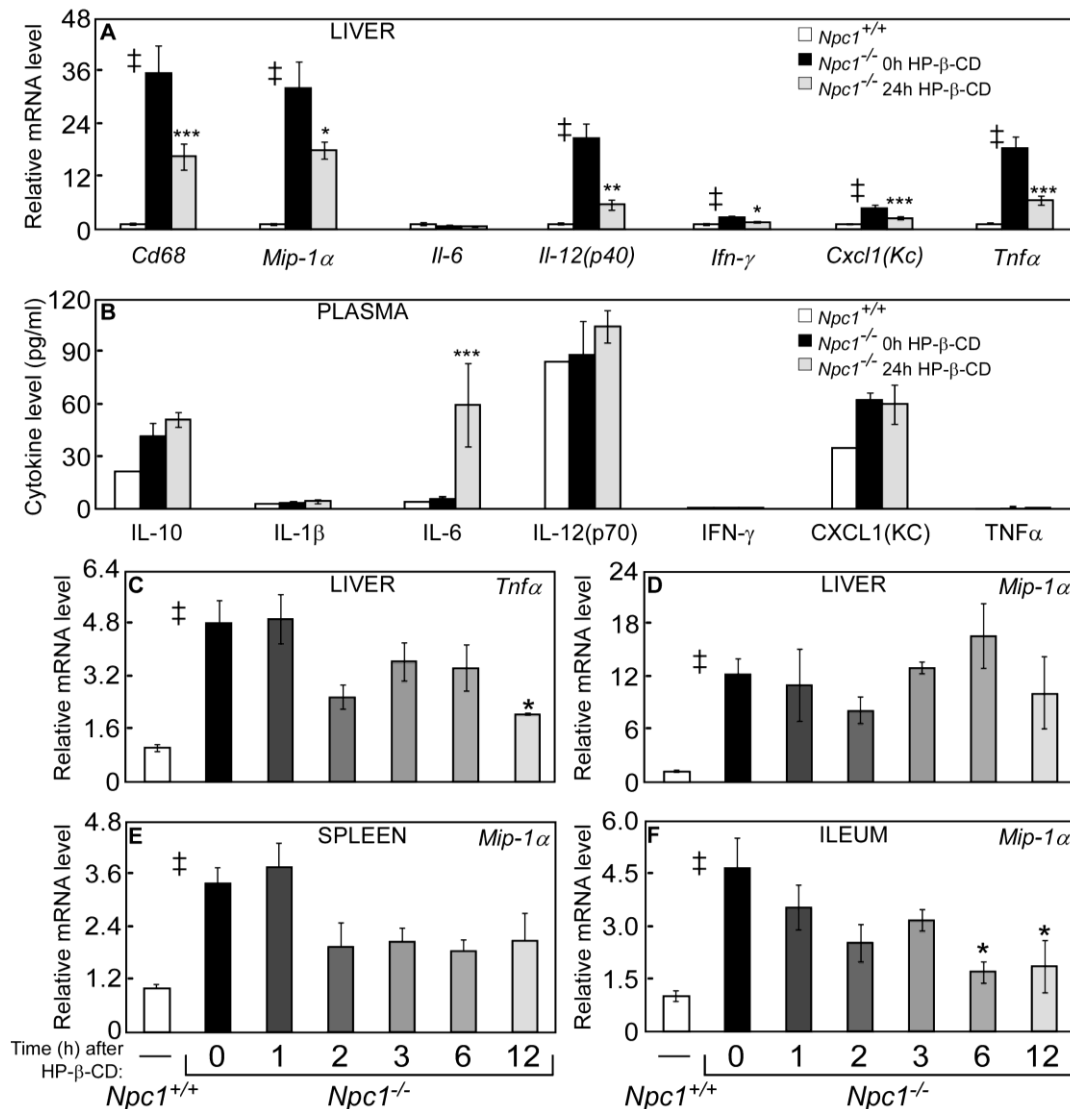
Figure 3.5 *Markers of inflammation after HP-β-CD Treatment.* Livers were collected from 49-day-old $Npc1^{+/+}$ and $Npc1^{-/-}$ mice 24h after a saline or HP-β-CD injection (4,000 mpk, sc). Hepatic RNA was harvested and used to survey changes in mRNA levels of cytokines and other inflammatory markers after HP-β-CD **(A)**. Blood was collected from the tail vein of 49-day-old $Npc1^{-/-}$ mice at 0, 3, 6, 12, and 24h after a HP-β-CD injection (4,000 mpk, sc). The same mice were used for all time points. Plasma was used to measure the protein levels of cytokines **(B)**. Liver, spleen, and ileum were collected from $Npc1^{-/-}$ mice 0, 1, 2, 3, 6, and 12h after HP-β-CD injections (see Figs. 2-3 for details) and processed for RNA. The relative mRNA level of cytokines and other inflammatory markers **(C-F)** were measured. Each bar represents the mean ± SEM for 4-6 mice. Statistically significant differences (*P*-value <0.05) between the $Npc1^{+/+}$ and the 0h $Npc1^{-/-}$ groups are represented by ‡, while differences after HP-β-CD treatment in $Npc1^{-/-}$ mice compared to the 0h group are represented by * (P <0.05) to *** (P <0.0005).

Because of the extreme reduction in the mRNA level of cytokines after HP-β-CD injection, it may be possible to use cytokines as a biomarker to track disease progression and drug improvement in human NPC patients; however, it would be impractical to do multiple liver biopsies for cytokine measurements. Fortuitously, cytokines are secreted into the plasma and are high in many disease states; therefore, there are many kits readily available to measure their circulating protein levels. Taking advantage of a multi-plex plate produced by MSD, the plasma levels of 7 cytokines were measured after HP-β-CD administration in $Npc1^{-/-}$ mice (**Fig. 3.5B**). While the mRNA levels of *Il-12p40*, *Ifn-γ*, *Cxcl1*, and *Tnfα* were much higher in the livers of $Npc1^{-/-}$ compared to $Npc1^{+/+}$ controls and were reduced with HP-β-CD treatment (**Fig. 3.5A**), these changes were not mirrored by the circulating protein levels of these cytokines in mouse plasma (**Fig. 3.5B**). The only significant difference 24h after HP-β-CD injection was an increase in IL-6, a pro-inflammatory cytokine. This increase in IL-6 was also apparent in the $Npc1^{+/+}$ HP-β-CD and $Npc1^{-/-}$ saline treated groups and reached a peak at 6h (**Fig. 3.6C, D**). Significant changes were also observed in the plasma concentrations IL-10 6h (**Fig. 3.6A, B**) and CXCL1 3-12h (**Fig. 3.6E, F**) after HP-β-CD in $Npc1^{-/-}$ mice; however, these increases were only transient and also occurred in the other treatment groups.

As nearly all hepatic cytokine mRNA levels were reduced 24h after HP-β-CD, liver, spleen, and ileum were harvested from $Npc1^{-/-}$ 0 to 12h after an injection of HP-β-CD in order to measure the time course of HP-β-CD effect on cytokines. For each tissue, the mRNA levels for several genes were measured; however, only a representative group is shown in (**Fig. 3.5 C-F**). For all tissues, there was a significant difference between $Npc1^{+/+}$ and $Npc1^{-/-}$, but there were very few reductions after HP-β-CD treatment. There was a trend towards decreased levels of *Tnfα* in liver following HP-β-CD administration, which reached significance by 12h (**Fig. 3.5 C**); nonetheless, there was no decrease in *Mip1α* mRNA in liver or spleen by 12h (**Fig. 3.5 D,E**). There was, however, a significant decrease in *Mip1α* mRNA in ileum as early as 6h (**Fig. 3.5 F**). In summary, changes in cytokine expression in tissues of $Npc1^{-/-}$ mice were absent or modest during the first 12h after HP-β-CD despite dramatic reductions in mRNA and

protein levels in liver by 24h, suggesting that the anti-inflammatory effects of HP-β-CD are secondary to changes in sterol homeostasis.
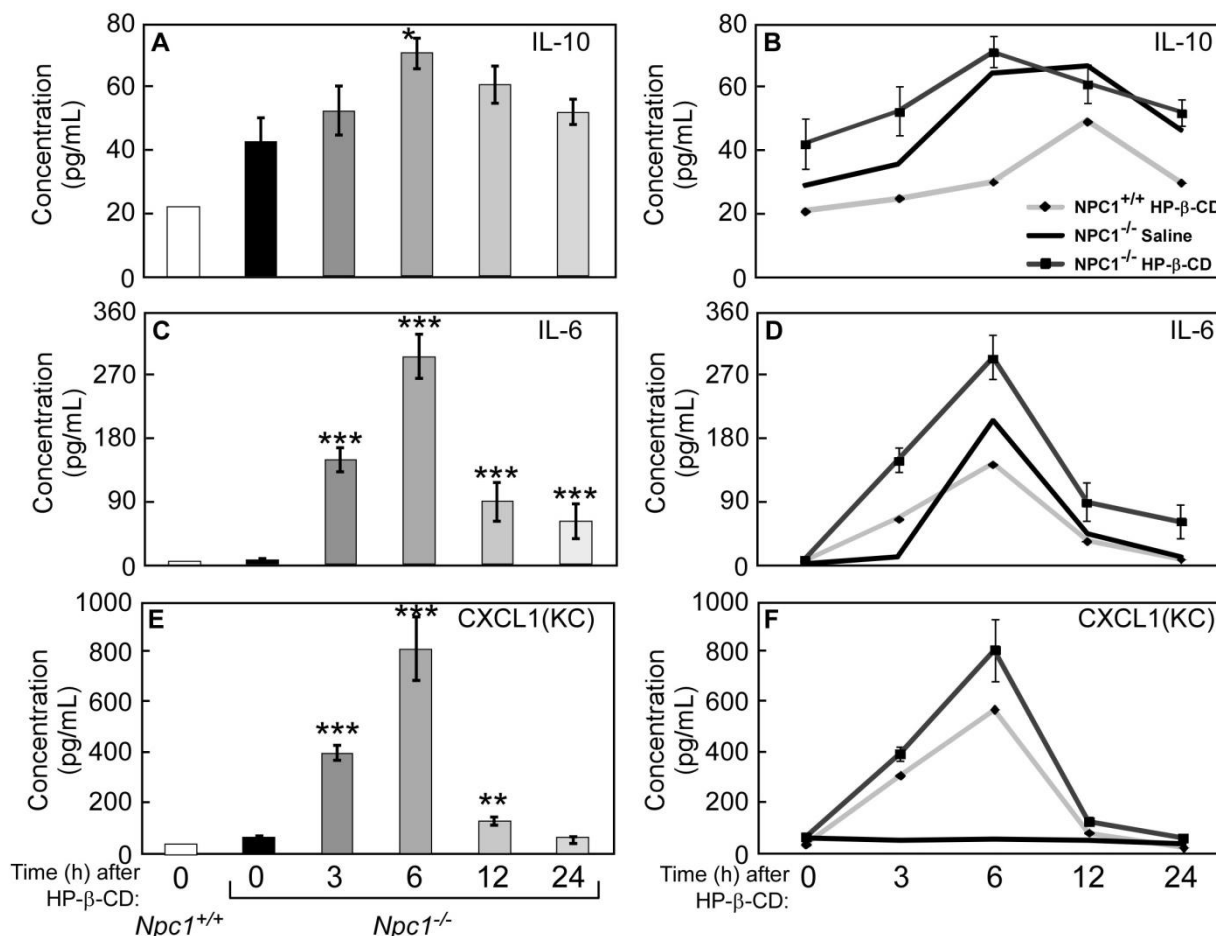
Figure 3.6 *Cytokine levels over time after HP-β-CD Treatment.* Blood was collected from the tail vein of 49-day-old *Npc1*^{-/-} mice at 0, 3, 6, 12, and 24h after a HP-β-CD injection (4,000 mpk, sc). The same mice were used for all time points. Plasma was used to measure the protein levels of cytokines **(A-F)**. Each bar represents the mean ± SEM for 4-6 mice. Statistically significant differences (*P*-value <0.05) after HP-β-CD treatment in *Npc1*^{-/-} mice compared to the 0h group are represented by * (P <0.05) to *** (P <0.0005).

Significant changes in mRNA levels were observed in *Npc1*^{-/-} cells treated with HP-β-CD and SBE-β-CD in culture:

Another possible mechanism of action for HP-β-CD's effect on the *Npc1*^{-/-} mouse is that it could act specifically on one tissue, which would lead to the release of a humoral factor that then could elicit the release of lysosomal cholesterol in other tissues. One way to test this hypothesis is to harvest homogenous cell types from *Npc1*^{-/-} mice and treat them in culture with HP-β-CD. If HP-β-CD has an
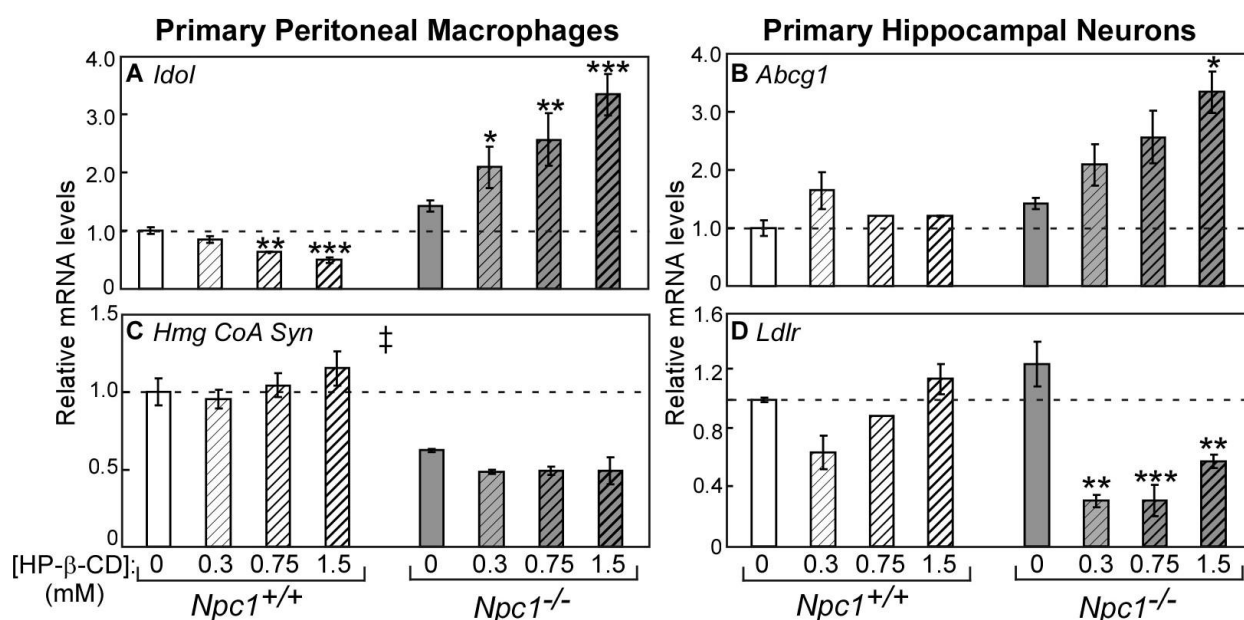
Figure 3.7 *Acute effects of HP-β-CD in cultured cells from Npc1⁻ᐟ⁻ mice.* Thioglycollate-elicited peritoneal macrophages (from 49-day-old mice) and hippocampal neurons (from neonatal mouse pups) were obtained from $Npc1^{+/+}$ and $Npc1^{-/-}$ mice. These cells were treated in FBS-containing culture media with increasing amounts of HP-β-CD (0.3mM to 1.5mM) or an equivalent volume of vehicle (saline). 4h later, the cells were harvested for RNA isolation, and the relative mRNA levels of LXR target genes, *Idol* (**A**) and *Abcg1* (**B**), and SREBP2 target genes, *Hmg CoA Syn* (**C**) and *Ldlr* (**D**) were determined by qPCR. Each bar represents the mean ± SEM of triplicate wells. A statistically significant difference ($P <0.05$) between saline-treated $Npc1^{+/+}$ and $Npc1^{-/-}$ cells is represented by ‡, and differences in RNA levels resulting from HP-β-CD treatment within cells of a given genotype are represented by asterisks * ($P <0.05$) to *** ($P <0.0005$).

effect on multiple primary cell types, it would prove that HP-β-CD is working directly in these cells and not by a yet unidentified humoral factor. Therefore, age-matched $Npc1^{+/+}$ and $Npc1^{-/-}$ mice were used to harvest peritoneal macrophage or hippocampal neurons. In the adult mouse, a single sc injection of HP-β-CD at 4,000 mpk is estimated to provide a maximal plasma concentration of 1.3 mM (Liu et al., 2010a); therefore, a relevant concentration range of HP-β-CD (0.3-1.5 mM) was applied *in vitro* to the primary macrophage and neurons (**Fig. 3.7**). As observed in whole animals, administration of HP-β-CD had virtually no effect in wildtype cultured cells. However after only 4h of HP-β-CD exposure, gene expression changes consistent with an increase in intracellular sterol were observed in $Npc1^{-/-}$ cells. Representative LXR target genes, *Idol* in macrophages (**Fig. 3.7A**) and *Abcg1* in neurons (**Fig. 3.7B**), exhibited a dose-dependent increase in mRNA level; while the mRNA levels of selected SREBP2 target genes, *Hmg CoA Syn* (**Fig. 3.7C**) and *low density lipoprotein receptor* (*Ldlr*) (**Fig. 3.7D),** were maximally

reduced with the minimal dose of 0.3 mM HP-β-CD. While the reduction in *Hmg CoA Syn* mRNA levels

was only a trend in macrophages, the decrease in *Ldlr* was statistically different between the vehicle and

HP-β-CD treated *Npc1^{-/-}* neurons.
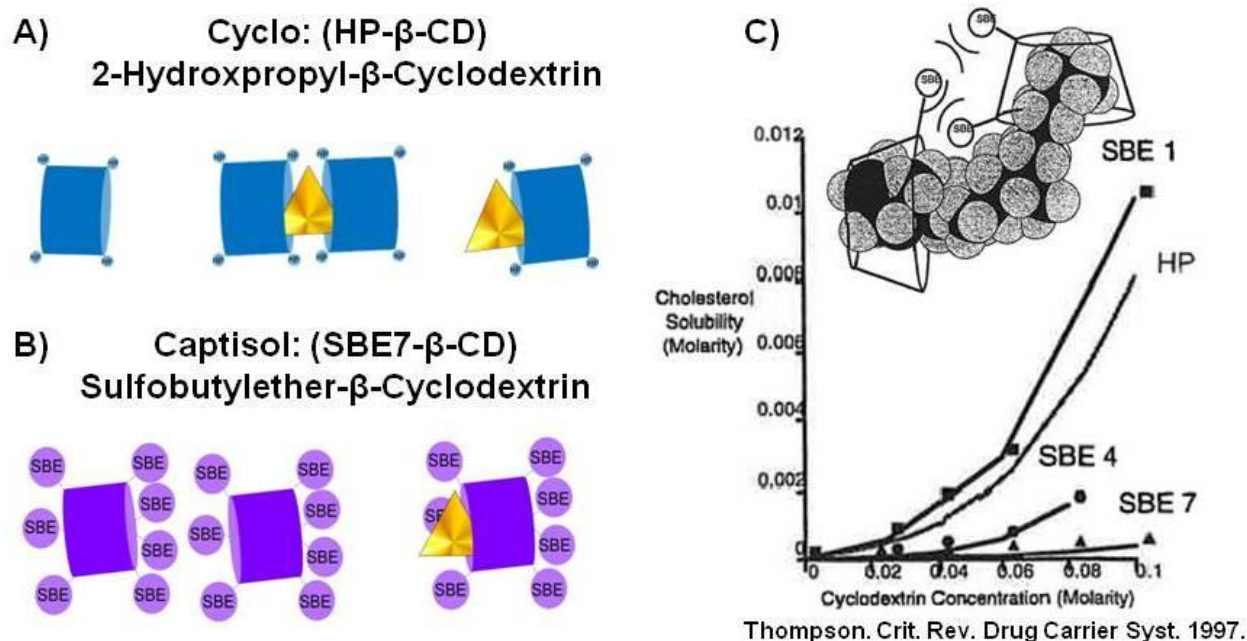
Figure 3.8 *Two forms of modified β-Cyclodextrin.* 2-hydroxypropyl-β-cyclodextrin (HP-β-CD) can bind to cholesterol either in a 2:1 or 1:1 conformation **(A)**; whereas sulfobutylether-β-cyclodextrin (SBE-β-CD) contains large head groups that sterically hinder it from dimerization, and thus can only bind to cholesterol in a 1:1 complex **(B)**. In order to fully solubilize cholesterol, which is required to extract the sterol from lipid membranes, cyclodextrins must bind cholesterol in a 2:1 ratio. This can be achieved at high concentration of HP-β-CD (HP), but can never be achieved with SBE7-β-CD (SBE7) **(C,** modified from Thompson, 1997).

The ability of various cyclodextrins to interact, adsorb, and ultimately extract unesterified

cholesterol from lipid membranes into an aqueous environment has been extensively studied (Puglisi et

al., 1996; Yancey et al., 1996; Atger et al., 1997; Thompson, 1997; Zidovetzki et al., 2007; Lopez et al.,

2011; McCauliff et al., 2011). Single β-CDs can accommodate a single unesterified cholesterol in their

hydrophobic pocket, but about one-third of the sterol molecule is expected to protrude from the CD

(Yancey et al., 1996; Lopez, de Vries, & Marrink, 2011). In this 1:1 configuration, all β-CDs appear

capable of facilitating the translocation of free cholesterol between membranes (or between donor and

acceptor lipid vesicles) – thus behaving as a "shuttle". In order to fully extract unesterified cholesterol

from membranes, β-CDs must form a 2:1 complex to allow for complete solubilization of the sterol into

an aqueous environment (Thompson, 1997) – thus acting as a "sink" (see **Fig. 3.8**). While HP-β-CD (2-hydroxypropyl-β-cyclodextrin, **Fig. 3.8A**) can bind to cholesterol either in a 2:1 or 1:1 confirmation; an alternate form of β-CD, sulfobutylether-β-cyclodextrin (SBE-β-CD, **Fig. 3.8B**), which harbors chemical modifications that sterically hinder it from dimerization, can only bind to cholesterol in a 1:1 complex (Rajewski et al., 1995; Thompson, 1997). Therefore, HP-β-CD potentially works by pulling cholesterol out of the cell membrane of an $Npc1^{-/-}$ cell, while SBE-β-CD can only bind cholesterol not incorporated into a membrane, such as the cholesterol trapped in the lysosome of $Npc1^{-/-}$ cells.
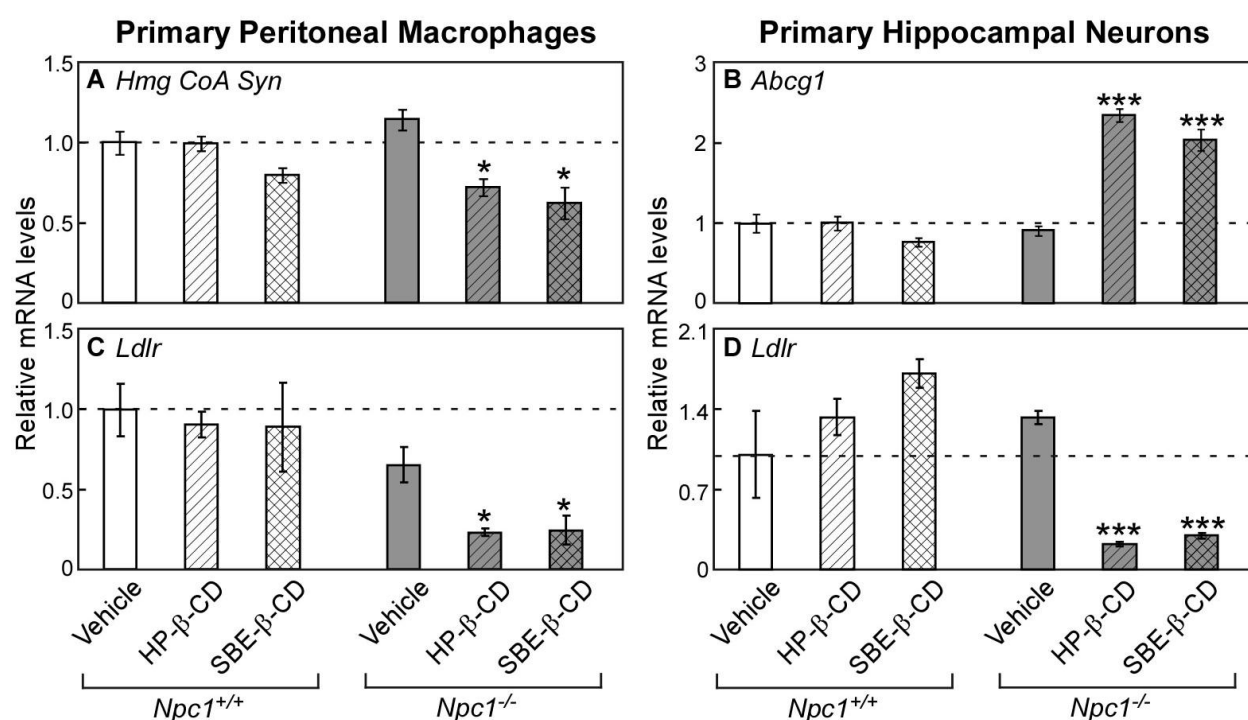
Figure 3.9 *Effects of HP-β-CD compared to SBE-β-CD in cultured cells from Npc1$^{-/-}$ mice.* Thioglycollate-elicited peritoneal (from 49-day-old mice) and hippocampal neurons (from neonatal mouse pups) were harvested from $Npc1^{+/+}$ and $Npc1^{-/-}$ mice. These cells were treated in FBS-containing culture media with vehicle (saline), 0.3mM HP-β-CD or 0.3mM SBE-β-CD. 16h later, the cells were harvested for RNA, and the relative mRNA levels of SREBP2 target genes, *Hmg CoA Syn* (**A**) and *Ldlr* (**C, D**), and the LXR target gene, *Abcg1* (**B**), were measured by qPCR. Each bar represents the mean ± SEM of triplicate wells. Statistically significant differences by CD treatment for cells of a given genotype compared to the vehicle-treated group are represented by * ($P <0.05$) to *** ($P <0.0005$).

In order to determine whether a solubilizing function of HP-β-CD is essential to its mechanism of action in $Npc1^{-/-}$ cells, the effects of HP-β-CD and SBE-β-CD were compared on primary cells *in vitro* (**Fig. 3.9**) using the concentration of 0.3 mM established in the previous experiment (**Fig. 3.7**). Both

forms of β-CD cause near equivalent reductions in *Hmg CoA Syn* and *Ldlr* mRNA levels in macrophages (**Fig. 3.9A, C**). In addition, SBE-β-CD and HP-β-CD exhibited comparable efficacy in inducing the LXR target gene, *Abcg1*, and decreasing *Ldlr* mRNA in neurons (**Fig. 3.9B, D**). Neither HP-β-CD nor SBE-β-CD treatment at 0.3mM had any effect on $Npc1^{+/+}$ cells. In addition, 0.05mM doses of SBE-β-CD and HP-β-CD were tested in primary macrophages and neurons (data not shown), and the resulting changes were very consistent with the changes observed in gene expression after 0.3mM treatment. Overall, these cell-based studies demonstrate a cell-autonomous activity of β-CDs, and further support a mechanism of action that does not rely on the ability of CDs to form a 2:1 complex with cholesterol in order to fully solubilize the sterol into an aqueous environment.

3.5 Discussion

The studies presented in this chapter provide a timeline for the pharmacological effects of HP-β-CD in $Npc1^{-/-}$ mice. Previous studies have shown that 24h after a single injection of HP-β-CD to 49-day-old $Npc1^{-/-}$ mice, there are significant modifications to cholesterol synthesis, cholesteryl ester concentrations, and mRNA levels of SREBP2 and LXR target genes as well as cytokines (Liu et al., 2010a). However within just 3h of HP-β-CD administration, there are significant reductions in *de novo* cholesterol synthesis in liver and spleen (**Fig. 3.1**) and significant increases in hepatic cholesteryl ester content (**Fig. 3.2**). By 6h, these changes reached a steady state, and significant differences in the levels of SREBP2 and LXR target genes were apparent in liver (**Fig. 3.1-2**). Corresponding shifts in mRNA levels were seen as early as 3h after HP-β-CD in spleen and intestine (**Fig. 3.3**). The pharmacological effects observed within the first 6h after HP-β-CD administration support a mechanism where the trapped lysosomal cholesterol in $Npc1^{-/-}$ cells is being released. Furthermore, the 3h to 6h timeframe in which sterol balance and corresponding gene changes occur is very consistent with the rate of HP-β-CD clearance in mice. The changes after a single injection of HP-β-CD have been summarized as a timeline in (**Fig. 3.10**).
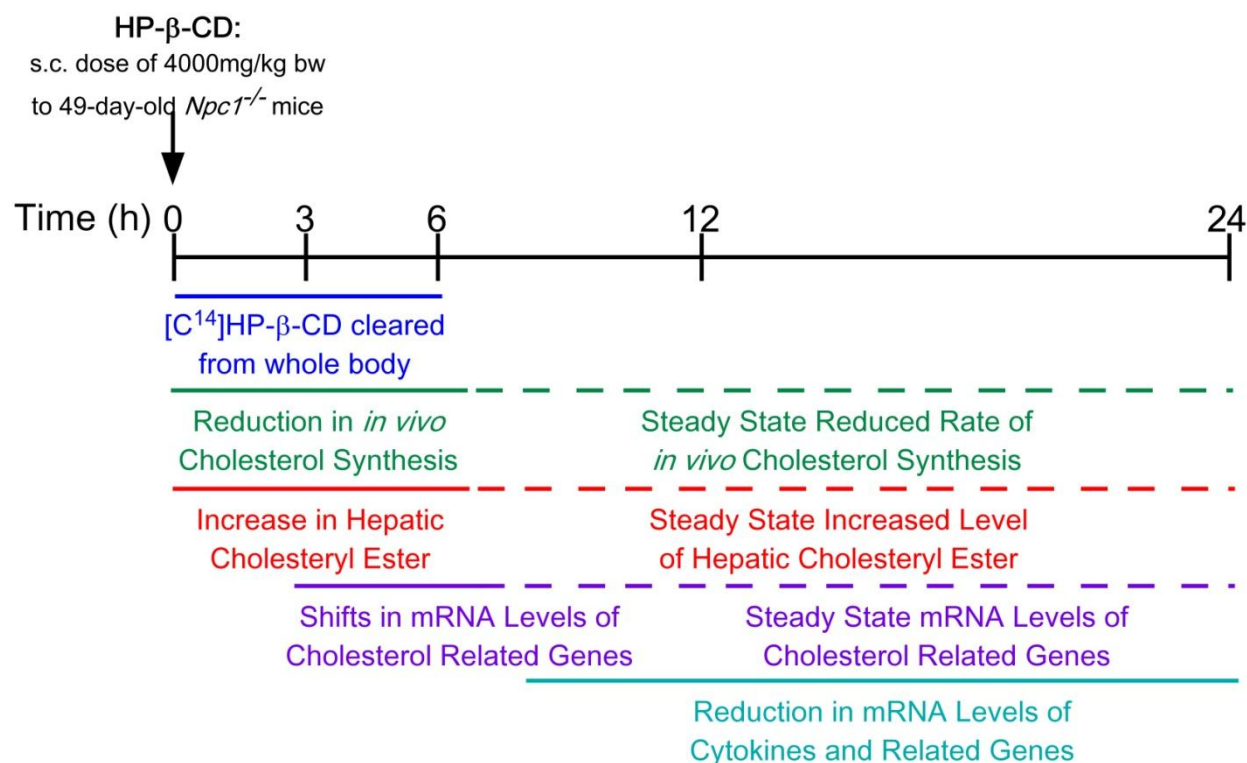
Figure 3.10 *Timeline of HP-β-CD's effects in Npc1$^{-/-}$ mice.* Within 3h of HPβCD administration to 49-day-old *Npc1*$^{-/-}$ mice, a significant reduction in *de novo* sterol synthesis and increase in cholesteryl ester (CE) occur in liver. By 6h, decreases in SREBP2 target genes and increases in LXR target genes are apparent. Finally 24h after HPβCD administration, inflammation is significantly reduced.

In addition to measuring the rate of sterol balance changes after HP-β-CD, the plasma concentration and hepatic mRNA levels of cytokines were also measured. While the mRNA levels of proinflammatory cytokines were higher in the *Npc1*$^{-/-}$ mouse and were brought down 24h after HP-β-CD treatment, there were very few changes in mRNA levels before 12h had elapsed (**Fig. 3.5**). In general, the plasma concentrations of the cytokines were very low and did not reflect an inflamed state in the *Npc1*$^{-/-}$ mouse as suggested by the increased mRNA levels of cytokines. The only significant increase in plasma cytokine protein levels measures 24h after HP-β-CD was in IL-6 (**Fig. 3.5B**). As IL-6 was also increased after 24h in the *Npc1*$^{+/+}$ HP-β-CD and *Npc1*$^{-/-}$ saline-treated groups (**Fig. 3.6 C,D**), this was most likely due to the stress of mouse handling for the repeated tail-vein blood collections. The stress of being handled also can explain the subtle increase in IL-10 at 6h (**Fig. 3.6 A,B**). Intriguingly, the increase in CXCL1 from 3h to 12h appears to be caused by the drug treatment as the change was observed in HP-β-CD treated *Npc1*$^{+/+}$

and *Npc1*^{-/-} but not in the saline treated *Npc1*^{-/-}group (**Fig. 3.6 E,F**). It is possible that an endotoxin present in the molecular grade Sigma form of HP-β-CD could cause this increase in cytokines. Overall, the reduction in proinflammatory cytokines was not as rapid as the changes in cholesterol balance, implying that the reduction in cytokines is secondary to the decrease in accumulated sterol.

Therefore while changes in cholesterol balance were seen as early as 3h after HP-β-CD in *Npc1*^{-/-} mice, secondary changes such as a reduction in cytokine levels did not appear until 12 to 24h after the initial dose (**Fig. 3.10**). Taken as a whole, the time course data demonstrate that even though HP-β-CD is cleared within 6h from mice, 24h is a good time point for studying the maximum effects of HP-β-CD *in vivo*. The short-term time course present here, however, does not address the pending question of how quickly the NPC diseased state returns after a HP-β-CD injection. From the original studies in 7-day-old *Npc1*^{-/-} mice, it was shown that by 6 weeks after a single HP-β-CD injection: the total cholesterol concentration was elevated to levels similar to those found in untreated *Npc1*^{-/-}, and cholesterol synthesis levels were even higher than without treatment (Liu et al., 2009). After this, serial dosing was shown to be effective in *Npc1*^{-/-} mice; however, both every other day (Davidson et al., 2009) and weekly dosing schemes (Ramirez et al., 2010) were used. To ultimately determine the most effective interval between doses of HP-β-CD in NPC patients, these time course studies need to be continued in mice past 24h up until 1 week after CD.

In order to test the hypothesis that HP-β-CD works in *Npc1*^{-/-} mice by carrying cholesterol through the bloodstream for urinary excretion, lipoprotein profiles and urinary cholesterol levels were evaluated after HP-β-CD. There were no detectable shifts in the amount cholesterol carried in the plasma (**Fig. 3.4 B,C**).; therefore, the released lysosomal cholesterol after HP-β-CD in *Npc1*^{-/-} mice does not move through the blood. In mice given a single injection of 4000mg of HP-β-CD/kg bw, there was no change in the level of cholesterol in urine (**Fig. 3.4 D**). However, an increase from 99.7 ±25.9μg/day to 171.6±57.0μg/day has been reported in wildtype rats given an iv dose of HP-β-CD as low as 100mg/kg (Frijlink et al., 1991). Nevertheless, my goal in measuring the cholesterol level in urine was not to

disprove that cholesterol could be excreted in the urine after HP-β-CD administration. Rather, my goal was to challenge the prevailing idea that a CD complex in the urine is the pathway by which cholesterol is freed from $Npc1^{-/-}$ mice after HP-β-CD treatment. There was, however, a subtle but significant increase in the level of cholesterol excreted within the urine of $Npc1^{-/-}$ compared to $Npc1^{+/+}$ mice. This observation is most probably a reflection of the increased levels of cellular cholesterol in $Npc1^{-/-}$, as trace amounts of cell lysate from epithelial cells that shed from the wall of the urinary tract may have been included in the urine samples. In summary, no complex of CD/cholesterol was evident in either the serum or urine of $Npc1^{-/-}$ mice (**Fig. 3.4**), which suggests that HP-β-CD does not serve as a cholesterol carrier in $Npc1^{-/-}$ cells. Alternatively these results suggest that HP-β-CD briefly shuttles cholesterol from the lysosome of $Npc1^{-/-}$ cells and then releases the previously trapped cholesterol within the cell. However, these *in vivo* data do not rule out the possibility that HP-β-CD acts in $Npc1^{-/-}$ mice to release a humoral factor from a single tissue.

Gene expression changes related to sterol homeostasis in $Npc1^{-/-}$ mouse tissues following acute HP-β-CD exposure were confirmed *in vitro* using primary cultured cells from $Npc1^{-/-}$ mice (**Fig. 3.7**). This suggests that HP-β-CD directly acts on cells to alter intracellular cholesterol trafficking and rules out a humoral intermediate. These observations extend findings from CHO cells and fibroblasts (Abi-Mosleh et al., 2009; Rosenbaum et al., 2010) to pertinent cell types: neurons and macrophages. While this manuscript was in preparation, the Vance group published an eloquent report detailing experiments from primary neurons, microglia, and astrocytes, which were harvested from $Npc1^{-/-}$ mice and treated in culture with doses from 0.1 to 10mM HP-β-CD (Peake et al., 2011). With the lowest dose of 0.1mM HP-β-CD, significant reductions in SREBP2 and its target genes were measured after 24h of treatment in $Npc1^{-/-}$ primary neurons (Peake et al., 2011). This is consistent with the decrease in LDLR measured in $Npc1^{-/-}$ neurons after 4h treatment with 0.3 to 1.5mM HP-β-CD reported in this chapter (**Fig. 3.7**). However, at a dose of 1mM HP-β-CD, Vance's group surprisingly observed a significant increase in SREBP2 target genes in neurons from both $Npc1^{+/+}$ and $Npc1^{-/-}$ mice, which is contradictory to the results presented in

this chapter for 0.75 and 1.5mM HP-β-CD. Many differences between the two experiments could account for this discord: 4h vs. 24h of treatment; hippocampal vs. cerebellar granule primary neurons; and media that contained or lacked a source of lipid (FBS).

Although no changes in $Npc1^{+/+}$ neurons were seen after HP-β-CD in my studies, a significant decrease in the mRNA level for an LXR target gene in $Npc1^{+/+}$ macrophages was observed with 0.75 and 1.5mM HP-β-CD (**Fig. 3.7**). So one can infer that at these high concentrations, HP-β-CD could be extracting cholesterol from the cellular membrane at least in macrophages, which is consistent with Vance's observations. In order to prove that at the lowest dose of 0.3 mM (most comparable to what is seen *in vivo*) HP-β-CD was not working through this undesirable mechanism that could disrupt cellular membranes, SBE-β-CD was utilized. This modified form of β-CD can only bind to cholesterol in a 1:1 complex and, therefore, can not fully solubilize cholesterol from membranes (**Fig. 3.8**). In both primary $Npc1^{-/-}$ macrophages and neurons, 0.3mM SBE-β-CD worked as effectively as 0.3mM HP-β-CD at altering mRNA expression (**Fig. 3.9**). These data support previous *in vivo* results, which showed that either HP-β-CD or SBE-β-CD at a dose of 4000 mg/kg bw could return cholesterol synthesis in the liver and spleen of 7-day-old $Npc1^{-/-}$ to wildtype levels (Ramirez et al., 2011).

Taken together, these data suggest that at low concentrations HP-β-CD can alleviate the build-up of cholesterol in $Npc1^{-/-}$ cells without altering cholesterol at the cellular membrane, which would require a 2:1 binding of cholesterol. Instead the data presented here point to the alternative hypothesis, presented first by Dietschy (Liu et al., 2009), that HP-β-CD enters the lysosome through bulk-phase endocytosis where it can bypass NPC1 to release the trapped lysosomal cholesterol within the cytoplasm for normal cellular processing. My work enhances this molecular mechanism by further suggesting that HP-β-CD works by binding cholesterol in a 1:1 confirmation within the lysosome (**Fig. 3.10**). In support of this, Maxfield and colleagues showed that a methyl-β-CD conjugated to a dextran with AlexaFluor546 was present within the lysosome of $Npc1^{-/-}$ cells and was able to diminish staining for free cholesterol within the lysosome (Rosenbaum et al., 2010).
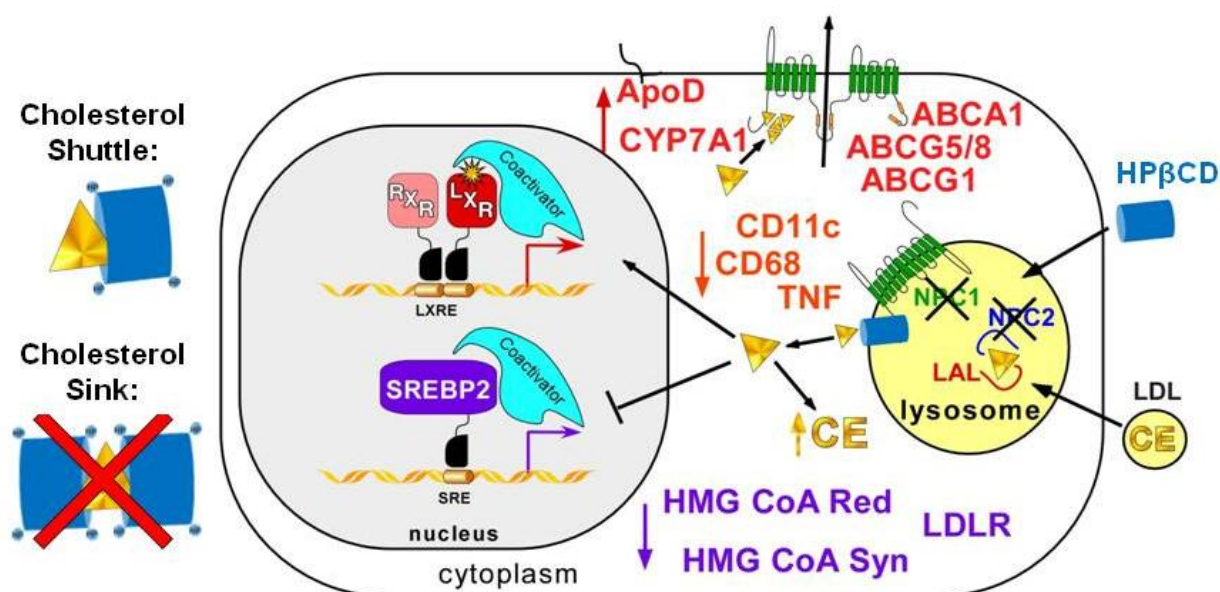
Figure 3.11 *Proposed molecular mechanism for HP-β-CD's effects in Npc1⁻/⁻ mice.* In cells without functional NPC1 or NPC2, the egress of free cholesterol (triangle) from the lysosome is blocked leading to massive lipid accumulation, enhanced cellular sterol synthesis (via SREBP2), decreased cholesteryl ester (CE) formation, reduced sterol elimination (via LXR), and increased inflammation. When cells are exposed to low concentrations of HPβCD, the cholesterol shuttle enters the lysosome and binds to free cholesterol in a 1:1 confirmation. HPβCD then releases the cholesterol across the limiting membrane of the lysosome into the cytosolic compartment allowing for: rapid decreases in sterol synthesis rates (via SREBP2), increases in cholesteryl ester (CE) formation and sterol elimination (via LXR), and ultimately decreases inflammation, which enhances cell survival.

In conclusion, comprehensive studies have been done to monitor the acute effects of HP-β-CD in *Npc1⁻/⁻* mice. Overall, these data suggest that HP-β-CD is not acting as a "sink" to bind and carry cholesterol out of cells into plasma and/or out of the body, but is liberating the trapped unesterified cholesterol from the lysosomes of *Npc1⁻/⁻* cells very rapidly by facilitating the egress of this cholesterol to intracellular sites for normal sterol processing.

CHAPTER FOUR:

Determining the Effect of Dual Cyclodextrin and Liver X Receptor Agonist

Therapy on the Progression of Niemann Pick Disease

4.1 Abstract

As there are no pharmacological agents approved by the US Food and Drug Administration to extend lifespan in patients with Niemann Pick Type C (NPC) disease, small bioavailable compounds have been sought that increase the lifespan of the $Npc1^{-/-}$ mouse. First, it was found that an agonist for the oxysterol nuclear hormone receptor, Liver X Receptor (LXR), increases cholesterol efflux from brain, reduces neuroinflammation, and delays neuronal cell death, which leads to a modest but significant increase in lifespan. However, the LXR agonist used causes hepatic steatosis and splenomegaly, two symptoms already aggravated in NPC disease. Then, 2-hydroxypropyl-β-cyclodextrin (HP-β-CD), a cholesterol-binding agent, was found to facilitate the release of trapped lysosomal cholesterol leading to a dramatic increase in lifespan. Unfortunately, HP-β-CD does not relieve the lung disease observed in the $Npc1^{-/-}$ mouse and does not appear to reach the brain after the mature blood-brain-barrier has formed. This observation led back to the LXR agonist, which has been shown in other models to reduce pulmonary inflammation and can cross the mature blood-brain-barrier, and stimulated the hypothesis that coadministration of HP-β-CD with an LXR agonist would have an additive effect on relieving NPC disease progression. To test this, wildtype and $Npc1^{-/-}$ mice were given weekly injections of HP-β-CD and fed the LXR agonist, T0901317. $Npc1^{-/-}$ mice treated with HP-β-CD and LXR agonist in combination lived significantly longer than those treated with vehicle; however, dual treatment provided no added benefit in survival over HP-β-CD alone. $Npc1^{-/-}$ mice had more difficulty breathing in pulmonary function tests than wildtype mice, which was not affected by either treatment. Overall, providing HP-β-CD and LXR agonist in combination had no added benefit greater than HP-β-CD administration alone. Notably, this suggests the two agents have overlapping mechanisms of action to relieve NPC disease progression.

4.2 Introduction

Niemann Pick Type C (NPC) disease is a rare lysosome storage disorder, which is estimated to affect 1 in 120,000 live births. NPC is transmitted by autosomal recessive inheritance, in which both parents are silent carriers of inactivating mutation(s) in one of two proteins required to transport cholesterol through the lysosomal compartment: NPC1 or NPC2 (Vanier, 2010) (Patterson et al., 2012). Mutations in NPC1, a large 13-transmembrane protein found in the late endosome/early lysosome (LE/L), are most common and represent 95% of NPC cases; while, mutations in the small (132 amino acids) soluble NPC2 protein account for the remaining NPC cases where the genetic cause has been identified (Ory, 2004). Regardless of the underlying mutation, patients with NPC typically suffer from progressive neurodegeneration, which presents in late infancy/early childhood with vertical supranuclear gaze palsy, cerebellar ataxia, gelastic cataplexy, and seizures; and die between 10 and 25 years of age (Vanier, 2010). In additional to the prominent neurological symptoms, children with NPC also suffer from preceding systemic disease, including hepatomegaly, splenomegaly, and chronic pulmonary disease (Patterson et al., 2012). Lung involvement is particularly common with NPC2 mutations (Millat et al., 2001; Bjurulf et al., 2008; Griese et al., 2010) but is also known to occur with NPC1 mutations (Palmeri et al., 2005). Indeed, respiratory distress, which is often difficult to diagnose as NPC, can be life-threatening in infancy before neurodegeneration has a chance to occur (Millat et al., 2001).

Once a child has been diagnosed with NPC either by identification of mutations in NPC1 or NPC2 or by a positive filipin test, which shows the characteristic accumulation of free cholesterol within cells, there is are virtually no therapeutic options to halt the progression of the disease. The prevailing management plan for NPC in patients is to treat individual symptoms as they occur in order to improve quality of life; for example, anti-epileptic therapy can be prescribed to control seizures (Patterson et al., 2012). Using animal models, several potential therapies for NPC have been discovered to reduce neurodegeneration and to ultimately extend lifespan, including: an inhibitor of glucosylceramide synthase (N-butyldeoxynojirimycin or miglustat) (Zervas et al., 2001b); a Liver X Recptor agonist (T0901317 or

Tcmpd) (Repa et al., 2007); and a modified cyclodextrin (2-hydroxypropyl-β-cyclodextrin or HP-β-CD) (Liu et al., 2009). Of these therapies, miglustat was first described in NPC and has been since tested in clinical trials. Although whether this drug extended lifespan in patients was inconclusive, neurological symptoms were delayed compared to untreated controls (Patterson et al., 2007). While miglustat was approved as a therapy for NPC in the European Union, the United States Food and Drug Administration denied the request based on reported severe side effects including weight loss and tremors (Patterson et al., 2012).

After miglustat, Tcmpd was shown to reduce inflammation, improve neuronal survival, and lead to a slight but significant extension of lifespan by 10 days in the $Npc1^{-/-}$ mouse model (Repa et al., 2007). As LXR agonists are known to induce lipogenesis leading to hepatic steatosis and splenomegaly (Repa et al., 2000a; Schultz et al., 2000; Jung et al., 2011), they were not pursued as a therapy in NPC patients. Then in 2009, a single dose of HP-β-CD was shown to lead to dramatic sterol balance changes in 7-day-old $Npc1^{-/-}$ pups and to significantly extend lifespan by 30% (Liu et al., 2009). Further work found that serial injections of HP-β-CD could lead to a remarkable doubling of lifespan (Davidson et al., 2009; Ramirez et al., 2010); that HP-β-CD is beneficial in every organ except lung (Ramirez et al., 2010; Muralidhar et al., 2011); and that systemically-administered HP-β-CD can not cross the blood brain barrier of an adult animal (Aqul et al., 2011; Ramirez et al., 2011).

These observations lead me to revisit Tcmpd as a therapy to use in combination with HP-β-CD for the treatment of NPC disease. Previous work demonstrated that Tcmpd is capable of crossing the blood-brain-barrier in adult animals to achieve concentrations well above the EC_{50} for LXRα/β resulting in altered gene expression in the CNS (Whitney et al., 2002). In addition, Tcmpd has been effective in two models of neurodegeneration: in an Alzheimer disease mouse model (Lefterov et al., 2007) and in the $Npc1^{-/-}$ mouse (Repa et al., 2007). In addition, Tcmpd treatment has been shown to protect against induced lung injury by reducing the immune response and reactive oxygen species in a variety of rodent models including the challenges of lipopolysaccharide (Birrell et al., 2007; Gong et al., 2009) or

carrageenan (Crisafulli et al., 2010) or after infection with *Mycobacterium tuberculosis* (Korf et al., 2009). Thus, Tcmpd may be able to target lung and adult brain, two affected organs recalcitrant to systemically administered HP-β-CD therapy.
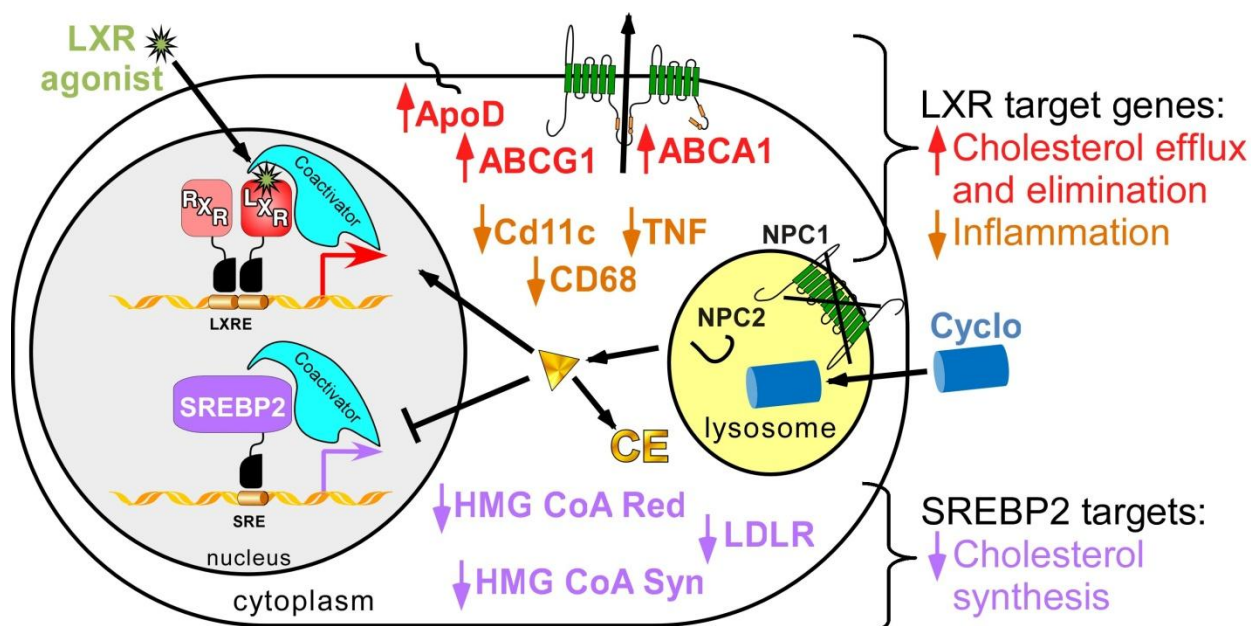
Figure 4.1 *Hypothetical model of dual HP-β-CD and LXR agonist treatment in a cell with mutant Npc1.* In cells without functional NPC1 or NPC2, the trafficking of free cholesterol (triangle) from the lysosome is blocked leading to massive lipid accumulation, enhanced cellular sterol synthesis (via SREBP2), decreased cholesteryl ester (CE) formation, reduced sterol elimination (via LXR), and increased inflammation. After **HPβCD** treatment, cholesterol will be released from the lysosome, resulting in: rapid decreases in sterol synthesis (via SREBP2), higher levels of CE content, as well as increases in sterol efflux and elimination (via LXR) and ultimately decreases inflammation, which the **LXR agonist** will further enhance.

These studies were designed to test if dual HP-β-CD and Tcmpd treatment would have an additive effect on alleviating the progression of NPC disease by improving pulmonary function, further enhancing Purkinje cell survival, and ultimately extending lifespan. In order to investigate this hypothesis (**Fig. 4.1**), wildtype and *Npc1*^{-/-} mice were treated with vehicle, HP-β-CD alone, Tcmpd alone, or dual HP-β-CD and Tcmpd treatment. Then, the mice were used to identify effects of treatment on pulmonary function, peripheral and neural inflammation, neurodegeneration, liver and kidney function, and survival. Overall, these studies provide novel insight into the molecular mechanisms by which HP-β-CD and Tcmpd delay the progression of NPC disease.

4.3 Materials and Methods

Animals and Treatments

Heterozygous (*Npc1*$^{+/-}$) mice were bred to generate wildtype (*Npc1*$^{+/+}$) and homozygous-null (*Npc1*$^{-/-}$) littermates (Loftus et al., 1997). For the ontogeny study, *Npc1*$^{+/+}$ and *Npc1*$^{-/-}$ littermates on a mixed BALB/c and C57BL/6 background were utilized. For all of other studies in this chapter, *Npc1*$^{+/+}$ and *Npc1*$^{-/-}$ mice were maintained on a pure BALB/c background. Mice were group-housed in plastic cages containing wood chip bedding in an animal facility with temperature-controlled rooms ($23 \pm 1°C$) and a maintained light cycle (12h light on/12h off). The mice were allowed *ad libitum* access to water and a standard rodent chow containing 0.02% w/w cholesterol (7001; Harlan Teklad, Madison, WI). For the dual treatment studies, 7-day-old pups were administered their first subcutaneous (sc) injection of HP-β-CD (H107, Sigma) at 4000 mg per kg body weight [mpk] or vehicle (saline at equivalent volume of 20 μl/g body weight (bw)). The mice continued to receive weekly HP-β-CD or saline treatments until their death. Pups were genotyped by 19 days of age and were weaned from their mothers at exactly 21 days of age. Beginning at 21-days-old, mice were fed a powdered form of Teklad 7001 diet with or without the synthetic LXR agonist, T0901317 (Tcmpd, #71810, Cayman Chemicals, Ann Arbor, MI), which was added at 0.1g per kg diet. Assuming a 25g mouse eats 5g of diet every day, the mice received a daily dose of 20 mpk until death. The mouse studies in this chapter utilized an equal number of age-matched males and females per group. All animal research was conducted in conformity with the Public Health Service Policy on Humane Care and Use of Laboratory Animals, and all experiments were performed with prior approval from University of Texas Southwestern Medical Center's Institutional Animal Care and Use Committee.

Assessment of survival and pulmonary function

Npc1$^{+/+}$ and *Npc1*$^{-/-}$ littermates (n= 10/mice group) were treated with vehicle (saline injection and fed chow), with HP-β-CD alone (HP-β-CD injection and fed chow), or with dual treatment (HP-β-CD

injection and fed Tcmpd in chow). Each week, weights of the mice were recorded. Beginning at 3 weeks

of age until death, pulmonary capacities were measured twice per week using a whole body

plethysmograph (#PLY4221, Buxco, Wilmington, NC). For the first 2 sessions, mice were allowed 10

minutes to acclimate to the chamber before the 5-minute recording was made. For each session

afterwards, mice were allowed 2 minutes rest before the recording. For each breathe, the enhanced pause

(Penh value) was calculated by (the peak expiratory height/ the peak inspiratory height) x the pause,

which is (the expiratory time/the time to expire 65% of the volume) -1(**Fig. 4.3A**). The average Penh

value over the 5 minutes was measured using the BioSystem XA: 2.11.2 software (Buxco). Penh is

defined by Buxco as a "unit-less index of airway hyper-reactivity." Although it is not a true measurement

of airway resistance, it is a powerful indicator of pulmonary function from awake, unrestrained animals.

For each treatment group, Penh value is plotted as average recording per week for 20 weeks, the area

under the curve, and as the average over lifespan.

For the survival study, all mice were given easy access to food and water by providing the powdered

form of 7001 diet on the floor of their cage and using water bottles with long spouts. At end stage, mice

were monitored twice daily. When a mouse could no longer intake food or water, this point was

considered death and the mouse was euthanized. Survival curves were plotted using GraphPad Prism5

software (GraphPad Software, Inc. San Diego, CA).

Measurement of relative mRNA levels

Tissues. For the ontogeny study, $Npc1^{+/+}$ and $Npc1^{-/-}$ littermates (n= 4 mice/ age) were studied at 10,

20, 30, 40, 50, 60, 70, and 80 days of age at the same point during the light cycle (3h after lights on or

Zeitgeber time (ZT) 3). Mice were exsanguinated; then lungs were collected and flash-frozen in liquid

nitrogen. For the dual-treatment study, $Npc1^{+/+}$ and $Npc1^{-/-}$ littermates (n= 6 mice/ group) were treated

with vehicle (saline injection and fed chow), with HP-β-CD alone (HP-β-CD injection and fed chow),

with Tcmpd alone (saline injection and fed Tcmpd in chow), or with dual treatment (HP-β-CD injection

and fed Tcmpd in chow). The mice were euthanized at exactly 50 days of age, 24h after receiving a final injection of saline or HP-β-CD, at the same point during the light cycle (ZT 2). Mice were exsanguinated; then liver, lung, brain (defined as the whole brain without cerebellum and brain stem), and cerebellum were collected and flash-frozen in liquid nitrogen.

All tissues were stored at -80°C until total RNA was isolated using RNA STAT-60 (Tel-Test, Inc.). RNA concentrations were determined by absorbance at 260nm with a Thermo Scientific Nanodrop 100 Spectrophotometer. 2ug of total RNA was treated with RNase-free DNase (Roche) and reverse-transcribed into cDNA with SuperScript II (Invitrogen) as previously described (Kurrasch et al., 2004; Valasek et al., 2005b). The cDNA was used to perform quantitative real-time PCR (qPCR) with the Applied Biosystems 7900HT sequence detection system. Each qPCR was analyzed in duplicate and contained in a final volume of 10 μl: 25 ng of cDNA, each primer at 150 nM, and 5 μl of 2x SYBR Green PCR Master Mix (Applied Biosystems). The nucleotide sequences of the primers used in this chapter are listed in Table C.3 of Appendix C. Results were evaluated by the comparative cycle number at threshold (C_T) method (Schmittgen et al., 2008) using cyclophilin as the invariant housekeeping gene (Dheda et al., 2004; Kosir et al., 2010), and mRNA levels were arithmetically adjusted to a unit of 1 for the *wildtype* control-treated group.

Histological examination of tissues

Tissues. $Npc1^{+/+}$ and $Npc1^{-/-}$ littermates (n= 4 mice/ group) were treated with vehicle (saline injection and fed chow), with HP-β-CD alone (HP-β-CD injection and fed chow), with Tcmpd alone (saline injection and fed Tcmpd in chow), or with dual treatment (HP-β-CD injection and fed Tcmpd in chow). The mice were euthanized at exactly 50 days of age, 24h after receiving a final injection of saline or HP-β-CD, at the same point during the light cycle (ZT 3). Under deep anesthesia, mice were perfused through the heart with saline (until the liver was completed blanched and the run-off was clear) followed by a 4% formaldehyde solution (HT501320, Sigma) for ~10 min (until all exposed organs were stiff to the touch).

Lungs were inflated by injecting 2mL of 4% formaldehyde directly into the trachea. Lungs, liver, and brain were carefully removed from the animal into a jar of 4% formaldehyde, which was kept during the day at ~23°C and overnight at 4°C. The following day, the tissues were washed 3x with PBS. At this point, the tissues were preserved in a PBS/0.02% sodium azide solution and stored at 4°C. Before sectioning, tissues were transferred to a 20% sucrose/PBS/0.02% sodium azide solution at 4°C for cryoprotection. Once the tissues were completely submerged in the sucrose solution (~2 days), they were sectioned.

Immunohistochemistry. All sectioning was done using a Leica CM 1850 cryostat at -20°C. Cerebella were dissected from the cryopreserved brains and were embedded in optimal cutting temperature compound (OCT, 4583, Tissue-Tek). The cerebella were sectioned along the sagital plane at 40uM. Sections were stored in a PBS/0.02% sodium azide solution at 4°C until the day of staining. Cryopreserved liver and lungs were embedded in OCT and sectioned at 6 μm and 10 μm, respectively. Sections were immediately placed on SuperFrost Plus glass slides (12-550-15; Fisher) and stored at -20°C until the day of staining. For macrophage and microglia identification, liver, lung, or cerebellar sections were stained for CD68 immunoreactivity. Sections were blocked with 3% goat serum and 0.25% Triton X-100 to permeabilize the cells. Then, sections were incubated with anti-CD68 (1:500; MCA1957T, AbD Serotec, Raleigh, NC) overnight at 4°C, followed by goat anti-rat Alexa 488 (1:1000; Invitrogen) for 2h. At this point the free floating cerebellar sections were mounted on slides. Slides were coverslipped with VectaShield Mounting medium w/ DAPI (H-1200, Vector Laboratories).

To show Purkinje cell structure, free-floating cerebellar sections were stained for calbindin immunoreactivity (Frank et al., 2003; Repa et al., 2007). Sections were blocked in 0.3% H_2O_2 to quench endogenous peroxidases and then with 3% goat serum and 0.25% Triton X-100 to permeabilize the cells. Then, sections were incubated with anti-calbindin D-28K (1:5000; AB1778, Millipore, Billerica, MA) overnight at 4°C, followed by biotinylated goat anti-rabbit (1:1000; BA-1000, Vector Laboratories, Burlingame, CA) for 2h, and NeutrAvidin-HRP (1:5000; 31030, Pierce, Rockford, IL) for 1h. The tissue-

bound peroxidase activity was revealed by incubating the sections in a 0.04% DAB/0.01% H_2O_2 (SK-4100, Vector Laboratories) for 2-3 min. Tissue sections were mounted on slides, dehydrated with increasing concentrations of EtOH, and then coverslipped with permount (SP15-100, Fisher). Each image shown is a representative histological section of 3 or more tissue slices stained from n=4 animals/group.

Evaluation of drug toxicity and liver function

Npc1$^{+/+}$ (n= 6/mice group) were treated with vehicle (saline injection and fed chow), with HP-β-CD alone (HP-β-CD injection and fed chow), or with dual treatment (HP-β-CD injection and fed Tcmpd in chow). The mice were injected with saline or HP-β-CD weekly beginning at 7 days of age and were fed Tcmpd daily beginning at 21 days of age. At 6 months of age, whole animal and liver weights were recorded. Blood samples were collected using heparin-coated syringes from the ascending vena cava of anesthetized mice. Plasma was separated from red blood cells by centrifugation at $1x10^4$x g for 10min at 4°C. Plasma samples were sent to UT Southwestern's Mouse Metabolic Phenotyping Core, where liver function tests (alanine aminotransferase (ALT); aspartate aminotransferase (AST); and alkaline phosphatase (ALP)) as well as other analytes (glucose, cholesterol, creatinine, and blood urea nitrogen) were measured. Analyses were performed using the Vitros 250 chemistry analyzer (Ortho-Clinical Diagnostics, Raritan, NJ). Liver function test results are reported as U per L of plasma; while, all other tests are reported as mg per dL of plasma. Liver weights are expressed as the percentage of whole body weight.

Data Analysis

All data are presented as the mean ± SEM. Statistically significant differences (*P*-value <0.05) between each group were determined using a one-way ANOVA followed by the Newman-Keuls multiple comparison test and are indicated by different letters. Significant differences in survival curves were determined by the Wilcoxon-Gehar and Log-rank analyses and are represented by **** (p<0.0001).

Significant differences in body weight curves were determined by calculating the area under the curve from 3 to 12 or 20 weeks and then performing a one-way ANOVA, which are also represented by *** ($p<0.001$). All statistical tests were performed using GraphPad Prism5 software (GraphPad Software, Inc. San Diego, CA).

4.4 Results

Pulmonary inflammation gradually increases over the lifespan of *Npc1*$^{-/-}$ mice:

Although the hallmark presentation of Niemann Pick Type C (NPC) disease is progressive neurodegeneration, pulmonary dysfunction is known to affect many patients and in some cases to be the cause of premature death (Millat et al., 2001). The *Npc1*$^{-/-}$ mouse has also be shown to display increased pulmonary inflammation and was recently shown to have decreased pulmonary function (Muralidhar et al., 2011). As HP-β-CD does not relieve the lung disease observed in the *Npc1*$^{-/-}$ mouse but appears to be beneficial to every other organ affected by NPC disease (Ramirez et al., 2010), this study was designed to test if an alternative treatment, an LXR agonist, known to extend lifespan in *Npc1*$^{-/-}$ mice could be given in combination with HP-β-CD to relieve pulmonary inflammation and improve lung function. Before beginning this dual treatment study, it was important to determine the age at which pulmonary inflammation began in *Npc1*$^{-/-}$ mice.

Npc1$^{+/+}$ and *Npc1*$^{-/-}$ mice were used in an ontogeny study to characterize lungs at various points in their lifespan from 10 to 80 days of age. The lungs of *Npc1*$^{-/-}$ mice had increased levels of a pro-inflammatory marker, *Cd11c* (**Fig. 4.2 A**), and of a cell surface marker for monocytes and macrophages, *Cd68* (**Fig. 4.2 B**) compared to *Npc1*$^{+/+}$ lungs starting as early as 20 days of age. While the markers stayed relatively constant in *Npc1*$^{+/+}$ mice, *Cd68* and *Cd11c* (**Fig. 4.2 A, B**) progressively increased over the lifespan of *Npc1*$^{-/-}$ mice. Therefore for the dual treatment study (**Fig. 4.2 C**), *Npc1*$^{+/+}$ and *Npc1*$^{-/-}$ littermates were given a weekly injection of HP-β-CD at 4000 mpk beginning at 7 days of age, along with

a low daily dose of LXR agonist, T0901317 (Tcmpd) at 20 mpk, in their diet beginning at 21 days of age.

The mice were then studied at 50 days of age after 7 doses of HP-β-CD and 4 weeks of daily Tcmpd

treatment or were allowed to live on to monitor survival and pulmonary function over their lifespan.
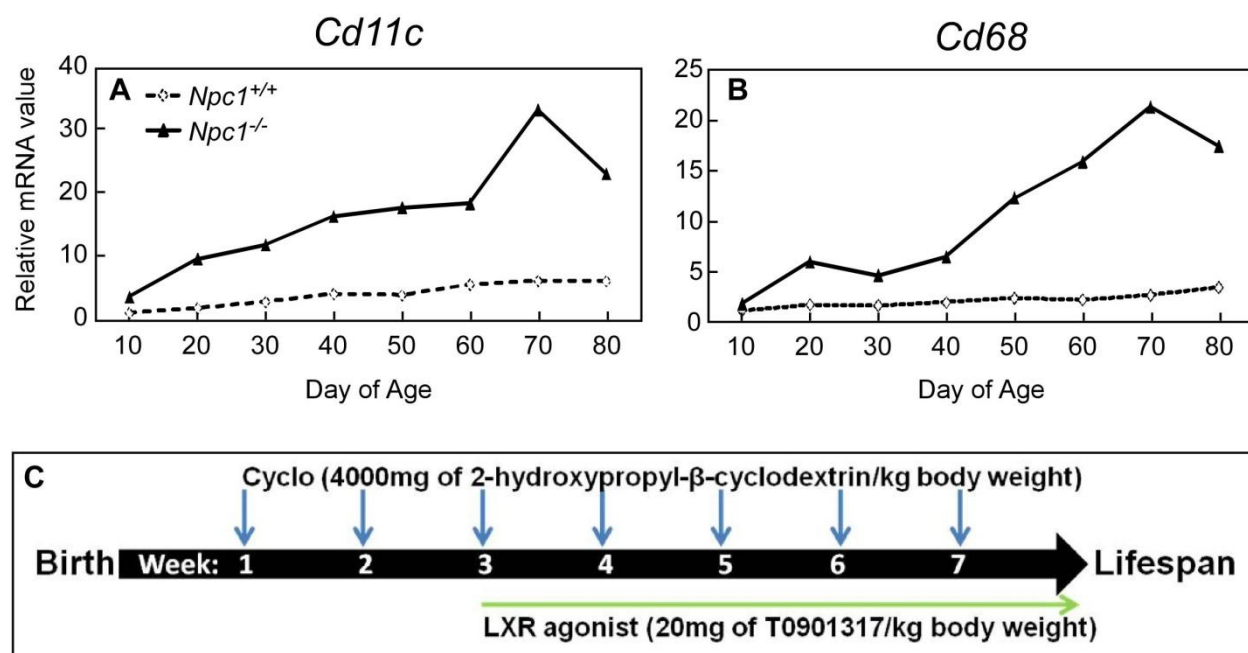
Figure 4.2 *Ontogeny of pulmonary inflammation in Npc1^{-/-} mice and dual treatment study design.* At 10, 20, 30, 40, 50, 60, 70, and 80 days of age, lungs were harvested from *Npc1*^{+/+} and *Npc1*^{-/-} mice (n=4 mice/ group). Total RNA was extracted from lungs and was pooled into groups. Relative mRNA levels for *Cd11c* (**A**), pro-inflammation marker, and *Cd68* (**B**), a marker for macrophages, were measured by qPCR using cyclophilin as the invariant housekeeping gene. As pulmonary inflammation was elevated is *Npc1*^{-/-} mice as early as 20 days of age compared to *Npc1*^{+/+}, the dual treatment plan (**C**) included weekly injections of HP-β-CD beginning at 7 days of age and daily doses of LXR agonist in the diet beginning at 21 days of age. Mice were evaluated after 7 weeks of treatment or were used for a survival study.

Decreased pulmonary function in *Npc1*^{-/-} mice is not improved by dual treatment:

Npc1^{+/+} and *Npc1*^{-/-} mice were treated with vehicle, HP-β-CD alone, or Tcmpd and HP-β-CD in

combination. Beginning at 3 weeks of age, the mice were placed twice per week in a whole body

plethysmograph (**Fig. 4.3A**) to monitor pulmonary function. The enhanced pause (Penh value, **Fig. 4.3A**),

which is a unitless index that represents the difficulty an animal experiences in breathing, was calculated

for each mouse. Over their lifespan, *Npc1*^{-/-} mice had a higher Penh value, indicating reduced pulmonary

function, compared to *Npc1*^{+/+} littermates (**Fig. 4.3B-D**). The Penh value was, on average, steady for each

individual *Npc1*^{-/-} mouse until the last week of life, which was after 10 weeks in vehicle-treated controls
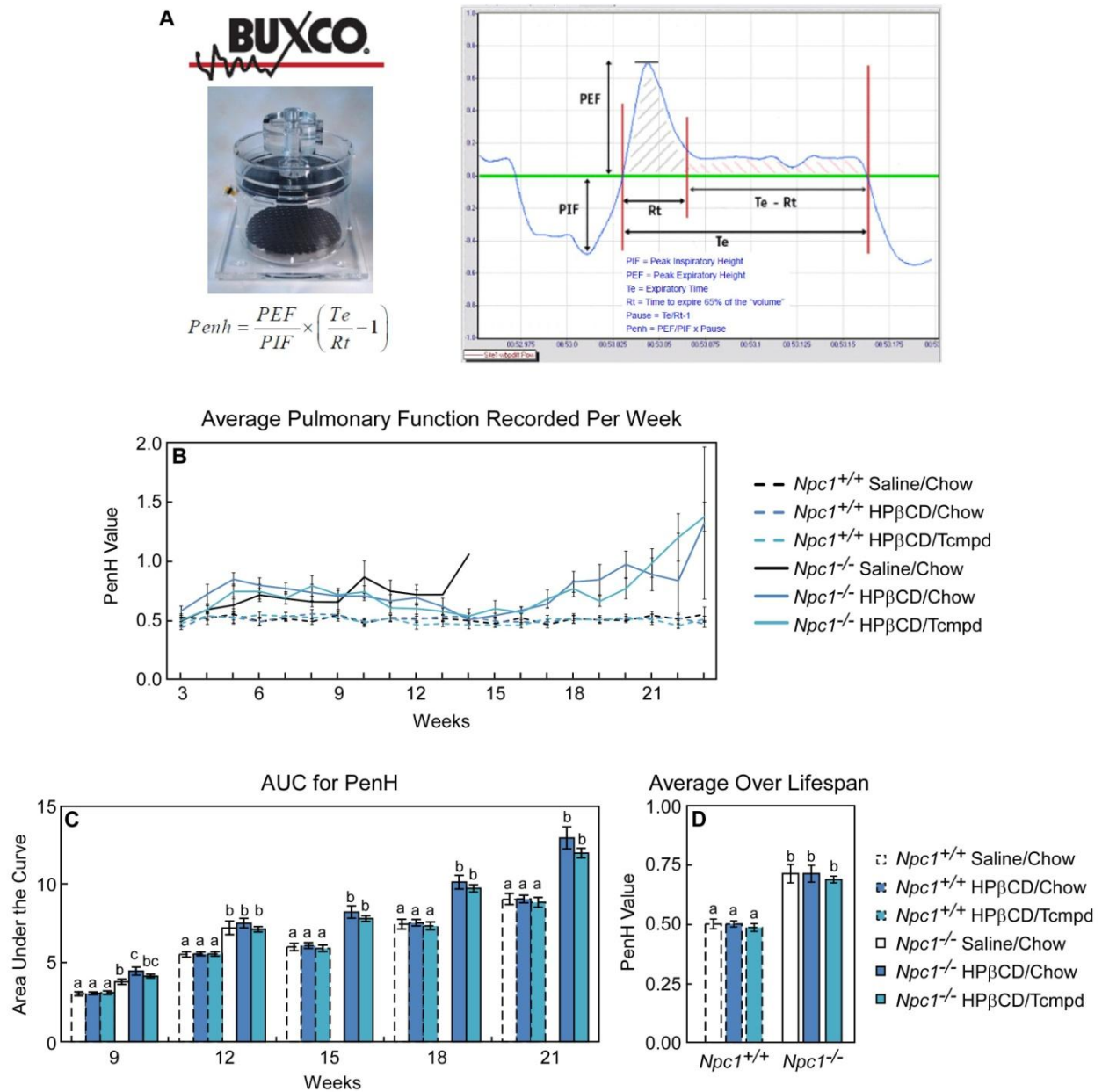
Figure 4.3 *Effect of HP-β-CD and Tcmpd on pulmonary function in Npc1$^{-/-}$ mice*. *Npc1$^{+/+}$* and *Npc1$^{-/-}$* littermates (n= 10/mice group) were treated over their lifespan with vehicle (saline injection and fed chow), with HP-β-CD alone (HP-β-CD injection and fed chow), or with dual treatment (HP-β-CD injection and fed Tcmpd in chow). Starting at 3 weeks of age, mice were placed in a Buxco Whole Body Unrestrained Plethysmograph twice per week to monitor pulmonary function by Penh (**A**). For each mouse, weekly averages of Penh value were determined, which are plotted as the mean per group ± SEM (**B**). In order to determine statistical significances between groups, the area under the curve (**C**) from averaged Penh values reported in (**A**) by week, as well as, the total average of all Penh values recorded over each mouse's lifespan (**D**) were calculated. Each bar represents the mean ± SEM. Statistically significant differences (P <0.05) between genotypes are indicated by different letters.

and after 20 weeks for the HP-β-CD alone and dual-treated groups. At this time point, the Penh value

dramatically increased, which can be seen when the average Penh for each group is plotted by week (**Fig.**

4.3B). HP-β-CD alone and dual treatment lead to no significant decrease in Penh value in *Npc1*^{-/-} mice compared to the control-treated group at any point (**Fig. 4.3C**). Importantly, neither treatment led to any increase in Penh value in *Npc1*^{+/+} mice (**Fig. 4.3C**). Overall, the results of the pulmonary function tests demonstrate that *Npc1*^{-/-} mice had more difficulty breathing than *Npc1*^{+/+}; however, dual treatment made this no better or worse (**Fig. 4.3D**).

LXR target genes were increased in liver, lung and brain by dual treatment of *Npc1*^{-/-}:

As dual Tcmpd and HP-β-CD treatment had no effect on pulmonary function *Npc1*^{-/-} mice, it was important to verify that Tcmpd reached the lung as well as other tissues effected by NPC disease such as liver and brain. To do so, *Npc1*^{+/+} and *Npc1*^{-/-} mice were treated with vehicle, HP-β-CD alone, Tcmpd alone, or dual treatment (Tcmpd and HP-β-CD in combination), and tissues were harvested at 50 days of age. *Npc1* mRNA levels confirmed genotype of *Npc1*^{+/+} and *Npc1*^{-/-} mice (**Fig. 4.3A-C**). After 4 weeks of daily Tcmpd treatment in chow, LXR target genes were found to be significantly higher than chow treated controls of both *Npc1*^{+/+} and *Npc1*^{-/-} mice in liver (*Abcg8*, **Fig. 4.3D**), lung (*Abcg1*, **Fig. 4.3E**), and brain (*Abca1*, **Fig. 4.3F**). Interestingly, dual Tcmpd and HP-β-CD treatment was able to significantly increase LXR target genes in liver over Tcmpd treatment alone in *Npc1*^{-/-} mice (**Fig. 4.3D**), but not in other *Npc1*^{-/-} tissues or in *Npc1*^{+/+} mice. This is consistent with previous reports where HP-β-CD was shown to increase the expression of LXR target genes in livers from *Npc1*^{-/-} mice (Liu et al., 2009) and to have no effect on cholesterol metabolism in *Npc1*^{+/+} mice or in *Npc1*^{-/-} lung and only limited effects in brains of adult *Npc1*^{-/-} mice (Liu et al., 2010a; Ramirez et al., 2010).

Livers and lungs, but not brains of *Npc1*^{-/-} mice have significantly higher levels of *de novo* cholesterol synthesis (Liu et al., 2010a) and of the transcriptional regulator of cholesterol synthesis, SREBP2, and its target genes, such as *HmgCoASyn* and *HmgCoARed* (**Fig. 4.3 H-J**). After 7 weekly doses of HP-β-CD, *HmgCoASyn* was significantly reduced down to wildtype levels in livers from *Npc1*^{-/-} mice (**Fig. 4.3 H)** but not in lung (**Fig. 4.3 I).** The addition of Tcmpd had no effect of SREBP2 targets alone or in

LIVER — LUNG — BRAIN

Relative mRNA Levels

A Npc1, B Npc1, C Npc1, D Abcg8, E Abcg1, F Abca1, G HmgCoASyn, H HmgCoASyn, I HmgCoARed, J Cd11c, K Cd11c, L Cd11c, M Cd68, N Cd68, O Cd68

Legend: Saline/Chow, HPβCD/Chow, Saline/Tcmpd, HPβCD/Tcmpd

$Npc1^{+/+}$ $Npc1^{-/-}$
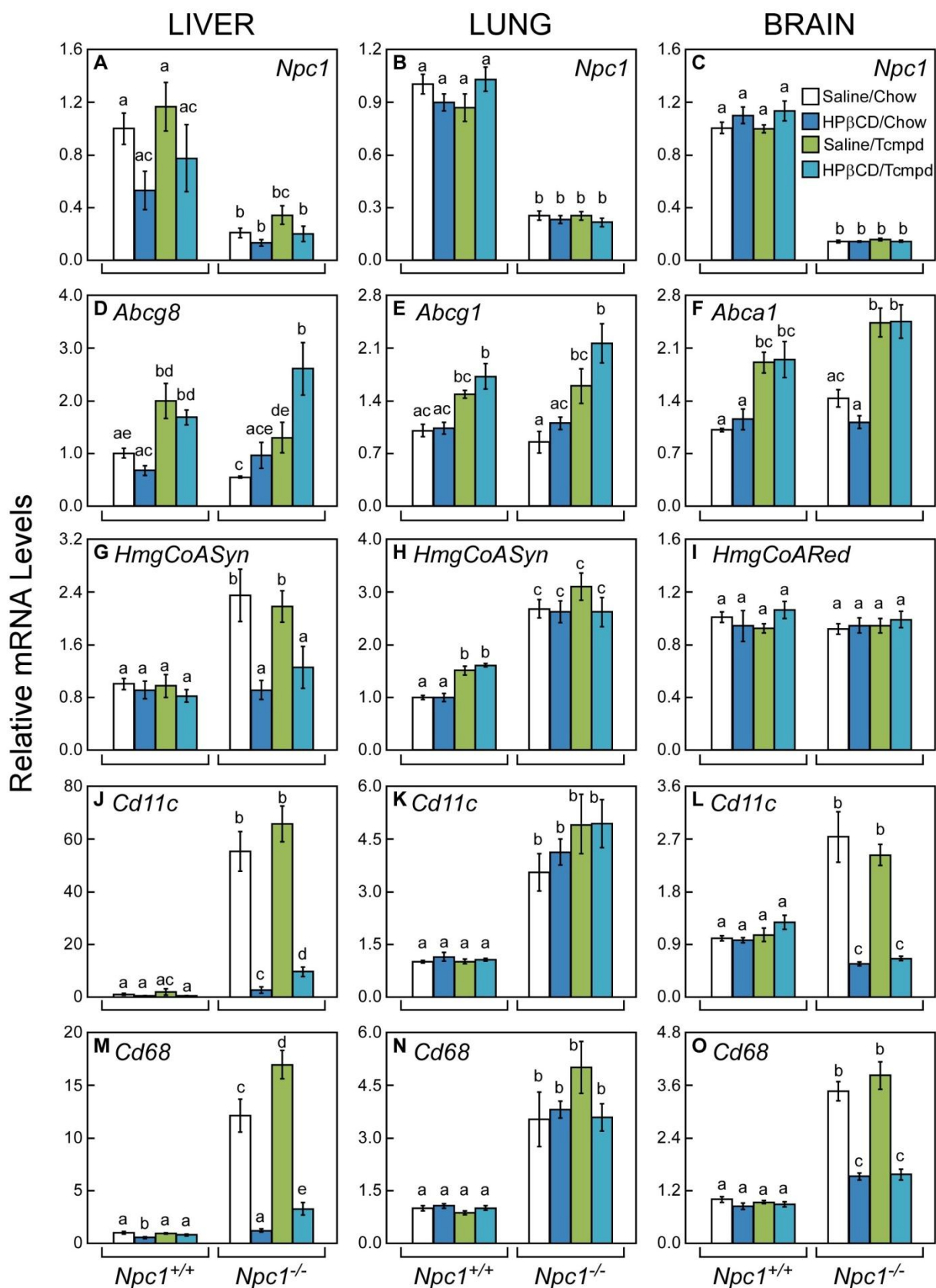
Figure 4.4 *Effect of HP-β-CD and Tcmpd on hepatic, pulmonary, and brain mRNA levels in Npc1$^{-/-}$ mice.* Tissues were harvested from 50-day-old *Npc1$^{+/+}$* and *Npc1$^{-/-}$*, which were treated with vehicle (saline injection and fed chow), with HP-β-CD alone (HP-β-CD injection and fed chow), with Tcmpd alone (saline injection and fed Tcmpd in chow), or with dual treatment (HP-β-CD injection and fed Tcmpd in chow). Total RNA was extracted from liver, lung, and brain. Relative mRNA levels of *Npc1* [**A-C**], LXR target genes [**D-F**], SREBP2 target genes [**G-I**], *Cd11c* [**J-L**], and *Cd68* [**M-O**] were measured by qPCR using cyclophilin as the invariant housekeeping gene. Each bar represents the mean ± SEM for 6 mice. Statistically significant differences (P <0.05) between groups are indicated by different letters.

combination with HP-β-CD in *Npc1$^{-/-}$* mice; however, Tcmpd was shown to significantly increase

HmgCoASyn in lung of *Npc1$^{+/+}$* mice. This suggested that Tcmpd could lead to an increase in cholesterol

synthesis in lungs of wildtype animals; although, future studies are needed to further investigate this

observation. Neither HP-β-CD nor Tcmpd had any effect on *HmgCoARed* expression in brain (**Fig. 4.3 J**).

Figure 4.5 *Effect of HP-β-CD and Tcmpd on hepatic inflammation in Npc1$^{-/-}$ mice.* *Npc1$^{+/+}$* and *Npc1$^{-/-}$* were treated with vehicle (saline injection and fed chow), with HP-β-CD alone (HP-β-CD injection and fed chow), with Tcmpd alone (saline injection and fed Tcmpd in chow), or with dual treatment (HP-β-CD injection and fed Tcmpd in chow). At 50-days-old, mice were perfused through the heart with saline followed by formalin. Livers were harvested and cryo-preserved in sucrose for sectioning at 6 μm. Liver sections were stained for CD68 immunoreactivity (**green**) to indicate microphage burden and co-stained with DAPI (**blue**) to show cell nuclei (**A-H**). Each image shown is a representative histological section from 3 or more slices stained from n=4 animals/group.

Peripheral inflammation is not further improved by dual treatment in *Npc1$^{-/-}$* mice:

mRNA analyses verified that Tcmpd was successfully delivered to its target tissues as LXR target

genes were significantly increased in liver, lung, and brain of Tcmpd-treated mice and that HP-β-CD was

delivered to liver as SREBP2 target genes were significantly reduced in $Npc1^{-/-}$ mice. Next, it was

evaluated whether HP-β-CD alone, Tcmpd alone, or dual-treatment could reduce the inflammation seen in

peripheral tissues of $Npc1^{-/-}$ mice. As shown throughout lifespan in lung (**Fig. 4.2 A,B**), at 50 days of age

Cd11c (**Fig. 4.4 J, K**) and *Cd68* (**Fig. 4.4 L, M**) were significantly increased in $Npc1^{-/-}$ mice compared to

$Npc1^{+/+}$ in both liver and lung. While HP-β-CD alone and dual treatment were able to significantly reduce

these markers in liver (**Fig. 4.4 J, M**), they had no effect on lung (**Fig. 4.4 K, N**). Dual Tcmpd and HP-β-

CD treatment had no benefit over HP-β-CD alone, and in fact had a slightly diminished effect at reducing

hepatic inflammation (**Fig. 4.4 J, M**), consistent with reports that Tcmpd alone can lead to hepatotoxicity
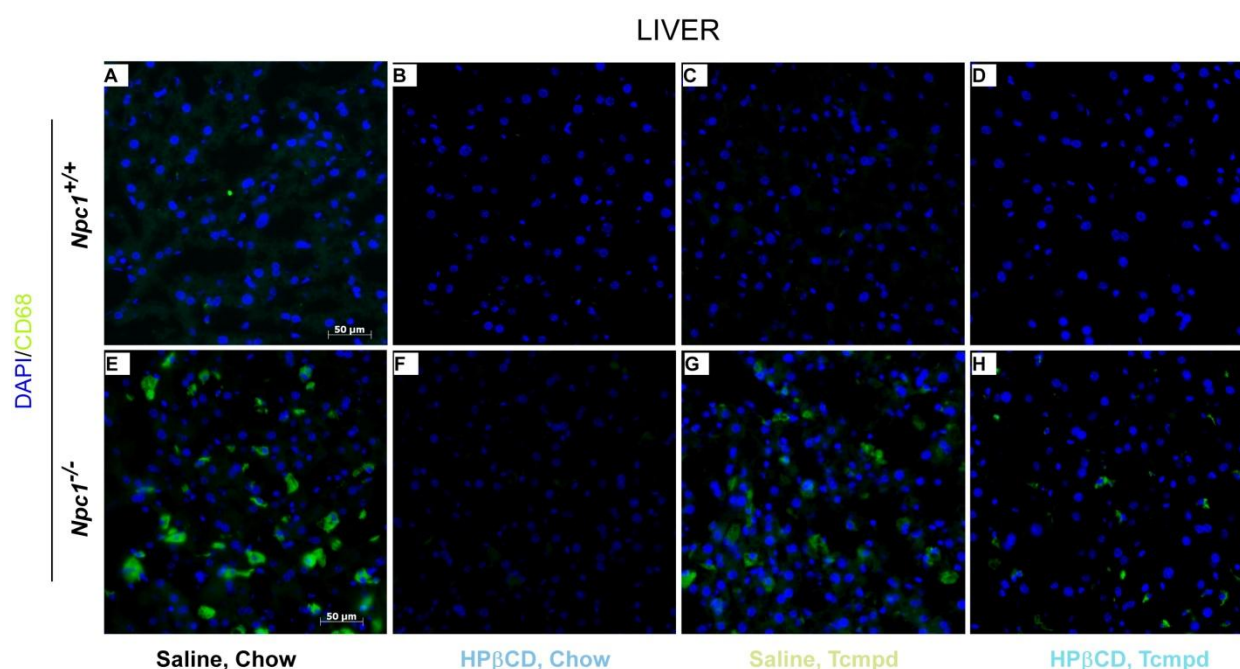
(Jung et al., 2011).
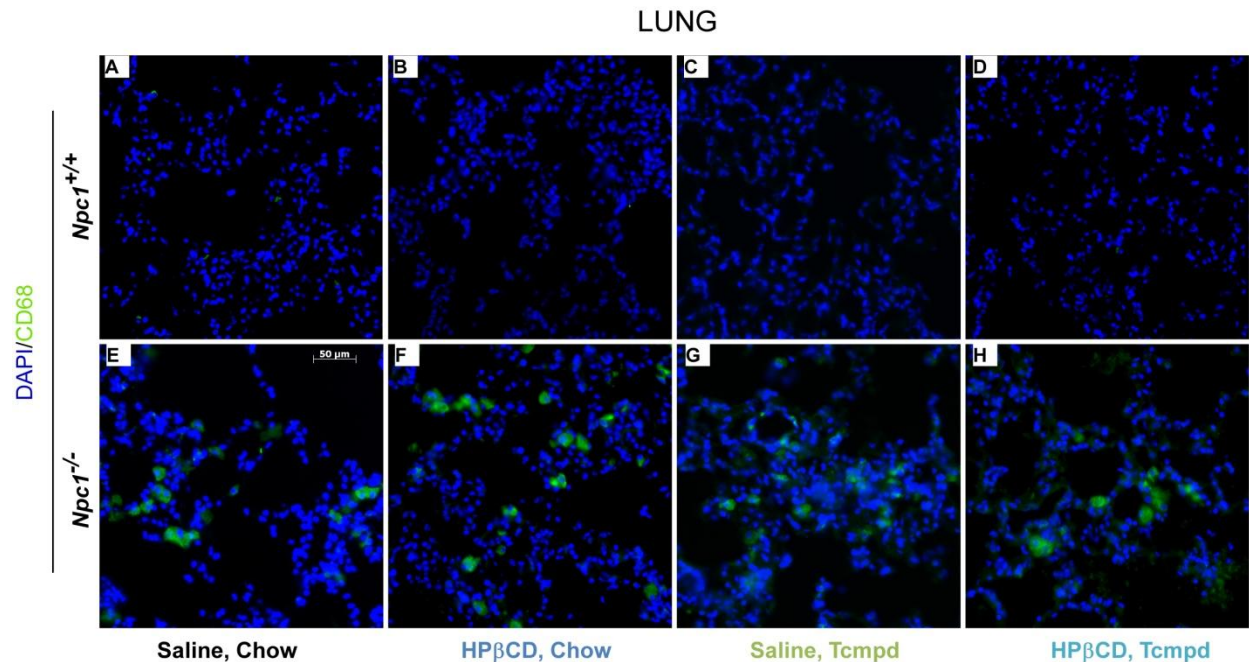
Figure 4.6 *Effect of HP-β-CD and Tcmpd on pulmonary inflammation in Npc1^{-/-} mice.* ** *Npc1^{+/+}* and *Npc1^{-/-}* were treated with vehicle (saline injection and fed chow), with HP-β-CD alone (HP-β-CD injection and fed chow), with Tcmpd alone (saline injection and fed Tcmpd in chow), or with dual treatment (HP-β-CD injection and fed Tcmpd in chow). At 50-days-old, mice were perfused through the heart with saline followed by formalin. Lungs were inflated by injecting formalin directly into the trachea. Lungs were harvested and cryo-preserved in sucrose for sectioning at 10 μm. Lung sections were stained for CD68 immunoreactivity (green**) to indicate macrophage burden and co-stained with DAPI (**blue**) to show cell nuclei (**A-H**). Each image shown is a representative histological section from 3 or more slices stained from n=4 animals/group.

In addition to the mRNA analyses, histology was used to evaluate macrophage infiltration in

peripheral tissues after vehicle, HP-β-CD alone, Tcmpd alone, or dual treatment. Livers from 50-day-old

vehicle-treated $Npc1^{-/-}$ mice **(Fig. 4.5E)** contained numerous with large CD68$^+$ macrophages, while virtually no macrophages were evident in $Npc1^{+/+}$ controls **(Fig. 4.5A)**. In liver, as observed for the mRNA levels of *Cd68*, the number of CD68$^+$ macrophages was reduced to wildtype levels with HP-β-CD alone **(Fig. 4.5F)** and were unchanged by Tcmpd treatment alone **(Fig. 4.5G).** Dual HP-β-CD and Tcmpd treatment **(Fig. 4.5H)** led to an overall reduction in the number and the size of CD68$^+$ cells; however, small macrophages were present in larger numbers compared HP-β-CD alone **(Fig. 4.5F)**. Neither treatment lead to a visible increase in CD68$^+$ cells in livers from $Npc1^{+/+}$ mice **(Fig. 4.5A-D)**. As in liver, lungs from 50-day-old vehicle treated $Npc1^{-/-}$ mice **(Fig. 4.6E)** contained large CD68$^+$ macrophages. HP-β-CD alone **(Fig. 4.6F)**, Tcmpd alone **(Fig. 4.6G)**, and dual treatment **(Fig. 4.6H)** were unable to reduce the number of macrophages in lung. The treatments did not lead to any increase in CD68$^+$ cells in either $Npc1^{+/+}$ **(Fig. 4.6A-D)** or $Npc1^{-/-}$ mice **(Fig. 4.6E-H)**.

Dual treatment does not further alter Purkinje cell survival or microglia burden in $Npc1^{-/-}$ brains:

When administered alone, Tcmpd (50 mg/kg starting at P21)(Repa et al., 2007) and HP-β-CD (4,000 mg/kg starting at P7)(Liu et al., 2009) have been shown to enhance Purkinje cell survival and to reduce neuronal inflammation in $Npc1^{-/-}$ mice compared to control animals. However, the two agents have never been compared directly or tested in combination; therefore, brains and cerebellum were evaluated from 50-day-old dual treated $Npc1^{+/+}$ and $Npc1^{-/-}$ mice. As observed in liver and lung (**Fig. 4.4**), the relative mRNA levels of *Cd11c* (**Fig. 4.4 L**) and *Cd68* (**Fig. 4.4 O**) in brain were significantly increased in $Npc1^{-/-}$ compared to $Npc1^{+/+}$ mice. HP-β-CD treatment significantly reduced *Cd11c* to levels lower than those seen in wildtype (**Fig. 4.4 L**) and decreased *Cd68* to levels approaching those in wildtype brain (**Fig. 4.4 O**). Tcmpd had no significant effect on reducing the inflammation markers in whole brain, and thus the dual Tcmpd and HP-β-CD treatment had no benefit over HP-β-CD alone.

Although dual treatment appeared to have no benefit in whole brain, cerebellum was further
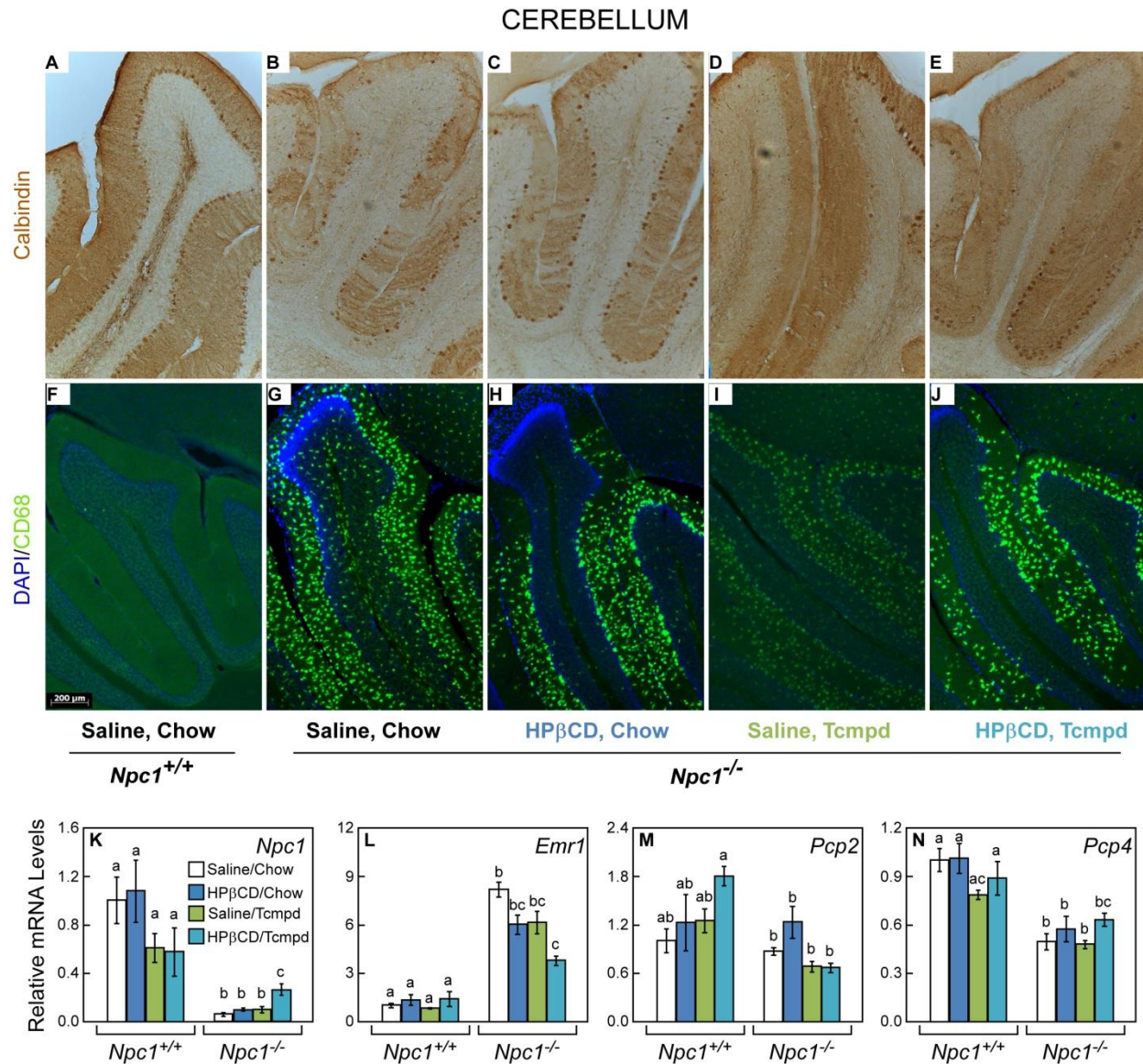
CEREBELLUM

Figure 4.7 *Effect of HP-β-CD and Tcmpd on Purkinje cell survival and inflammation in the cerebellum of Npc1^-/- mice. Npc1^+/+* and *Npc1^-/-* were treated with vehicle (saline injection and fed chow), with HP-β-CD alone (HP-β-CD injection and fed chow), with Tcmpd alone (saline injection and fed Tcmpd in chow), or with dual treatment (HP-β-CD injection and fed Tcmpd in chow). At 50-days-old, one cohort of mice was perfused through the heart with saline followed by formalin. Brains were harvested and cryo-preserved in sucrose for sectioning at 40uM. Free-floating cerebellar sections were stained for calbindin immunoreactivity (**brown**) to show Purkinje cell structure (**A-E**) or for CD68 immunoreactivity (**green**) to indicate microglia burden and co-stained with DAPI (**blue**) to show cell nuclei (**F-J**). Each image shown is a representative histological section from 3 or more cerebellar slices stained from n=4 animals/group. A second cohort was used at 50-days-old to harvest cerebellum for total RNA extractions. Relative mRNA levels of *Npc1* (**K**), *Emr1* (**L**), and *Pcp2/4* (**M-N**) were measured by qPCR using cyclophilin as the invariant housekeeping gene. Each bar represents the mean ± SEM for 6 mice. Statistically significant differences (P <0.05) between groups are indicated by different letters.

examined as it is most affected area of the brain by NPC (Vance, 2006). As shown previously (**Fig. 2.3**),

by 50-days of age, *Npc1^-/-* mice displayed an extensive loss of Purkinje cells (**Fig. 4.7 B**) and manifested a

dramatic increase in microglia burden **(Fig. 4.7 G)** compared to *wildtype* controls **(Fig. 4.7A, F)**. Both

HP-β-CD **(Fig. 4.7 C, H)** and Tcmpd **(Fig. 4.7 D, I)** alone led to some preservation of Purkinje cells and

reduction in microglia burden over vehicle-treated $Npc1^{-/-}$ mice. This improvement in Purkinje cell

survival and decrease neuroinflammation was also seen in the dual-treated animals **(Fig. 4.7 E, J)**;

however, using histology it was not feasible to determine whether any of the changes were significant

compared to the other treatments. Therefore, quantitative PCR was used to evaluate the mRNA levels of

the microglia cell-surface markers *Emr1* and *Cd68,* as well as, the Purkinje cell markers *Pcp2/4* in

cerebellum **(Fig. 4.7)**. *Npc1* levels confirmed genotype of $Npc1^{+/+}$ and $Npc1^{-/-}$ mice (**Fig. 4.7 K**). As seen

with CD68$^+$ in cerebellar slices, *Emr1* (**Fig. 4.7 L**) and *Cd68* (data not shown) were significantly higher in

vehicle treated $Npc1^{-/-}$ mice compared to $Npc1^{+/+}$. While there was only a trend towards a decrease in

Cd68 with treatment, *Emr1* was shown to be significantly decreased with dual treatment compared to

vehicle treated $Npc1^{-/-}$ mice but not compared to the HP-β-CD or Tcmpd alone (**Fig. 4.7 L**). *Pcp2* (**Fig.**

4.7 M) and *Pcp4* (**Fig. 4.7 N**) were both found not to be significantly increased by HP-β-CD or Tcmpd

treatment in $Npc1^{-/-}$ mice. Therefore, although treatment increased calbindin$^+$ cells and reduced CD68$^+$

cells, overall this was not significant.

Dual treatment does not further extend lifespan in $Npc1^{-/-}$ mice over HP-β-CD treatment alone:

Weekly treatment with HP-β-CD (4,000 mpk starting at P7) was shown to double the lifespan of

$Npc1^{-/-}$ mice from ~85 days in saline treated animals to 160 days (Ramirez et al., 2010); while daily

treatment with Tcmpd (50 mg/kg starting at P21) was shown to modestly but significantly extend the

lifespan of $Npc1^{-/-}$ mice by 10 days (Repa et al., 2007). In this dual treatment survival study, $Npc1^{-/-}$ mice

from the control group receiving standard chow containing low (0.02% w/w) cholesterol and weekly

injections of saline lived to be an average of 84.6±2.9 days **(Fig. 4.8 A)**. Weekly HP-β-CD (4,000 mg/kg

starting at P7) injections significantly extended lifespan by 44% to 151.5±3.5 days; whereas, the addition

of daily Tcmpd treatment (20 mg/kg starting at P21) to the weekly HP-β-CD injections increased lifespan

beyond the control group by 47% to 159.4±2.8 days (**Fig. 4.8 A**). Although the dual HP-β-CD and Tcmpd

treated *Npc1*$^{-/-}$ mice lived slightly longer than the HP-β-CD alone group, this difference did not reach

statistical significance. Weekly weights were recorded during the survival study, which showed that the

vehicle-treated *Npc1*$^{-/-}$ mice gained weight until 7 weeks of age and then gradually began losing weight

until their death around 12 weeks of age (**Fig. 4.8 B**). No difference was seen between the HP-β-CD alone

and dual-treated *Npc1*$^{-/-}$ groups, which gained weight until 12 weeks of age and then gradually began

losing weight until their death around 22 weeks of age (**Fig. 4.8 B**). Of note, neither HP-β-CD or dual

treatment had any effect on survival (data not shown) or on body weight in *Npc1*$^{+/+}$ mice (**Fig. 4.8 B**).
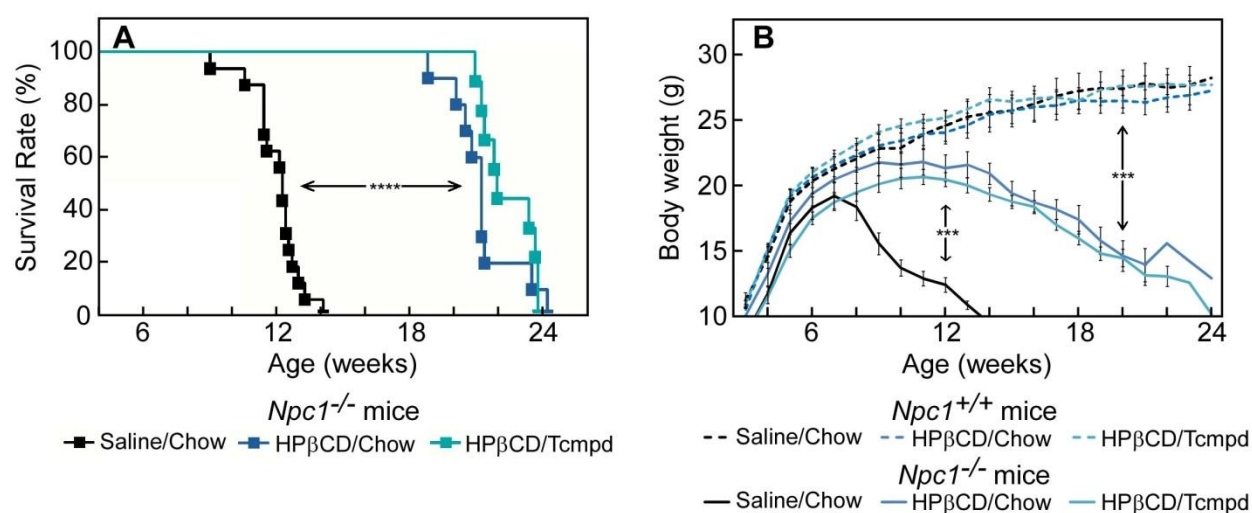
Figure 4.8 *Effect of HP-β-CD and Tcmpd on lifespan and body weight in the Npc1$^{-/-}$ mice. Npc1$^{+/+}$ and Npc1$^{-/-}$*
littermates (n=10/group) were treated over their lifespan with vehicle (saline injection and fed chow), with HP-β-
CD alone (HP-β-CD injection and fed chow), or with dual treatment (HP-β-CD injection and fed Tcmpd in chow).
Beginning at 7d, mice received weekly injections of saline or HP-β-CD. At 21d, mice were weaned on to standard
chow (0.02% cholesterol) with or without Tcpmd. (**A**) *Npc1*$^{-/-}$ mice treated with dual treatment (159d) or HP-β-CD
alone (152d) alone survived significantly longer than those treated with vehicle (86d, p<0.0001). Significant
differences in survival curves were determined by Wilcoxon-Gehar and Log-rank analyses using GraphPad Prism
software. (**B**) Body weights were recorded weekly. **Not Shown:** Treatment had no effect on survival in wildtype
mice.

Dual treatment of Tcmpd and HP-β-CD does not lead to liver or kidney toxicity in mice:

Long-term serial treatment with HP-β-CD has been suggested to lead to some damage of the lung

(Davidson et al., 2009) or kidney (Ramirez et al., 2010), while chronic administration of an LXR agonist,

such as Tcmpd, causes lipogenesis leading to hepatic steatosis (Schultz et al., 2000) (Jung et al., 2011). In

these studies, neither weekly HP-β-CD treatment or daily Tcmpd treatment was shown to have any
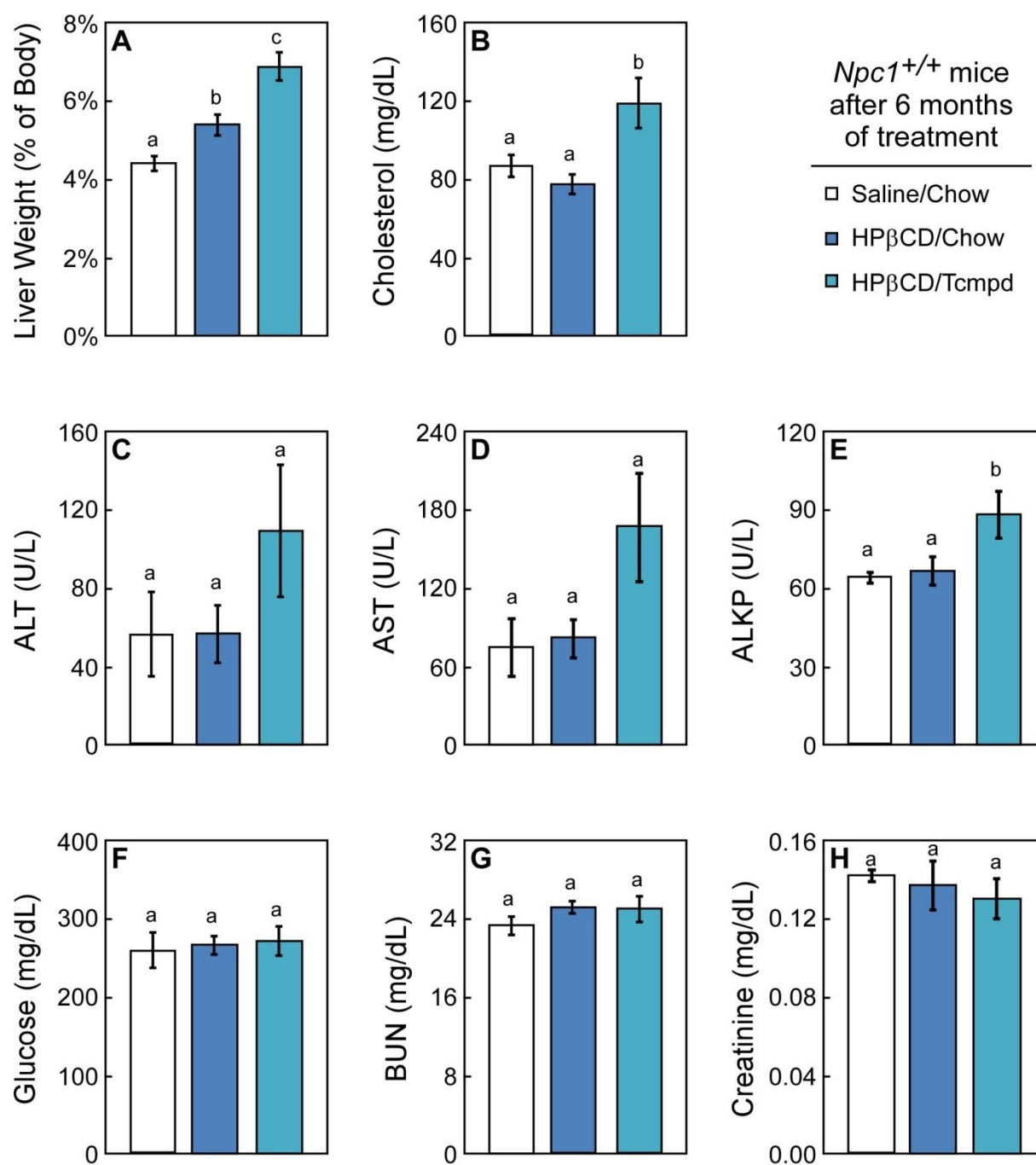
Figure 4.9 *Effect of HP-β-CD and Tcmpd on circulating markers of liver and kidney function in mice. Npc1⁺/⁺* mice were treated with vehicle (saline injection and fed chow), with HP-β-CD alone (HP-β-CD injection and fed chow), or with dual treatment (HP-β-CD injection and fed Tcmpd in chow). After 6 months of treatment, blood samples were collected, and liver weights (**A**) were recorded. Plasma was separated from whole blood and used to measure cholesterol (**B**); liver function (**C-E**) (alanine aminotransferase (ALT), aspartate aminotransferase (AST), and alkaline phosphatase (ALKP)); glucose (**F**); and kidney function (**G-H**) (blood urea nitrogen (BUN) and creatinine (Crea)). Each bar represents the mean ± SEM for 6 mice. Statistically significant differences (P <0.05) between groups are indicated by different letters.

negative impact on pulmonary function (**Fig. 4.3)** or to increase inflammation in lung (**Fig. 4.4,6)** in either $Npc1^{+/+}$ or $Npc1^{-/-}$ mice. To further investigate Tcmpd and HP-β-CD effects on liver and kidney function, liver and plasma were harvested from $Npc1^{+/+}$ after 6 months of chronic treatment with vehicle, HP-β-CD alone, or a combination of HP-β-CD and Tcmpd. As predicted by Tcmpd effects, liver weights from the mice receiving dual HP-β-CD and Tcmpd treatment were significantly higher than those receiving vehicle or HP-β-CD alone (**Fig. 4.9A)**, which correlated with a significant increase in plasma cholesterol (**Fig. 4.9B)**. However unexpectedly, there was a significant increase in the liver weights of HP-β-CD compared to vehicle-treated Npc1$^{+/+}$ mice (**Fig. 4.9A)**, which will need to be further investigated. The increase in liver weight did not appear to be a sign of liver toxicity as neither HP-β-CD alone nor dual treatments led to a significant increase in liver function tests, alanine aminotransferase (ALT, **Fig. 4.9C)** or aspartate aminotransferase (AST, **Fig. 4.9D)**, or in liver inflammation (**Fig. 4.4,5)** in $Npc1^{+/+}$ mice. Dual treatment did led to a modest but significant increase in alkaline phosphatase (ALP, **Fig. 4.9E)**, which is also a marker for liver function. Neither treatment led to any changes in plasma glucose (**Fig. 4.9F**) or in markers of kidney function, blood urea nitrogen (BUN, **Fig. 4.9G**) and creatinine (**Fig. 4.9H**). In summary, although chronic dual HP-β-CD and Tcmpd had no added benefit in $Npc1^{-/-}$ mice over HP-β-CD alone, it does not appear to have any toxic effects even up to 6 months of treatment.

4.5 Discussion

Although pulmonary dysfunction is known to be a symptom of Niemann Pick Type C (NPC) disease (Millat et al., 2001), compared with more prominent phenotypes such as neurodegeneration, relatively little is known about the progression of lung disease in NPC patients and animal models. Of the few reports describing lung disease in the $Npc1^{-/-}$ mouse, only two have looked at histology in similarly treated animals at more than one time point (Manabe et al., 1995; Ramirez et al., 2010) and only one has measured lung function, which was done at a single time point (Muralidhar et al., 2011). In this chapter,

the ontogeny of lung disease is first described in the untreated $Npc1^{-/-}$ mouse compared to $Npc1^{+/+}$ littermates. The lack of functional NPC1 was shown to lead to a progressive increase in mRNA markers for macrophage burden and inflammatory state in lung (**Fig. 4.2**). The difference between the lungs of $Npc1^{-/-}$ and $Npc1^{+/+}$ mice was apparent as early as 3 weeks of age and continued to increase until 10 weeks of age. $Npc1^{-/-}$ mice were also found to have reduced pulmonary function compared to $Npc1^{+/+}$ mice, which was evident by 6 weeks of age and to exacerbate at 10 weeks of age, about a week prior to death (**Fig. 4.3**). This finding of decreased pulmonary function using alert animals in Whole Body Unrestrained Plethysmograph is consistent with the previous findings performed with 10-11 week old $Npc1^{-/-}$ mice using more extensive terminal pulmonary function tests, which require surgical ventilation of the animals (Muralidhar et al., 2011).

In addition to monitoring the ontogeny of lung disease in the $Npc1^{-/-}$ mice, these studies evaluated the potential effects of dual HP-β-CD and Tcmpd treatment on lung inflammation and pulmonary function. Previously, systemically administered HP-β-CD had been shown to lead to dramatic improvements in cholesterol metabolism in every organ except lung (Ramirez et al., 2010). Furthermore, HP-β-CD given chronically was suggested by one group to lead to increased pulmonary inflammation in mice (Davidson et al., 2009); while, Tcmpd has been shown to help prevent induced pulmonary injury (Birrell et al., 2007). Neither HP-β-CD alone nor dual treatment had any effect on pulmonary function in $Npc1^{+/+}$ or $Npc1^{-/-}$ mice (**Fig. 4.3D**). Tcmpd alone and dual treatment led to a significant increase in LXR target genes showing that the LXR agonist was effectively delivered to the lung; however, no treatment had any effect on reducing mRNA markers of inflammation or cholesterol synthesis (**Fig. 4.4**). In agreement, HP-β-CD and Tcmpd treatment were unable to reduce the number of macrophages in $Npc1^{-/-}$ lung compared to control group; however, the treatments also did not lead to an increase in macrophage burden in either $Npc1^{+/+}$ or $Npc1^{-/-}$ mice (**Fig. 4.6**). Overall, these results show that HP-β-CD does not increase inflammation in lung. Instead, they support the alternative hypothesis suggested by Ramirez (Ramirez et al., 2010) and Muralidhar (Muralidhar et al., 2011) that HP-β-CD treatment reduces NPC symptoms in

other tissues leading to an extension of lifespan and allowing more time for pulmonary disease to progress. While these findings show that Tcmpd was delivered to lung but had no effect in NPC, it is unclear whether HP-β-CD is able to penetrate the lung. In order to treat the pulmonary component of NPC, it will be important to determine in future studies if HP-β-CD is simply not getting into lung or if lung is resistant to its benefit.

As Tcmpd (Whitney et al., 2002) but not HP-β-CD (Ramirez et al., 2011) can cross the blood-brain-barrier of a mature animal, dual HP-β-CD and Tcmpd treatment was also hypothesized to improve Purkinje cell survival and to reduce neuroinflammation in NPC. Even though dual treatment significantly decreased microglia infiltration in brain and delayed neuronal loss in the cerebellum compared to untreated $Npc1^{-/-}$ mice (**Fig. 4.4,7**), it produced no obvious improvements over HP-β-CD treatment alone. In these studies, Tcmpd alone did not have as powerful of an effect at improving neuronal survival and inflammation as had been previously reported in $Npc1^{-/-}$ mice (Langmade et al., 2006; Repa et al., 2007). In both of these previous studies, mice were treated daily with 50 mg/kg Tcmpd. Thus, this discrepancy is likely due to the lower dose of 20 mg/kg, which was used in this study to circumvent the extreme hepatomegaly induced by the LXR agonist. Although it is possible that using a higher dose of Tcmpd along with weekly injections of HP-β-CD may have a stronger effect than HP-β-CD alone, this is unlikely as the lower dose of Tcmpd significantly increased LXR target genes in brain over HP-β-CD alone (**Fig. 4.4F**), which did not lead to a further rescue of neurons or a reduction in inflammation.

Although Tcmpd is known to stimulate hepatic lipogenesis leading to steatosis (Schultz et al., 2000; Jung et al., 2011), this is the first report to test hepatic inflammation and liver function after Tcmpd treatment in $Npc1^{-/-}$ mice. The low dose of Tcmpd was effectively delivered to liver in $Npc1^{+/+}$ and $Npc1^{-/-}$ mice, as it was able to induce a significant increase in the expression of LXR target gene, $Abcg8$ (**Fig. 4.4D**). In $Npc1^{-/-}$ mice, which already have dramatically increased hepatic inflammation compared to $Npc1^{+/+}$ animals, Tcmpd caused a slight but significant upregulation in the mRNA level of $Cd68$ but no obvious increase in number of $CD68^{+}$ cells in liver slices (**Fig. 4.4,5**). The addition of Tcmpd to weekly

HP-β-CD treatment in *Npc1*^{-/-} mice lead to increased inflammatory markers and CD68^{+} cells over HP-β-CD treatment alone (**Fig. 4.4,5**). Six months of dual Tcmpd and HP-β-CD treatment caused a significant increase in liver weight and plasma levels of cholesterol and ALKP, but no change in liver function tests, ALT and AST (**Fig. 4.9**). Tcmpd also did not have pro-inflammatory effects in any tissue examined from *Npc1*^{+/+} animals (**Fig. 4.4-6**). Six months of weekly HP-β-CD injections were found to exert no changes in liver or kidney function or alter any other plasma markers of toxicity examined compared to vehcile-treated *Npc1*^{+/+} mice (**Fig. 4.9**) suggesting that it is well tolerated by mice even at the extremely high dose of 4000 mg/kg.

As the addition of daily Tcmpd doses to weekly injections of HP-β-CD did not further improve lung function or neuronal survival, it was not unexpected that dual treatment led to no significant increase in the lifespan of *Npc1*^{-/-} mice over weekly HP-β-CD treatments (88.4% compared to 79.1%, **Fig. 4.8**). In a previous study testing the effect of the neurosteroid allopregnanolone, *Npc1*^{-/-} mice were given a single injection of allopregnanolone prepared in HP-β-CD (4000 mg/kg) at 7 days of age and then were fed Tcmpd (50 mg/kg) daily beginning at weaning. This dual treatment strategy was shown to significantly extend lifespan in *Npc1*^{-/-} mice compared to a single dose of allopregnanolone prepared in HP-β-CD (Langmade et al., 2006). Although this combination therapy study is complicated by the addition of allopregnanolone (which has since been shown to have no effect on lifespan in *Npc1*^{-/-} mice (Liu et al., 2009)), they show that daily Tcmpd treatment with a single dose of HP-β-CD extended lifespan by 72% compared to vehicle treated *Npc1*^{-/-} mice (Langmade et al., 2006). As weekly HP-β-CD alone led to a 79.1% increase in the lifespan of *Npc1*^{-/-} mice in the studies presented in this chapter, dual Tcmpd and HP-β-CD treatment did not appear to have any added benefit over weekly HP-β-CD administration alone. This suggests that Tcmpd, with the risk of hepatic toxicity, should not be pursued as a combination therapy with HP-β-CD for NPC disease. However, these results do not refute the importance of LXR activation in alleviating the progression of NPC disease. They only suggest that the initial level of LXR activation achieved by HP-β-CD alone is sufficient (**Fig. 4.1**) and that additional activation by an LXR

agonist has no added benefit. In order to fully address LXR contribution to HP-β-CD effect in NPC, the $Npc1^{-/-}$ mouse will need to be bred onto an LXRα/β deficient mouse strain and treated with HP-β-CD.

Overall, the data presented in this chapter suggest that Tcmpd and HP-β-CD act via a similar molecular mechanism to delay the progression of NPC. Further, the results advocate that only one of the compounds should be given at a time. As high doses of Tcmpd can lead to hepatotoxicty and HP-β-CD appears to have more substantial effects, serial HP-β-CD therapy is currently the best candidate for the treatment of NPC disease in patients.

CHAPTER FIVE:

Conclusions and Recommendations

5.1 Overall Conclusions and Implications

Cholesterol is essential to mammalian life; therefore, the synthesis, entry, and efflux of cholesterol are tightly regulated processes within the body. In some rare disease states, such as in Niemann-Pick Type C (NPC), cholesterol balance is lost resulting in premature death. NPC disease, which is estimated to affect 1:120,000 live births, is caused by inactivating mutations in one of two cholesterol trafficking proteins, NPC1 or NPC2, leading to the entrapment and accumulation of unesterified cholesterol within the lysosome. Regardless of the underlying mutation, patients with NPC typically suffer from progressive neurodegeneration, which presents in late infancy/early childhood with vertical supranuclear gaze palsy, cerebellar ataxia, gelastic cataplexy, and seizures; and die between 10 and 25 years of age (Vanier, 2010). In addition to the prominent neurological symptoms, children with NPC also suffer from systemic disease, including liver dysfunction, hepatosplenomegaly, and chronic pulmonary disease (Patterson et al., 2012).

Currently there are no pharmacological agents that have been approved by the US Food and Drug Administration (FDA) to extend lifespan in children with NPC. However, small-molecule therapeutics, including a Liver X Receptor (LXR) agonist (Repa et al., 2007) and a modified cyclodextrin (Liu et al., 2009), have been shown to increase lifespan in the $Npc1^{-/-}$ mouse model, which displays many of the symptoms found in patients with NPC. Although both of these potential therapies are known to alter cholesterol dynamics in the cell, the molecular mechanism(s) through which they are able to overcome the defect in NPC and ultimately to enhance survival have not been fully elucidated, which was the main focus of this dissertation. Overall, this work further clarifies the mechanism(s) of action by which LXR agonists and cyclodextrins delay disease progression and could lead to the development of more effective therapies for patients with NPC.

5.1.1 LXR agonists and Niemann-Pick Type C Disease

One primary aim of this work was to evaluate a potential molecular mechanism by which modulations in LXR activity alter NPC disease progression.The ATP-binding cassette transporter G1 (*Abcg1*) is a LXR target gene known to play an important role in the efflux of cholesterol from macrophages (Baldan et al., 2006a; Kim et al., 2008)and has been suggested to be involved in the intracellular transport of cholesterol (Tarling et al., 2011). Thus, the $Npc1^{-/-}Abcg1^{-/-}$ mouse was generated and evaluated. These mice die significantly earlier (10d) than $Npc1^{-/-}$ littermates, which was consistent with the 10d reduction in lifespan of the $Npc1^{-/-}$ mice when they are on a *Lxrβ*-deficient background (Repa et al., 2007). Sterol balance studies, histological evaluations, and mRNA analyses in tissues from *wildtype*, $Abcg1^{-/-}$, $Npc1^{-/-}$, and $Npc1^{-/-}Abcg1^{-/-}$ mice overall revealed very few changes to account for the reduction in survival. While there were no differences evident in Purkinje cell survival or neuroinflammatory burden in the cerebella of the mice, $Npc1^{-/-}Abcg1^{-/-}$ mice displayed a significant increase in macrophage infiltration of peripheral tissues compared to $Npc1^{-/-}$ littermates. Further, primary macrophages from $Npc1^{-/-}Abcg1^{-/-}$ showed significantly higher cytokine secretion after lipopolysaccharide challenge than $Npc1^{-/-}$ macrophages. Taken together these data imply that in Niemann-Pick Type C disease, ABCG1 plays a vital role in reducing the peripheral inflammatory response, possibly through the intracellular transport and efflux of cholesterol from macrophages (models depicted in **Figs. 2.9 and 2.10**).

5.1.2 Cyclodextrins and Niemann-Pick Type C Disease

Another aim of this work was to evaluate the time course of changes elicited by a modified β-cyclodextrin (HP-β-CD) in $Npc1^{-/-}$ mice within the first 24h after administration to further understand HP-β-CD's mechanism(s) of action in NPC disease. Within 3h of HP-β-CD administration to 49-day-old $Npc1^{-/-}$ mice, a significant reduction in *de novo* sterol synthesis and increase in cholesteryl ester (CE) content occurred in liver; while, decreases in SREBP2 target genes and increases in LXR target genes

were apparent by 6h. Finally, 24h after HP-β-CD administration, inflammation was significantly reduced in *Npc1*$^{-/-}$ mice. These results (summarized in **Fig. 3.10**) imply that immediately after HP-β-CD administration in *Npc1*$^{-/-}$ cells, there is a large influx of cholesterol into the metabolically active pool of cholesterol within the cytoplasm, which is able to be utilized and sensed by the cell. Furthermore, the reduction in cytokines appears to be secondary to the changes in cholesterol dynamics after HP-β-CD. Taken as a whole, the time course data demonstrated that although HP-β-CD is cleared within 6h from mice, 24h is an adequate time point for studying the maximum effects of HP-β-CD *in vivo*.

In addition, no changes in cholesterol were evident in the urine or plasma of *Npc1*$^{-/-}$ mice within 24h after HP-β-CD administration, which suggest that HP-β-CD does not utilize a mechanism to carry cholesterol with it through the bloodstream to be secreted intact by the kidneys into the urine. Instead, studies performed in primary macrophages and neurons from *Npc1*$^{-/-}$ mice imply that HP-β-CD works by shuttling cholesterol intracellularly, as direct application of HP-β-CD to cells can elicit the decreases in SREBP2 target genes and increases in LXR target genes seen *in vivo*. Finally, SBE-β-CD, an alternative modified β-cyclodextrin which is sterically hindered from fully solubilizing cholesterol (model depicted in **Fig. 3.8**), was used alongside HP-β-CD in culture cell systems to establish that the mechanism of action for cyclodextrins in *Npc1*$^{-/-}$ cells does not rely on extracting cholesterol from membranes. Overall, these data suggest that HP-β-CD's mechanism of action (depicted in **Fig. 3.11**) is through liberating the trapped unesterified cholesterol from the lysosomes of *Npc1*$^{-/-}$ cells very rapidly by facilitating the egress of this cholesterol to intracellular sites for normal sterol processing.

5.1.3 Combination therapies for Niemann-Pick Type C Disease

In addition to the work described to define the mechanism(s) of action for the LXR agonist and cyclodextrin, a primary aim was to determine if a co-administration of the two agents had an additive effect on relieving NPC disease progression. *Npc1*$^{-/-}$ mice were given weekly injections of HP-β-CD beginning at 7 days of age and were fed a diet with added LXR agonist, T0901317 (Tcmpd), beginning at

21 days of age. *Npc1*$^{-/-}$ mice treated with the dual HP-β-CD and Tcmpd therapy lived significantly longer than those treated with vehicle; however, the dual-treatment provided no added extension in survival over HP-β-CD alone. Consistently, the combination of daily Tcmpd and weekly HP-β-CD injections in *Npc1*$^{-/-}$ mice had no advantage over HP-β-CD alone at preventing Purkinje cell loss, reducing peripheral or neural inflammation, or at decreasing molecular markers of cholesterol synthesis; however, dual treatment did further enhance the expression of LXR target genes showing that it was successfully delivered to liver, lung, and brain. Overall, these results imply that Tcmpd and HP-β-CD have overlapping mechanisms of action and suggest that only one of the compounds should be given at a time to delay the progression of NPC.

Long-term co-administration of Tcmpd and HP-β-CD in wildtype and *Npc1*$^{-/-}$ mice also provided insight into the safety of these small-molecule therapeutics. Although neither compound was found to improve pulmonary function or inflammation in *Npc1*$^{-/-}$ mice, Tcmpd and HP-β-CD had no negative effects in the lungs of wildtype or *Npc1*$^{-/-}$ mice. Additionally in wildtype mice, Tcmpd and HP-β-CD were shown to have no adverse effect on kidney function. Although daily dosing with Tcmpd did lead to a significant increase in hepatomegaly and plasma levels of alkaline phosphatase, it did not alter other liver function tests (alanine aminotransferase and aspartate aminotransferase) or increase hepatic inflammation in wildtype mice. As high doses of LXR agonists can lead to hepatotoxicty and HP-β-CD appears to have more substantial effects at preventing disease progression, serial HP-β-CD therapy appears to currently be the best option for the treatment of NPC disease.

5.2 Recommendations for Future Studies

5.2.1 Regarding LXR agonists

In the studies presented in this dissertation, the functional deletion of a single LXR target gene,

Abcg1, was shown to significantly reduce the lifespan of *Npc1*^{-/-} mice. Although these data suggested that the deletion of ABCG1 led to increased peripheral inflammation in *Npc1*^{-/-} mice, they did not address whether increased activity of ABCG1 would be beneficial in NPC (depicted in **Fig. 2.10**). This could be evaluated by breeding *Npc1*^{-/-} mice to a transgenic mouse model that overexpresses *Abcg1*, which has already be generated and described (Kennedy et al., 2005). As other therapies, besides LXR agonists, become available that increase either the expression or activity of ABCG1, they could also be tested in the *Npc1*^{-/-} mouse model. Additionally, more detailed analyses should be performed to compare peripheral inflammation and its effects on *Npc1*^{-/-} and *Npc1*^{-/-}*Abcg1*^{-/-} mice (which have now been backcrossed onto a pure BALB/c strain). As ABCG1 is known to play a significant role in maintaining pulmonary cholesterol homeostasis (Baldan et al., 2006b; Thomassen et al., 2007; Baldan et al., 2008; Wojcik et al., 2008), it may be particularly informative to evaluate the surfactant composition and perform pulmonary function testing on the *Npc1*^{-/-}*Abcg1*^{-/-} mice. Also to address if Tcmpd therapy, which led to an extension of lifespan in *Npc1*^{-/-} mouse, is working through ABCG1 in NPC disease, a survival study to test the effect of Tcmpd treatment should be performed in *Npc1*^{-/-} and *Npc1*^{-/-}*Abcg1*^{-/-} mice.

In addition to studies with ABCG1, the *Npc1*^{-/-}*Lxrβ*^{-/-} mice should be revisited. Although these mice were shown to have a statistically shorter lifespan compared to the *Npc1*^{-/-} mutant (Repa et al., 2007), no further analyses were done to determine why lifespan was shortened. It would be informative to know if these mice, like the *Npc1*^{-/-}*Abcg1*^{-/-} mice, have increased peripheral inflammation.

Finally although Tcmpd was found to significantly increase lifespan in *Npc1*^{-/-} mice (Repa et al., 2007), it is known to induce lipogenesis leading to hepatic steatosis and splenomegaly (J. J. Repa et al., 2000; Schultz et al., 2000), two symptoms already present in NPC disease. It is likely that while Tcmpd reduced neuroinflammation and delayed neuronal cell death, it further aggravated hepatosplenomegaly in *Npc1*^{-/-} mice. Therefore, it may be valuable to test the effects of other LXR agonists, which have been shown to have little impact on lipogensis (Miao et al., 2004; Peng et al., 2008), at extending lifespan in *Npc1*^{-/-} mice.

5.2.2 Regarding Cyclodextrins

Although the short-term time course after HP-β-CD administration in $Npc1^{-/-}$ mice demonstrated that cholesterol is cleared very rapidly within cells, it did not address the pending question of how quickly the NPC disease state returns after a HP-β-CD injection. From the original studies in 7-day-old $Npc1^{-/-}$ mice, it was shown that by 6 weeks after a single HP-β-CD injection: the total cholesterol concentration was elevated back to that of an untreated $Npc1^{-/-}$, and cholesterol synthesis levels were even higher than without treatment (Liu et al., 2009). After this, repeated dosing was shown to be effective in $Npc1^{-/-}$ mice; however, both every other day (Davidson et al., 2009) and weekly dosing schemes (Ramirez et al., 2010) were used. To ultimately determine the most effective interval between doses of HP-β-CD in NPC patients, the time course studies presented here need to be extended in mice to include time-points past 24h up until 1 week after HP-β-CD administration.

As a single high dose of HP-β-CD led to an immediate and irreversible hearing loss in both wildtype and NPC-affected cats (Ward et al., 2010), another future study that needs to be performed is to evaluate the hearing threshold after HP-β-CD is given to another animal model, such as the mouse (see **Appendix B**). If hearing loss is also seen in mice, it would be important to determine the mechanism by which HP-β-CD raises hearing threshold before it is moved into patients. If the mechanism of action involves extracting cholesterol from the plasma membrane of cells in the inner ear, it is possible that an alternative form of cyclodextrin, such as SBE-β-CD, could have the beneficial effects of HP-β-CD without causing hearing loss.

Another remaining question is why HP-β-CD improves cholesterol dynamics in every organ tested except lung. Although studies presented here prove that weekly injection of HP-β-CD does not lead to lung damage, they do not address if HP-β-CD is able to penetrate the lung. It will be important to determine in future studies if HP-β-CD is simply not getting into lung or if lung is resistant to its benefit. The most direct way to address this would be to administer a labelled-form of HP-β-CD (sc at 4,000 mpk)
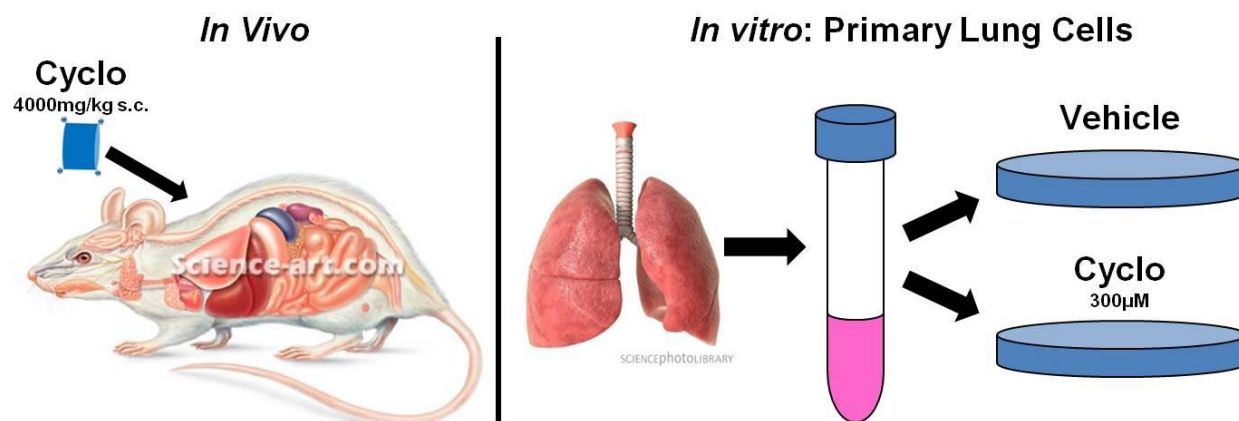
Figure 5.1 *Experimental design to determine if HP-β-CD reaches lung.* Currently it is unknown if HP-β-CD is able to penetrate the lung when it is administrator (sc at 4,000 mpk) to mice. In order to determine if HP-β-CD can elicit effects in lung, primary cells will be harvested from *Npc1*^{-/-} lungs and plated in culture. Once the cells have adhered, they will be treated with Cyclo (HP-β-CD at 300μM) or vehicle (PBS). 16h later, the cells will be harvested for RNA in order to evaluate SREBP2 and LXR target genes. Pictures of the mouse and lung were modified from http://science-art.com and http://www.sciencephoto.com, respectively.

and determine if it is getting into the lungs of *Npc1*^{-/-} mice. Unfortunately, there currently is no such labelled HP-β-CD available. Previously, a ^{14}C-labelled HP-β-CD was used in mice (Liu et al., 2010a); however, this compound is no longer being commercially produced. The ideal labelled-form of HP-β-CD would be able to be assessed visually in real-time at both the whole animal level and the intracellular level. Attaching a commercially available infrared probe (BrightSite IRdyes, LiCOR) to HP-β-CD may provide the desired resolution and is being pursued. Another less direct approach, which is currently underway, to address whether HP-β-CD is getting into lung is to harvest primary cells from lung and to treat them in culture with HP-β-CD (modeled in **Fig. 5.1**). If HP-β-CD is able to elicit decreases in SREBP2 target genes and increases in LXR target genes in *Npc1*^{-/-} lung cells as was seen in primary macrophages and neurons, it will show that HP-β-CD is capable of having an effect in lung. This will further suggest that HP-β-CD is not getting into lung through the current administration route and will recommend using more direct means to deliver the compound to lungs, such as aerosolization or nasal delivery.

5.2.3 Regarding other therapies

Although dual HP-β-CD and Tcmpd therapy was not able to further extend lifespan in *Npc1*$^{-/-}$ mice over HP-β-CD alone, it is possible that other combination therapies could be beneficial to NPC. In particular, any therapy that is found to improve pulmonary function in *Npc1*$^{-/-}$ mice should be tested in combination with HP-β-CD to see if co-administration has an additive effect on lifespan. As miglustat has been approved as a therapy for NPC in the European Union, it is likely that any pharmaceutical agent which is tested in clinic will be prescribed in combination with it; therefore, it would be valuable to test HP-β-CD, as well Tcmpd, with miglustat in *Npc1*$^{-/-}$ mice. Finally, it is possible that therapies, such as Tcmpd and HP-β-CD, which have been shown to restore cholesterol balance and ultimately to reduce neurodegeneration could be beneficial in other neurodegenerative diseases linked to cholesterol dysregulation. Finally, cholesterol has been shown to accumulate in many other lysosomal storage diseases besides NPC. Therefore, Tcmpd and HP-β-CD could be tested in mouse models for Alzheimer, Parkinson, and Huntington diseases, as well as, various lysosomal storage disorders.

Testing Histone Deacetylase Inhibitors as Potential Therapies for Niemann Pick Type C Disease

A.1 Abstract

As there are no pharmacological agents approved by the US Food and Drug Administration to extend lifespan in patients with Niemann Pick Type C (NPC) disease, small bioavailable compounds have been sought to serve as therapies for NPC disease. Several compounds, including a Liver X Receptor (LXR) agonist and 2-hydroxypropyl-β-cyclodextrin (HP-β-CD), have been found to extend lifespan in the $Npc1^{-/-}$ mouse; however, each agent tested so far has had limitations. The LXR agonist causes hepatic steatosis and splenomegaly, two symptoms already aggravated in NPC disease; while HP-β-CD does not relieve the lung disease observed in the $Npc1^{-/-}$ mouse and appears not to reach the brain after the mature blood-brain-barrier has formed. Recently, a screen performed in fibroblasts from NPC patients identified histone deacetylase inhibitors (HDACi), which alleviated the accumulated lysosomal cholesterol that is characteristic to NPC disease. In order to further evaluate these compounds as a therapy for NPC, four unique HDACi were tested alongside an LXR agonist and HP-β-CD in primary macrophages harvested from $wildtype$, $Npc1^{-/-}$, and $Npc2^{-/-}$ mice. In particular, the HDACi LBH589, even at very low doses, was shown to alter gene expression of cholesterol-related genes and to reduce cytokine secretion from macrophages. In addition, the expression of histone deacetylases in macrophages was assessed. These studies showed that $Hdac5$ and the class I $Hdac$s (all potently inhibited by LBH589) are highly expressed in macrophages. Overall, this work extends the finding that HDACi could serve as potential therapies for NPC from human fibroblasts to an *in vitro* mouse macrophage model and leads to the recommendation that LBH598 therapy be further evaluated *in vivo* in $Npc1^{-/-}$ and $Npc2^{-/-}$ mice.

A.2 Introduction

Niemann Pick Type C (NPC) disease is a lysosome storage disorder, which is estimated to affect 1 in 120,000 live births. NPC is caused by inactivating mutation(s) in one of two proteins required to transport cholesterol through the late endosome/early lysosome (LE/L): NPC1 or NPC2 (Vanier, 2010) (Patterson et al., 2012). Mutations in NPC1 are most common and represent 95% of NPC cases; while, mutations in NPC2 protein account for the remaining NPC cases where the genetic cause has been identified (Ory, 2004) (Vanier, 2010) (Patterson et al., 2012). Regardless of the underlying mutation, patients with NPC typically suffer from progressive neurodegeneration, which presents in late infancy/early childhood with vertical supranuclear gaze palsy, cerebellar ataxia, gelastic cataplexy, and seizures; and die between 10 and 25 years of age (Vanier, 2010). In additional to the prominent neurological symptoms, children with NPC also suffer from preceding systemic disease, including hepatomegaly, splenomegaly, and chronic pulmonary disease (Patterson et al., 2012). Once a child has been diagnosed with NPC either by identification of mutations in NPC1 or NPC2 or by a positive filipin test that confirms the characteristic accumulation of free cholesterol within cells, there are virtually no therapeutic options to halt the progression of the disease. The prevailing management plan for NPC in patients is to treat individual symptoms as they occur in order to improve quality of life (Patterson et al., 2012).

Using animal models, several potential therapies for NPC have been discovered to reduce neurodegenertation and to ultimately extend lifespan, including: a Liver X Receptor agonist (T0901317 or Tcmpd) (Repa et al., 2007) and a modified cyclodextrin (2-hydroxypropyl-β-cyclodextrin or HP-β-CD) (Liu et al., 2009). Tcmpd was shown to reduce inflammation, improve neuronal survival, and lead to a slight but significant extension of lifespan by 10 days in the $Npc1^{-/-}$ mouse model (Repa et al., 2007). As LXR agonists are known to induce lipogenesis leading to hepatic steatosis and splenomegaly (Repa et al., 2000a; Schultz et al., 2000; Jung et al., 2011), they were not pursued as a therapy in NPC patients. A single dose of HP-β-CD was shown to lead to dramatic sterol balance changes in 7-day-old $Npc1^{-/-}$ pups and to significantly extend lifespan by 30% (Liu et al., 2009). Further work found that serial injections of

HP-β-CD could lead to a remarkable doubling of lifespan (Davidson et al., 2009; Ramirez et al., 2010). However, HP-β-CD appears to have no effect on the pulmonary dysfunction in the *Npc1*$^{-/-}$ mouse (Ramirez et al., 2010; Muralidhar et al., 2011), can not cross the blood brain barrier of an adult animal (Aqul et al., 2011; Ramirez et al., 2011), and causes hearing loss, at least in a feline model (Ward et al., 2010). Therefore, the search for an optimal NPC therapy that could be used to treat patients continues.

A powerful, non-biased approach to identify novel therapeutic agents for NPC disease was performed by Fred Maxfield's group at Cornell University. This group is screening small-molecule libraries to indentify compounds able to reduce filipin staining in fibroblasts cultured from NPC patients (Rosenbaum et al., 2009). Recently, using this approach a new class of compounds, histone deacetylase inhibitors (HDACi), was shown to alleviate the accumulated lysosomal unesterified cholesterol in fibroblast lines derived from patient with mutantions in *NPC1*. HDACi can lead to global changes in transcription by preventing histone deacetylase (HDACs) proteins from cleaving acetyl groups off of histones, transcription factors, and chaperone proteins (Pipalia et al., 2011). As two HDACi have been approved by the US Food and Drug Administration (FDA) for treatment of cancer and several more are currently in clinical trials (Tan et al., 2010), this class of drugs has the potential to move quickly into the clinic as a therapy for NPC. Before this can occur, the compounds must be fully evaluated in animal models of NPC disease and the most effective HDACi needs to be selected. Therefore, a series of studies was performed to evaluate four of the compounds identified in Dr. Maxfield's screen, alongside an LXR agonist and HP-β-CD, in primary macrophages harvested from wildtype, *Npc1*$^{-/-}$, and *Npc2*$^{-/-}$ mice. The experiments were designed: 1) to characterize the distribution of *Hdac*s in wildtype versus *Npc1*$^{-/-}$ and *Npc2*$^{-/-}$ macrophages; 2) to determine if HDACi alter mRNA expression of sterol-related genes; 3) to evaluate if HDACi affect cytokine secretion from macrophages. Together, the results of these studies lead to a recommendation of LBH589 as the HDACi to be further studied *in vivo* as a potential therapy for NPC disease.

A.3 Materials and Methods

Compounds

The synthetic LXR agonist, T0901317 (Tcmpd, #71810, Cayman Chemicals, Ann Arbor, MI) was

prepared in DMSO and used at a final concentration of 1 μM for all studies. 2-hydroxypropyl-β-

cyclodextrin (HP-β-CD, H107, Sigma) was made in PBS and used at a final concentration of 300 μM for

all studies. Since all other compounds were prepared in DMSO, an equivalent volume of DMSO (1 uL/

mL of media) was used as the vehicle and was added to each well treated with HP-β-CD. All wells also

received PBS. The histone deacetylase inhibitors (HDACi) used in this chapter were gifts from Paul

Helquist of the University of Notre Dame and are listed in **Table A.1**. The synthesis and characterization

of these HDACi was previously described in the supplementary text of (Pipalia et al., 2011). All four

HDACi (LBH589, SAHA, CI994, and racTSA) were prepared in DMSO and were used in a range of

concentrations, which is specified within each figure legend.

Animals

Heterozygous (*Npc1*$^{+/-}$) mice on a BALB/c background were bred to generate wildtype (*Npc1*$^{+/+}$) and

homozygous-null (*Npc1*$^{-/-}$) littermates (Loftus et al., 1997). Heterozygous (*Npc2*$^{+/-}$) mice on a BALB/c

background were bred to generate wildtype (*Npc2*$^{+/+}$) and homozygous-null (*Npc2*$^{-/-}$) littermates (Sleat et

al., 2004). As genetic shift may have occurred between the two pure BALB/c lines, each homozygous-

null mouse was only compared to its respective wildtype littermates. Litters were genotyped upon

weaning, between 19-21 days of age. Mice were group-housed in plastic cages containing wood chip

bedding in an animal facility with temperature-controlled rooms (23 ± 1°C) and a maintained light cycle

(12h light on/12h off). The mice were allowed *ad libitum* access to water and a standard rodent chow

containing 0.02% w/w cholesterol (7001; Harlan Teklad, Madison, WI). All studies in this chapter

utilized either all males or females as indicated, and macrophages were obtained from 2-month-old mice.

All animal research was conducted in conformity with the Public Health Service Policy on Humane Care

and Use of Laboratory Animals, and all experiments were performed with prior approval from the University of Texas Southwestern Medical Center's Institutional Animal Care and Use Committee.
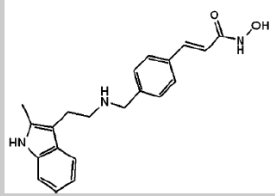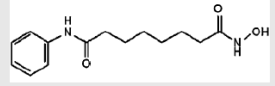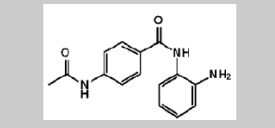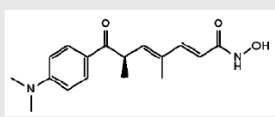
HDACi	Abbr.	Common Name	Molecular Weight	IC_{50} for HDACs	EC_{50} in NPC	Chemical Structure
LBH-589	LBH589	Panobinostat	349.43	0.1 nM	<5 nM	
Suberoylanilide hydroxamic acid	SAHA	Vorinostat; Zolinza	264.32	10 nM	500 nM	
CI-994	CI994	Tacedinaline	269.30	500 nM	500 nM	
Trichostatin A (racemic form)	racTSA	-	302.37	0.1 nM	50 nM	

Table A.1 *Histone Deacetylase Inhibitors.* The histone deacetylase inhibitors (HDACi) used in this chapter were synthesized by Paul Helquist of the University of Notre Dame. Each HDACi is listed name, which is followed by: the abbreviation as it is written in this text; the common name; the molecular weight; the concentration to achieve 50% inhibition of histone deacetylase activity, which was provided by Paul Helquist; the concentration of the compounds which leads to a 50% reduction in filipin labeling in NPC human fibroblast (EC_{50}), which were published in (Pipalia et al., 2011); and the chemical structures, which are from the supplementary text of (Pipalia et al., 2011).

Primary Macrophage Harvest

Npc1$^{+/+}$, *Npc1$^{-/-}$*, *Npc2$^{+/+}$*, or *Npc2$^{-/-}$* mice (n=3 to 4 mice/group) received a 1 mL ip injection of 3% thioglycollate (autoclaved and aged for 3 months; #211717, Becton Dickinson) to elicit macrophages. Three days later, mice were euthanized, and macrophages were harvested from the peritoneal cavity by sterile lavage using ice-cold PBS. Lavage solutions from mice of the same genotype were pooled, and cells were collected by centrifugation for 5 min at 150x g at 4°C. Cell pellets were resuspended in medium [high-glucose DMEM (Invitrogen) containing 10% heat-inactivated fetal calf serum (FBS; Atlanta Biologicals) and 1% Pen/Strep (Invitrogen)]. The primary macrophages were counted and plated

(at 1.05×10^5 cells/cm^2 for mRNA evaluations or 2.1×10^5 cells/cm^2 for cytokine secretion assays) on tissue-culture treated plates (Corning). Once plated, the cells were maintained in a humid incubator at 37°C with 5% CO_2. Six hours later, cells were washed with PBS and exposed to fresh media.

Measurement of relative mRNA levels

To determine the relative mRNA abundance of *Hdac*s, thioglycollate-elicited peritoneal macrophages were harvested for RNA 6h after plating. To compare the effects of various compounds, peritoneal macrophages were treated for 16hr in fresh media with: vehicle (1μL/mL DMSO), 1μM Tcmpd, 300μM HPβCD, 0.1nM-10μM LBH589, 0.01-10μM SAHA, 0.5-10μM Cl-994, or 0.1-100nM racTSA. To harvest total RNA from cells, culture medium was aspirated from each well, and 500 uL of RNA STAT-60 (Tel-Test, Inc) was used to lyse cells and isolate RNA. RNA concentrations were determined by absorbance at 260nm with a Thermo Scientific Nanodrop 100 Spectrophotometer. 2 ug of total RNA was treated with RNase-free DNase (Roche) and reverse-transcribed into cDNA with SuperScript II (Invitrogen) as previously described (Kurrasch et al., 2004; Valasek et al., 2005b). The cDNA was used to perform quantitative real-time PCR (qPCR) with the Applied Biosystems 7900HT sequence detection system. Each qPCR was analyzed in duplicate and contained in a final volume of 10 μl: 25 ng of cDNA, each primer at 150 nM, and 5 μl of 2x SYBR Green PCR Master Mix (Applied Biosystems). The nucleotide sequences of the primers used in this chapter are listed in **Table D.1** of Appendix C. Results were evaluated by the comparative cycle number at threshold (C_T) method (Schmittgen et al., 2008) using cyclophilin or β-actin as the invariant housekeeping gene (Dheda et al., 2004; Kosir et al., 2010). For the *Hdac* distribution, mRNA levels were arithmetically adjusted to a unit of 100% for the most hightly expressed *Hdac* in wildtype cells. For all other analyses, relative mRNA levels were arithmetically adjusted to a unit of 1 for the wildtype, vehicle-treated group.

Measurement of secreted cytokine concentrations

Thioglycollate-elicited peritoneal macrophages were cultured in fresh media with vehicle (1μL DMSO), 1μM Tcmpd, 300μM HPβCD, or 40nM LBH589. After 16 h of treatment, the macrophages were challenged with lipopolysaccharide (LPS; L4391, Sigma) prepared in saline by replacing the culture media with fresh media containing: either vehicle (DMSO) or treatment (Tcmpd, HPβCD, or LBH589) and either vehicle (saline) or 100ng/mL LPS. After 4h, the culture medium from each well was transferred to a tube, flash frozen in liquid nitrogen, and stored at -80°C until analyses for cytokine levels were performed. 25 μL of each sample was analyzed in duplicate, alongside cytokine standards, on a 7-plex mouse cytokine plate (#K15012B-1, MesoScale Discovery, Gaithersburg, Maryland) according to the manufacturer's instructions. The plate was analyzed using a SECTOR® Imager 2400 instrument (MesoScale Discovery). Concentrations for IFNγ, IL-1β, IL-6, IL-10, IL-12p70, CXCL1 (KC), and TNF are reported as pg of protein per mL of media.

Data Analysis

All data are presented as the mean ± SEM. Statistically significant differences were evaluated using a one-way ANOVA followed by the Dunnett's post-hoc test. Differences between the vehicle and treatment groups within a given genotype were determined and are indicated by "**a**" or "**c**" for wildtype samples ($Npc1^{+/+}$ and $Npc2^{+/+}$) and by "**b**" or "**d**" for homozygous-null ($Npc1^{-/-}$ and $Npc2^{-/-}$) samples. A significant difference between vehicle-treated samples of different genotypes is denoted by "*****" or "**x**". All statistical tests were performed using GraphPad Prism5 software (GraphPad Software, Inc. San Diego, CA).

A.4 Results

***Hdac5* and Class 1 *Hdac*'s are highly expressed in primary mouse macrophages:**

Histone deacetylases (HDACs) are a group of proteins responsible for cleaving the acetyl group off of histones, which leads to more tightly wound DNA and ultimately a global reduction in transcription. In

addition to histones, HDACs have also been shown to deacetylate other proteins, such as transcription factors and chaperone proteins (Pipalia et al., 2011). HDACs are separated into four distinct classes, which can be further grouped into the classical HDACs and the sirtuin family (class III). The classical HDAC family includes class I (HDAC 1-3,8), class II (HDAC 4-7, 9-10), and class IV (HDAC 11). Of the classical HDACs, those belonging to class I are considered to be widely expressed throughout the body, while class II and IV members are restricted to certain cell types (De Ruijter et al., 2003). In order to determine which of the HDACs were present in macrophages (the model used for the studies described in this chapter), I designed and validated primers that distinctly recognized the mouse mRNA species for *Hdac1-9* and *Hdac11* (see Appendix C). As *Hdac10* has only been found in a rare subset of B cells in mouse, it was not included. Primary thioglycollate-elicited peritoneal macrophages were harvested from $Npc1^{+/+}$ and $Npc2^{+/+}$ Balb/c wildtype mice and the relative levels of the *Hdacs* were evaluated. As no differences were seen between the two wildtype strains, only $Npc1^{+/+}$ are shown (**Fig. A.1,** white bars). *Hdac5* was expressed at the highest level with a C_T value of 21.6, which was followed by *Hdac1-3,8* (all members of class I). *Hdac11* showed the lowest expression in macrophages with a C_T value of 29.9.
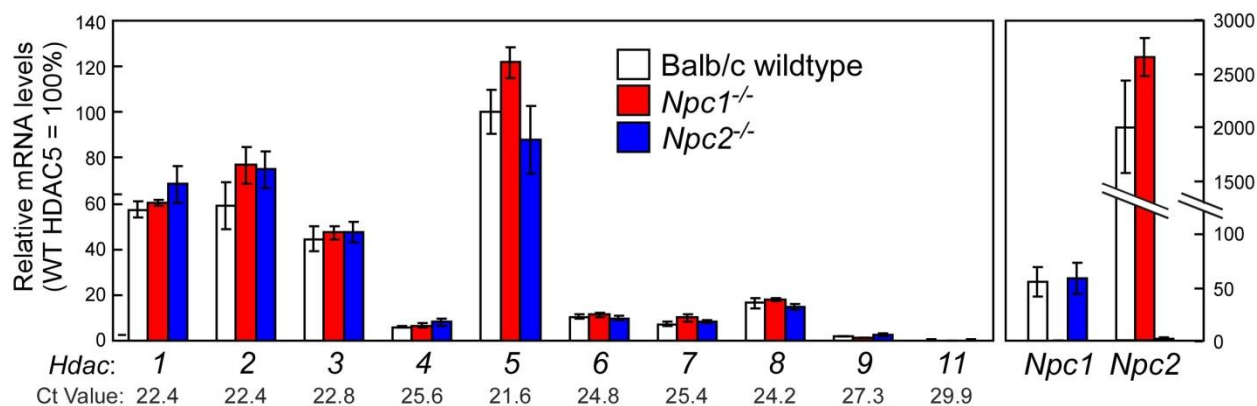
Figure A.1 *Distribution of Hdac's in primary macrophages harvested from wildtype, Npc1^{-/-}, and Npc2^{-/-} mice.* Thioglycollate-elicited peritoneal macrophages were obtained from 2 month old male Balb/c wildtype (white bars), $Npc1^{-/-}$ (red bars), and $Npc2^{-/-}$ mice (blue bars). RNA was harvested, and gene expression of *Hdac1-9, Hdac11*, *Npc1*, and *Npc2* was determined by qPCR, using cyclophilin as the invariant housekeeping gene. mRNA levels were arithmetically adjusted to a unit of 100% for the highest expressed *Hdac* in the wildtype group, *Hdac5*. Each bar represents the mean ± SEM for 3 wells. Average Ct values of *Hdac* for the wildtype group are indicated below each gene symbol.

As *Hdac* expression is known to be altered in some disease states (Atadja, 2009), I next wanted to

evaluate the distribution of *Hdac*s in mouse models for Niemann Pick Type C (NPC) disease. Primary peritoneal macrophages were harvested from $Npc1^{-/-}$ and $Npc2^{-/-}$, and their relative expression of *Hdac*s was compared to that of Balb/c wildtype mice. Overall, $Npc1^{-/-}$ (**Fig. A.1,** red bars) and $Npc2^{-/-}$ (**Fig. A.1,** blue bars) macrophages have the same relative mRNA abundance of *Hdac1-9* and *Hdac11* as was found in wildtype cells. The relative expression of *Npc1* and *Npc2* confirmed the genotypes of the primary macrophages (**Fig. A.1**).

HDACi alter mRNA expression of sterol-related genes in primary mouse macrophages:

Although the expression of *Hdac*s does not appear to be altered in NPC disease (at least in macrophages from two mouse models), four HDACi (described in **Table A.1**) were shown to alleviate filipin staining in fibroblast lines derived from patients with mutations in *NPC1* (Pipalia et al., 2011). In order to determine if these HDACi also could elicit changes in a mouse model for NPC disease, primary thioglycollate-elicited peritoneal macrophages were harvested from $Npc1^{+/+}$ and $Npc1^{-/-}$ littermate mice and were treated in culture with the HDACi. At the time this initial study was performed, Maxfield and colleagues had not determined the concentration of HDACi that was required to lead to a 50% reduction in filipin labeling in NPC human fibroblast (EC_{50}), which has since been reported in (Pipalia et al., 2011). Also, it was unknown if the HDACi would be toxic to the primary mouse macrophages; therefore, an extremely low dose (the reported IC_{50} required to reduce histone deacetylase activity) was used: LBH589 (0.1nM), SAHA (0.01μM), Cl994 (0.5μM), or racTSA (0.1nM) (**Fig. A.2**).

Sixteen hours after treatment with the low dose of HDACi, gene expression changes were compared to vehicle (a negative control) and to Tcmpd and HP-β-CD (two positive controls known to induce changes in cholesterol-related genes). The relative expression of *Npc1* was evaluated to confirm the genotypes of the macrophages; however, quite unexpectedly, *Npc1* was found to be significantly increased with LBH589 treatment in $Npc1^{+/+}$ mice (**Fig. A.2A**). In addition, racTSA was shown in $Npc1^{-/-}$ mice to induce a significant increase in the expression of *scavenger receptor B* (*Srb1*), which encodes the

cell receptor for High Density Lipoproteins (HDL) and may be protective against atherosclerosis (**Fig. A.2C**). While LBH589, like Tcmpd, led to an increase in the SREBP2 target gene, *Hmg-CoA-Red*, in *Npc1*^{+/+} mice; SAHA and CI994, like HP-β-CD, reduced the expression of *Hmg-CoA-Red* in *Npc1*^{-/-} mice (**Fig. A.2H**). Although overall very few changes were induced by HDACi treatment at these low concentrations, the results from this preliminary experiment were encouraging as no toxic effects were seen in the macrophages, which was assessed by the number of dead cells in each well compared to vehicle treatment before RNA harvest.

Figure A.2 *Effect of HDACi treatment at IC$_{50}$ concentrations on gene expression in wildtype and Npc1$^{-/-}$ macrophages.* Thioglycollate-elicited peritoneal macrophages were obtained from 2 month old male *Npc1*^{+/+} (white bars) and *Npc1*^{-/-} (red bars). The cells were treated in culture with vehicle (1μL/mL DMSO), Tcmpd (1μM), HPβCD (300μM), LBH589 (0.1nM), SAHA (0.01μM), Cl994 (0.5μM), or racTSA (0.1nM) for 16 hours. RNA was harvested and gene expression (**A-I**) was determined by qPCR, using β-actin as the invariant housekeeping gene. Each bar represents the mean ± SEM for 3 wells. Statistically significant differences (P <0.05) between treatments are indicated by "**a**" for *Npc1*^{+/+} samples or "**b**" *Npc1*^{-/-} samples; while a significant variance between vehicle-treated samples of different genotypes is denoted by *****.

Next, the studies were extended to evaluate the effect of HDACi on gene expression using doses at least 2 fold higher than the EC$_{50}$ for NPC human fibroblast, which were published in (Pipalia et al., 2011). Primary peritoneal macrophages were harvested from *Npc1*^{+/+} and *Npc1*^{-/-} (**Fig. A.3**) and from *Npc2*^{+/+}

and *Npc2*^{-/-} (**Fig. A.4**) littermate mice, and then were treated in culture with: vehicle (1μL/mL DMSO), Tcmpd (1μM), HPβCD (300μM), LBH589 (40nM), SAHA (10μM), CI994 (10μM), or racTSA (100nM). LBH589, SAHA, and to a lesser extent racTSA led to an increase in *Npc1*, *Npc2*, and *Srb1* expression in mouse macrophages (**Fig. A.3, 4 A-C**). The only exceptions were that *Npc1* expression was not increased in *Npc1*^{-/-}animals (**Fig. A.3 A**), and *Npc2* expression was unchanged in *Npc2*^{-/-}mice (**Fig. A.4 B**). Although the LXR target genes, *ABC transporter a1 (Abca1)* and *g1(Abcg1)*, were relatively unaffected by HDACi treatment (**Fig. A.3, 4 D-E**); *the inducible degrader of LDLR* [*Idol*] another LXR target gene, was increased by LBH589, SAHA, and racTSA albeit not to the same extend as by Tcmpd (**Fig. A.3, 4**
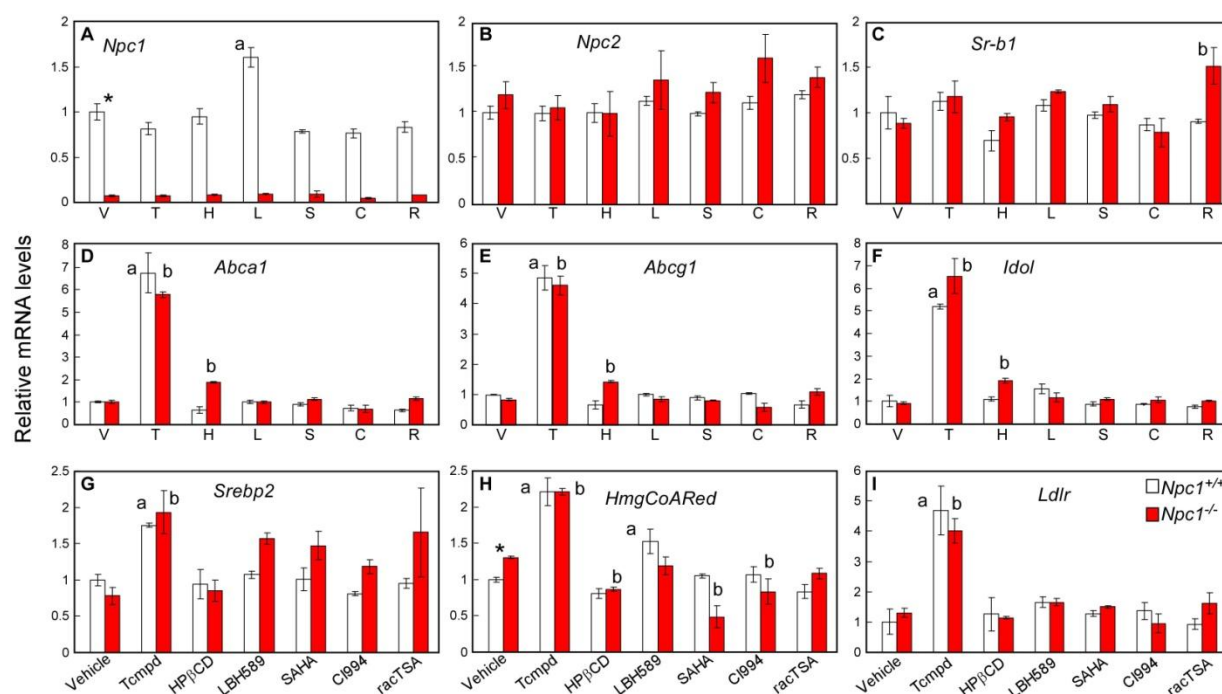

Figure A.3 *Effect of HDACi treatment at higher concentrations on gene expression in wildtype and Npc1*^{-/-} *macrophages.* Thioglycollate-elicited peritoneal macrophages were obtained from 2 month old female *Npc1*^{+/+} (white bars) and *Npc1*^{-/-} (red bars). The cells were treated in culture with vehicle (1μL/mL DMSO), Tcmpd (1μM), HPβCD (300μM), LBH589 (40nM), SAHA (10μM), CI994 (10μM), or racTSA (100nM) for 16 hours. RNA was harvested and gene expression (**A-I**) was determined by qPCR, using βactin as the invariant housekeeping gene. mRNA levels were arithmetically adjusted to 1 for the vehicle-treated wildtype group. Each bar represents the mean ± SEM for 3 wells. Statistically significant differences (P <0.05) between treatments are indicated by "**a**" for *Npc1*^{+/+} samples or "**b**" *Npc1*^{-/-} samples; while a significant variance between vehicle-treated samples of different genotypes is denoted by *****.

was increased by LBH589, SAHA, and racTSA albeit not to the same extend as by Tcmpd (**Fig. A.3, 4 F**). Srebp2 and its target genes were also increased by HDACi treatment (**Fig. A.3, 4 G-I**). Overall, it appears that treatment with LBH589 (40nM), SAHA (10μM), and racTSA (100nM), but not with CI994 (10μM), induces a global increase in the transcription of cholesterol-related genes irrespective of *Npc1* and *Npc2* genotype.
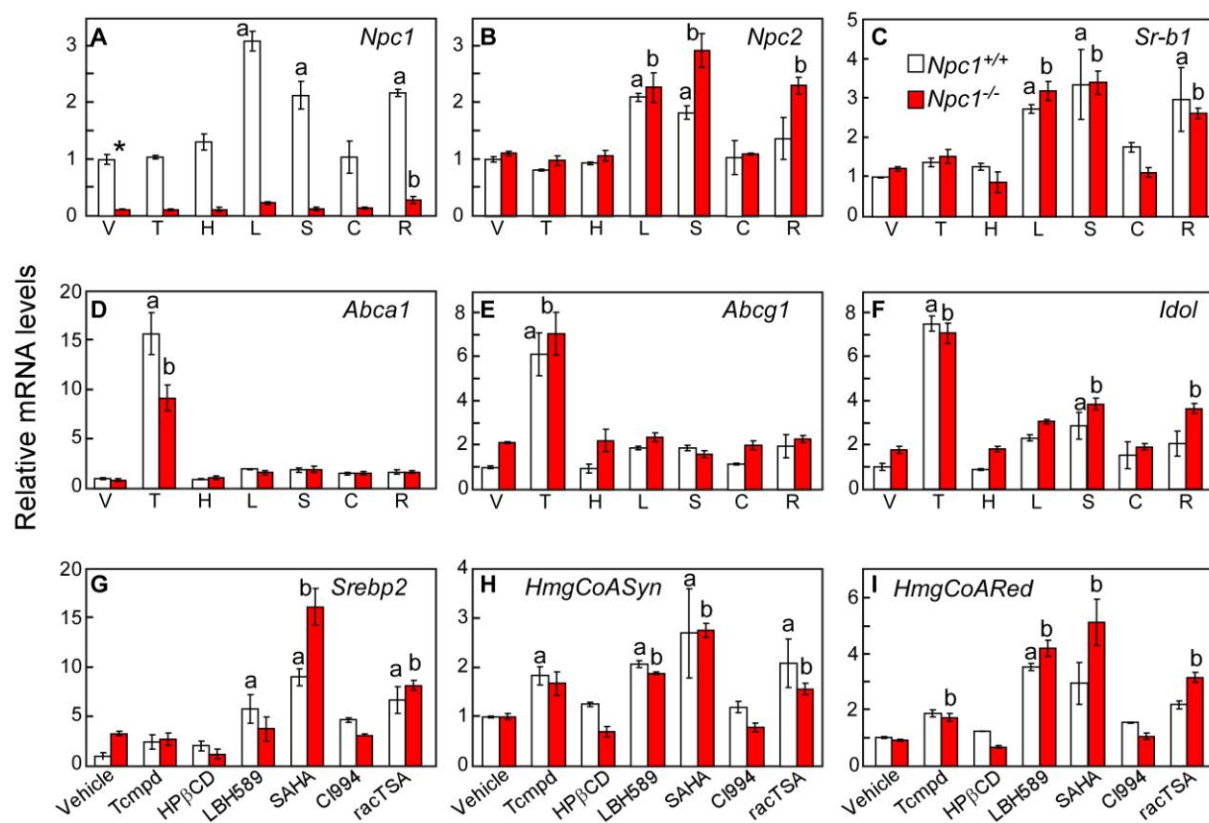

Figure A.4 *Effect of HDACi treatment on gene expression in wildtype and Npc2$^{-/-}$ macrophages.* Thioglycollate-elicited peritoneal macrophages were obtained from 2 month old male *Npc2$^{+/+}$* (white bars) and *Npc2$^{-/-}$* (blue bars). The cells were treated in culture with vehicle (1μL/mL DMSO), Tcmpd (1μM), HPβCD (300μM), LBH589 (40nM), SAHA (10μM), CI994 (10μM), or racTSA (100nM) for 16 hours. RNA was harvested and gene expression (**A-I**) was determined by qPCR, using βactin as the invariant housekeeping gene. mRNA levels were arithmetically adjusted to 1 for the vehicle-treated wildtype group. Each bar represents the mean ± SEM for 3 wells. Statistically significant differences (P <0.05) between treatments are indicated by "**a**" for *Npc2$^{+/+}$* samples or "**b**" *Npc2$^{-/-}$* samples; while a significant variance between vehicle-treated samples of different genotypes is denoted by **∗**.

LBH589 reduces cytokine secretion from primary mouse macrophages:

Of the HDACi used in this chapter, the three which led to the most dramatic changes in gene expression (LBH589, SAHA, and racTSA) are classified as pan-deacetylase inhibitors, which means that they serve as inhibitors to all class I (HDAC 1-3,8) and class II (HDAC 4-7, 9-10) members
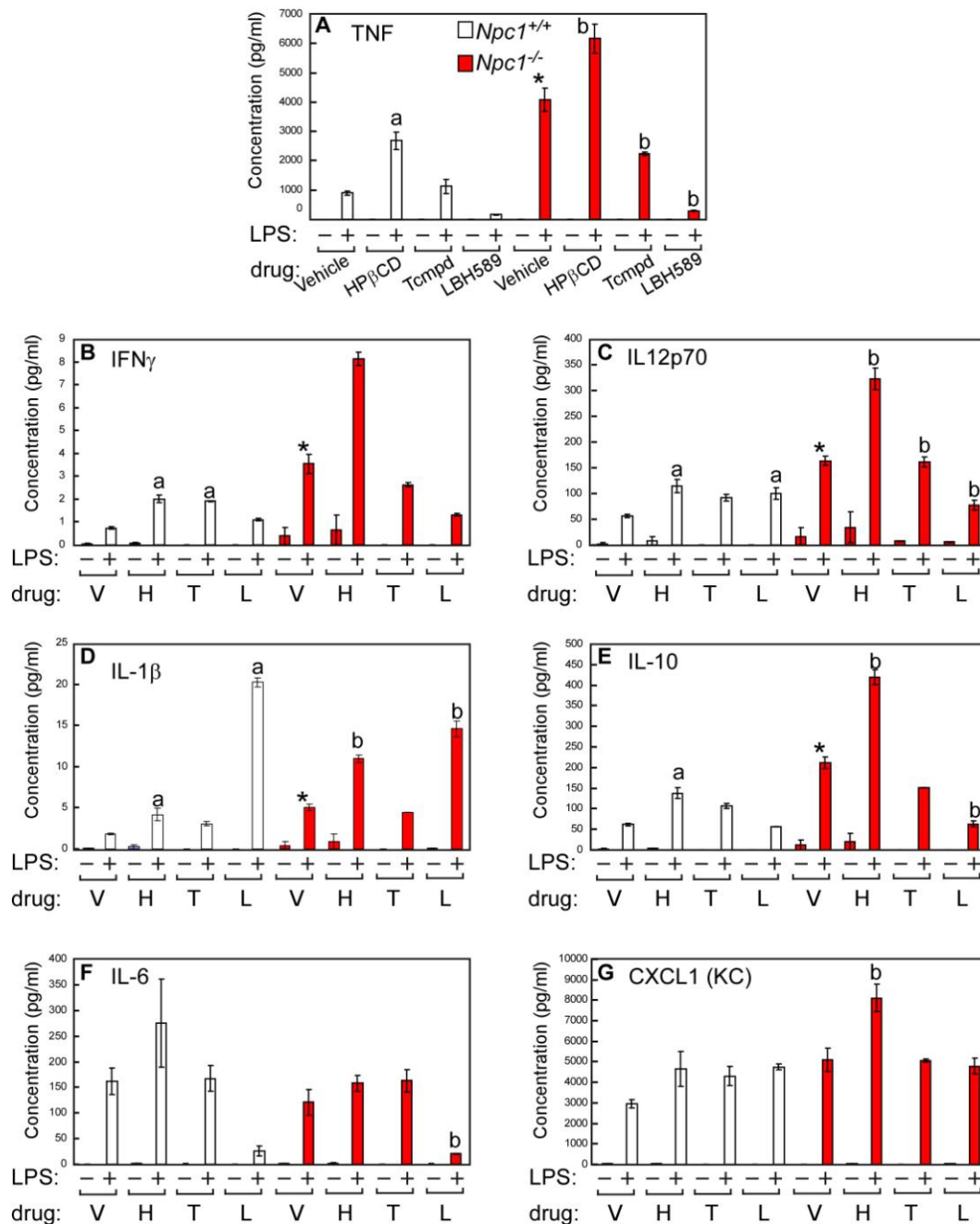
Figure A.5 *Effect of treatment on cytokine secretion from wildtype and Npc1⁻ᐟ⁻ macrophages.* Thioglycollate-elicited peritoneal macrophages were obtained from 2 month old male $Npc1^{+/+}$ (white bars) and $Npc1^{-/-}$ (red bars). The cells were pretreated for 16h with vehicle (1μL/mL DMSO), Tcmpd (1μM), HPβCD (300μM), or LBH589 (40nM). After 16h pretreatment, the cells were stimulated for 4hr with Lipopolysaccharide (LPS, 100ng/mL). Media was harvested to measure the protein levels of cytokines secreted by the macrophages: TNF (**A**), INF-γ (**B**), IL-12p70 (**C**), IL-1β (**D**), IL-10 (**E**), IL-6 (**F**), and CXCL1 (**G**) Each bar represents the mean ± SEM for 3 wells. Statistically significant differences (P <0.05) between treatments after LPS stimulation are indicated by "**a**" for $Npc1^{+/+}$ samples or "**b**" $Npc1^{-/-}$ samples; while a significant variance between vehicle-treated samples of different genotypes after LPS stimulation is denoted by *****. No significant differences were seen between any non-LPS stimulated group.
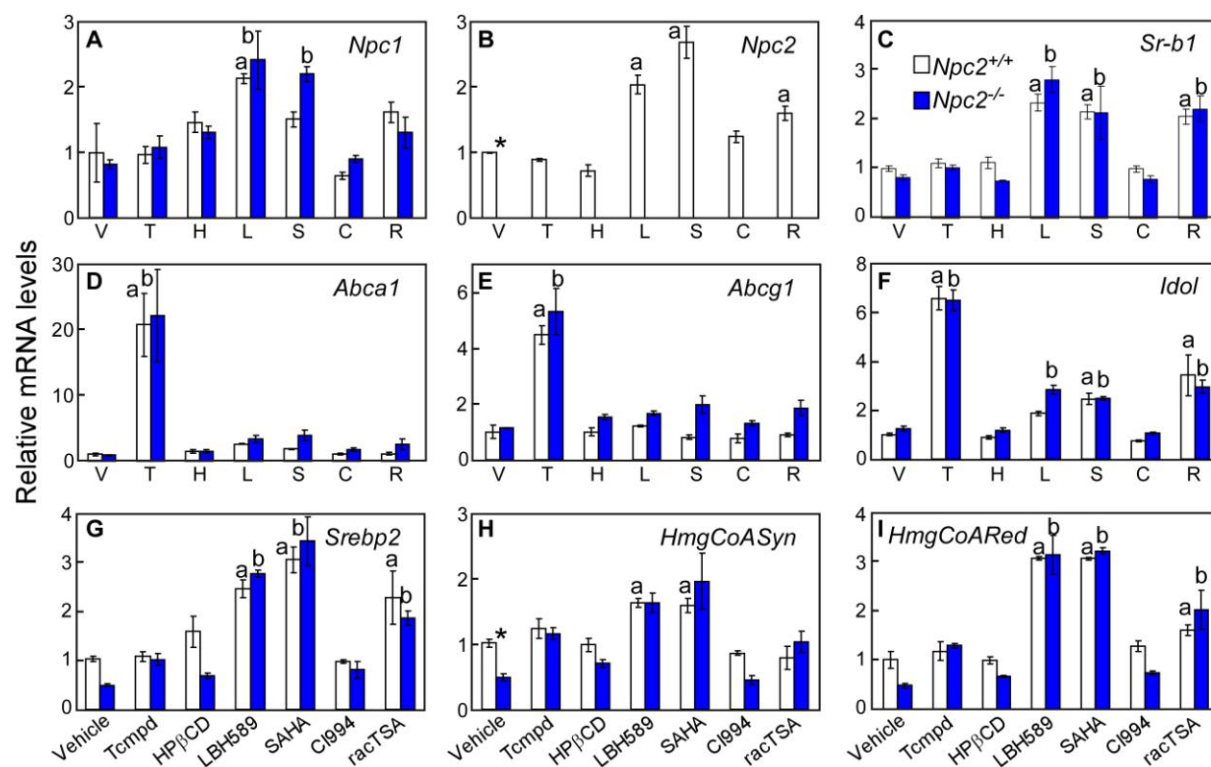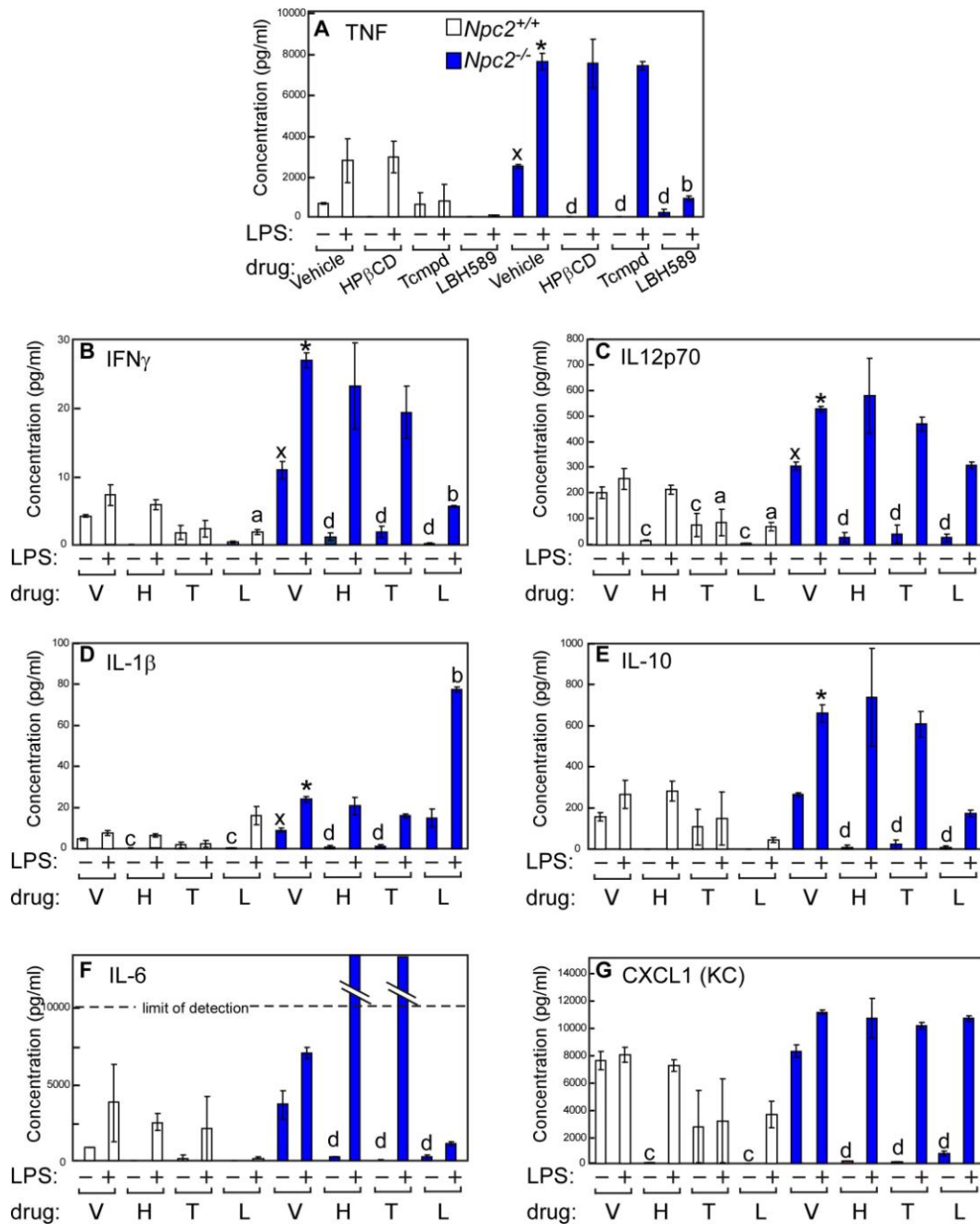
Figure A.6 *Effect of treatment on cytokine secretion from wildtype and Npc2$^{-/-}$ macrophages.* Thioglycollate-elicited peritoneal macrophages were obtained from 2 month old male *Npc2$^{+/+}$* (white bars) and *Npc2$^{-/-}$* (blue bars). The cells were pretreated for 16h with vehicle (1μL/mL DMSO), Tcmpd (1μM), HPβCD (300μM), or LBH589 (40nM). After 16h pretreatment, the cells were stimulated for 4hr with Lipopolysaccharide (LPS, 100ng/mL). Media was harvested to measure the protein levels of cytokines secreted by the macrophages: TNF (**A**), INF-γ (**B**), IL-12p70 (**C**), IL-1β (**D**), IL-10 (**E**), IL-6 (**F**), and CXCL1 (**G**) Each bar represents the mean ± SEM for 3 wells. Statistically significant differences (P <0.05) between treatments after LPS stimulation are indicated by "**a**" for *Npc2$^{+/+}$* samples or "**b**" *Npc2$^{-/-}$* samples; while a significant variance between vehicle-treated samples of different genotypes after LPS stimulation is denoted by *****. Statistically significant differences (P <0.05) between treatments with no LPS stimulation are indicated by "**c**" for *Npc2$^{+/+}$* samples or "**d**" *Npc2$^{-/-}$* samples; while a significant variance between vehicle-treated samples of different genotypes without LPS stimulation is denoted by **x**.

(Atadja, 2009). As LBH589 at a dose of 40nM produced roughly equivalent effects to SAHA, which was used at a dose 250-fold higher (10μM), LBH589 was selected as the HDACi to continue studying. As all studies performed have been in primary macrophages, next I wanted to evaluate if LBH589 had an anti-inflammatory effect. To test this, primary macrophages were harvested from the peritoneal cavity of *Npc1*^{+/+} and *Npc1*^{-/-} (**Fig. A.5**) and from *Npc2*^{+/+} and *Npc2*^{-/-} (**Fig. A.6**) and then were treated in culture with vehicle (1μL/mL DMSO), Tcmpd (1μM), HPβCD (300μM), or LBH589 (40nM) in order to measure levels of cytokine secretion. After the16hr treatment, lipopolysaccharide (LPS), which is known to elicit an immune response, was used to challenge the macrophages. Of the 7 cytokines (IFNγ, IL-1β, IL-6, IL-10, IL-12p70, CXCL1/KC, and TNF) measured, all were increased by LPS-stimulation of wildtype*, Npc1*^{-/-} (**Fig. A.5**), and *Npc2*^{-/-} macrophages (**Fig. A.6**). In *Npc1*^{-/-} and *Npc2*^{-/-} macrophages, which overall secrete more cytokines than the cells harvested from their wildtype littermates, treatment with LBH589 reduced the LPS-stimulated secretion of IFNγ, IL-6, IL-10, IL-12p70, and TNF (**Fig. A.5,6 A-C, E-F**). Although LBH589 treatment did lead to an increase in IL-1β secretion after LPS stimulation (**Fig. A.5,6 D**), LBH589 treatment alone caused no increase in the secretion of any of the cytokines (**Fig. A.5,6**).
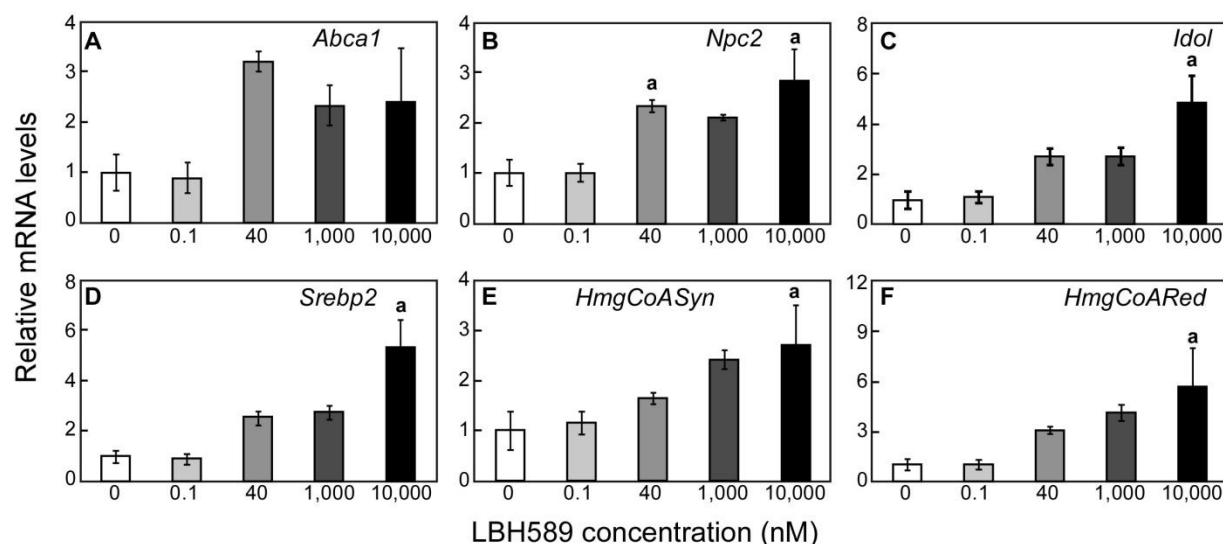
Figure A.7 *Dose-response of LBH589 on gene expression in macrophages.* Thioglycollate-elicited peritoneal macrophages were obtained from 2 month old male Balb-c mice. The cells were treated in culture with DMSO as a vehicle (0nM LBH589) or LBH589 at increasing concentrations (0.1nM, 40nM, 1μM, or 10μM) for 16 hours. RNA was harvested and gene expression (**A-F**) was determined by qPCR, using βactin as the invariant housekeeping gene. Each bar represents the mean ± SEM for 3 wells. Statistically significant differences (P <0.05) between treatments are indicated by "**a**".

LBH589 produces a dose responsive increase in gene expression in primary mouse macrophages:

To further evaluate LBH589, thioglycollate-elicited peritoneal macrophages were harvested from Balb-c wildtype mice and were treated in culture with increasing concentrations (0.1nM, 40nM, 1μM, or 10μM) of this pan-deacetylase inhibitor. The relative expression of the cholesterol-related genes including LXR target genes (**Fig. A.7 A,C**), a cholesterol trafficking gene (**Fig. A.7 B**), and *Srebp2* and its target genes (**Fig. A.7 D-F**) all exhibited a dose-dependent response to increasing levels of LBH589 that trended towards significance. Even the highest dose of 10μM LBH589 was well tolerated by the macrophages during the 16hr treatment period.

A.5 Discussion

Histone deacetylases (HDACs) are a group of transcriptional modulators that regulate gene expression, without altering gene sequence by controlling the acetylation state of histones (De Ruijter et al., 2003). Histone deacetylase inhibitories (HDACi) have been primarily used to cancer progression by inducing growth arrest, differentiation, and/or apoptosis in cancer cells; and the HDACi, SAHA, has been FDA-approved for the treatment of cutaneous T cell lymphoma (Munkacsi et al., 2011). However, HDACi have also been shown to have beneficial effects in other diseases such as Sickle cell anemia (Bradner et al., 2010), Gaucher disease (Lu et al., 2011), and Cystic fibrosis (Hutt et al., 2010). Furthermore, valproic acid has also been shown to induce neuronal differentiation and improve cholesterol trafficking in neural stem cells from $Npc1^{-/-}$ mice (Kim et al., 2007). Recently, a screen performed in fibroblasts from NPC patients found that HDACi could alleviate the accumulated lysosomal cholesterol that is characteristic to NPC disease (Pipalia et al., 2011). This is the first study to evaluate the HDACi (LBH589, SAHA, CI994, and racTSA) identified in the human fibroblast screen in a NPC mouse model and to begin to address the mechanism of action of HDACi in $Npc1^{-/-}$ and $Npc2^{-/-}$ mice.

Of the HDACi used in this chapter, three of the compounds (LBH589, SAHA, and racTSA) led to

dramatic increases in the expression of cholesterol-related genes (**Fig. A.2-4**). These increases were seen equally in wildtype, *Npc1*^{-/-} and *Npc2*^{-/-} mice, which is in contrast to the studies in human fibroblast where decreases in filipin staining were seen in fibroblasts from patients with mutations in *NPC1* but not *NPC2* (Pipalia et al., 2011). This suggests that HDACi could be working through multiple mechanisms, which is likely since LBH589, SAHA, and recTSA are pan-deacetylases (meaning HDACi that inhibit all class I and class II HDACs). On the other hand, CI994, which led to minimal changes in the expression of cholesterol-related genes, is a Class I specific HDACi and has little to no effect on other HDAC from Class II-IV. This leads to the possibility that the pan-deacetylases are inducing their gene expression changes through one of the Class II HDACs. As *Hdac5* was the highest expressed *Hdac* in macrophages (**Fig. A.1**), it is a likely candidate and should be evaluated further using HDAC5-specific HDACi or *Hdac5* knockout strategies.

Another possible mechanism by which the HDACi could be working is by increasing the protein levels of NPC2 in *Npc1*^{-/-} animals or NPC1 in *Npc2*^{-/-} mice, which could allow some movement of cholesterol out of the lysosome. Although the HDACi increase the mRNA level of *Npc1* and *Npc2* (**Fig. A.2-4**), it is currently unclear whether this reflects a change in the protein levels of NPC1 or NPC2 in cells from mouse, as was reported for NPC1 in human fibroblast (Pipalia et al., 2011). Western analyses for NPC1 protein levels were performed in macrophages harvested from wildtype mice 16h and 48h after treatment with vehicle or 40nM LBH589 (data not shown). However, these results were inconclusive, and protein levels after LBH589 treatment need to be further evaluated in macrophages.

Overall, the studies presented in this chapter lead to the recommendation that LBH589, which was the most potent HDAC at inducing changes in macrophage gene expression and cytokine secretion, be further evaluated as a potential treatment for NPC disease. As LBH589 is currently undergoing clinical trials for the treatment of myeloma (Atadja, 2009), it has the potential to be moved quickly into trials for NPC patients. *Npc1*^{-/-} and *Npc2*^{-/-} mouse models can be used to test LBH589 effects on cholesterol metabolism *in vivo* through measurements of cholesterol synthesis rates and the ratio of unesterified cholesterol to

cholesteryl esters in tissues. In addition, the mice can be used to determine if LBH589 leads to any negative side effects and if it is able to target all tissues, including lung and brain which are unaffected by systemically delivered HPβCD. Ultimately, survival studies need to be performed in mice to determine if LBH589 treatment leads to an extension in lifespan before HDACs can be moved into the clinic to benefit patients with NPC disease.

APPENDIX B:

Evaluating Cyclodextrin's Effects on Hearing in Mice

B.1 Abstract

In 2009, a single injection of 2-hydroxypropyl-β-cyclodextrin (HP-β-CD) administered to young $Npc1^{-/-}$ mice was found to relieve tissue lipid accumulation and greatly extended lifespan, while the same dose had no noticeable effect in wildtype mice. In the following year, the first adverse effect after HP-β-CD therapy was reported in studies using the feline model of Niemann Pick Type C disease (NPC) disease. Repeated or high doses of HP-β-CD were shown to increase the hearing threshold in both NPC-affected and wildtype cats; however, the mechanism of action through which HP-β-CD causes hearing loss was not determined. As membrane cholesterol is important to the integrity of hair cells within the inner ear, it is plausible that HP-β-CD is absorbing cholesterol from the plasma membrane of hair cells leading to the change in hearing threshold. In order to test this hypothesis and to validate that HP-β-CD causes an increase in hearing threshold in another species, I evaluated hearing by Auditory Brainstem Response (ABR) testing in wildtype mice before and after treatment with HP-β-CD or sulfobutylether-β-CD (SBE-β-CD), an alternative form of β-cyclodextrin that can interact with sterol but can not fully solubilize cholesterol or extract it from membranes. Hearing threshold was significantly elevated in mice that received a single high-dose or repeated small-doses of HP-β-CD; however, SBE-β-CD and vehicle treatment had no effect on hearing. These data support the hypothesis that HP-β-CD's site of action in hearing loss is at the plasma membrane and further suggest that SBE-β-CD may serve as a safer alternative therapy for NPC patients.

B.2 Introduction

β-cyclodextrins (CDs) are cyclic oligosaccharides composed of 7 glucopyranosides, which form a

134

barrel-shaped molecule. CDs have a hydrophilic exterior that renders the compound water-soluble and a hydrophobic core that can harbor small hydrophobic molecules, such as lipids. Both of these properties make CDs, which have been approved by the US Food and Drug Administration (FDA) as a delivery agent, ideal vehicles to increase the solubility of hydrophobic drugs (Irie et al., 1992; Thompson, 1997; Gould et al., 2005; Stella et al., 2008). In addition to the natural CDs that are products of starch, several modified forms of β-CD, which have less toxic effects *in vivo* including 2-hydroxypropyl (HP-β-CD) and sulfobutylether (SBE-β-CD), have been synthesized and FDA-approved. These CDs were considered to possess no therapeutic effect until 2009, when a single dose of HP-β-CD (4,000 mg per kg, mpk) in 7-day-old $Npc1^{-/-}$ pups was shown to lead to dramatic sterol balance changes in just 24h and to a significant extension in the lifespan by 40%. Intriguingly, the measurable shifts in cholesterol synthesis rates and the ratio of esterified/unesterified cholesterol observed in $Npc1^{-/-}$ mice after HP-β-CD administration were not seen in wildtype mice given the same dose of HP-β-CD (Liu et al., 2009). This suggested that HP-β-CD was correcting the cholesterol imbalance by facilitating the release of the lysosomal pool of unesterified cholesterol from NPC-deficient cells and was not acting at the plasma membrane.

Since the initial mouse studies, HP-β-CD was evaluated in the feline model of NPC (Somers et al., 2003) in order to confirm the effectiveness of HP-β-CD at extending lifespan. However, these studies uncovered a previously unreported side effect in both wildtype and NPC-affected cats (Ward et al., 2010). A single, high dose of HP-β-CD (8,000 mpk) administered subcutaneously (sc) caused a sudden hearing loss in the cats (**Fig. B.1A**). In addition, weekly sc injections of HP-β-CD (4,000 mpk) led to a progressive increase in hearing threshold, which was significant by the 5th dose; while, a single, low dose of HP-β-CD (4,000 mpk) administered intrathecally caused significant hearing loss in just 1 week. With all three treatment regiments, the hearing loss caused by HP-β-CD appeared to be irreversible, as no improvements in hearing threshold were measurable even up to 12 weeks after the final drug administration (Ward et al., 2010). Ward and colleagues hypothesized that the hearing loss after HP-β-CD could be due to direct damage to a structure in the inner ear, such as the stria vascularis, the inner and

outer hair cells, or the auditory nerve (2010); however, no histopathology was done of the inner ear after

HP-β-CD administration to identify the site or the mechanism of action for the irreversible deafness.
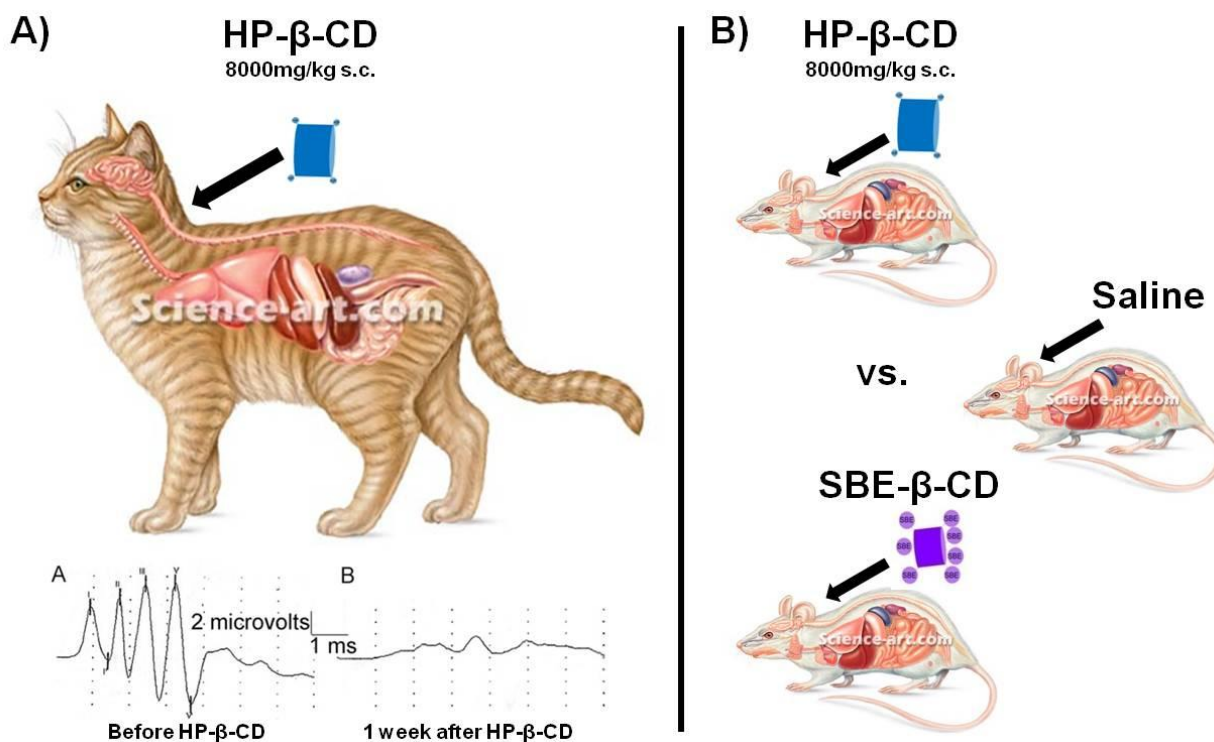
Figure B.1 *Experimental design to determine if HP-β-CD causes hearing loss in mice.* A single dose of 2-hydroxypropyl-β-cyclodextrin (HP-β-CD) at 8,000 mpk sc or 4,000 mpk intrathecal was shown to lead to a sudden and irreversible decrease in hearing threshold in cats **(A)**. Studies will be performed to validate this side effect in mice compared to treatment with saline or with sulfobutylether-β-cyclodextrin (SBE-β-CD), which contains large head groups that sterically hinder it from dimerization and thus can only bind to cholesterol in a 1:1 complex. In order to fully solubilize cholesterol, which is required to extract the sterol from lipid membranes, cyclodextrins must bind cholesterol in a 2:1 ratio. This can be achieved at high concentration of HP-β-CD but can never be achieved with SBE-β-CD **(B)**. Pictures of the cat and mice were modified from http://science-art.com. Brainstem auditory evoked response recordings from cats were modified from (Ward et al., 2010).

Although the study in felines was the first to report a shift in hearing threshold after the *in vivo*

administration of HP-β-CD (Ward et al., 2010), it was not the first study to test the effects of a β-

cyclodextrin in the inner ear. Several reports utilized another β-cyclodextrin, methyl (M-β-CD), to both

cholesterol-load and sterol-deplete outer hairs cells (OHCs) in culture, which had been harvested from

guinea pigs (Rajagopalan et al., 2007; Canis et al., 2009; Organ et al., 2009; Brownell et al., 2011) or

chick embryos (Levic et al., 2011). Overall these studies suggested that alterations in the amount of

cholesterol found in the plasma membrane of OHCs can lead to defects in the motility and electric

potential, which could ultimately impact hearing. The critical role for cholesterol in the plasma membrane of OHCs lead to the hypothesis that HP-β-CD is changing hearing threshold *in vivo* by extracting cholesterol from the plasma membrane of hair cells. Therefore, studies were performed in mice to test this potential mechanism of action and to confirm HP-β-CD's effect on hearing in an additional species beyond felines (**Fig. B.1B**). Together these experiments give insight into the role of cholesterol in the inner ear and identify an alternative treatment to HP-β-CD for NPC disease, which does not lead to hearing loss.

B.3 Materials and Methods

Animals and Treatments

Female wildtype mice on a pure BALB/c background were used for the following studies. All mice were group-housed in plastic cages containing wood-chip bedding in an animal facility with temperature-controlled rooms ($23 \pm 1°C$) and a maintained light cycle (12h light on/12h off). The mice were allowed *ad libitum* access to water and a standard rodent chow containing 0.02% w/w cholesterol (7001; Harlan Teklad, Madison, WI). For the single-injection studies, 5 to 6-month-old mice were administered a sc injection of HP-β-CD (H107, Sigma; molecular weight (MW) = 1396) at 8000 mpk, SBE-β-CD (Captisol™, CYDEX Pharmaceuticals, Inc.; MW = 2163) at 12350 mpk (the equivalent Molar dose), or vehicle (saline at the equivalent volume of 40 μl/g body weight (bw)). For the repeat injection studies, mice were administered their first sc injection of HP-β-CD (4000 mpk) or vehicle (saline at equivalent volume of 20 μl/g bw) at 4-5 months of age. Mice continued to receive weekly injections of HP-β-CD or vehicle until they were studied after 8 weeks (a total of 9 injections). All animal research was conducted in conformity with the Public Health Service Policy on Humane Care and Use of Laboratory Animals, and all experiments were performed with prior approval from University of Texas Southwestern Medical Center's Institutional Animal Care and Use Committee.

Assessment of hearing threshold

Before the wildtype mice were treated with vehicle, HP-β-CD, or SBE-β-CD as described above, a baseline hearing threshold for each animal was established with Auditory Brainstem Response (ABR) testing. For ABR testing, mice were anesthetized with a cocktail of Ketamine (100 mpk)/ Xylazine (10 mpk)/Acepromazine (2 mpk) at a dose of 100uL/25g bw. When the mice were no longer responsive to a foot/tail-pinch test, the mice were placed on a warm heating pad in the ABR chamber. Then, a lubricating ointment was applied to their eyes, and the three electrodes were positioned: the negative (-) was placed in the ipsilateral superior postauricular area, the positive (+) was placed in the vertex, and a ground electrode was deeply inserted into the muscles of the left leg. The thresholds of sensitivity for the left ear were determined for Blackman windowed tones presented at 4, 16, and 32 kHz using the testing parameters previously described for rats (Pawlowski et al., 2013). The frequencies were designed to specifically test regions of the organ of Corti from basal (32 kHz) to apical regions (4 kHz) along the basilar membrane. To determine the hearing threshold at each frequency, a stimulus was presented in 512 sweeps starting at 70 decibel (dB). Once an ABR response was detected in duplicate, the stimulus amplitude was decreased in 10 dB and then 5 dB intervals until the ABR response was no longer identifiable. If an ABR response was not detectable at 70 dB, then the testing was started at the highest available stimuli for each frequency (103 dB for 4 kHz, 99 dB for 16 kHz, and 87 dB for 32 kHz) and was reduced in intervals until the ABR response was no longer identifiable. If no ABR response was detectable at the highest available stimulus for a given frequency, 5dB was added and this value was recorded as the hearing threshold. For example, a mouse that had no detectable ABR response for 4 kHz at 103 dB was recorded at 108 dB. All ABR thresholds were determined by a reviewer, blinded to treatment regimens.

Throughout the testing, the mouse's heart rate was evaluated periodically to ensure that the mouse was still alive. Immediately after the ABR testing, mice received a reversal agent, Atipamezole (2.5 mpk) at a dose of 100uL/25g bw, and were moved into a mouse cage on a heating pad. Each mouse was

continuously monitored until it was fully alert and freely roaming around the cage. At a set time after the single- or repeated- injections of vehicle, HP-β-CD, or SBE-β-CD, each mouse was retested with ABR as described above. After the final ABR testing while the mice were still deeply anesthetized, the mice were decapitated, and the inner ears were collected for histology.

To determine the shift in hearing threshold after treatment at a given frequency, the baseline hearing threshold for each individual mouse was subtracted from its retest threshold. For each treatment group, the shift in hearing threshold for the individual mice was calculated and averaged, which is reported in decibel (dB) for each frequency.

Data Analysis

All data are presented as the mean ± SEM. When only two treatments were used, statistically significant differences were tested using an unpaired Student's t-test and are represented by * (P <0.05) to ** (P <0.005). When three treatments were used, significant differences between the vehicle-treated group and those treated with HP-β-CD or SBE-β-CD were determined using a one-way ANOVA followed by Dunnett's post-hoc analysis and are represented by * (P <0.05) to *** (P <0.0005). All statistical tests were performed using GraphPad Prism5 software (GraphPad Software, Inc. San Diego, CA).

B.4 Results

A single large dose of HP-β-CD causes an increase in hearing threshold in mice:

In wildtype and NPC-affected cats, a single high dose of HP-β-CD (8,000 mpk, sc) caused a sudden and irreversible increase in hearing threshold (Ward et al., 2010). To establish if this side effect is limited to cats or is a universal feature of HP-β-CD tratment, I chose to test the effects of HP-β-CD on hearing in wildtype and $Npc1^{-/-}$ mice. However in preliminary results (not shown), I observed that the $Npc1^{-/-}$ mice

Figure B.2 *Effect of HP-β-CD on hearing loss in mice.* Baseline ABR tests were performed on 5 to 6 month old wildtype Balb-c mice at 4, 16, and 32 kHz. After the baseline recordings, mice (n=3/treatment) were injected with HP-β-CD (8,000 mpk, sc) or saline. One week after the injection, ABR responses were re-evaluated. An example ABR recording is shown at 16kHz from a mouse before and after saline (**A**) or HP-β-CD (**B**) treatment. To calculate the change in hearing threshold, the baseline threshold for each individual mouse was subtracted from its re-test threshold (**C**). Each bar represents the mean ± SEM. Statistically significant differences between treatment groups are indicated by * (P <0.05) to ** (P <0.005).

had significant changes to the structure of the inner ear compared to wildtype animals, which is consistent with the reported hearing phenotype in NPC patients (Pikus, 1991) and the feline NPC model (Vite et al., 2008). In order to avoid the complications of testing a potentially ototoxic drug in a mouse model that already has damage to the inner ear, studies of HP-β-CD were performed only in wildtype animals. Using the testing parameters previously described for ABR evaluations in rats (Pawlowski et al., 2013), the average baseline thresholds of sensitivity for the wildtype Balb/c mice (n=50) used in this study were determined to be 40 dB at 4kHz, 45 dB at 16kHz, and 65 dB at 16kHz; although, the standard deviation varied as much as 10 dB within each frequency. Because of the variation seen in the hearing threshold in age- and gender-matched wildtype, each mouse was used as its own control.

In these studies, the threshold at which each individual animal had an ABR response (seen as two consecutive peaks at ~3 and ~4 mS after the tone sounds) was determined at 4, 16, and 32 kHz using the left ear. For example, the baseline at 16kHz for Mouse #4 was 40 dB (**Fig. B.2A**), while Mouse #5 had a baseline hearing threshold of 30dB for 16 kHz (**Fig. B.2B**). After the baselines were established, mice were allowed 1 week to recover and then were injected with saline as a vehicle or with a single high dose of HP-β-CD (8,000 mpk, sc) as was used in the cat studies (Ward et al., 2010). One week following the single injection, the ABR responses of the mice were re-evaluated. While saline had no effect on the hearing threshold (**Fig. B.2A**), HP-β-CD led to a dramatic increase in hearing threshold. For example, Mouse #5 went from a baseline of 30dB to 90 dB at 16 kHz after HP-β-CD (**Fig. B.2B**). At each frequency tested, there was a statistically significant increase in hearing threshold measurable 1 week after a single injection of HP-β-CD (8,000 mpk, sc) compared to saline treatment (**Fig. B.2C**).

Repeated therapeutic doses of HP-β-CD lead to a gradual increase in hearing threshold in mice:

Once hearing loss after HP-β-CD was confirmed in mice, the next question to address was whether this ototoxic effect seen after a large bolus dose was relevant at therapeutic doses for NPC disease. In previous mouse studies, a single dose of HP-β-CD (4,000 mpk, sc) in 7-day-old $Npc1^{-/-}$ pups was shown

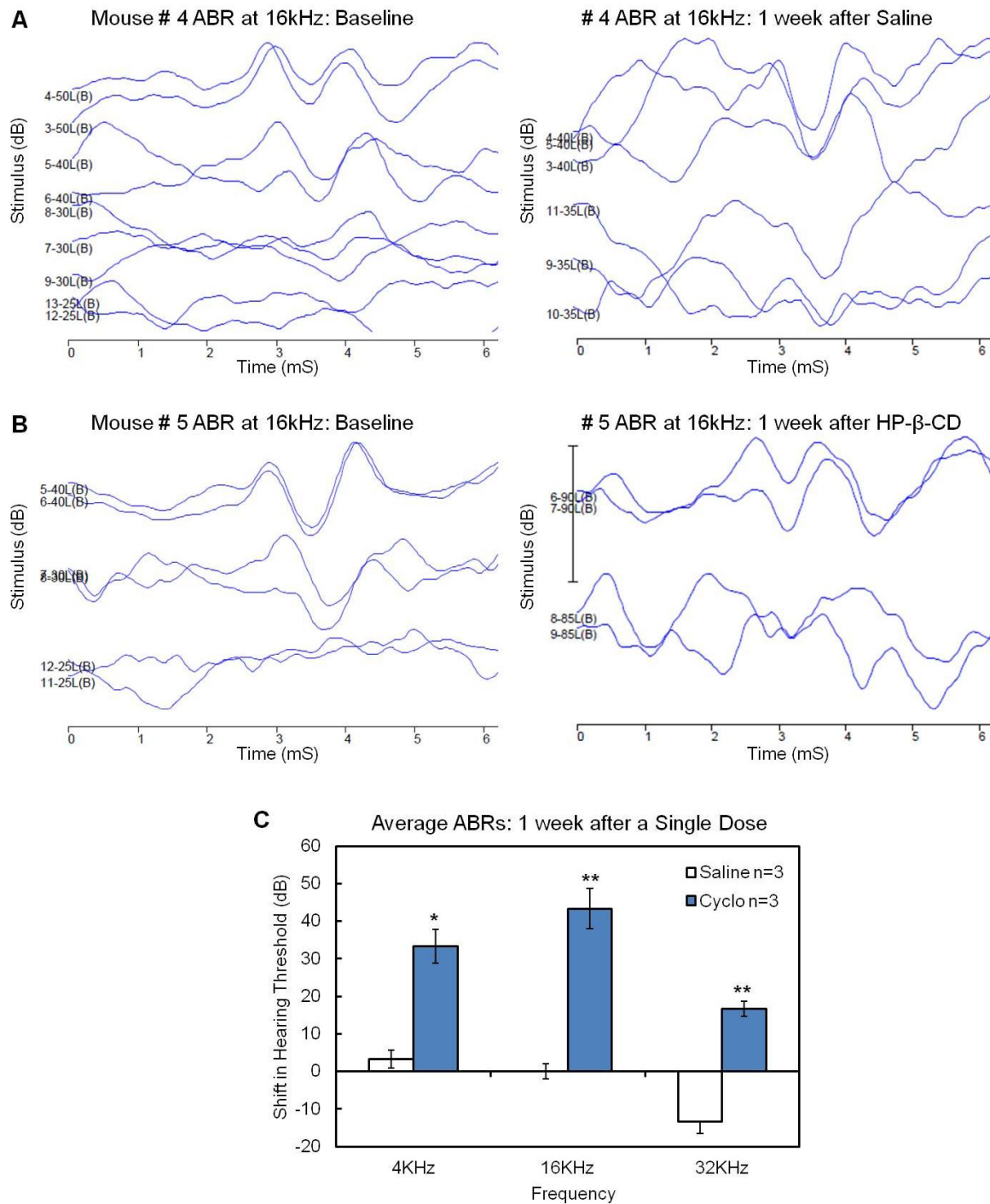**Figure B.3** *Effect of repeated low doses of HP-β-CD on hearing loss in mice.* Baseline ABR tests were performed on 4 to 5 month old wildtype Balb-c mice at 4, 16, and 32 kHz. After the baseline recordings, mice (n=3+/treatment) were injected weekly with HP-β-CD (4,000 mpk, sc) or saline. 4 weeks after the initial dose (5 total injections), ABR responses after therapy were evaluated. Then, the ABR responses were re-evaluated 8 weeks after the initial dose (9 total injections). An example ABR recording is shown at 4kHz from a mouse before and after serial doses of saline (**A**) or HP-β-CD (**B**). To calculate the change in hearing threshold 4 weeks (**C**) and 8 weeks (**D**) after treatment, the baseline threshold for each individual mouse was subtracted from the re-test threshold. Each bar represents the mean ± SEM. The statistically significant difference between treatment groups is indicated by * (P

extend lifespan by 40% (Liu et al., 2009); whereas, weekly injections of HP-β-CD (4,000 mpk, sc,

starting at P7) were shown to almost double the lifespan of *Npc1*^{-/-} mice (Ramirez et al., 2010). In order to

determine if serial treatment of HP-β-CD (4,000 mpk, sc) can led to hearing loss, mice began receiving

weekly injections of saline or HP-β-CD after baseline ABR response thresholds were recorded. After 5

injections (4 weeks after the initial dose), each mouse's hearing threshold was re-evaluated. At this point,

there was no sign of hearing loss in mice receiving HP-β-CD compared to saline treatment (**Fig. B.3C**).

The mice were allowed to recover from anesthesia after ABR testing and continued to receive injections

for an addition 4 weeks. After a total of 9 injections (8 weeks after the initial dose), no increase in hearing

threshold was seen after saline treatment (**Fig. B.3A**); however, weekly HP-β-CD led to eventual hearing

loss. For example, Mouse #14 had a baseline of 40dB at 4 kHz. Mouse #14's hearing threshold remained

around 40dB after 4 weeks of HP-β-CD (4,000 mpk, sc) treatment, but increased to 70dB after 8 weeks of

injections (**Fig. B.3B**). Although there were trends to an increase in hearing threshold at each frequency

tested after 8 weeks of treatment, there was only a statistically significant increase compared to saline

treatment at 32kHz (**Fig. B.3D**).

SBE-β-CD does not lead to a shift in hearing threshold in mice:

As HP-β-CD was found to cause ototoxicity in cats and now in mice, it will be important to determine

the mechanism by which HP-β-CD raises hearing threshold before it is moved into the clinic as a therapy

for NPC disease. Alterations in the plasma membrane concentrations of cholesterol have been found to

lead to defects in outer hair cells, which play a critical role within the inner ear (Canis et al., 2009; Levic

et al., 2011). In order to evaluate if HP-β-CD is affecting hearing by drawing cholesterol out of the

plasma membrane of cells, an alternative form of β-cyclodextrin, sulfobutylether-β-cyclodextrin (SBE-β-

CD), was tested (**Fig. B.1B**). Whereas HP-β-CD is capable of binding to cholesterol in a 1:1 or a 2:1

complex, SBE-β-CD contains chemical modifications that sterically hinder it from dimerization and thus

can only bind to cholesterol in a 1:1 complex (Rajewski et al., 1995; Thompson, 1997). In order to fully

extract unesterified cholesterol from lipid membranes, cyclodextrins must form a 2:1 complex to allow

for complete solubilization of the sterol into an aqueous environment. This can be achieved at high

concentration of HP-β-CD, but SBE-β-CD is incapable of extracting cholesterol from plasma membranes

(Thompson, 1997).

In order to determine if SBE-β-CD, like HP-β-CD, can led to hearing loss, mice were given a single

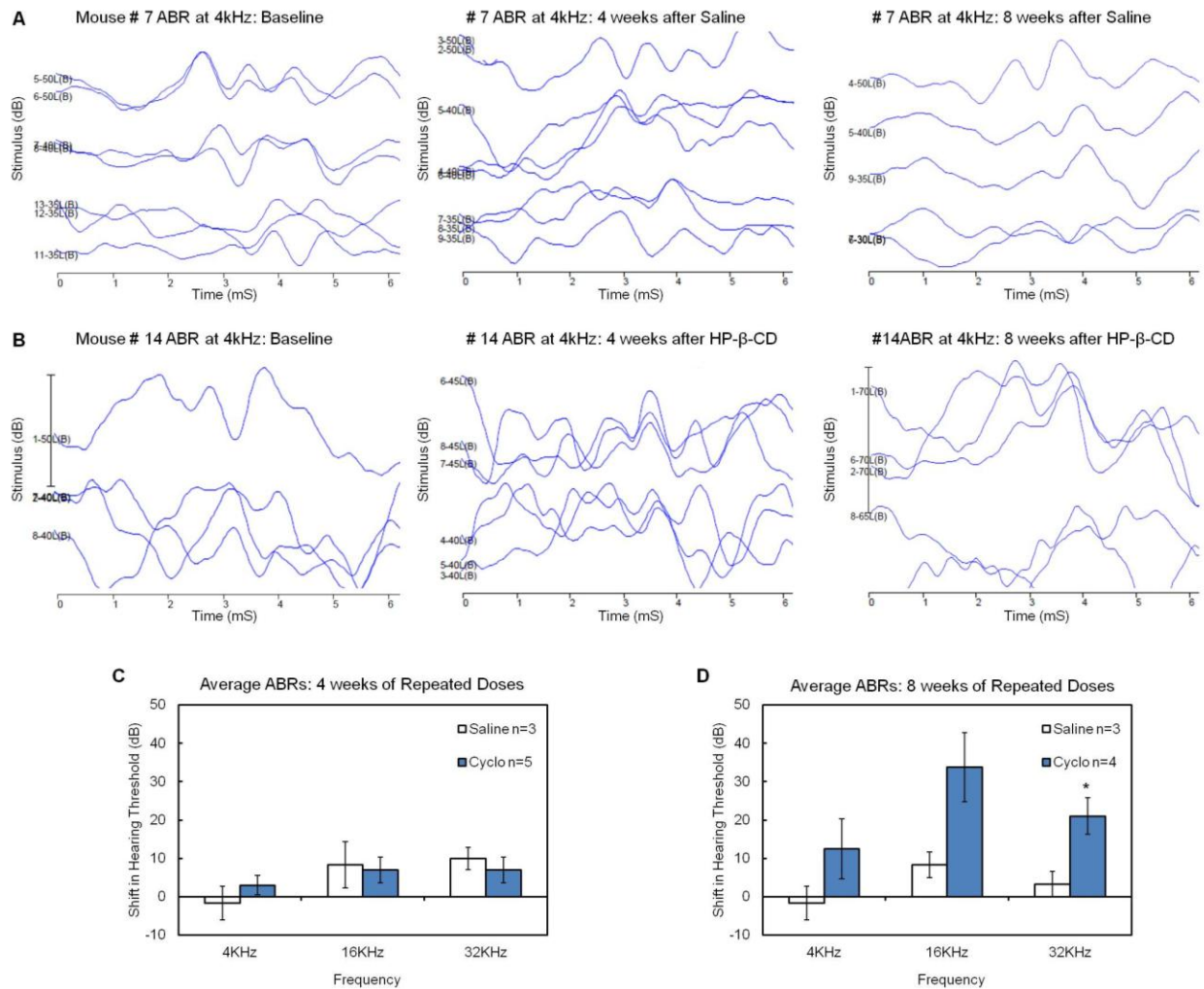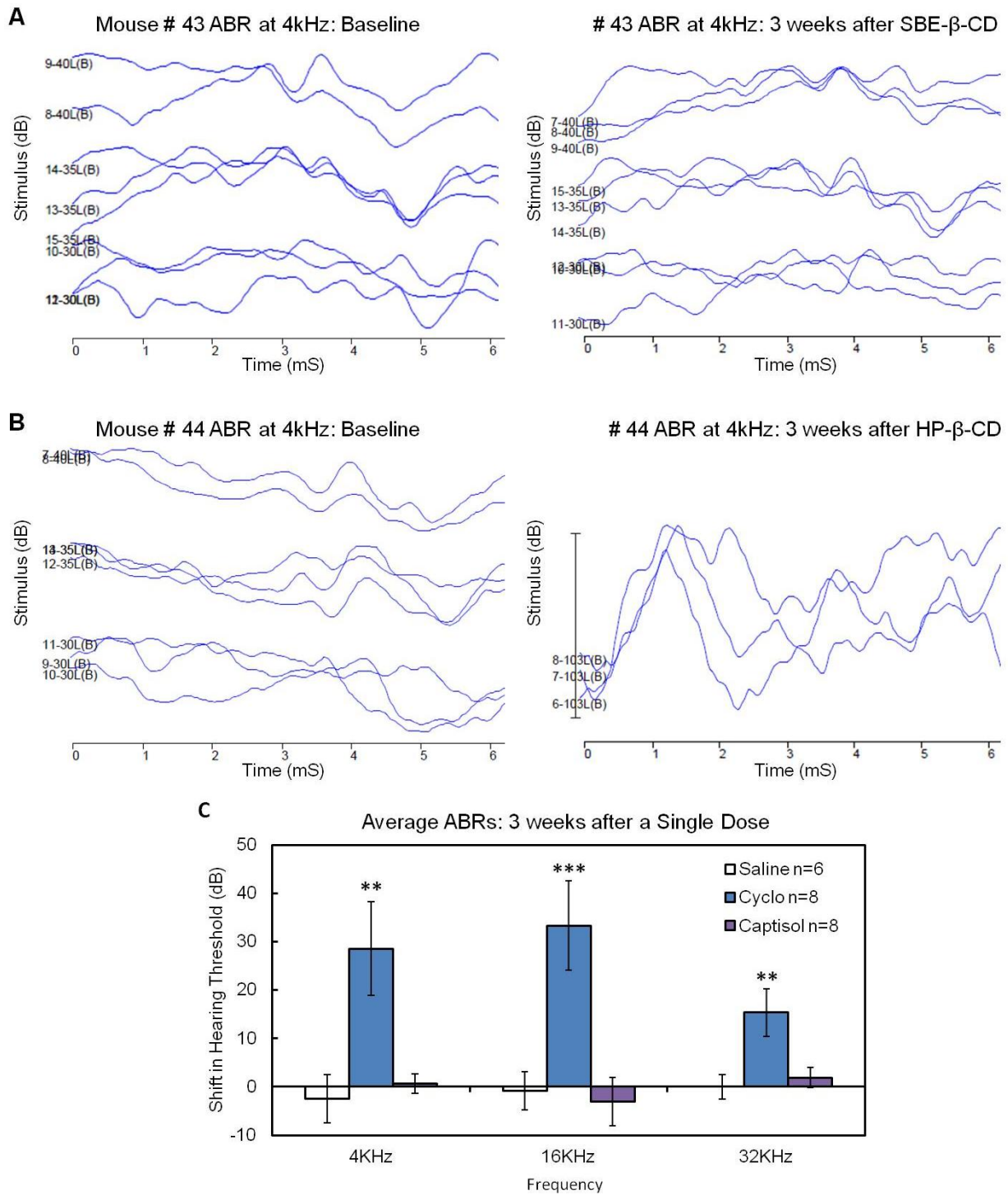**Figure B.4** *Effect of SBE-β-CD on hearing loss in mice.* Baseline ABR tests were performed on 5 to 6 month old wildtype Balb-c mice at 4, 16, and 32 kHz. After the baseline recordings, mice (n=6+/treatment) were injected with HP-β-CD (12,350 mpk, sc), HP-β-CD (8,000 mpk), or saline. Three weeks after the injection, ABR responses were re-evaluated. An example ABR recording is shown at 4kHz from a mouse before and after SBE-β-CD (**A**) or HP-β-CD (**B**) treatment. To calculate the change in hearing threshold, the baseline threshold for each individual mouse was subtracted from its re-test threshold (**C**). Each bar represents the mean ± SEM. Statistically significant differences between treatment groups are indicated by * (P <0.05) to ** (P <0.005).

dose of vehicle or either β-CD after baseline ABR response thresholds were recorded. In order to directly compare the effects of the two β-CD, SBE-β-CD was given at a dose of 12,350 mpk, which is the equivalent Molar dose to 8,000 mpk of HP-β-CD. Three weeks following the single injection, the ABR responses of the mice were re-evaluatd. While SBE-β-CD, like saline, caused no change in hearing threshold (**Fig. B.4A**), HP-β-CD led to a dramatic increase in hearing threshold. For example, Mouse #44 went from a 4 kHz baseline threshold of 35dB to an undetectable ABR response of 103dB at 3 weeks after a single injection of HP-β-CD (**Fig. B.4B**). At each frequency tested compared to saline treatment, there was a statistically significant increase in hearing threshold measurable after HP-β-CD (8,000 mpk, sc) but no change after SBE-β-CD (12,350 mpk, sc) treatment (**Fig. B.4C**).

B.5 Discussion

Unesterified cholesterol is an integral component of plasma membranes, and its concentration is tightly regulated within cells. Any alterations in cholesterol balance can lead to detrimental effects throughout the body, including the inner ear. In fact, eating a diet rich in cholesterol has been linked with hearing loss, while taking medicines that lower LDL cholesterol levels, such as statins, has been suggested to have a beneficial effect on hearing in humans (Gopinath et al., 2011). Mechanistically, hypercholesterolemia by cholesterol feeding in chinchillas has been shown to induce ultrastructural changes in the cochlea, which could explain the reported hearing loss (Gratton et al., 1992). In addition, several genetic disorders caused by mutations in genes required for cholesterol synthesis and trafficking, including Niemann Pick Type C (NPC) disease, have been associated with hearing loss in both patients (Pikus, 1991) and in animal models (Vite et al., 2008). Most recently, the cholesterol-binding pharmaceutical agent, HP-β-CD, which is FDA-approved and widely used as a vehicle, was shown to cause increased hearing threshold in cats (Ward et al., 2010).

In the studies presented in this chapter, the hearing loss induced by HP-β-CD was confirmed in

another animal model, the mouse. Within just 1 week, a single injection was HP-β-CD at 8,000 mpk led

to a significant increase in hearing threshold compared to saline treatment (**Fig. B.2**). Since there were

significant changes in threshold at 4, 16, and 32 kHz, this suggested that HP-β-CD caused damage all

along the basilar membrane of the organ of Corti from the basal (32 kHz) to the more apical regions (4

kHz). In addition to the single-bolus dose, 2 months of weekly HP-β-CD injections at 4,000 mpk also

induced an increase in hearing threshold, which was significant at 32 kHZ, representative of damage

within the basal region of the organ of Corti (**Fig. B.3**). Together these studies show that very high

concentrations of HP-β-CD are immediately ototoxic and suggest that lower concentrations of HP-β-CD

can led to hearing loss over time. A likely scenario to explain this would be that HP-β-CD is not fully

cleared from the closed circulatory system of the inner ear. Therefore, with each repeated dose of HP-β-

CD more accumulates, which ultimately reaches a critical concentration that causes ototoxity.

At high concentrations, HP-β-CD is capable of fully solubilizing cholesterol by forming a 2:1 ratio

with the sterol, which is required in order to fully extract cholesterol from plasma membranes. The ability

of cyclodextrin to form a 2:1 ratio and to fully solubilize cholesterol from membranes was shown not to

be required to relieve accumulated sterol in NPC disease. This was supported by several lines of

evidence: 1) The changes in sterol balance after HP-β-CD administration were only seen in $Npc1^{-/-}$ mice,

never in wildtype mice (Liu et al., 2009); 2) SBE-β-CD (a cyclodextrin which can not extract cholesterol

from membranes) was capable of reducing cholesterol synthesis in the liver and spleen of 7-day-old $Npc1^{-/-}$

mice to wildtype levels (Ramirez et al., 2011); and 3) SBE-β-CD was able to elicit alterations in gene

expression indicative of increased intracellular cholesterol in primary $Npc1^{-/-}$ macrophages and neurons

(Taylor et al., 2012). As HP-β-CD's effect in the inner ear was seen in wildtype animals and appears to

require a critical concentration, it suggests that the mechanism of action could be through altering

cholesterol levels at the plasma membrane. In support of this, a single dose of SBE-β-CD (at 12,350 mpk,

an equal molar concentration to 8,000 mpk HP-β-CD) did not alter hearing threshold in mice even after 3

weeks, while HP-β-CD (at 8,000 mpk) led to significant hearing loss at all three frequencies tested after 3

weeks (**Fig. B.4**).

Overall these studies confirm that HP-β-CD causes hearing loss in mice and begin to address the mechanism. Currently histopathological examination of the inner ears collected from these mice on their final day of ABR testing are underway, which should grant additional insight into HP-β-CD's mechanism of action in the inner ear. The studies presented in this chapter also supply an alternative therapy for the treatment of NPC disease; however, the efficacy of SBE-β-CD needs to be further evaluated in $Npc1^{-/-}$ mice. The results of ongoing survival studies after SBE-β-CD injections in $Npc1^{-/-}$ mice will provide evidence to determine if SBE-β-CD, which is also FDA-approved, should be utilized instead of HP-β-CD as a therapy for NPC disease.

APPENDIX C:

Primers used for Quantitative Real-time PCR

C.1 Designing and Validating Primers

Quantitative Real-time PCR (qPCR) is a powerful technique, which provides a precise assessment of changes in mRNA levels among samples in a relatively short amount of time with a small quantity of material (Valasek et al., 2005a). However, the accuracy and specificity by which each qPCR reaction is able to measure the relative expression of a gene target is very dependent on the primer set used to amplify the gene of interest. For example, if a primer set was designed to anneal to "Gene A" but also had an off-target effect and annealed to "Gene B", the results obtained from the qPCR reaction would include the relative expression of both genes and could lead to the wrong interpretation of the results. Because of this, all of the qPCR primers used for the research presented in this dissertation were designed and validated to meet specific guidelines. To design primers, programs including Primer Express software (Version 3, Applied Biosystems) and a variety of online primer design algorithms [DLux (Invitrogen,https:// orf.invitrogen.com/lux/); PrimerBlast (NCBI, http:// ncbi.nlm.nih.gov/tools/primer-blast); Integrated DNA Technology (http://idtdna.com/scitools/applications/RealTimePCR/ default.aspx)] were used. Specifically, primers were designed to target only the gene of interest and to span an intron in order to distinguish cDNA from gDNA. Once primers were designed, the oligonucleotides were ordered (Integrated DNA Technology), and then were validated by analysis of template titration and dissociation curves as previously described (Chuang et al., 2008).

C.2 Primer Tables 1-4

The primers used in this dissertation research have been compiled into tables according to the chapter or appendix in which they appear. Each primer set is listed by the gene abbreviation as it is written in this text followed by: the full name of the gene with any recognized alternative names in parenthesis; the NCBI accession number, the forward (F) and reverse (R) primer sequences, and the location of the region on the gene amplified by these primers (the amplicon position).

Table C.1: PCR Primers Used to Quantify Mouse mRNA Levels in Chapter 2				
Gene Symbol	**Full Name (Alternative Name)**	**Accession Number**	**Sequence of Primers (5' to 3')**	**Amplicon position**
Housekeeping Gene:				
βactin	Cytoplasmic βactin	NM_007393	F: CATCGTGGGCCGCTCTA	178 - 245
			R: CACCCACATAGGAGTCCTTCTG	
Cyclo	Cyclophilin; Peptidylprolyl isomerase B (PP1B)	NM_011149	F: TGGAGAGCACCAAGACAGACA	642-707
			R: TGCCGGAGTCGACAATGAT	
Genes of Interest:				
Abca1	ATP-binding cassette A1 (ABC1)	NM_013454	F: CGTTTCCGGGAAGTGTCCTA	6805-6883
			R: GCTAGAGATGACAAGGAGGATGGA	
Abcg1	ATP-binding cassette G1 (ABC8)	NM_009593	F: GCTGTGCGTTTTGTGCTGTT	1676-1759
			R: TGCAGCTCCAATCAGTAGTCCTAA	
Api6	Apoptosis Inhibitory 6 (Cd5 antigen like, Cd5l)	NM_009690	F: GCTGGCCATCTTGAGCATT	145-214
			R: TCCCACTAGCTGCACTTTGG	
Casp1	Caspase 1	NM_009807	F: TGGCACATTTCCAGGACTGA	566-637
			R: TCTTTCCATAACTTCTGGGCTTT	
Casp3	Caspase 3	NM_009810	F: CATAAGAGCACTGGAATGTCATCTC	229-302
			R: CCCATGAATGTCTCTCTGAGGTT	
Casp6	Caspase 6	NM_009690	F: AATTCACGAGGTGTCGACTTCA	341-480
			R: CGTGGCTCAGGAAGACACA	
Cd68	CD68 antigen	NM_009853	F: CCTCCACCCTCGCCTAGTC	343-460
			R: TTGGGTATAGGATTCGGATTTGA	
Cd11c	CD11c antigen (Integrin alpha X, Itgax)	NM_021334	F: CTTCATTCTGAAGGGCAACCT	3211-3284
			R: CACTCAGGAGCAACACCTTTTT	
Ch25h	Cholesterol 25-hydroxylase	NM_009890	F: CACAAGGTGCATCACCAGAACT	478-564
			R: CGAAGAAGGTCAGCGAAAGC	
HmgCoARed	3-Hydroxy-3-methylglutaryl-Coenzyme A Reductase (HMGCR)	NM_008255	F: CTTGTGGAATGCCTTGTGATTG	578-653
			R: AGCCGAAGCAGCACATGAT	
Ldlr	Low density lipoprotein receptor	NM_010700	F: GAGGAACTGGCGGCTGAA	2620-2858
			R: GTGCTGGATGGGGAGGTCT	
Mip1α	Chemokine (C-C motif) ligand 3 (CCL3)	NM_011337	F: TTCATCGTTGACTATTTTGAAACCA	237-312
			R: GCCGGTTTCTCTTAGTCAGGA	
Npc1	Niemann-Pick type C1	NM_008720	F: CCCTTCGGGCCTCCAT	1437-1514
			R: TGCGGTGATGCTTTCAATG	
Pcp2	Purkinje cell protein 2 (L7)	NM_008790	F: CACTTCTGAGCCCCATTTCC	51 - 118
			R: GTGGGTCAGCAGGTTGAAGA	
Pcp4	Purkinje cell protein 4 (PEP19)	NM_008791	F: GAGTCAGGCCAACATGAGTGA	164-232
			R: TCTCCTGACGTCTTGTCTTTTCC	
Tnf	Tumor necrosis factor alpha	NM_013693	F: CTGAGGTCAATCTGCCCAAGTAC	791-866
			R: CTTCACAGAGCAATGACTCCAAAG	
Srebp2	Sterol regulatory element binding factor 2 (SREBF2)	NM_033218	F: ACAAACTTGCTCTGAAAACAAATC	157-287
			R: GCGTTCTGGAGACCATGGA	

Table C.2: PCR Primers Used to Quantify Mouse mRNA Levels in Chapter 3				
Gene Symbol	**Full Name (Alternative Name)**	**Accession Number**	**Sequence of Primers (5' to 3')**	**Amplicon position**
Housekeeping Gene:				
Cyclo	Cyclophilin; Peptidylprolyl isomerase B (PP1B)	NM_011149	F: TGGAGAGCACCAAGACAGACA R: TGCCGGAGTCGACAATGAT	642-707
Genes of Interest:				
Abca1	ATP-binding cassette A1 (ABC1)	NM_013454	F: CGTTTCCGGGAAGTGTCCTA R: GCTAGAGATGACAAGGAGGATGGA	6805-6883
Abcg1	ATP-binding cassette G1 (ABC8)	NM_009593	F: GCTGTGCGTTTTGTGCTGTT R: TGCAGCTCCAATCAGTAGTCCTAA	1676-1759
Abcg8	ATP-binding cassette G8	NM_026180	F: TGCCCACCTTCCACATGTC R:ATGAAGCCGGCAGTAAGGTAGA	1759-1831
Cd68	CD68 antigen	NM_009853	F: CCTCCACCCTCGCCTAGTC R: TTGGGTATAGGATTCGGATTTGA	343-460
Cxcl1	Chemokine (C-X-C motif) ligand 1 (KC, GRO1)	NM_008176	F: AACCGAAGTCATAGCCACAC R: CAGACGGTGCCATCAGAG	249-395
Cyp7A1	Cytochrome P450 7A1 (Cholesterol 7 alpha hydroxylase)	NM_007824	F: AGCAACTAAACAACCTGCCAGTACTA R: GTCCGGATATTCAAGGATGCA	1073-1154
HmgCoARed	3-Hydroxy-3-methylglutaryl-Coenzyme A Reductase (HMGCR)	NM_008255	F: CTTGTGGAATGCCTTGTGATTG R: AGCCGAAGCAGCACATGAT	578-653
HmgCoASyn	3-Hydroxy-3-methylglutaryl-Coenzyme A synthase (HMGCS1)	NM_145942	F: GCCGTGAACTGGGTCGAA R: GCATATATAGCAATGTCTCCTGCAA	534-610
Idol	Inducible Degrader of the LDL receptor (MYLIP)	NM_153789	F: TGTGCTATGTGACGAGGCCG R: CCTGCACACCTGGTTGAGACA	220 - 311
Il-6	Interleukin 6	NM_031168	F: CTGCAAGAGACTTCCATCCAGTT R: AAGTAGGGAAGGCCGTGGTT	45-113
Il-12(p40)	Interleukin 12 subunit beta (IL-12β)	NM_008352	F: GGAAGCACGGCAGCAGAATA R: AACTTGAGGGAGAAGTAGGAATGG	792-971
Ifn-γ	Interferon gamma (INF-γ)	NM_008337	F: TGGCATAGATGTGGAAGAAAAGA R: TGCAGGATTTTCATGTCACCAT	228-308
Ldlr	Low density lipoprotein receptor	NM_010700	F: GAGGAACTGGCGGCTGAA R: GTGCTGGATGGGGAGGTCT	2620-2858
Mip1α	Chemokine (C-C motif) ligand 3 (CCL3)	NM_011337	F: TTCATCGTTGACTATTTTGAAACCA R: GCCGGTTTCTCTTAGTCAGGA	237-312
Tnfα	Tumor necrosis factor alpha	NM_013693	F: CTGAGGTCAATCTGCCCAAGTAC R: CTTCACAGAGCAATGACTCCAAAG	791-866
Srebp2	Sterol regulatory element binding factor 2 (SREBF2)	NM_033218	F: ACAAACTTGCTCTGAAAACAAATC R: GCGTTCTGGAGACCATGGA	157-287

Table C.3: PCR Primers Used to Quantify Mouse mRNA Levels in Chapter 4				
Gene Symbol	**Full Name (Alternative Name)**	**Accession Number**	**Sequence of Primers (5' to 3')**	**Amplicon position**
Housekeeping Gene:				
Cyclo	Cyclophilin; Peptidylprolyl isomerase B (PP1B)	NM_011149	F: TGGAGAGCACCAAGACAGACA R: TGCCGGAGTCGACAATGAT	642-707
Genes of Interest:				
Abca1	ATP-binding cassette A1 (ABC1)	NM_013454	F: CGTTTCCGGGAAGTGTCCTA R: GCTAGAGATGACAAGGAGGATGGA	6805-6883
Abcg1	ATP-binding cassette G1 (ABC8)	NM_009593	F: GCTGTGCGTTTTGTGCTGTT R: TGCAGCTCCAATCAGTAGTCCTAA	1676-1759
Abcg8	ATP-binding cassette G8	NM_026180	F: TGCCCACCTTCCACATGTC R:ATGAAGCCGGCAGTAAGGTAGA	1759-1831
Cd68	CD68 antigen	NM_009853	F: CCTCCACCCTCGCCTAGTC R: TTGGGTATAGGATTCGGATTTGA	343-460
Cd11c	CD11c antigen (Integrin alpha X, Itgax)	NM_021334	F: CTTCATTCTGAAGGGCAACCT R: CACTCAGGAGCAACACCTTTTT	3211-3284
Emr1	EGF-like module receptor 1 (F4/80)	NM_010130	F: CCAGCAATGGACAAACCAACTTT R: GGTGAGTCACTTTGAAGACATTCG	234-312
HmgCoARed	3-Hydroxy-3-methylglutaryl-Coenzyme A Reductase (HMGCR)	NM_008255	F: CTTGTGGAATGCCTTGTGATTG R: AGCCGAAGCAGCACATGAT	578-653
HmgCoASyn	3-Hydroxy-3-methylglutaryl-Coenzyme A synthase (HMGCS1)	NM_145942	F: GCCGTGAACTGGGTCGAA R: GCATATATAGCAATGTCTCCTGCAA	534-610
Npc1	Niemann-Pick type C1	NM_008720	F: CCCTTCGGGCCTCCAT R: TGCGGTGATGCTTTCAATG	1437-1514
Pcp2	Purkinje cell protein 2 (L7)	NM_008790	F: CACTTCTGAGCCCCATTTCC R: GTGGGTCAGCAGGTTGAAGA	51 - 118
Pcp4	Purkinje cell protein 4 (PEP19)	NM_008791	F: GAGTCAGGCCAACATGAGTGA R: TCTCCTGACGTCTTGTCTTTTCC	164-232

Table C.4: PCR Primers Used to Quantify Mouse mRNA Levels in Appendix A				
Gene Symbol	**Full Name (Alternative Name)**	**Accession Number**	**Sequence of Primers (5' to 3')**	**Amplicon position**
Housekeeping Gene:				
βactin	Cytoplasmic βactin	NM_007393	F: CATCGTGGGCCGCTCTA R: CACCCACATAGGAGTCCTTCTG	178 - 245
Cyclo	Cyclophilin; Peptidylprolyl isomerase B (PP1B)	NM_011149	F: TGGAGAGCACCAAGACAGACA R: TGCCGGAGTCGACAATGAT	642-707
Genes of Interest:				
Abca1	ATP-binding cassette A1 (ABC1)	NM_013454	F: CGTTTCCGGGAAGTGTCCTA R: GCTAGAGATGACAAGGAGGATGGA	6805-6883
Abcg1	ATP-binding cassette G1 (ABC8)	NM_009593	F: GCTGTGCGTTTTGTGCTGTT R: TGCAGCTCCAATCAGTAGTCCTAA	1676-1759
Hdac1	Histone Deacetylase 1	NM_008228	F: ATGACCAACCAGAACACTAACG R: GGGCAGCATCCTCAAGTTCTC	1065-1139
Hdac2	Histone Deacetylase 2	NM_008229	F: GGATGGAGAAGACCCGGACAA R: TCTTCATCGCAAGCTATCCG	1399-1467
Hdac3	Histone Deacetylase 3	NM_010411	F: CGCTGAAGAGAGAGGTCCCG R: CCACATCACTTTCCTTGTCGTTG	1257-1354
Hdac4	Histone Deacetylase 4	NM_207225	F: AGGAACCACCACTGTAGCCCG R: CTTGGCTGAGCTTCAAGACAGA	3331 -3398
Hdac5	Histone Deacetylase 5	NM_010412	F: CCCTCCTACAAATTGCCTTTGC R: AACGTACTTTTAAGTTGGGTTCCG	1047-1140
Hdac6	Histone Deacetylase 6	NM_010413	F: CGTGGTGGAAAGAAGTGTGCT R: TGCCTTTCTTCTTTACCTCCG	439-505
Hdac7	Histone Deacetylase 7	NM_019572	F: CCAGTAGTAGCAGCACACCCG R: GCAGGCGAGAGGGTAAGGTG	1055-1267
Hdac8	Histone Deacetylase 8	NM_027382	F: CGAGTATGTCAGCATCTGCG R: GGGCATAGGCTTCGATCAGAGA	150-232
Hdac9	Histone Deacetylase 9	NM_024124	F: CAAAAGACACTCCAACCAATGG R: GCAGCCGTGTACCAGAGCTT	801-870
Hdac11	Histone Deacetylase 11	NM_144919	F: ACACGAGGCGCTATCTCAACG R: TGCACAAGGAAGTTGGGAAGAAA	255-351
HmgCoARed	3-Hydroxy-3-methylglutaryl-Coenzyme A Reductase (HMGCR)	NM_008255	F: CTTGTGGAATGCCTTGTGATTG R: AGCCGAAGCAGCACATGAT	578-653
HmgCoASyn	3-Hydroxy-3-methylglutaryl-Coenzyme A synthase (HMGCS1)	NM_145942	F: GCCGTGAACTGGGTCGAA R: GCATATATAGCAATGTCTCCTGCAA	534-610
Idol	Inducible Degrader of the LDL receptor (MYLIP)	NM_153789	F: TGTGCTATGTGACGAGGCCG R: CCTGCACACCTGGTTGAGACA	220 - 311
Ldlr	Low density lipoprotein receptor	NM_010700	F: GAGGAACTGGCGGCTGAA R: GTGCTGGATGGGGAGGTCT	2620-2858
Npc1	Niemann-Pick type C1	NM_008720	F: CCCTTCGGGCCTCCAT R: TGCGGTGATGCTTTCAATG	1437-1514
Npc2	Niemann-Pick type C2	NM_023409	F: GCACAAAGGCCAGTCCTACA R: CGTGCTGTTCTGGGACTGA	392-458
Sr-b1	Scavenger Receptor class B Member 1 (SCARB1)	NM_016741	F: TCCCCATGAACTGTTCTGTGAA R: TGCCCGATGCCCTTGA	1351-1417
Srebp2	Sterol regulatory element binding factor 2 (SREBF2)	NM_033218	F: ACAAACTTGCTCTGAAAACAAATC R: GCGTTCTGGAGACCATGGA	157-287

BIBLIOGRAPHY

2012 Alzheimer's disease facts and figures. (2012). *Alzheimer's & Dementia: the Journal of the Alzheimer's Association, 8*, 131-168.

Abi-Mosleh, L., Infante, R. E., Radhakrishnan, A., Goldstein, J. L., & Brown, M. S. (2009). Cyclodextrin overcomes deficient lysosome-to-endoplasmic reticulum transport of cholesterol in Niemann-Pick type C cells. *Proceedings of the National Academy of Sciences USA, 106*, 19316-19321.

Alvarez, A. R., Klein, A., Castro, J., Cancino, G. I., Amigo, J., Mosqueira, M., Vargas, L. M., Yevenes, L. F., Bronfman, F. C., & Zanlungo, S. (2008). Imatinib therapy blocks cerebellar apoptosis and improves neurological symptoms in a mouse model of Niemann-Pick type C disease. *FASEB Journal, 22*, 3617-3627.

Aqul, A., Liu, B., Ramirez, C. M., Pieper, A. A., Estill, S. J., Burns, D. K., Liu, B., Repa, J. J., Turley, S. D., & Dietschy, J. M. (2011). Unesterified cholesterol accumulation in late endosomes/lysosomes causes neurodegeneration and is prevented by driving cholesterol export from this compartment. *Journal of Neuroscience, 31*, 9404-9413.

Assmann, G., & Seedorf, U. (2001). Acid lipase deficiency: Wolman disease and cholesteryl ester storage disease. In C. R. Scriver (Ed.), *The Metabolic and Molecular Bases of Inherited Disease.* (8th Ed. ed., Vol. 3, pp. 3551-3572). New York: McGraw-Hill.

Atadja, P. (2009). Development of the pan-DAC inhibitor panobinostat (LBH589): successes and challenges. *Cancer Letters, 280*, 233-241.

Atger, V. M., de la Llera-Moya, M., Stoudt, G. W., Rodrigueza, W. V., Phillips, M. C., & Rothblat, G. H. (1997). Cyclodextrins as catalysts for the removal of cholesterol from macrophage foam cells. *Journal of Clinical Investigation, 99*, 773-780.

Baldan, A., Gomes, A. V., Ping, P., & Edwards, P. A. (2008). Loss of ABCG1 results in chronic pulmonary inflammation. *Journal of Immunology, 180*, 3560-3568.

Baldan, A., Tarr, P., Lee, R., & Edwards, P. A. (2006a). ATP-binding cassette transporter G1 and lipid homeostasis. *Current Opinion in Lipidology, 17*, 227-232.

Baldan, A., Tarr, P., Vales, C. S., Frank, J., Shimotake, T. K., Hawgood, S., & Edwards, P. A. (2006b). Deletion of the transmembrane transporter ABCG1 results in progressive pulmonary lipidosis. *Journal of Biological Chemistry, 281*, 29401-29410.

Beltroy, E. P., Liu, B., Dietschy, J. M., & Turley, S. D. (2007). Lysosomal unesterifed cholesterol content correlates with liver cell death in murine Niemann-Pick type C disease. *Journal of Lipid Research, 48*, 869-881.

Birrell, M. A., Catley, M. C., Hardaker, E., Wong, S. S. N., Willson, T. M., McCluskie, K., Leonard, T., Farrow, S. N., Collins, J. K., Haj-Yahia, S., & Belvisi, M. G. (2007). Novel role for the liver X nuclear receptor in the suppression of lung inflammatory responses. *Journal of Biological Chemistry, 282*, 31882-31890.

Bjurulf, B., Spetalen, S., Erichsen, A., Vanier, M. T., Strom, E. H., & Stromme, P. (2008). Niemann-Pick disease type C2 presenting as fatal pulmonary alveolar lipoproteinosis: morphological findings in lung and nervous tissue. *Medical Science Monitor, 14*, CS71-75.

Bojanic, D. D., Tarr, P. T., Gale, G. D., Smith, D. J., Bok, D., Chen, B., Nusinowitz, S., Lovgren-Sandblom, A., Bjorkhem, I., & Edwards, P. A. (2010). Differential expression and function of ABCG1 and ABCG4 during development and aging. *Journal of Lipid Research, 51*, 169-181.

Boothe, A. D., Weintroub, H., Pentchev, P. G., Jones, J., Butler, J., Barry, J. E., Neumeyer, B., Stivers, J. A., & Brady, R. O. (1984). A lysosomal storage disorder in the BALB/c mouse: bone marrow transplantation. *Veterinary Pathology, 21*, 432-441.

Bradner, J. E., Mak, R., Tanguturi, S. K., Mazitschek, R., Haggarty, S. J., Ross, K., Chang, C. Y., Bosco, J., West, N., Morse, E., Lin, K., Shen, J. P., Kwaiatkowski, N. P., Gheldof, N., Dekker, J. M., DeAngelo, D. J., Carr, S. A., Schreiber, S. L., Golub, T. R., & Ebert, B. L. (2010). Chemical

genetic strategy identified histone deacetylase 1 (HDAC1) and HDAC2 as therapeutic targets in sickle cell disease. *Proceedings of the National Academy of Sciences USA, 107*, 12617–12622.

Brown, D. E., Thrall, M. A., Walkley, S. U., Wenger, D. A., Mitchell, T. W., Smith, M. O., Royals, K. L., March, P. A., & Allison, R. W. (1994). Feline Niemann-Pick disease type C. *The American Journal of Pathology, 144*, 1412-1415.

Brownell, W. E., Jacob, S., Hakizimana, P., Ulfendahl, M., & Fridberger, A. (2011). Membrane cholesterol modulates cochlear electromechanics. *Pflugers Archiv, 461*, 677-686.

Camargo, F., Erickson, R. P., Garver, W. S., Hossain, G. S., Carbone, P. N., Heidenreich, R. A., & Blanchard, J. (2001). Cyclodextrins in the treatment of a mouse model of Niemann-Pick C disease. *Life Sciences, 70*, 131-142.

Canis, M., Schmid, J., Olzowy, B., Jahn, K., Strupp, M., Berghaus, A., & Suckfuell, M. (2009). The influence of cholesterol on the motility of cochlear outer hair cells and the motor protein prestin. *Acta Oto-Laryngologica, 129*, 929-934.

Carstea, E. D., Morris, J. A., Coleman, K. G., Loftus, S. K., Zhang, D., Cummings, C., Gu, J., Rosenfeld, M. A., Pavan, W. J., Krizman, D. B., Nagle, J., Polymeropoulos, M. H., Sturley, S. L., Ioannou, Y. A., Higgins, M. E., Comly, M., Cooney, A., Brown, A., Kaneski, C. R., Blanchette-Mackie, E. J., Dwyer, N. K., Neufeld, E. B., Chang, T. Y., Liscum, L., Strauss, J. F., 3rd, Ohno, K., Zeigler, M., Carmi, R., Sokol, J., Markie, D., O'Neill, R. R., van Diggelen, O. P., Elleder, M., Patterson, M. C., Brady, R. O., Vanier, M. T., Pentchev, P. G., & Tagle, D. A. (1997). Niemann-Pick C1 disease gene: homology to mediators of cholesterol homeostasis. *Science, 277*, 228-231.

Chuang, J.-C., Cha, J.-Y., Garmey, J. C., Mirmira, R. G., & Repa, J. J. (2008). Nuclear hormone receptor expression in the endocrine pancreas. *Molecular Endocrinology, 22*, 2353-2363.

Costet, P. (2010). Molecular pathways and agents for lowering LDL-cholesterol in addition to statins. *Pharmacology & Therapeutics, 126*, 263-278.

Crisafulli, C., Mazzon, E., Paterniti, I., Galuppo, M., Bramanti, P., & Cuzzocrea, S. (2010). Effects of liver X receptor agonist treatment on signal trandsuction pathways in acute lung inflammation. *Respiratory Research, 11*, 19.

Crocker, A. C. (1961). The cerebral defect in Tay-Sachs disease and Niemann-Pick disease. *Journal of Neurochemistry, 7*, 69-80.

Davidson, C. D., Ali, N. F., Micsenyi, M. C., Stephney, G., Renault, S., Dobrenis, K., Ory, D. S., Vanier, M. T., & Walkley, S. U. (2009). Chronic cyclodextrin treatment of murine Niemann-Pick C disease ameliorates neuornal cholesterol and glycosphingolipid storage and disease progression. *PLoS One, 4*, e6951.

De Ruijter, A. J. M., Van Gennip, A. H., Caron, H. N., Kemp, S., & Van Kuilenburg, A. B. P. (2003). Histone deacetylases (HDACs): characterization of the classical HDAC family. *Biochemical Journal, 370*, 737-749.

DeBarber, A. E., Eroglu, Y., Merkens, L. S., Pappu, A. S., & Steiner, R. D. (2011). Smith-Lemli-Opitz syndrome. *Expert Reviews in Molecular Medicine, 13*, e24.

Dheda, K., Huggett, J. F., Bustin, S. A., Johnson, M. A., Rook, G., & Zumla, A. (2004). Validation of housekeeping genes for normalizing RNA expression in real-time PCR. *BioTechniques, 37*, 112-119.

Dietschy, J. M. (1984). Regulation of cholesterol metabolism in man and in other species. *Klinische Wochenschrift, 62*, 338-345.

Dietschy, J. M. (1998). Dietary fatty acids and the regulation of plasma low density lipoprotein cholesterol concentrations. *Journal of Nutrition, 128*, 444S-448S.

Dietschy, J. M. (2009). Central nervous system: cholesterol turnover, brain development and neurodegeneration. *Biological Chemistry, 390*, 287-293.

Dietschy, J. M., & Spady, D. K. (1984). Measurement of rates of cholesterol synthesis using tritiated water. *Journal of Lipid Research, 25*, 1469-1476.

Dietschy, J. M., & Turley, S. D. (2004). Cholesterol metabolism in the central nervous system during early development and in the mature animal. *Journal of Lipid Research, 45*, 1375-1397.

Du, H., Cameron, T. L., Garger, S. J., Pogue, G. P., Hamm, L. A., White, E. K., Hanley, K. M., & Grabowski, G. A. (2008). Wolman disease/choesteryl ester storage disease: efficacy of plant-produced human lysosomal acid lipase in mice. *Journal of Lipid Research, 49*, 1646-1657.

Du, H., Witte, D. P., & Grabowski, G. A. (1996). Tissue and cellular specific expression of murine lysosomal acid lipase mRNA and protein. *Journal of Lipid Research, 37*, 937-949.

Elrick, M. J., Pacheco, C. D., Yu, T., Dadgar, N., Shakkottai, V. G., Ware, C., Paulson, H. L., & Lieberman, A. P. (2010). Conditional Niemann-Pick C mice demonstrate cell autonomous Purkinje cell neurodegeneration. *Human Molecular Genetics, 19*, 837-847.

Frank, T. C., Nunley, M. C., Sons, H. D., Ramon, R., & Abbott, L. C. (2003). Fluoro-jade identification of cerebellar granule cell and Purkinje cell death in the α_{1A} calcium ion channel mutant mouse, leaner. *Neuroscience, 118*, 667-680.

Frijlink, H. W., Eissens, A. C., Hefting, N. R., Poelstra, K., Lerk, C. F., & Meijer, D. K. F. (1991). The effect of parenterally administered cyclodextrins on cholesterol levels in the rat. *Pharmaceutical Research, 8*, 9-16.

Frolov, A., Zielinski, S. E., Crowley, J. R., Dudley-Rucker, N., Schaffer, J. E., & Ory, D. S. (2003). NPC1 and NPC2 regulate cholesterol homeostasis through generation of LDL cholesterol-derived oxysterols. *Journal of Biological Chemistry, 278*, 25517-25526.

German, D. C., Liang, C.-L., Song, T., Yazdani, U., Xie, C., & Dietschy, J. M. (2002). Neurodegeneration in the Niemann-Pick C mouse: glial involvement. *Neuroscience, 109*, 437-450.

German, D. C., Quintero, E. M., Liang, C., Xie, C., & Dietschy, J. M. (2001a). Degeneration of neurons and glia in the Niemann-Pick C mouse is unrelated to the low-density lipoprotein receptor. *Neuroscience, 105*, 999-1005.

German, D. C., Quintero, E. M., Liang, C. L., Ng, B., Punia, S., Xie, C., & Dietschy, J. M. (2001b). Selective neurodegeneration, without neurofibrillary tangles, in a mouse model of Niemann-Pick C disease. *The Journal of Comparative Neurology, 433*, 415-425.

Goldstein, J. L., & Brown, M. S. (2009). The LDL receptor. *Arteriosclerosis, Thrombosis, and Vascular Biology, 29*, 431-438.

Goldstein, J. L., DeBose-Boyd, R. A., & Brown, M. S. (2006). Protein sensors for membrane sterols. *Cell, 124*, 35-46.

Goldstein, J. L., Hobbs, H. H., & Brown, M. S. (1995). Familial hypercholesterolemia. In C. R. Scriver, A. L. Beaudet, W. S. Sly & D. Valle (Eds.), *The Metabolic and Molecular Bases of Inherited Disease.* (7th ed., pp. 2073-2099). New York: McGraw-Hill, IOnc.

Gong, H., He, J., Lee, J. H., Mallick, E., Gao, X., Li, S., Homanics, G. E., & Xie, W. (2009). Activation of the liver X receptor prevents lipopolysaccharide-induced lung injury. *Journal of Biological Chemistry, 284*, 30113-30121.

Gopinath, B., Flood, V. M., Teber, E., McMahon, C. M., & Mitchell, P. (2011). Dietary intake of cholesterol is positively associated and use of cholesterol-lowering medication is negatively associated with prevalent age-related hearing loss. *Journal of Nutrition, 141*, 1355-1361.

Gould, S., & Scott, R. C. (2005). 2-Hydroxypropyl-β-cyclodextrin (HP-β-CD): A toxicology review. *Food and Chemical Toxicology, 43*, 1451-1459.

Gratton, M. A., & Wright, C. G. (1992). Alterations of ineer ear morphology in experimental hypercholesterolemia. *Hearing Research, 61*, 97-105.

Griese, M., Brasch, F., Aldana, V. R., Cabrera, M. M., Goelnitz, U., Ikonen, E., Karam, B. J., Liebisch, G., Linder, M. D., Lohse, P., Meyer, W., Schmitz, G., Pamir, A., Ripper, J., Rolfs, A., Schams, A., & Lezana, F. J. (2010). Respiratory disease in Niemann-Pick type C2 is caused by pulmonary alveolar proteinosis. *Clinical Genetics, 77*, 119-130.

Griffin, L. D., Gong, W., Verot, L., & Mellon, S. H. (2004). Niemann-Pick type C disease involves disrupted neurosteroidogenesis and responds to allopregnanolone. *Nature Medicine, 10*, 704-711.

Grundy, S. M., Cleeman, J. I., Merz, C. N. B., Brewer, H. B., Clark, L. T., Hunninghake, D. B., Pasternak, R. C., Smith, S. C., & Stone, N. J. (2004). Implications of recent clinical trials for the National Cholesterol Education Program Adult Treatment Panel III guidelines. *Arteriosclerosis Thrombosis and Vascular Biology, 24*, e149-e161.

Horton, J. D., Goldstein, J. L., & Brown, M. S. (2002). SREBPs: activators of the complete program of cholesterol and fatty acid synthesis in the liver. *Journal of Clinical Investigation, 109*, 1125-1131.

Huang, X., Suyama, K., Buchanan, J., Zhu, A. J., & Scott, M. P. (2005). A *Drosophila* model of the Niemann-Pick type C lysosome storage disease: *dnpc1a* is required for molting and sterol homeostasis. *Development, 132*, 5155-1524.

Huang, X., Warren, J. T., Buchanan, J., Gilbert, L. I., & Scott, M. P. (2007). Drosophila Niemann-Pick type C-2 genes control sterol homeostasis and steroid biosynthesis: a model of human neurodegenerative disease. *Development, 134*, 3733-3742.

Hutt, D. M., Herman, D., Rodrigues, A. P., Noel, S., Pilewski, J. M., Matteson, J., Hoch, B., Kellner, W., Kelly, J. W., Schmidt, A., Thomas, P. J., Matsumura, Y., Skach, W. R., Gentzsch, M., Riordan, J. R., Sorscher, E. J., Okiyoneda, T., Yates, J. R., 3rd, Lukacs, G. L., Frizzell, R. A., Manning, G., Gottesfeld, J. M., & Balch, W. E. (2010). Reduced histone deacetylase 7 activity restores function to misfolded CFTR in cystic fibrosis. *Nature Chemical Biology, 6*, 25-33.

Irie, T., Fukunaga, K., Garwood, M. K., Carpenter, T. O., Pitha, J., & Pitha, J. (1992). Hydroxypropylcyclodextrins in parenteral use. II: Effects on transport and disposition of lipids in rabbit and humans. *Journal of Pharmaceutical Sciences, 81*, 524-528.

Janowski, B. A., Grogan, M. J., Jones, S. A., Wisely, G. B., Kliewer, S. A., Corey, E. J., & Mangelsdorf, D. J. (1999). Structural requirements of ligands for the oxysterol liver X receptors LXRα and LXRβ. *Proceedings of the National Academy of Sciences USA, 96*, 266-271.

Jung, U. J., Millman, P. N., Tall, A. R., & Deckelbaum, R. J. (2011). n-3 Fatty acids ameliorate hepatic steatosis and dysfunction after LXR agonist ingestion in mice. *Biochimica Biophysica Acta, 1811*, 491-497.

Karasinska, J. M., & Hayden, M. R. (2011). Cholesterol metabolism in Huntington disease. *Nature Reviews: Neurology, 7*, 561-572.

Karten, B., Campenot, R. B., Vance, D. E., & Vance, J. E. (2006). Expression of ABCG1, but not ABCA1, correlates with cholesterol release by cerebellar astroglia. *Journal of Biological Chemistry, 281*, 4049-4057.

Kennedy, M. A., Barrera, G. C., Nakamura, K., Baldan, A., Tarr, P. T., Fishbein, M. C., Frnak, J., Francone, O. L., & Edwards, P. A. (2005). ABCG1 has a critical role in mediating cholesterol efflux to HDL and preventing cellular lipid accumulation. *Cell Metabolism, 1*, 121-131.

Kim, S.-J., Lee, B.-H., Lee, Y.-S., & Kang, K.-S. (2007). Defective cholesterol traffic and neuronal differentiation in neural stem cells of Niemann-Pick type C disease improved by valproic acid, a histone deacetylase inhibitor. *Biochemical and Biophysical Research Communications, 360*, 593-599.

Kim, W. S., Weickert, C. S., & Garner, B. (2008). Role of ATP-binding cassette transporters in brain lipid transport and neurological disease. *Journal of Neurochemistry, 104*, 1145-1166.

Kodam, A., Maulik, M., Peake, K., Amritraj, A., Vetrivel, K. S., Thinakaran, G., Vance, J. E., & Kar, S. (2010). Altered levels and distribution of amyloid precursor protein and its processing enzymes in Niemann-Pick type C1-deficient mouse brains. *Glia, 58*, 1267-1281.

Korf, H.-W., Vander Beken, S., Romano, M., Steffensen, K. R., Stijlemans, B., Gustafsson, J.-A., Grooten, J., & Huygen, K. (2009). Liver X receptors contribute to the protective immune response against *Mycobacterium tuberculosis* in mice. *Journal of Clinical Investigation, 119*, 1626-1637.

Kosir, R., Acimovic, J., Golicnik, M., Perse, M., Majdic, G., Fink, M., & Rozman, D. (2010). Determination of reference genes for circadian studies in different tissues and mouse strains. *BMC Molecular Biology, 11*, 60.

Kotti, T. J., Ramirez, D. M. O., Pfeiffer, B. E., Huber, K. M., & Russell, D. W. (2006). Brain cholesterol turnover required for geranylgeraniol production and learning in mice. *Proceedings of the National Academy of Sciences USA, 103*, 3869-3874.

Kurrasch, D. M., Huang, J., Wilkie, T. M., & Repa, J. J. (2004). Quantitative real-time polymerase chain reaction measurement of regulators of G-protein signaling mRNA levels in mouse tissues. *Methods in Enzymology, 389*, 3-15.

Kuwamura, M., Awakura, T., Shimada, A., Umemura, T., Kagota, K., Kawamura, N., & Naiki, M. (1993). Type C Niemann-Pick disease in a boxer dog. *Acta Neuropathologica, 85*, 345-348.

Kwon, H. J., Abi-Mosleh, L., Wang, M. L., Deisenhofer, J., Goldstein, J. L., Brown, M. S., & Infante, R. E. (2009). Structure of N-terminal domain of NPC1 reveals distinct subdomains for binding and transfer of cholesterol. *Cell, 137*, 1213-1224.

Langmade, S. J., Gale, S. E., Frolov, A., Mohri, I., Suzuki, K., Mellon, S. H., Walkley, S. U., Covey, D. F., Schaffer, J. E., & Ory, D. S. (2006). Pregnane X receptor (PXR) activation: a mechanism for neuroprotection in a mouse model of Niemann-Pick C disease. *Proceedings of the National Academy of Sciences USA, 103*, 13807-13812.

Lefterov, I., Bookout, A., Wang, Z., Staufenbiel, M., Mangelsdorf, D., & Koldamova, R. (2007). Expression profiling in APP23 mouse brain: inhibition of Aβ amyloidosis and inflammation in response to LXR agonist treatment. *Molecular Neurodegeneration, 2*, 1-15.

Levic, S., & Yamoah, E. N. (2011). Plasticity in membrane cholesterol contributes toward electrical matruation of hearing. *Journal of Biological Chemistry, 286*, 5768-5773.

Li, H., Repa, J. J., Valasek, M. A., Beltroy, E. P., Turley, S. D., German, D. C., & Dietschy, J. M. (2005). Molecular, anatomical, and biochemical events associated with neurodegeneration in mice with

Niemann-Pick Type C disease. *Journal of Neuropathology and Experimental Neurology, 64*, 323-333.

Li, J., Brown, G., Ailion, M., Lee, S., & Thomas, J. H. (2004). NCR-1 and NCR-2, the C. elegans homologs of the human Niemann-Pick type C1 disease protein, function upstream of DAF-9 in the dauer formation pathways. *Development, 131*, 5741-5752.

Liu, B., Li, H., Repa, J. J., Turley, S. D., & Dietschy, J. M. (2008). Genetic variations and treatments that affect the lifespan of the NPC1 mouse. *Journal of Lipid Research, 49*, 663-669.

Liu, B., Ramirez, C. M., Miller, A. M., Repa, J. J., Turley, S. D., & Dietschy, J. M. (2010a). Cyclodextrin overcomes the transport defect in nearly every organ of NPC1 mice leading to excretion of sequestered cholesterol as bile acid. *Journal of Lipid Research, 51*, 933-944.

Liu, B., Turley, S. D., Burns, D. K., Miller, A. M., Repa, J. J., & Dietschy, J. M. (2009). Reversal of defective lysosomal transport in NPC disease ameliorates liver dysfunction and neurodegeneration in the *npc1$^{-/-}$* mouse. *Proceedings of the National Academy of Sciences USA, 106*, 2377-2382.

Liu, J.-P., Tang, Y., Zhou, S., Toh, B. H., McLean, C., & Li, H. (2010b). Cholesterol involvement in the pathogenesis of neurodegenerative diseases. *Molecular and Cellular Neuroscience, 23*, 33-42.

Loftus, S. K., Morris, J. A., Carstea, E. D., Gu, J. Z., Cummings, C., Brown, A., Ellison, J., Ohno, K., Rosenfeld, M. A., Tagle, D. A., Pentchev, P. G., & Pavan, W. J. (1997). Murine model of Niemann-Pick C disease: mutation in a cholesterol homeostasis gene. *Science, 277*, 232-235.

Lopez, C. A., de Vries, A. H., & Marrink, S. J. (2011). Molecular mechanism of cyclodextrin mediated cholesterol extraction. *PLoS Computational Biology, 7*, e1002020.

Lowenthal, A. C., Cummings, J. F., Wenger, D. A., Thrall, M. A., Wood, P. A., & de Lahunta, A. (1990). Feline sphingolipidosis resembling Niemann-Pick disease type C. *Acta Neuropathologica, 81*, 189-197.

Lu, J., Yang, C., Chen, M., Ye, D. Y., Lonser, R. R., Brady, R. O., & Zhuang, Z. (2011). Histone deacetylase inhibitors prevent the degradation and restore the activity of glucocerebrosidase in Gaucher disease. *Proceedings of the National Academy of Sciences USA, 108.* , 21200–21205.

Malathi, K., Higaki, K., Tinkelenberg, A. H., Balderes, D. A., Almanzar-Paramio, D., Wilcox, L. J., Erdeniz, N., Redican, F., Padamsee, M., Liu, Y. Q., Khan, S. A., Alcantara, F., Carstea, E. D., Morris, J. A., & Sturley, S. L. (2004). Mutagenesis of the putative sterol-sensing domain of yeast Niemann Pick C-related protein reveals a primordial role in subcellular sphingolipid distribution. *Journal of Cell Biology, 164*, 547-556.

Manabe, T., Yamane, T., Higashi, Y., Pentchev, P. G., & Suzuki, K. (1995). Ultrastructural changes in the lung in Niemann-Pick type C mouse. *Virchows Archives, 427*, 77-83.

Maue, R. A., Burgess, R. W., Wang, B., Wooley, C. M., Seburn, K. L., Vanier, M. T., Rogers, M. A., Chang, C. C. Y., Chang, T.-Y., Harris, B. T., Graber, D. J., Penatti, C. A. A., Porter, D. M., Szwergold, B. S., Henderson, L. P., Totenhagen, J. W., Trouard, T. P., Borbon, I. A., & Erickson, R. P. (2012). A novel mouse model of Niemann Pick type C disease carrying a D1005G-Npc1 mutation comparable to commonly observed human mutations. *Human Molecular Genetics, 21*, 730-750.

McCauliff, L. A., Xu, Z., & Storch, J. (2011). Sterol transfer between cyclodextrin and membranes: similar but not identical mechanism to NPC2-mediated cholesterol transfer. *Biochemistry, 50*, 7341-7349.

Miao, B., Zondlo, S., Gibbs, S., Cromley, D., Hosagrahara, V. P., Kirchgessner, T. G., Billheimer, J., & Mukherjee, R. (2004). Raising HDL cholesterol without inducing hepatic steatosis and hypertriglyceridemia by a selective LXR modulator. *Journal of Lipid Research, 45*, 1410-1417.

Millat, G., Chikh, K., Naureckiene, S., Sleat, D. E., Fensom, A. H., Higaki, K., Elleder, M., Lobel, P., & Vanier, M. T. (2001). Niemann-Pick disease type C: spectrum of HE1 mutations and

genotype/phenotype correlations in the NPC2 group. *American Journal of Human Genetics, 69*, 1013-1021.

Morris, M. D., Bhuvaneswaran, C., Shio, H., & Fowler, S. (1982). Lysosome lipid storage disorder in NCTR-BALB/c mice. I. Description of the disease and genetics. *The American Journal of Pathology, 108*, 140-149.

Munkacsi, A. B., Chen, F. W., Brinkman, M. A., Higaki, K., Gutierrez, G. D., Chaudhari, J., Layer, J. V., Tong, A., Bard, M., Boone, C., Ioannou, Y. A., & Sturley, S. L. (2011). An "exacerbate-reverse" strategy in yeast identifies histone deacetylase inhibition as a correction for cholesterol and sphingolipid transport defects in human Niemann-Pick type C disease. *Journal of Biological Chemistry, 286*, 23842-23851.

Muralidhar, A., Borbon, I. A., Esharif, D. M., Ke, W., Manacheril, R., Daines, M., & Erickson, R. P. (2011). Pulmonary function and pathology in hydroxypropyl-beta-cyclodextrin-treated and untreated *Npc1$^{-/-}$* mice. *Molecular Genetics and Metabolism, 103*, 142-147.

Naureckiene, S., Sleat, D. E., Lackland, H., Fensome, A., Vanier, M. T., Wattiaux, R., Jadot, M., & Lobel, P. (2000). Identification of *HE1* as the second gene of Niemann-Pick C disease. *Science, 290*, 2298-2301.

Ong, W. Y., Kumar, U., Switzer, R. C., Sidhu, A., Suresh, G., Hu, C. Y., & Patel, S. C. (2001). Neurodegeneration in Niemann-Pick type C disease mice. *Experimental Brain Research, 141*, 218-231.

Organ, L. E., & Raphael, R. M. (2009). Lipid lateral mobility in cochlear outer hair cells: regional differences and regulation by cholesterol. *Journal of the Association for Research in Otolaryngology, 10*, 383-396.

Orth, M., & Bellosta, S. (2012). Cholesterol: its regulation and role in central nervous system disorders. *Cholesterol, 2012*, 292598.

Ory, D. S. (2004). The Niemann-Pick Disease Genes Regulators of Cellular Cholesterol Homeostasis. *Trends in Cardiovascular Medicine, 14*, 66-72.

Palmeri, S., Tarugi, P., Sicurelli, F., Buccoliero, R., Malandrini, A., De Santi, M. M., Marciano, G., Battisti, C., Dotti, M. T., Calandra, S., & Federico, A. (2005). Lung involvement in Niemann-Pick disease type C1: improvement with bronchoalveolar lavage. *Neurological Sciences, 26*, 171-173.

Panda, S., Antoch, M. P., Miller, B. H., Su, A. I., Schook, A. B., Straume, M., Schultz, P. G., Kay, S. A., Takahashi, J. S., & Hogenesch, J. B. (2002). Coordinated transcription of key pathways in the mouse by the circadian clock. *Cell, 109*, 307-320.

Parihar, R. K., Razaq, M., & Saini, G. (2012). Homozygous familial hypercholesterolemia. *Indian Journal of Endocrinology and Metabolism, 16*, 643-645.

Patterson, M. C. (2003). A riddle wrapped in a mystery: understanding Niemann-Pick disease, type C. *The Neurologist, 9*, 301-310.

Patterson, M. C., Hendriksz, C. J., Walterfang, M., Sedel, F., Vanier, M. T., Wijburg, F., & Group, N.-C. G. W. (2012). Recommendations for the diagnosis and management of Niemann-Pick disease type C: an update. *Molecular Genetics and Metabolism, 106*, 330-344.

Patterson, M. C., Vanier, M. T., Suzuki, K., Morris, J. A., Carstea, E. D., Neufeld, E. B., Blanchette-Mackie, J. E., & Pentchev, P. G. (2001). Niemann-Pick Disease Type C: a lipid trafficking disorder. In C. R. Scriver (Ed.), *The Metabolic and Molecular Bases of Inherited Disease.* (8th Ed. ed., Vol. 3, pp. 3611-3633). New York: McGraw-Hill.

Patterson, M. C., Vecchio, D., Prady, H., Abel, L., & Wraith, J. E. (2007). Miglustat for treatment of Niemann-Pick C disease: a randomized controlled study. *Lancet Neurology, 6*, 765-772.

Pawlowski, K., Koulich, E., Wright, C. G., & Roland, P. (2013). Ototopic Applications of Povidone Iodine/Dexamethasone in the Rat. *Otology & Neurotology, 34*, 167-174.

Peake, K. B., & Vance, J. E. (2010). Defective cholesterol trafficking in Niemann-Pick C-deficient cells. *FEBS Letters, 584*, 2731-2739.

Peake, K. B., & Vance, J. E. (2011). Normalization of cholesterol homeostasis by 2-hydroxypropyl-β-cyclodextrin in neurons and glia from Niemann-Pick C1 (NPC1)-deficient mice. *Journal of Biological Chemistry, 287*, 9290-9298.

Peng, D., Hiipakka, R. A., Dai, Q., Guo, J., Reardon, C. A., Getz, G. S., & Liao, S. (2008). Antiatherosclerotic effects of a novel synthetic tissue-selective steroidal liver X receptor agonist in low-density lipoprotein receptor-deficient mice. *The Journal of Pharmacology and Experimental Therapeutics, 327*, 332-342.

Pentchev, P. G. (2004). Niemann-Pick C research from mouse to gene. *Biochimica Biophysica Acta, 1685*, 3-7.

Pikus, A. (1991). Audiologic profile in Niemann-Pick C. *Annals of the New York Academy of Sciences, 630*, 313-314.

Pipalia, N. H., Cosner, C. C., Huang, A., Chatterjee, A., Bourbon, P., Farley, N., Helquist, P., Wiest, O., & Maxfield, F. R. (2011). Histone deacetylase inhibitor treatment dramatically reduces cholesterol accumulation in Niemann-Pick type C1 mutant human fibroblasts. *Proceedings of the National Academy of Sciences USA, 108*, 5620-5625.

Pringsheim, T., Wiltshire, K., Day, L., Dykeman, J., Steeves, T., & Jette, N. (2012). The incidence and prevalence of Huntington's disease: a systematic review and meta-analysis. *Movement Disorders, 27*, 1083-1091.

Puglisi, G., Fresta, M., & Ventura, C. A. (1996). Interaction of natural and modified β-cyclodextrins with a biological membrane model of dipalmitoylphosphatidylcholine. *Journal of Colloid and Interface Science, 180*, 542-547.

Raal, F. J., & Santos, R. D. (2012). Homozygous familial hypercholesterolemia: current perspectives on diagnosis and treatment. *Atherosclerosis, 223*, 262-268.

Rajagopalan, L., Greeson, J. N., Xia, A., Liu, H., Sturm, A., Raphael, R. M., Davidson, A. L., Oghalai, J. S., Pereira, F. A., & Brownell, W. E. (2007). Tuning of the outer hair cell motor by membrane cholesterol. *Journal of Biological Chemistry, 282*, 36659-36670.

Rajewski, R. A., Traiger, G., Bresnahan, J., Jaberaboansari, P., Stella, V. J., & Thompson, D. O. (1995). Preliminary safety evaluation of parenterally administered sulfoalkyl ether β-cyclodextrin derivatives. *Journal of Pharmaceutical Sciences, 84*, 927-932.

Ramirez, C. M., Liu, B., Aqul, A., Taylor, A. M., Repa, J. J., Turley, S. D., & Dietschy, J. M. (2011). Quantitative role of LAL, NPC2, and NPC1 in lysosomal cholesterol processing defined by genetic and pharmacological manipulations. *Journal of Lipid Research, 52*, 688-698.

Ramirez, C. M., Liu, B., Taylor, A. M., Repa, J. J., Burns, D. K., Weinberg, A. G., Turley, S. D., & Dietschy, J. M. (2010). Weekly cyclodextrin administration normalizes cholesterol metabolism in nearly every organ of the Niemann-Pick type C1 mouse and markedly prolongs life. *Pediatric Research, 68*, 309-315.

Repa, J. J., Li, H., Frank-Cannon, T. C., Valasek, M. A., Turley, S. D., Tansey, M. G., & Dietschy, J. M. (2007). Liver X receptor activation enhances cholesterol loss from the brain, decreases neuroinflammation, and increases survival of the NPC1 mouse. *Journal of Neuroscience, 27*, 14470-14480.

Repa, J. J., Liang, G., Ou, J., Bashmakov, Y., Lobaccaro, J.-M. A., Shimomura, I., Shan, B., Brown, M. S., Goldstein, J. L., & Mangelsdorf, D. J. (2000a). Regulation of mouse sterol regulatory element-binding protein-1c gene (SREBP-1c) by oxysterol receptors, LXRα and LXRβ. *Genes & Development, 14*, 2819-2830.

Repa, J. J., & Mangelsdorf, D. J. (2000b). The role of orphan nuclear receptors in the regulation of cholesterol homeostasis. *Annual Reviews in Cell and Developmental Biology, 16*, 459-481.

Repa, J. J., & Mangelsdorf, D. J. (2002). The liver X receptor gene team: potential new players in atherosclerosis. *Nature Medicine, 8*, 1243-1248.

Rosenbaum, A. I., Rujoi, M., Huang, A. Y., Du, H., Grabowski, G. A., & Maxfield, F. R. (2009). Chemical screen to reduce sterol accumulation in Niemann-Pick C disease cells identified novel lysosomal acid lipase inhibitors. *Biochimica Biophysica Acta, 1791*, 1155-1165.

Rosenbaum, A. I., Zhang, G., Warren, J. D., & Maxfield, F. R. (2010). Endocytosis of beta-cyclodextrins is responsible for cholesterol reduction in Niemann-Pick type C mutant cells. *Proceedings of the National Academy of Sciences USA, 107*, 5477-5482.

Roy, A., & Pahan, K. (2011). Prospects of statins in Parkinson disease. *Neuroscientist, 17*, 244-255.

Russell, D. W., Halford, R. W., Ramirez, D. M. O., Shah, R., & Kotti, T. (2009). Cholesterol 24-hydroxylase: an enzyme of cholesterol trunover in the brain. *Annual Reviews in Biochemistry, 78*, 1017-1040.

Schmittgen, T. D., & Livak, K. J. (2008). Analyzing real-time PCR data by the comparative C_T method. *Nature Protocols, 3*, 1101-1108.

Schuchman, E. H., & Desnick, R. J. (2001). Niemann-Pick Disease Types A and B: acid sphingomyelinase deficiencies. In C. R. Scriver (Ed.), *The Metabolic and Molecular Bases of Inherited Disease.* (8th Ed. ed., Vol. 3, pp. 3589-3610). New York: McGraw-Hill.

Schultz, J. R., Tu, H., Luk, A., Repa, J. J., Medina, J. C., Li, L., Schwendner, S., Wang, S., Thoolen, M., Mangelsdorf, D. J., Lustig, K. D., & Shan, B. (2000). Role of LXRs in control of lipogenesis. *Genes & Development, 14*, 2831-2838.

Sleat, D. E., Wiseman, J. A., El-Banna, M., Price, S. M., Verot, L., Shen, M. M., Tint, G. S., Vanier, M. T., Walkley, S. U., & Lobel, P. (2004). Genetic evidence for nonredundant functional cooperativity between NPC1 and NPC2 in lipid transport. *Proceedings of the National Academy of Sciences USA, 101*, 5886-5891.

Smith, D., Wallom, K.-L., Williams, I. M., Jeyakumar, M., & Platt, F. M. (2009). Beneficial effects of anti-inflammatory therapy in a mouse model of Niemann-Pick disease type C1. *Neurobiology of Disease, 36*, 242-251.

Somers, K. L., Royals, M. A., Carstea, E. D., Rafi, M. A., Wenger, D. A., & Thrall, M. A. (2003). Mutation analysis of feline Niemann-Pick C1 disease. *Mol Genet Metab, 79*, 99-103.

Stella, V. J., & He, Q. (2008). Cyclodextrins. *Toxicologic Pathology, 36*, 30-42.

Swaroop, M., Thorne, N., Rao, M. S., Austin, C. P., McKew, J. C., & Zheng, W. (2012). Evaluation of Cholesterol Reduction Activity of Methyl-beta-cyclodextrin Using Differentiated Human Neurons and Astrocytes. *Journal of Biomolecular Screening, 17*, 1243-1251.

Sym, M., Basson, M., & Johnson, C. (2000). A model for niemann-pick type C disease in the nematode Caenorhabditis elegans. *Current Biology, 10*, 527-530.

Tan, J., Cang, S., Ma, Y., Petrillo, R. L., & Liu, D. (2010). Novel histone deacetylase inhibitors in clinical trials as anti-cancer agents. *Journal of Hematology & Oncology, 3*, 5.

Tarling, E. J., & Edwards, P. A. (2011). ATP binding cassette transporter G1 (ABCG1) is an intracellular sterol transporter. *Proceedings of the National Academy of Sciences USA, 108*, 19719-19724.

Tarr, P. T., & Edwards, P. A. (2008). ABCG1 and ABCG4 are coexpressed in neurons and astrocytes of the CNS and regulate cholesterol homeostasis through SREBP-2. *Journal of Lipid Research, 49*, 169-182.

Taylor, A. M., Liu, B., Mari, Y., Liu, B., & Repa, J. J. (2012). Cyclodextrin mediates rapid changes in lipid balance in Npc1-/- mice without carrying cholesterol through the bloodstream. *Journal of Lipid Research, 53*, 2331-2342.

Thomassen, M. J., Barna, B. P., Malur, A. G., Bonfield, T. L., Farver, C. F., Malur, A., Dalrymple, H., Kavuru, M. S., & Febbraio, M. (2007). ABCG1 is deficient in alveolar macrophages of GM-CSF knockout mice and patients with pulmonary alveolar proteinosis. *Journal of Lipid Research, 48*, 2762-2768.

Thompson, D. O. (1997). Cyclodextrins - enabling excipients: their present and future use in pharmaceuticals. *Critical Reviews in Therapeutic Drug Carrier Systems, 14*, 1-104.

Turley, S. D., Herndon, M. W., & Dietschy, J. M. (1994). Reevaluation and application of the dual-isotope plasma ratio method for the measurement of intestinal cholesterol absorption in the hamster. *Journal of Lipid Research, 35*, 328-339.

Valasek, M. A., & Repa, J. J. (2005a). The power of real-time PCR. *Advances in Physiology Education, 29*, 151-159.

Valasek, M. A., Weng, J., Shaul, P. W., Anderson, R. G. W., & Repa, J. J. (2005b). Caveolin-1 is not required for murine intestinal cholesterol transport. *Journal of Biological Chemistry, 280*, 28103-28109.

Van Den Eeden, S. K., Tanner, C. M., Bernstein, A. L., Fross, R. D., Leimpeter, A., Bloch, D. A., & Nelson, L. M. (2003). Incidence of Parkinson's disease: variation by age, gender, and race/ethnicity. *American Journal of Epidemiology, 157*, 1015-1022.

Vance, J. E. (2006). Lipid imbalance in the neurological disorder, Niemann-Pick C disease. *FEBS Letters, 580*, 5518–5524.

Vance, J. E. (2012). Dysregulation of cholesterol balance in the brain: contribution to neurodegenerative diseases. *Disease Models & Mechanisms, 5*, 746-755.

Vanier, M. T. (2010). Niemann-Pick disease type C. *Orphanet Journal of Rare Diseases, 5*, 16.

Vite, C. H., Ding, W., Bryan, C., O'Donnell, P. E., Cullen, K., Aleman, D., Haskins, M. E., & Van Winkle, T. (2008). Clinical, electrophysiological, and serum biochemical measures of progressive neurological and hepatic dysfunction in feline Niemann-Pick type C disease. *Pediatric Research, 64*, 544-549.

Ward, S., O'Donnell, P., Fernandez, S., & Vite, C. H. (2010). 2-Hydroxypropyl-β-cyclodextrin raises hearing threshold in normal cats and in cats with Niemann-Pick type C disease. *Pediatric Research, 68*, 52-56.

Whitney, K. D., Watson, M. A., Colins, J. L., Benson, W. G., Stone, T. M., Numerick, M. J., Tippin, T. K., Wilson, J. G., Winegar, D. A., & Kliewer, S. A. (2002). Regulation of cholesterol

homeostasis by the liver X receptors in the central nervous system. *Molecular Endocrinology, 16*, 1378-1385.

Willy, P. J., & Mangelsdorf, D. J. (1997). Unique requirements for retinoid-dependent transcriptional activation by the orphan receptor LXR. *Genes & Development, 11*, 289-298.

Wojcik, A. J., Skaflen, M. D., Srinivasan, S., & Hedrick, C. C. (2008). A critical role for ABCG1 in macrophage inflammation and lung homeostasis. *Journal of Immunology, 180*, 4273-4282.

Wu, Y.-P., Mizukami, H., Matsuda, J., Saito, Y., Proia, R. L., & Suzuki, K. (2005). Apoptosis accompanied by up-regulation of TNF-α death pathway genes in the brain of Niemann-Pick type C disease. *Molecular Genetics and Metabolism, 84*, 9-17.

Xie, C., Burns, D. K., Turley, S. D., & Dietschy, J. M. (2000). Cholesterol is sequestered in the brains of mice with Niemann-Pick Type C disease but turnover is increased. *Journal of Neuropathology and Experimental Neurology, 59*, 1106-1117.

Xie, C., Turley, S. D., & Dietschy, J. M. (1999a). Cholesterol accumulation in tissues of the Niemann-Pick type C mouse is determined by the rate of lipoprotein-cholesterol uptake through the coated-pit pathway in each organ. *Proceedings of the National Academy of Sciences USA, 96*, 11992-11997.

Xie, C., Turley, S. D., Pentchev, P. G., & Dietschy, J. M. (1999b). Cholesterol balance and metabolism in mice with loss of function of Niemann-Pick C protein. *American Journal of Physiology, 276*, E336-E344.

Xie, X., Brown, M. S., Shelton, J. M., Richardson, J. A., Goldstein, J. L., & Liang, G. (2011). Amino acid substitution in NPC1 that abolishes cholesterol binding reproduces phenotype of complete NPC1 deficiency in mice. *Proceedings of the National Academy of Sciences USA, 108*, 15330-15335.

Xu, M., Liu, K., Swaroop, M., Porter, F. D., Sidhu, R., Finkes, S., Ory, D. S., Marugan, J. J., Xiao, J., Southall, N., Pavan, W. J., Davidson, C., Walkley, S. U., Remaley, A. T., Baxa, U., Sun, W., McKew, J. C., Austin, C. P., & Zheng, W. (2012). delta-Tocopherol Reduces Lipid Accumulation

in Niemann-Pick Type C1 and Wolman Cholesterol Storage Disorders. *The Journal of Biological Chemistry, 287*, 39349-39360.

Yancey, P. G., Rodriguez, W. V., Kilsdonk, E. P. C., Stoudt, G. W., Johnson, W. J., Phillips, M. C., & Rothblat, G. H. (1996). Cellular cholesterol efflux mediated by cyclodextrins. Demonstration of kinetic pools and mechanism of efflux. *Journal of Biological Chemistry, 271*, 16026-16034.

Yu, T., Shakkottai, V. G., Chung, C. C., & Lieberman, A. P. (2011). Temporal and cell-specific deletion establishes that neuronal *Npc1* deficiency is sufficient to mediate neurodegeneration. *Human Molecular Genetics, 20*, 4440-4451.

Zervas, M., Dobrenis, K., & Walkley, S. U. (2001a). Neurons in Niemann-Pick disease type C accumulate gangliosides as well as unesterified cholesterol and undergo dendritic and axonal alterations. *Journal of Neuropathology and Experimental Neurology, 60*, 49-64.

Zervas, M., Somers, K. L., Thrall, M. A., & Walkley, S. U. (2001b). Critical role for glycosphingolipids in Niemann-Pick disease type C. *Current Biology, 11*, 1283-1287.

Zidovetzki, R., & Levitan, I. (2007). Use of cyclodextrins to manipulate plasma membrane cholesterol content: evidence, misconceptions and control strategies. *Biochimica Biophysica Acta, 1768*, 1311-1334.